

Electronic Thesis and Dissertation Repository

---

12-9-2020 11:45 AM

## Longitudinal Partitioning Waveform Relaxation Methods For The Analysis of Transmission Line Circuits

Tarik Menkad, *The University of Western Ontario*

Supervisor: Anestis Dounavis, *The University of Western Ontario*

A thesis submitted in partial fulfillment of the requirements for the Doctor of Philosophy degree in Electrical and Computer Engineering

© Tarik Menkad 2020

Follow this and additional works at: <https://ir.lib.uwo.ca/etd>



Part of the [Electrical and Electronics Commons](#), [Numerical Analysis and Computation Commons](#), [Numerical Analysis and Scientific Computing Commons](#), [Other Electrical and Computer Engineering Commons](#), [Signal Processing Commons](#), and the [VLSI and Circuits, Embedded and Hardware Systems Commons](#)

---

### Recommended Citation

Menkad, Tarik, "Longitudinal Partitioning Waveform Relaxation Methods For The Analysis of Transmission Line Circuits" (2020). *Electronic Thesis and Dissertation Repository*. 7547.  
<https://ir.lib.uwo.ca/etd/7547>

This Dissertation/Thesis is brought to you for free and open access by Scholarship@Western. It has been accepted for inclusion in Electronic Thesis and Dissertation Repository by an authorized administrator of Scholarship@Western. For more information, please contact [wlsadmin@uwo.ca](mailto:wlsadmin@uwo.ca).

## Abstract

Three research projects are presented in this manuscript. Projects one and two describe two waveform relaxation algorithms (WR) with longitudinal partitioning for the time-domain analysis of transmission line circuits. Project three presents theoretical results about the convergence of WR for chains of general circuits.

The first WR algorithm uses an assignment-partition procedure that relies on inserting external series combinations of positive and negative resistances into the circuit to control the speed of convergence of the algorithm. The convergence of the subsequent WR method is examined, and fast convergence is cast as a generic optimization problem in the frequency-domain. An automatic suboptimal numerical solution of the min-max problem is presented and a procedure to construct its objective function is suggested. Numerical examples illustrate the parallelizability and good scaling of the WR algorithm and point out to the limitation of resistive coupling.

In the second WR algorithm, resistances from the previous insertion are replaced with strictly dissipative impedances to address the slow convergence of standard resistive coupling of the first algorithm for low-loss highly reactive circuits. The pertinence and feasibility of impedance coupling are demonstrated and the properties of the subsequent WR method are studied. A new coupling strategy proposes judicious approximations of the optimal convergence conditions for faster speed of convergence. The proposed strategy avoids the difficult problem of optimisation and uses coarse macromodeling of the transmission line to construct approximations with delay under circuit form. Numerical examples confirm a superior speed of convergence and further runtime saving.

Finally, new results concerning the nilpotent WR algorithm are presented for chains of circuits when dissipative impedance coupling is used. It is shown that optimal local convergence is necessary to achieve the optimal WR algorithm. However, the converse is not correct: the WR algorithm with null local convergences factors can be nilpotent yet not optimal or even be non-nilpotent at all. The second analysis concerns resistive coupling. It is demonstrated that WR always converges for chains circuits. More

precisely, it is shown that WR will converge independently of the length of the chain when this late is made of identical symmetric circuits.

## Keywords

Circuit simulation, transmission line, non-overlapping, waveform relaxation, iteration solver, ODE, DAE, resistive coupling, optimization, dissipative impedance coupling, transmission coupling conditions, iteration matrix, convergence analysis, local and global convergence, nilpotent operator, optimal convergence.



## Summary for Lay Audience

The continuous demand for faster data processing in electronic systems requires stricter verification of their integrity. The interconnections which are responsible of transporting data between different parts of these systems are sensitive to the speed of operation. A high operating speed gives birth to physical phenomena which degrade data and causes errors. It is essential to address these issues in the early stages of the design cycle. To this end, simulation tools used in the design cycle must be reliable and fast. Indeed, a reliable simulation which takes a lot of time can be impractical for some design cycles. The computational core of conventional simulation tools uses the so-called direct methods to solve the mathematical models of such systems. These methods however can become time consuming and memory intensive for large design problems. Another class of computational methods namely relaxation methods, divide large simulation problems into smaller ones and solve them repetitively at the same time until solution is reached. If the number of cycles is decreased, then it is possible to reduce drastically the simulation time. This following thesis presents a research effort intended to accelerate these relaxation methods.

## Co-Authorship Statement

In all my papers, I am the first author and my PhD supervisor Prof. Anestis Dounavis is the second author.

## Acknowledgments

Throughout the writing of this dissertation, I have received a great deal of support and assistance.

I would like to thank my supervisor, Professor Anestis Dounavis, whose expertise was invaluable in formulating the research questions and methodology. His insightful feedback and criticism pushed me to sharpen my thinking and brought my work to a higher level.

I would like to thank Professor Robert Corless and Professor Martin Gander of the Applied Mathematics Departments of Western University, London Ontario, Canada and of l'Université de Genève, Geneva Switzerland for providing me with a valuable insight through the numerous discussions we had on numerical methods and on domain decomposition techniques. I would also like to thank Professor kazimierz Adamiak of the Department of Electrical and Computer Engineering of Western University for his teaching of Computational Electromagnetic course. I am honored that he incorporated my Matlab codes as a template in his later course assignments.

I would also like to thank the department chair Professor Kenneth McIsaac and acting chair Professor Abdallah Shami for giving me the opportunity to teach undergraduate courses as a lecturer in the department of Electrical and Computer Engineering at Western. I would like to extend my gratitude to the administrative team of the Electrical and Computer Engineering Department of Western for their professionalism and dedication.

Finally, I thank my wife for her unconditional support, council and sympathetic ear.

à ma famille, avec tout mon amour.

# Table of Contents

Abstract .....	ii
Keywords .....	iv
Summary for Lay Audience .....	v
Co-Authorship Statement.....	vi
Acknowledgments.....	vii
Table of Contents .....	ix
List of Tables .....	xii
List of Figures .....	xiii
Chapter 1 .....	1
1 Introduction .....	1
1.1 Initial Value Problem .....	1
1.2 A Circuit Simulation Problem .....	3
1.3 Review of Numerical Techniques for Initial-Value Problems .....	3
1.3.1 Linear Solution Methods.....	4
1.3.2 Nonlinear Solution Methods.....	9
1.3.3 Integration Methods .....	12
1.3.4 Waveform Methods .....	14
1.4 Waveform Relaxation Analysis of Transmission Line Circuits .....	18
1.5 Contribution of the present research thesis .....	22
Chapter 2.....	24
2 Resistive Coupling-based Waveform Relaxation Algorithm for Analysis of Interconnect Circuits .....	24
2.1 Proposed WR Algorithm.....	24
2.1.1 Development of partitioning interface .....	24

2.1.2	Local convergence analysis of WR algorithm .....	27
2.1.3	Two-subsystem problem.....	29
2.1.4	Multi–subsystem problem.....	31
2.1.5	Construction of the optimization problem .....	36
2.1.6	LP-WR .....	40
2.2	Numerical Examples .....	43
2.2.1	Example One-Proof of concept.....	43
2.2.2	Example Two-Low loss distributed circuit-perfect dielectric. ....	50
2.2.3	Example Three-Chain connection.....	51
2.2.4	Example Four Tree structure-scalability with respect to number of CPUs. ....	56
2.2.5	Example Five-Tree structure-scalability with respect to the partition size. ....	66
2.3	Conclusion .....	69
Chapter 3.....		70
3	Using Strictly Dissipative Impedance Coupling in the Waveform Relaxation Method for the Analysis of Interconnect Circuits.....	70
3.1	Strictly dissipative impedance coupling .....	70
3.2	Proposed WR algorithm.....	73
3.2.1	Relevance of strictly dissipative impedance coupling .....	73
3.2.2	Feasibility.....	76
3.2.3	Properties of impedance coupling based WR .....	77
3.2.4	Coupling strategy .....	84
3.2.5	Computational cost analysis .....	87
3.2.6	Concluding remarks .....	89
3.3	Numerical Examples .....	90

3.3.1	Example One-Proof of Concept.....	91
3.3.2	Example Two-Chain connection.....	102
3.3.3	Example Three-Tree structure. ....	111
3.3.4	Example Four-RLCG single line problem [77]. ....	120
3.4	Conclusion .....	123
Chapter 4	.....	124
4	Some Convergence Results on Waveform Relaxation for Chains of Circuits.....	124
4.1	Nilpotency of Strictly Dissipative Impedance Coupling based Waveform Relaxation Algorithm.....	124
4.2	Convergence of Resistive Coupling-based Waveform Relaxation for Chains of Identical Symmetric Parts .....	141
4.2.1	Illustrative Example .....	145
4.3	Construction of iteration matrices.....	152
4.3.1	Gauss-Jacobi iteration matrix .....	153
4.3.2	Gauss-Seidel iteration matrix.....	156
4.4	Conclusion .....	159
Chapter 5	.....	161
5	Conclusion .....	161
5.1	Summary .....	161
5.2	Future work.....	162
5.2.1	Towards multi-conductor transmission line circuits.....	162
5.2.2	In the presence of nonlinear loads .....	162
Bibliography	.....	163
Curriculum Vitae	.....	171

## List of Tables

Table 2.1: Pseudocode. WR algorithm for a two-subsystem partition. GJ relaxation.....	26
Table 2.2: Pseudocode. WR algorithm for a two-subsystem partition. GS relaxation .....	27
Table 2.3: Formulation of the objective function. ....	39
Table 2.4: Summary of steps for the proposed parallel GS-WR algorithm.....	41
Table 2.5: Performance of proposed algorithm. Example Four.....	62
Table 2.6: Scaling with respect to the number of transmission lines. Example Five. ....	67
Table 3.1: Coefficients. Computational cost analysis.....	89
Table 3.2: P.U.L parameters. Example One. ....	91
Table 3.3: Performance of proposed algorithm. Example One. ....	96
Table 3.4: Performance of proposed algorithm. Example Two.....	103
Table 3.5: Performance of proposed algorithm. Example Three.....	115
Table 3.6: Cost and performance. Load: 1pF. Example Four. ....	121
Table 3.7: Cost and performance. Load: 50Ω. Example Four.....	121



## List of Figures

Figure 1.1: A (non-exhaustive) taxonomy of methods for solving IVP's [39].	4
Figure 2.1: Partitioning of system $N$ . (a) Localization of splitting node $X$ . (b) Insertion of a series connection of three resistances $-R_1$ , $R_1 + R_2$ and $-R_2$ at node $X$ . (c) Creation of an overlap partitioning for $N$ into $N_1$ and $N_2$ (d) Resulting two-subsystem partition of $N$ with corresponding Norton interface.	25
Figure 2.2: (a) Cascade connection. (b) Upstream input impedance of $N_l$ at interface $(k, l)$ . (c) Downstream input impedance of $N_l$ at interface $(l, m)$ .	33
Figure 2.3: (a) Branch connection. (b) Input impedance of $N_l$ at interface $(l, m_h)$ .	34
Figure 2.4: Potential locations for partitioning. (a) Series. (b) Branch.	40
Figure 2.5: Circuit of Example One. (a) Original circuit. (b) Partitioned circuit—capacitive load (c) Partitioned circuit—resistive load.	44
Figure 2.6: Magnitude of convergence coefficient $\rho$ . Example One.	44
Figure 2.7: Iteration waveform. (a) Far-end line 1. Example One.	45
Figure 2.8: Iteration waveform. (a) Near-end line 1. Example One.	46
Figure 2.9: Iteration waveform. (a) Far-end line 2. Example One.	47
Figure 2.10: Logarithm of error after seven WR iterations. Example One (b).	48
Figure 2.11: Logarithm of error after seven WR iterations. Example One (c).	49
Figure 2.12: Magnitude of convergence coefficient $\rho$ . Example Two.	50
Figure 2.13: Circuit of Example Three.	51
Figure 2.14: Magnitude of local convergence coefficients $\rho_{k,l}$ . Example Three.	52

Figure 2.15: Maximum values of $r_{k,l}$ vs $\rho_{k,l}$ . Example Three.....	52
Figure 2.16: Iteration waveforms, Node b11. Example Three. ....	53
Figure 2.17: Iteration waveforms. Node a12. Example Three.....	54
Figure 2.18: Iteration waveforms. Node b21. Example Three. ....	55
Figure 2.19: Number of rounds to converge. Sweep on the diagonal. Example Three. ...	56
Figure 2.20: Circuit of Example Four.....	57
Figure 2.21: Local convergence coefficients $\rho_{k,l}$ . Example Four.....	58
Figure 2.22: Iteration waveform. Node A. Example Four.....	59
Figure 2.23: Iteration waveform. Node B. Example Four. ....	60
Figure 2.24: Iteration waveform. Node C. Example Four. ....	61
Figure 2.25: Speedup. Example Four. ....	63
Figure 2.26: $\max r_{k,l}$ vs. $\max \rho_{k,l}$ . (a) 128 points. (b) 164 points. Example Four. ....	64
Figure 2.27: Local convergence coefficients $\rho_{k,l}$ after adding instances (164 points). Example Four.....	65
Figure 2.28: Error evolution. Example Four.....	66
Figure 2.29: Circuit of Example Five. ....	67
Figure 2.30: Iteration waveform. Node A. Example Five. ....	68
Figure 3.1: Parts $N_1$ and $N_2$ are connected directly. ....	70
Figure 3.2: Parts $N_1$ and $N_2$ are connected via a strictly dissipative element $Z_0$ .....	70
Figure 3.3: Dissipative coupling of parts $N_1$ and $N_2$ . Node c is put to Ground.....	71

Figure 3.4: Circuit partitioning. No circuit overlap. ....	74
Figure 3.5: Convergence analysis circuit. ....	79
Figure 3.6: Computation of order $m$ of coarse DEPACT model. ....	86
Figure 3.7: Main steps in the application of the WR-LP algorithm. ....	87
Figure 3.8: Circuit of Example One. ....	91
Figure 3.9: Impedance mismatch for low-loss 7,12. (a) Z-R disposition (b) R-Z disposition. Example One. ....	93
Figure 3.10: Augmented subcircuits $N_1$ and $N_2$ of $N_1$ and $N_2$ . Low-loss 7,12. Arrangement R-Z. Example One. ....	94
Figure 3.11: Sparsity pattern of MNA matrices. Low-loss 7,12. Top: Resistive coupling [97]. Bottom: Proposed R-Z. Example O. ....	95
Figure 3.12: Error decay. Lossy 6,10. Example One. ....	97
Figure 3.13: Error decay. Low-loss 7,12. Example One. ....	98
Figure 3.14: Rate of convergence. Low-loss 7,12. Top: Resistive coupling [97]. Middle: Proposed Z-R. Bottom: ___ R-Z. Example One. ....	99
Figure 3.15: Farend iteration waveform. Low-loss 7,12. (b) Proposed (R-Z). Iteration one. Example One. ....	100
Figure 3.16: Farend iteration waveform. Low-loss 7,12. (a) Resistive coupling [97]. Left: Iteration one. Middle: iteration twenty. Right: Iteration forty. Example One. ....	101
Figure 3.17: Circuit of Example Two. ....	102
Figure 3.18: Sparsity pattern of MNA matrices. Interior odd numbered subcircuit. Left: in arrangement A. Right: in arrangement B. Example Two. ....	103

Figure 3.19: Global error. $T = 30\text{ns}$ . Example Two.....	104
Figure 3.20: Local convergence factors. Resistive coupling based WR [97]. Example Two. ....	104
Figure 3.21: Local convergence factors-II. Proposed, arrangement A. Example Two. ...	105
Figure 3.22: Local convergence factors-I. Proposed, arrangement A. Example Two.....	105
Figure 3.23: Farend. Left: Resistive coupling [97]. Right: Proposed (B). Round 1. Example Two. ....	107
Figure 3.24: Resistive coupling [97]. Right: Proposed (B). Round 2. Example Two. ...	108
Figure 3.25: Farend. Left: Resistive coupling [97]. Right: Proposed (B). Round 10. Example Two. ....	109
Figure 3.26: Farend. Left: Resistive coupling [97]. Right: Proposed (B). Round 17. Example Two. ....	110
Figure 3.27: Circuit of Example Three. ....	112
Figure 3.28: Sparsity pattern of MNA matrix of entire circuit. Example Three. ....	113
Figure 3.29: Sparsity pattern of MNA matrices of subcircuits $L_1$ and $L_6$ . Top: Resistive coupling [97]. Bottom: Proposed. Example Three. ....	113
Figure 3.30: Augmented subcircuit $L_6$ . Example Three. ....	114
Figure 3.31: Iteration waveform. Left: Resistive coupling [97]. Right: Impedance coupling. Round 1. Example Three. ....	116
Figure 3.32: Iteration waveform. Left: Resistive coupling [97]. Right: Impedance coupling. Round 2. Example Three. ....	117
Figure 3.33: Iteration waveform. Left: Resistive coupling [97]. Right: Impedance coupling. Round 4. Example Three. ....	118

Figure 3.34: Global error, simulation time $T = 30\text{ns}$ . Example Three.....	119
Figure 3.35: Speedup: Theoretical vs actual. Example Three. ....	120
Figure 3.36: Error decay. $T = 5000\text{ns}$ . Load $50\Omega$ . Example Four.....	122
Figure 4.1: (I) Cascade connection of $N$ parts $P_n$ , $1 \leq n \leq N$ . (II) Frequency-domain representation of part $P_n$ .....	125
Figure 4.2: Dissipative coupling of the chain. ....	126
Figure 4.3: WR converge analysis circuit. The homogeneous problem. ....	126
Figure 4.4: Resistive coupling of a chain of identical symmetric parts.....	142
Figure 4.5: WR converge analysis circuit. The homogeneous problem. ....	142
Figure 4.6: Norms $\ (J'_N)^2\ _1$ . $N \in 3,5,10,50,100,150,200,250,300$ . Illustrative example. ....	146
Figure 4.7: Spectral norms $\ (J'_N)^2\ _2$ , $N \in 3,5,10,50,100,150,200,250,300$ . Illustrative example. ....	147
Figure 4.8: Spectral radii $\rho((J'_N)^2)$ , $N = 3, 5, 10$ . Illustrative example. ....	147
Figure 4.9: Spectral radii $\rho((J'_N)^2)$ , $N = 50, 100, 150$ . Illustrative example. ....	148
Figure 4.10: Spectral radii $\rho((J'_N)^2)$ , $N = 200, 250, 300$ . Illustrative example. ....	148
Figure 4.11: Frequency-domain representation of decoupled parts. (I) Left end. (II) Right end. Interior (III). ....	152

# Chapter 1

## 1 Introduction

The current chapter takes the reader for a quick overview of the main methods and numerical techniques for the solution of the initial value problem through sections 1.1 to 1.3. Those who are familiar with this topic or decide to skip these introductory sections, can start reading section 1.4 and 1.5. Section 1.4 summarizes the state-of-the art in using waveform relaxation methods for the analysis of transmission line circuits. Section 1.5 describes the contribution of the present work and positions it vis-a-vis published results in the literature.

### 1.1 Initial Value Problem

Many interesting applications can be modeled as an initial value problem (IVP), eg.,

$$\begin{aligned} \mathbf{F}(\mathbf{x}'(t), \mathbf{x}(t), t) &= \mathbf{0} \\ \mathbf{x}(0) &= \mathbf{x}_0 \end{aligned} \tag{1.1}$$

where  $\mathbf{x}(t) \in \mathbb{R}^n$  and  $F: \mathbb{R}^{2n+1} \rightarrow \mathbb{R}^n$ . Here, (1.1) can describe an IVP for an ordinary differential equation (ODE) system or for a differential algebraic equation (DAE) system. It is assumed that function  $\mathbf{F}$  is such that solution  $\mathbf{x}$  exists and is unique on a simulation interval of interest, say,  $t \in [0, T]$ , and that the initial condition is consistent for the DAE case.

In general, an analytic solution to (1.1) cannot be found, so the problem must be solved numerically. With the typical approach, (1.1) is first discretized in time with an integration method. Since DAE and stiff ODE systems require the use of implicit integration schemes, the time discretization will generate a sequence of nonlinear algebraic problems which are solved with an iterative method, usually a modified Newton method. The sequence of linear algebraic systems generated at each iteration of the non-linear solution are then solved with Gaussian elimination. The above process is

the “implicit-integration, Newton, direct method” canon and forms the basis for most general-purpose codes for solving large-scale IVP’s [1].

The standard approach has two computational bottlenecks (which bottleneck will dominate depends on the problem):

*Function evaluation* – computation of  $F(\cdot)$  and the associated Jacobian  $J_F(\cdot)$ . The cost of evaluating  $J_F$  grows with the problem size and with the degree of coupling. For densely coupled problems, evaluating  $J_F$  can be as low as  $O(n)$ .

*Linear system solution* – solving the linear system at each iteration of the nonlinear solution process. The complexity of direct elimination methods for solving systems of equations is polynomial in  $n$ , typically from  $O(n^{1.5})$  for sparse problems to  $O(n^3)$  for dense problems.

When using the standard Newton method, the function evaluation and the linear system solution are performed at each iteration of each nonlinear system at each timestep. However, certain modified Newton methods recalculate the Jacobian only at certain intervals (eg., every third Newton iteration) [2], thereby reducing the work required, although not the complexity, by a constant factor.

Efforts to improve the computational efficiency for numerically solving IVP’s focus on improving the efficiency of the function evaluation and the linear system solution. These efforts fall into two general (overlapping) categories: algorithmic improvement and hardware improvement. For example, one could use an iterative method for the linear system solution or implement the solver on a vector or parallel processing machine. For some problems, such an approach might be highly effective, but for other problems, such an approach might be a disaster. It seems that *general-purpose* codes for solving IVP’s must follow the “implicit-integration, Newton, direct method” canon because such codes are written to be able to reliably handle the largest possible class of problems. However, this formula can be quite limiting for specific problems that can benefit from the application of more specialized algorithms.

## 1.2 A Circuit Simulation Problem

The nodal analysis formulation of the circuit transient simulation problem is described by

$$\frac{d}{dt}q(v(t), t) + i(v(t), t) = 0 \quad (1.2)$$

$$v(0) = v_0$$

where  $v(t)$ ,  $q(v(t), t)$ ,  $i(v(t), t) \in \mathbb{R}^n$  are the vectors of node voltages, sums of node charges, and the sums of node resistive currents, respectively, and  $n$  is the total number of nodes in the circuits.

Numerical techniques for solving (1.2) are very well developed—for all practical purposes, the general circuit simulation problem has been solved [3],[4]. Programs like SPICE [5] and ASTAP [6]—which follow the “implicit-integration, Newton, direct method” approach to solving (1.2) – are capable of simulating virtually any circuit, given enough time. Unfortunately, for some of circuits, “enough time” might be a burden for simulation that leads to longer circuit design cycles.

## 1.3 Review of Numerical Techniques for Initial-Value Problems

There exists a myriad of approaches for solving initial value problems—a non-exhaustive taxonomy is presented in Figure 1.1. To solve the IVP, the system is first decomposed in time (for point-wise solution methods) or space (for waveform methods). The point-wise solution is computed with the application of an integration method, possibly followed by a nonlinear algebraic solution step. The waveform methods treat the nonlinear IVP as a nonlinear problem on a function space.

In this chapter, techniques for solving initial-value problems are reviewed. Although the techniques are applied in top-down fashion (eg., integration, nonlinear solution, linear solution), these techniques are presented in somewhat of a bottom-up order since the “top” algorithms generally build upon the “bottom” algorithms. Figure 1.1 presents a



roadmap that keeps different algorithms in their proper context within the frame of solving IVP's.

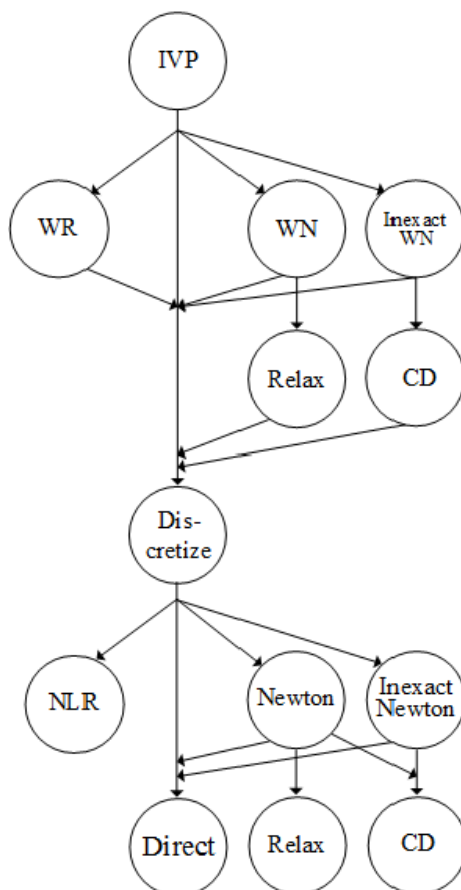


**Figure 1.1:** A (non-exhaustive) taxonomy of methods for solving IVP's [39].

### 1.3.1 Linear Solution Methods

In this section, methods are reviewed for solving the  $n$ -dimensional linear system of equations

$$\mathbf{Ax} = \mathbf{b} \tag{1.3}$$

where  $\mathbf{x}, \mathbf{b} \in \mathbb{R}^n$  and  $\mathbf{A}: \mathbb{R}^n \rightarrow \mathbb{R}^n$  and is assumed to be non-singular.

### 1.3.1.1 Direct Methods

The classical direct method for solving linear systems is Gaussian elimination, typically implemented with LU factorization techniques. This algorithm decomposes the matrix  $A$  into lower and upper triangular factors  $L$  and  $U$ , respectively, such that  $A = LU$ . The solution  $\mathbf{x}$  to (1.3) is computed by a forward elimination process followed by a backward substitution. A discussion of direct methods can be found in most linear algebra or numerical methods texts, see [7],[8] for dense matrix problems and [9],[10] for sparse matrix problems.

The main advantage of direct methods is reliability. With exact arithmetic, the solution  $\mathbf{x}$  can be computed exactly in a fixed number of steps. However, direct methods have two major disadvantages: computational complexity and storage. The complexity of direct elimination methods for solving linear systems of equations is polynomial in  $n$ , typically form  $O(n^{1.5})$  for sparse problems to  $O(n^3)$  for dense problems. For direct methods, the matrix itself must be stored in memory. This might not be particularly disadvantageous for the matrix itself, if the matrix is sparse. However, direct methods also require storage for the fill-in elements, ie. matrix zero locations which become non-zero as the elimination process proceeds. Most iterative methods for solving linear systems only require that the matrix itself be stored, so the fill-in storage, which can be quite substantial, is not needed. Moreover, certain nonlinear solution methods such as the so-called “matrix-free methods” do not require an explicit representation of the matrix at all. Relaxation and conjugate direction iterative methods for linear systems are presented in Sections 1.3.1.2 and 1.3.1.3. Matrix-free methods are discussed in Section 1.3.2.4.

### 1.3.1.2 Relaxation Methods

Linear relaxation methods seek to solve (1.3) by first decomposing the problem in space (i.e., pointwise) and then solving the decomposed problem in an iterative loop. The simplest relaxation method is the Richardson iteration [11],[12] which solves (1.3) by solving the following equation

$$\mathbf{x}^{(k+1)} = \mathbf{x}^{(k)} + \mathbf{b} - A\mathbf{x}^{(k)} \quad (1.4)$$

and the Gauss-Jacobi (GJ) and the Gauss-Seidel (GS) algorithms as

$$\mathbf{D}\mathbf{x}^{(k+1)} = \mathbf{b} - (\mathbf{L} + \mathbf{U})\mathbf{x}^{(k)} \quad (1.5)$$

and

$$(\mathbf{L} + \mathbf{D})\mathbf{x}^{(k+1)} = \mathbf{b} - \mathbf{U}\mathbf{x}^{(k)} \quad (1.6)$$

This shows that that GJ and GS algorithms are in fact the Richardson iteration of the system (1.3) preconditioned with  $\mathbf{D}^{-1}$  and  $(\mathbf{L} + \mathbf{U})^{-1}$  respectively. Matrices  $\mathbf{L}$ ,  $\mathbf{U}$  and  $\mathbf{D}$  are the strictly lower triangular, strictly upper triangular, and diagonal of the matrix  $\mathbf{A}$ .

In general, splitting of  $\mathbf{A}$  can be described by letting  $\mathbf{A} = \mathbf{M} - \mathbf{N}$ , so a generic relaxation method can be written as:

$$\mathbf{x}^{(k+1)} = \mathbf{M}^{-1}\mathbf{N}\mathbf{x}^{(k)} + \mathbf{M}^{-1}\mathbf{b} \quad (1.7)$$

the error equation for the relaxation method is then given by:

$$\mathbf{e}^{(k+1)} = \mathbf{M}^{-1}\mathbf{N}\mathbf{e}^{(k)} = (\mathbf{M}^{-1}\mathbf{N})^{k+1}\mathbf{e}^{(0)} \quad (1.8)$$

Where  $\mathbf{e}^{(k)} = \mathbf{x}^{(k)} - \mathbf{x}^*$  represents the error at the  $k^{th}$  iteration and  $\mathbf{x}^*$  the exact solution of (1.3). The asymptotic convergence rate of linear relaxation is determined by the spectral radius of matrix  $\mathbf{M}^{-1}\mathbf{N}$ . In order to guarantee convergence of the method for arbitrary  $\mathbf{e}^{(0)}$ , the spectral radius of  $\mathbf{M}^{-1}\mathbf{N}$  must be strictly less than unity [12].

### 1.3.1.3 Conjugate Direction Methods

The Richardson iteration produces updates of the form

$$\mathbf{x}^{(k+1)} = \mathbf{x}^{(0)} + q_R^{(k)}(\mathbf{A})\mathbf{r}^{(0)} \quad (1.9)$$

where  $q_R^{(k)}(\mathbf{A})$  is a polynomial of order  $k$  given recursively by

$$q_R^{(k)}(\mathbf{A}) = \mathbf{I} + (\mathbf{I} - \mathbf{A})q_R^{(k-1)}(\mathbf{A}) \quad (1.10)$$

with  $\mathbf{q}_R^{(0)} = \mathbf{I}$  and where  $\mathbf{r}^{(0)} = \mathbf{b} - \mathbf{A}\mathbf{x}^{(0)}$  is the initial residual. Considering the Richardson iteration as a polynomial highlights the weakness of the method; the Richardson iteration always generates the same sequence of polynomials, regardless of the problem to which the method is applied. One implication of this is that, generically, the iteration will not terminate in a finite number of iterations. However, by the Cayley-Hamilton theorem, there exists an  $n^{\text{th}}$  order polynomial which is exactly  $\mathbf{A}^{-1}$ , but in general, the polynomial of order  $n$  generated by the Richardson iteration will not correspond to Cayley-Hamilton polynomial. One way of considering conjugate direction methods is that they are methods which at each iteration, generate an optimal polynomial for calculating  $\mathbf{x}^{(k+1)}$  (optimal in the sense that  $\mathbf{x}^{(k+1)}$  minimizes a pre-defined cost function).

As an example, consider the conjugate gradient (CG) method [13] used to solve (1.3) for the case of symmetric and positive-definite  $\mathbf{A}$ . This method again generates  $\mathbf{x}^{(k+1)}$  with polynomials of  $\mathbf{A}$ :

$$\mathbf{x}^{(k+1)} = \mathbf{x}^{(0)} + \mathbf{q}_{CG}^{(k)}(\mathbf{A})\mathbf{r}^{(0)} \quad (1.11)$$

but does so by seeking to minimize the cost functional

$$\Phi(\mathbf{x}) = \langle \mathbf{x}, \mathbf{b} - \frac{1}{2}\mathbf{A}\mathbf{x} \rangle \quad (1.12)$$

where  $\langle \cdot, \cdot \rangle$  is the standard Euclidean inner product on  $\mathbb{R}^n$ . The relation  $\mathbf{x}^{(k)} = \mathbf{x}^{(0)} + \mathbf{q}_{CG}^{(k-1)}(\mathbf{A})\mathbf{r}^{(0)}$  implies that  $\mathbf{x}^{(k)} \in \mathbf{x}^{(0)} + \mathbb{K}^{(k)}(\mathbf{r}^{(0)}, \mathbf{A})$ , where  $\mathbb{K}^{(k)}(\mathbf{r}^{(0)}, \mathbf{A})$  is the  $k$ -dimensional Krylov space:

$$\mathbb{K}^{(k)}(\mathbf{r}^{(0)}, \mathbf{A}) = \text{span}\{\mathbf{r}^{(0)}, \mathbf{A}\mathbf{r}^{(0)}, \dots, \mathbf{A}^{k-1}\mathbf{r}^{(0)}\} \quad (1.13)$$

The minimization of  $\Phi$  can be accomplished for each iteration  $k$  by enforcing the Galerkin condition that the gradient of  $\Phi$  be zero on  $\mathbb{K}^{(k)}(\mathbf{r}^{(0)}, \mathbf{A})$ , i.e.,

$$\langle \nabla\Phi(\mathbf{x}^{(k)}), \mathbf{y} \rangle = 0 \quad \forall \mathbf{y} \in \mathbb{K}^{(k)}(\mathbf{r}^{(0)}, \mathbf{A}) \quad (1.14)$$

It suffices to enforce the Galerkin condition on any basis of  $\mathbb{K}^{(k)}(\mathbf{r}^{(0)}, \mathbf{A})$  that might be chosen. In particular, by choosing  $\{\mathbf{P}^{(0)}, \dots, \mathbf{P}^{(m)}\}$  as a basis for  $\mathbb{K}^{(m+1)}(\mathbf{r}^{(0)}, \mathbf{A})$ , such that

$$\langle \mathbf{A}\mathbf{P}^{(i)}, \mathbf{P}^{(j)} \rangle = 0, \quad i \neq j \quad (1.15)$$

and using the update

$$\mathbf{x}^{(k+1)} = \mathbf{x}^{(k)} + \frac{\langle \mathbf{r}^{(k)}, \mathbf{p}^{(k)} \rangle}{\langle \mathbf{A}\mathbf{p}^{(k)}, \mathbf{p}^{(k)} \rangle} \mathbf{p}^{(k)} \quad (1.16)$$

The sequence  $(\mathbf{x}^{(k)})_{k \geq 1}$  can be generated iteratively so that  $\mathbf{x}^{(k+1)}$  minimizes  $\Phi$  on  $\mathbb{K}^{(k)}(\mathbf{r}^{(0)}, \mathbf{A})$  for each  $k \in [0, m]$  [14]. Since the amount of work in the CG iteration is in the matrix-vector product, the CG algorithm requires only a modest increase in work per iteration when compared to Richardson-based iteration methods. However, the optimality of the CG algorithm provides a guarantee of finite termination (by Cayley-Hamilton) plus much better convergence properties prior to termination [15]. In fact, the convergence rate of the CG algorithm is bounded by:

$$\|\mathbf{e}^{(k)}\|_A \leq 2 \left( \frac{\sqrt{\kappa(\mathbf{A})} - 1}{\sqrt{\kappa(\mathbf{A})} + 1} \right)^k \|\mathbf{e}^{(0)}\|_A \quad (1.17)$$

where  $\|\mathbf{e}\|_A = \langle \mathbf{A}\mathbf{e}, \mathbf{e} \rangle^{\frac{1}{2}}$  is the  $A$ -norm of  $\mathbf{e}$ , and  $\kappa(\mathbf{A})$  is the condition number of the matrix  $\mathbf{A}$ . In practice, the bounds given in (1.17) are not necessarily sharp, particularly when  $\mathbf{A}$  has clustered eigenvalues.

For non-symmetric matrices, the CG algorithm cannot be directly applied. Krylov space methods which are appropriate for non-symmetric systems include CG applied to the normal equations (CGNR) [13], generalized conjugate residual algorithm (GCR) [16], the generalized minimum residual algorithm (GMRES) [17], and the conjugate gradient squared algorithm (CGS) [18]. These methods are quite powerful and are widely used, but none completely preserves the elegance of the original CG algorithm, see [19] for a

discussion of necessary and sufficient conditions for the existence of a conjugate gradient method.

The CGNR algorithm solves (1.3) for non-symmetric  $\mathbf{A}$  by applying CG to the equivalent symmetric system

$$\mathbf{A}^T \mathbf{A} \mathbf{x} = \mathbf{A}^T \mathbf{b}, \quad (1.18)$$

where the superscript  $T$  denotes the algebraic transposition. However, convergence of CGNR can be drastically slower than convergence of CG, convergence of CG is bounded by (1.17), so convergence of CGNR is bounded by

$$\|\mathbf{e}^{(k)}\|_{\mathbf{A}'\mathbf{A}} \leq 2 \left( \frac{\sqrt{\kappa(\mathbf{A}^t \mathbf{A})} - 1}{\sqrt{\kappa(\mathbf{A}^t \mathbf{A})} + 1} \right)^k \|\mathbf{e}^{(0)}\|_{\mathbf{A}^t \mathbf{A}} = 2 \left( \frac{\kappa(\mathbf{A}) - 1}{\kappa(\mathbf{A}) + 1} \right)^k \|\mathbf{e}^{(0)}\|_{\mathbf{A}^t \mathbf{A}} \quad (1.19)$$

For large  $\kappa(\mathbf{A})$ , the convergence of CG is essentially a function of  $\sqrt{\kappa(\mathbf{A})}$ , whereas convergence of CGNR is essentially a function of  $\kappa(\mathbf{A})$ .

The GCR and GMRES algorithms are theoretically equivalent algorithms which seek to minimize  $\|\mathbf{r}\|^2$  at each iteration. To do this, the basis of the Krylov space must be formed explicitly with an orthogonalization scheme at each iteration so that the work at each iteration grows linearly with the iteration number. The CGS algorithm [18] uses low-order recurrence relation at each iteration and abandons guaranteed minimization properties altogether. This is a theoretical drawback, but in practice, CGS seems to work quite reliably.

### 1.3.2 Nonlinear Solution Methods

In this section, some methods are discussed for solving systems of nonlinear equations

$$\mathbf{F}(\mathbf{x}) = \mathbf{0}, \quad (1.20)$$

where  $\mathbf{x} \in \mathbb{R}^n$  and  $\mathbf{F}: \mathbb{R}^n \rightarrow \mathbb{R}^n$ .

### 1.3.2.1 Newton's Method

The most popular method for solving (1.20) is undoubtedly Newton's method, where the  $n$  –dimensional linear system of equations

$$\mathbf{J}_F(\mathbf{x}^m)\mathbf{x}^{m+1} = \mathbf{J}_F(\mathbf{x}^m)\mathbf{x}^m - \mathbf{F}(\mathbf{x}^m) \quad (1.21)$$

is solved for  $\mathbf{x}^{m+1}$  in an iterative loop. Here,  $\mathbf{J}_F$  is the Jacobian of  $\mathbf{F}$ . Newton's method converges quadratically, provided the initial guess,  $\mathbf{x}^0$ , is sufficiently close to the exact solution [14]. The standard Newton method has some drawbacks. First, a linear system solution is required at each iteration. This can be expensive in terms of computation and storage, especially if a direct factorization method is used. Second, global convergence can be problematic if the initial guess is not close enough to the exact solution. Alternative nonlinear solution methods seek to improve the computation, storage, and /or the convergence properties of the standard Newton method.

### 1.3.2.2 Nonlinear Relaxation

As an alternative to the standard Newton method, (1.20) can be decomposed into smaller sub-problems, each of which is solved independently in an iterative loop, using fixed values from previous iterations for the variables from other sub-problems. Two common decompositions produce the Jacobi-Newton and Seidel-Newton algorithms [14]. These methods can be seen as generalizations of the corresponding linear Gauss-Jacobi and Gauss-Seidel relaxation methods. The Jacobi-Newton algorithm solves (1.20) by solving equations

$$f_i(x_1^m, \dots, x_{i-1}^m, x_i^{m+1}, x_{i+1}^m, \dots, x_n^m) = 0 \quad (1.22)$$

for  $x_i^{m+1}$ , usually with a scalar form of Newton's method. Similarly, the Seidel-Newton algorithm solves (1.20) by solving equations

$$f_i(x_1^{m+1}, \dots, x_{i-1}^{m+1}, x_i^{m+1}, x_{i+1}^m, \dots, x_n^m) = 0 \quad (1.23)$$

for  $x_i^{m+1}$ . The essential difference between Jacobi-Newton and Seidel-Newton is that, when computing  $x_i^{m+1}$  Seidel-Newton uses the values of  $x_j^{m+1}$  for the  $j^{th}$  subsystem if it

has been already computed, otherwise  $x_j^m$  is used. In some sense, Seidel-Newton uses the most recently computed information that is available. The class of nonlinear solution algorithms to which Jacobi-Newton and Seidel-Newton belong are referred to as relaxation-Newton algorithms. Each iteration of a relaxation-Newton method requires solving a scalar nonlinear problem to determine  $x_i^{m+1}$ —usually with a scalar form of Newton’s method. Even if the scalar nonlinear solution is iterated until convergence, the outer loop will generally not converge to  $x$ . This suggests that in the early iterations,  $x_i^{m+1}$  does not need to be determined very precisely. The  $n$ -step relaxation-Newton methods take a predetermined fixed number,  $n$ , of scalar Newton iterations—often as few as one [14].

### 1.3.2.3 Inexact Newton Methods

The class of nonlinear solution methods known as inexact Newton methods are obtained by combining Newton’s method with a linear solution method that only solves the linear system approximately. As in [20], the linear system that is solved with an inexact Newton method can be specified as

$$J_F(\mathbf{x}^m)\Delta\mathbf{x}^m = -F(\mathbf{x}^m) + \mathbf{r}^m$$

$$\mathbf{x}^{m+1} = \mathbf{x}^m + \Delta\mathbf{x}^m \tag{1.24}$$

where  $\mathbf{r}^m$  is the residual and represents the difference between  $J_F(\mathbf{x}^m)\Delta\mathbf{x}^m$  and  $F(\mathbf{x}^m)$ . One common context in which inexact Newton methods arise is when an iterative linear solver is used to solve (1.21). In this case, the linear system is only solved approximately within the convergence criterion of the iteration method. Here, methods combining Newton with linear relaxation are referred to as Newton–relaxation methods, methods combining Newton with conjugate direction method are referred to as Newton-Krylov methods.

A typical Newton-relaxation or Newton-Krylov method uses the ratio of the linear residual  $\mathbf{r}^k$  at iteration  $k$  to the initial linear residual  $\mathbf{r}^0$ . As discussed in [20], choosing a fixed convergence criterion  $\epsilon \in ]0,1[$  for all  $m$  will result in linear convergence of the



nonlinear iteration. However, by scheduling a sequence  $\{\epsilon^0, \epsilon^1, \dots\}$  so that  $\epsilon^m \in ]0, 1[$  for all  $m$  and  $\epsilon^m \rightarrow 0$  as  $m \rightarrow \infty$ , the nonlinear iteration will converge superlinearly.

### 1.3.2.4 Matrix-Free Methods

One modification that can be made to Newton-relaxation or Newton-Krylov methods is to dispense with the explicit formation of the Jacobian. The iterative linear solvers require only the result of a matrix-vector product, not the matrix itself. Since the matrix for the linear system in question is the Jacobian of nonlinear function  $\mathbf{F}$ , an approximate matrix-vector product can be calculated according to

$$J_{\mathbf{F}}(\mathbf{x})\mathbf{p} = \frac{\partial \mathbf{F}(\mathbf{x})}{\partial \mathbf{x}}\mathbf{p} \approx \frac{1}{\sigma}[\mathbf{F}(\mathbf{x} + \sigma\mathbf{p}) - \mathbf{F}(\mathbf{x})] \quad (1.25)$$

where  $\sigma$  is a small scalar parameter. The use of matrix-free Newton-Krylov methods within the context of solving stiff systems of ODE's was first studied by Gear and Saad in [21] and subsequently studied by Brown and Hindmarch [22],[23] and Chan and Jackson [24]. Matrix-free Newton-Krylov methods with global convergence properties are examined in [25]

### 1.3.3 Integration Methods

In conventional time-domain electrical simulation, superior numerical accuracy is commonly looked for through the employment of multistep backward-differentiation-formulas (BDF) techniques (also referred to as Gear's methods) [26]. These methods use past points information to achieve approximation order ranging from 2 to 6. In recent work [27], certain implicit RK methods were shown to be more reliable than BDF in the simulation of important classes of circuits, such as oscillators, filters and strongly nonlinear switching circuits for which accuracy and reliability are key. Despite these results it seems that BDF are still the dominant integration methods adopted by general purpose circuit simulator like SPICE.

Many IVP' admit an explicit representation as

$$\frac{d}{dt}\mathbf{x}(t) = \mathbf{F}(\mathbf{x}(t), t) \quad (1.26)$$

$$\mathbf{x}(0) = \mathbf{x}_0$$

where  $\mathbf{x}(t) \in \mathbb{R}^n$  and  $\mathbf{F} : \mathbb{R}^{n+1} \rightarrow \mathbb{R}^n$ . A  $k$  –linear multistep integration formula applied to solving (1.23) is expressed by:

$$\sum_{i=0}^k \alpha_i \mathbf{x}(\tau_{m+1-i}) = h_m \sum_{i=0}^k \beta_i \mathbf{F}(\mathbf{x}(\tau_{m+1-i}), \tau_{m+1-i}) \quad (1.27)$$

where  $h_m = \tau_{m+1} - \tau_m$  is the discretization timestep,  $\mathbf{x}(\tau_m)$  is the estimated value of the solution at  $t = \tau_m$ ,  $\mathbf{F}(\mathbf{x}(t), t)$  represents the dynamics of the equation at the given timepoint using the estimated value. The parameters  $\alpha_i$  and  $\beta_i$  are chosen for accuracy within stability limits and  $k$  is the order of the formula [26],[28]. For problems such as (1.26), explicit methods, when  $\beta_0 = 0$ , present a significant advantage over implicit counterpart,  $\beta_0 \neq 0$ , because there is no need to perform a nonlinear system solution which results in a substantial reduction in computation as well as storage. Unfortunately, explicit methods work well only for non-stiff problems, ie when system eigenvalues do not differ by orders of magnitude. For stiff problems, most problems in electrical engineering are of stiff nature, explicit methods present stability issues that jeopardize their reliability and implicit methods are a preferred alternative. The stability of implicit methods allows for substantially larger timesteps, resulting in lower overall computational work for the simulation.

It is worth noting that explicit methods lose their advantage when the differential portion of the IVP is itself implicit, eg., the circuit transient simulation problem

$$\frac{d}{dt} \mathbf{q}(\mathbf{v}(t), t) + \mathbf{i}(\mathbf{v}(t), t) = \mathbf{0} \quad (1.28)$$

$$\mathbf{v}(0) = \mathbf{v}_0$$

A linear multistep integration formula applied to solving (1.28) is expressed by

$$\sum_{i=0}^k \alpha_i \mathbf{q}(\mathbf{v}(\tau_{m+1-i})) = h_m \sum_{i=0}^k \beta_i \mathbf{i}(\mathbf{v}(\tau_{m+1-i}), \tau_{m+1-i}) \quad (1.29)$$

This expression is implicit in  $\mathbf{v}(\tau_{m+1})$  even if an explicit integration method is used. A nonlinear step is still required, but the stability inherent to implicit integration methods is not retained. Implicit integration methods are therefore recommended when handling stiff problems

### 1.3.4 Waveform Methods

The discussion in the previous sections concentrated on different methods that could replace the three components of the “implicit-integration, Newton, direct method” approach. Another means of obtaining a computational advantage in solving (1.1) is the adoption of a different level of abstraction, to be more precise extending the already introduced recipes to a new space, a function space. Application of alternative decompositions to the nonlinear and linear system solution steps produces nonlinear and linear relaxation algorithms. If this type of decomposition is applied at the ODE level, waveform methods are obtained. The operator formulation of the IVP can be written as

$$\mathcal{F}\mathbf{x} = \mathbf{0} \quad (1.30)$$

where  $\mathbf{x}$  belongs to some function space and  $\mathcal{F}$  is a nonlinear differential operator, as an example

$$\mathcal{F} = \frac{d}{dt} + \mathbf{F} \quad (1.31)$$

where  $\mathbf{x} \in \mathcal{C}^1(\mathbf{x}_0, [0, T], \mathbb{R}^n)$ ,  $\mathcal{F}: \mathcal{C}^1(\mathbf{x}_0, [0, T], \mathbb{R}^n) \rightarrow \mathcal{C}^1(\mathbf{x}_0, [0, T], \mathbb{R}^n)$  and the function space  $\mathcal{C}^1(\mathbf{x}_0, [0, T], \mathbb{R}^n)$  is defined as

$$\mathcal{C}^1(\mathbf{x}_0, [0, T], \mathbb{R}^n) = \{\mathbf{f} \in \mathcal{C}^1([0, T], \mathbb{R}^n) | \mathbf{f}(0) = \mathbf{x}_0\} \quad (1.32)$$

Given the operator formulation of the IVP in (1.30), abstract forms of the methods described in section 1.3.2 can be applied to yield various nonlinear waveform methods. These methods are reviewed in the following sections.

### 1.3.4.1 Waveform Newton Methods

As indicated by its name, it is an abstracted form of Newton's method applied to (1.30). This method is discussed in [29] and applied to the circuit simulation problem in [30],[31]. The waveform Newton method is expressed as

$$\mathbf{J}_{\mathcal{F}}(\mathbf{x}^m)\Delta\mathbf{x}^m = -\mathcal{F}(\mathbf{x}^m) \quad (1.33)$$

$$\mathbf{x}^{m+1} = \mathbf{x}^m + \Delta\mathbf{x}^m$$

where  $\mathbf{J}_{\mathcal{F}}$  is the Frechet derivative of  $\mathcal{F}$  defined by

$$\mathbf{J}_{\mathcal{F}}\mathbf{x}(t) = \frac{d}{dt}\mathbf{x}(t) + \mathbf{J}_{\mathcal{F}}(\mathbf{x}(t), t) \quad (1.34)$$

Using (1.31) and (1.34), the waveform Newton method can be expressed as

$$\left(\frac{d}{dt} + \mathbf{J}_{\mathcal{F}}(\mathbf{x}^m(t), t)\right)\Delta\mathbf{x}^m = -\frac{d}{dt}\mathbf{x}^m(t) - \mathcal{F}(\mathbf{x}^m(t), t) \quad (1.35)$$

$$\mathbf{x}^{m+1}(0) = \mathbf{x}_0$$

Expression (1.35) yields a linear IVP as follows

$$\left(\frac{d}{dt} + \mathbf{J}_{\mathcal{F}}(\mathbf{x}^m)\right)\mathbf{x}^{m+1} = \mathbf{J}_{\mathcal{F}}(\mathbf{x}^m)\mathbf{x}^m - \mathcal{F}(\mathbf{x}^m) \quad (1.36)$$

$$\mathbf{x}^{m+1}(0) = \mathbf{x}_0$$

This linear IVP can be solved with a variety of methods, as can be seen in Figure 1.1. For instance, the problem can be immediately discretized and a linear solver can be used to solve the resulting sequence of matrix problems or as in [30], this  $n$ -dimensional linear IVP discretized with  $l$  timepoints can be treated as one  $nl \times nl$  problem instead of a

sequence of  $l$  separate  $n \times n$  systems. Alternatively, the linear IVP can be solved iteratively with a linear waveform relaxation method or a conjugate direction waveform method. In this case, the problem is discretized within the main loop. A discussion of the convergence properties of the waveform Newton method can be found in [30].

### 1.3.4.2 Waveform Relaxation Methods

As with the linear and nonlinear relaxation methods, the nonlinear IVP can be decomposed in space and solved iteratively. The Jacobi waveform relaxation algorithm solves (1.1) by solving the scalar IVP's

$$\frac{d}{dt} x_i^{k+1}(t) + f_i(x_1^k(t), \dots, x_{i-1}^k(t), x_i^{k+1}(t), x_{i+1}^k(t), \dots, x_n^k(t), t) = 0 \quad (1.37)$$

$$x_i^{k+1}(0) = x_{i,0}$$

for each  $x_i^{k+1}(t)$  with a scalar integration scheme. The historical basis for the waveform relaxation methods is the Picard–Lindelöf iteration, used to demonstrate existence and uniqueness of solutions to IVP's [31]. Waveform relaxation, or dynamic iteration, has been very successful for simulating VLSI circuits [33][34]. Convergence theory for the linear time-invariant case is studied in [35] for ODE systems and in [36] for DAE systems. It is worth noticing that the convergence study of [35] and [36] has been carried out with the assumption that IVP's are solved exactly in other words the effect of time discretization is ignored, which is of course an idealization since WR is primarily meant to be a numerical method. The study of the convergence of the discretized WR algorithm, viewed as a nonstationary algorithm, was demonstrated in [34]. The implementation of this algorithm for systems in normal form and in the context of linear multistep methods was shown to converge provided the size of the timestep was kept small and linear interpolation was used to exchange information between subsystems [34], the multirate discretized WR algorithm was therefore shown to converge when linear interpolation operator is used, However experiments showed that other types of interpolations also lead to convergence of WR though the convergence theorem was not successfully extended to include other interpolation operators.

### 1.3.4.3 Inexact Waveform Newton Relaxation

One can continue to maintain the analogy between nonlinear solution methods and waveform methods and construct the class of inexact waveform Newton methods. These methods would result from the combination of the waveform Newton method and an iterative linear waveform method. The combination of waveform Newton with a linear waveform method is sometimes known as waveform Newton relaxation (WNR) and is discussed in [37]. The combination of waveform Newton with a linear conjugate direction method is presented in [38] and developed more fully in [39].

### 1.3.4.4 Acceleration of Waveform Relaxation Methods

The convergence rate of standard waveform relaxation can be slow for many problems of interest. As with the relaxation-based approaches for linear algebra, eg. Jacobi, application of appropriate acceleration is necessary to make the waveform approach practical. Such approaches include the shifted Picard iteration [40], multigrid [41],[42], successive overrelaxation (SOR) [41], Chebyshev acceleration [43], convolution SOR [44],  $\mathbb{L}^2$  Krylov subspace methods [39], and adaptive window size selection [45]. Many of these waveform acceleration techniques are analogous to acceleration methods for iteratively solving linear systems of equations. However, in most cases the generalization of these approaches to waveform relaxation does not accelerate convergence to the same degree as their linear algebra counterparts [35]. An analysis of why linear acceleration of waveform relaxation can, in general, be expected to be limited is given in [46]. Two acceleration methods for waveform relaxation that do, in fact, provide the same degree of acceleration as their analogous linear algebra methods are the convolution SOR developed in [44],[47] and convolution Krylov subspace methods developed in [48]. The stated methods for the acceleration of WR, apply on normal form ODEs. Unfortunately, in the context of circuit simulation, modified nodal analysis (MNA) equation formulation does not generally generate ODE systems in the normal form, one exception to this rule is Resistor-and-Grounded-Capacitor (RGC) networks [34].

## 1.4 Waveform Relaxation Analysis of Transmission Line Circuits

Parallel processing techniques based on waveform relaxation (WR) have emerged as valid methods to speed up transient analysis of large systems. An essential part of WR methods [33],[49] consists in splitting or partitioning these structures into smaller subcircuits or subsystems. WR methods iteratively solve each part independently from the others over the entire simulation interval by updating the coupling effects to approach the system response. The advantage of WR resides in the fact that every subsystem can be solved with its largest time step or with a different integration method or even solution method. This way the stiffness of the whole problem is overcome, and cost effectiveness can be reached. The state of the art of WR circuit computing can be found in [50].

Circuit partitioning is performed based on some pertinent properties for maximum efficiency of the WR algorithm. For example, directionality was used to subdivide metal oxide semiconductor (MOS) transistor circuits [51]-[55]. In multi-conductor transmission line (MTL) and fully coupled high-speed channels problems, weak electromagnetic coupling between conductors was exploited to subdivide such structures into individual transmission lines.

Since the pioneering work of F. Chang [56]-[58] on the application of WR to interconnect circuits, WR methods have been extensively used to analyze this class of circuits with essentially two partitioning schemes; transverse and longitudinal [59]-[84]. Transverse partitioning applies exclusively on MTL structures by breaking them down into a collection of single lines through the relaxation of the electromagnetic field coupling between lines [59]-[62]. Longitudinal partitioning (LP) applies on general circuits and divides them along the signal path with node splitting in general [63]-[84]. Waveform relaxation with transverse partitioning is naturally parallelizable for the Gauss-Jacobi iteration (GJ) and is convergent when coupling between lines is weak [61]. Waveform relaxation with longitudinal partitioning (WR-LP) on the other hand is inherently serial and naturally uses a Gauss-Seidel (GS) relaxation. It also produces tightly coupled subsystems for which classical WR generally takes excessive number of

iterations to converge. A situation which becomes aggravated when the number of serial subsystems is large [63]-[84].

In the analysis of VLSI MTL systems, R. Wang and O. Wing [63],[64] presented an overlapped partition for their bi-level WR-LP algorithm. Their objective was to ensure the algorithm always converges and to have control over its speed of convergence. They inserted a neutral series connection of three resistances ( $-R_o$ ),  $2R_o$ , and ( $-R_o$ ),  $R_o > 0$ , between every channel or TL and its terminations. Their intuitive approach was based on a careful study of the conventional WR methods which shows that there are usually overlaps between parts corresponding to the assignment-partition process of waveform relaxation. R. Wang and O. Wing [63],[64] took resistance  $R_o$  equal to the DC characteristic impedance of the interconnect to improve the speed of convergence of WR [63],[64]. Later, W. Beyene [65] used same insertion  $\{-R_o, 2R_o, -R_o\}$  in his WR-LP for the simulation of interconnect-dominated nonlinear networks. S. Grivet-Talocia et al. [66]-[73] set resistance  $R_o$  at the channel's reference impedance to eliminate signal reflections and reduce the number of iterations. Despite the seriality of these WR-LP algorithms, their application to the fully coupled channel with non-linear terminations led to efficient solutions compared to direct methods [63]-[73]. These WR methods essentially focused on drastically reducing the cost of the GS iteration. First, they target fully coupled systems in order to take advantage of the high complexity of the corresponding dense problems, Second, they all divide the whole system into two levels; a step which reduces the seriality of GS iteration to a minimum. Third, they replace the standard SPICE transmission line macromodels and SPICE transistor models by tailored delay rational macromodels and behavioral models [66]-[73] and pole residue models with FFT/IFFT [65]. Unlike SPICE, such tailored analysis methods scale well with the number of coupled links. These sophisticated methods cannot be used in sparse circuit problems like single TL circuits where coupling between lines is ignored. In this case, an efficient WR-LP method must focus primarily on lowering the number of iterations to converge.



Before we move on to describe another class of waveform relaxation methods, we conclude with the following two important points regarding resistive coupling in WR methods

- First, resistive coupling provides a simple way yet general to decompose transmission line circuits, it allows to keep the distributive nature of lines and hence works for any time-domain line macromodel. The speed of the WR method however depends on the values of its coupling resistances. M. Kabir and C. Christoffersen [82],[83] expressed the need for a way that systematically computes the best values for the reference resistances, or relaxation resistances that will yield the fastest speed of convergence. A problem which was not addressed in all the WR-LP algorithms discussed so far.
- Second, V. Loggia, S. Grivet-Talocia and H. Hu [70] confirmed a well-known experimental observation; resistive coupling works well for lossy problems with small to moderate reactive behavior but is slow to converge and even diverges when the losses start to decrease and when the circuit exhibits a high reactance. An inefficiency which restricts the use of this general coupling scheme.

To improve WR convergence, different overlap-type circuit techniques were proposed and summarized in [53]. Other techniques introduced additional circuit elements to suppress local feedback and enhance convergence [85],[86]. The quest to reduce the number of WR iterations effectively started in the PDE research community where F. Nataf, F. Rogier and E. de Sturler [87] were first to derive optimal interface conditions for domain decomposition methods. Later. M. Gander, L. Halpern, and F. Nataf [88]-[91] presented different versions for these optimal conditions in their work on overlapping and non-overlapping Schwarz waveform relaxation for time dependent problems. It was M. Gander, M. Al Khaleel, and A. Ruehli [74]-[79] who brought the idea of optimal WR convergence to circuit problems. Their work led to the emergence of a class of WR methods which involved an optimization step and hence was called optimized WR (oWR). These methods are suitable for strongly coupled serial circuits. Gander et al. [74]-[79] showed that faster and more uniform convergence can be reached while keeping the partitioning effort simple if an appropriate combination of current and

voltage waveforms are exchanged between subcircuits instead of just a current or a voltage, as in classical WR. The exchange of these combinations is implemented in the so-called transmission conditions (TC) equations of the waveform relaxation algorithm. Gander et al. [75],[84] showed that optimal convergence for general circuits uses nonlocal operators in the TC equations and therefore is expensive. To bypass this obstacle, they calculated constant and first degree polynomial approximations of the optimal conditions specifically for RC ladder circuit [75],[80],[81], for one lumped RLCG line type circuit [74],[76]-[78], and for the PEEC circuit [79]. We conclude our brief overview of optimized WR methods with the following important observations.

- The derivation of low-order approximations in [74]-[81] relies on extensive analysis and it applies to very similar/identical parts, a requirement difficult to fulfill in general. The approach concerns circuits for which the derivation of a closed form formula of the convergence factor with respect to complex frequency is feasible. This approach however becomes challenging when high-order approximations are sought. It leads to more complicated expressions of the convergence factors even for simple circuits like RC ladder RLCG line circuits or more general RGC circuits.
- Even for simple circuits like RC and RLCG ladders, the adoption of rational and rational-with-delay approximations of the optimal convergence conditions requires the use of nonlocal operators in the TC equations. This would jeopardize the cost efficiency of the oWR methods when they are applied to these circuits.
- The analysis used for RC and RLCG circuits cannot be applied to general TL circuits like MTLs, TL trees, interconnect dominated networks or high-speed channels where lines must keep their distributive nature and are usually represented by delay-extraction macromodels. In addition, the granularity of the partitioning used in these methods [74]-[78],[80],[81] will lead to a very large number of subcircuits whose solution requires implementation of WR algorithms with complex ordering and scheduling mechanisms.

## 1.5 Contribution of the present research thesis

In Chapter 2, the aim is to address the problem of determining the best coupling resistances that will yield the fastest speed of convergence for the WR method. First, we allow every two relaxation resistances to take different values at the interface between any two adjacent subcircuits. This will prove more efficient to decouple subcircuits with different input impedances. Every insertion  $\{-R_o, 2R_o, -R_o\}$ ,  $R_o > 0$  is replaced with  $\{-R_1, R_1 + R_2, -R_2\}$ ,  $R_1, R_2 > 0$ . For a given circuit partition, we state that the fastest possible global speed convergence is approached when all local convergence factors have low values, precisely less than one, over the frequency interval of interest and are uniform. This is the same experimental condition which Gander et al. [74]-[79] observed in their analysis of RC and RLCG circuits. Fast convergence is cast as a generic min-max optimization problem which is solved in the suboptimal sense. The reason is that the optimization problem cannot be solved directly as explained in Chapter 2. However, the steps that lead to this suboptimal solution are well defined, which allows to automate the solution algorithm to handle any TL architecture. To assess the efficiency of the min-max solution, a parallel WR algorithm with basic scheduling [53] is implemented. Simulation results confirm that: 1) Faster local convergence is generally observed when coupling resistances take different values especially for neighboring sub-systems with different input impedances, 2) The WR solution of arborescent TL circuits (trees) results in CPU run time savings when compared to SPICE-like solvers. It is important to keep in mind that transmission lines are represented in the time-domain with the same standard macromodeling algorithms implemented on SPICE and SPICE-like simulators.

In Chapter 3, the aim is to address the slow convergence/divergence of resistive coupling-based WR algorithm for low-loss and highly reactive transmission line circuits. We consider a more general coupling scheme; we replace coupling resistances with strictly dissipative impedances. Every insertion  $\{-R_1, R_1 + R_2, -R_2\}$ ,  $R_1, R_2 > 0$ , is replaced by a neutral series connection of three impedances  $\{-\zeta_1, \zeta_\Sigma, -\zeta_2\}$ . Coupling impedances  $\zeta_1$  and  $\zeta_2$  are strictly positive-real complex functions of complex frequency  $s$ ,  $\Re(s) \geq 0$ , and  $\zeta_\Sigma$  represents the created circuit overlap. We demonstrate the relevance of the proposed generalization, and we address its feasibility. We assert the consistency

of the subsequent WR algorithm. We also examine its convergence for any linear time invariant system, and we define the conditions for optimal convergence. Finally, we propose a coupling strategy for the WR analysis of single TL circuits. Every two adjacent subcircuits in the decomposed TL circuit, are decoupled with customized rational-with-delay impedance and resistance. Every rational-with-delay impedance approximates the input impedance of its corresponding subcircuit or part to approach the local optimal convergence condition. The approximation step avoids the expensive optimization and uses a coarse DEFACT [102] macromodeling of the transmission line to build the rational-with-delay function directly in circuit form. Numerical examples confirm that dissipative coupling further enhances the speed of convergence of the WR. It addresses the weakness of resistive coupling and produces a fast WR solution for low-loss highly reactive TL circuits.

The focus in chapters 2 and 3 is on system interfacing schemes that enhance the speed of convergence of WR and decrease its computational cost. The solution of the resulting subcircuits uses conventional stepping methods and standard transmission line macromodels.

Chapter 4 presents two theoretical studies about the application of WR to chains of circuits. The first analysis concerns the nilpotent WR algorithm when its partition-assignment step uses strictly dissipative impedance coupling. The second analysis concerns the convergence of WR when its partition-assignment step uses resistive coupling. In the first study, we show that a nilpotent WR operator must have null local convergence factors. However, the way these local factors are zeroed affects the degree of nilpotency of the WR operator and can even destroy it. The second study demonstrates the global convergence of the resistive coupling based WR when the cascaded circuits in the chain are symmetric and identical. We show that WR converges independently of the chain length.

## Chapter 2

### 2 Resistive Coupling-based Waveform Relaxation Algorithm for Analysis of Interconnect Circuits

A parallel waveform relaxation algorithm is presented for efficient transient analysis of large distributed interconnect networks. The proposed algorithm partitions interconnect circuits using a Norton interface derived from positive and negative resistors. A theoretical framework is provided to study the convergence properties of the proposed algorithm. From this discussion, a procedure emerges for an effective selection of the relaxation resistances' values. Numerical examples illustrate the parallelizability and good scaling of the proposed method with respect to the size of the network and the number of central processing units.

#### 2.1 Proposed WR Algorithm

##### 2.1.1 Development of partitioning interface

Consider a linear time-invariant system  $N$  with the following property; there exists a node  $X$  in  $N$  where it can be divided into two disjoint subsystems  $N_1$  and  $N_2$  with no feedback loop (Figure 2.1(a)). A series combination of three resistances  $-R_1$ ,  $(R_1 + R_2)$  and  $-R_2$ ,  $R_1, R_2 > 0$ , is inserted at node  $X$ . Since these resistances add up to zero, their presence does not change the solution of system  $N$  (Fig. 2.1(b)). Resistance  $(R_1 + R_2)$  is used to create an overlap partitioning of system  $N$  into two parts where each one contains subsystem  $N_1$  or  $N_2$  (Fig. 2.1(c)). Neighboring subsystems  $N_1$  or  $N_2$  are decoupled via a Norton interface (Fig. 2.1(d)) similar to the one used in [79]. Transient responses of system  $N$  on an interval  $[0, T]$ ,  $T$  refers to the duration of analysis, are obtained through the application of a classical WR algorithm on the two-subsystem partition of  $N$ . Subsystems  $N_1$  and  $N_2$  are solved separately on  $[0, T]$  and WR iterations are carried out using a GJ or GS relaxation with the following transmission conditions (TC) [79].

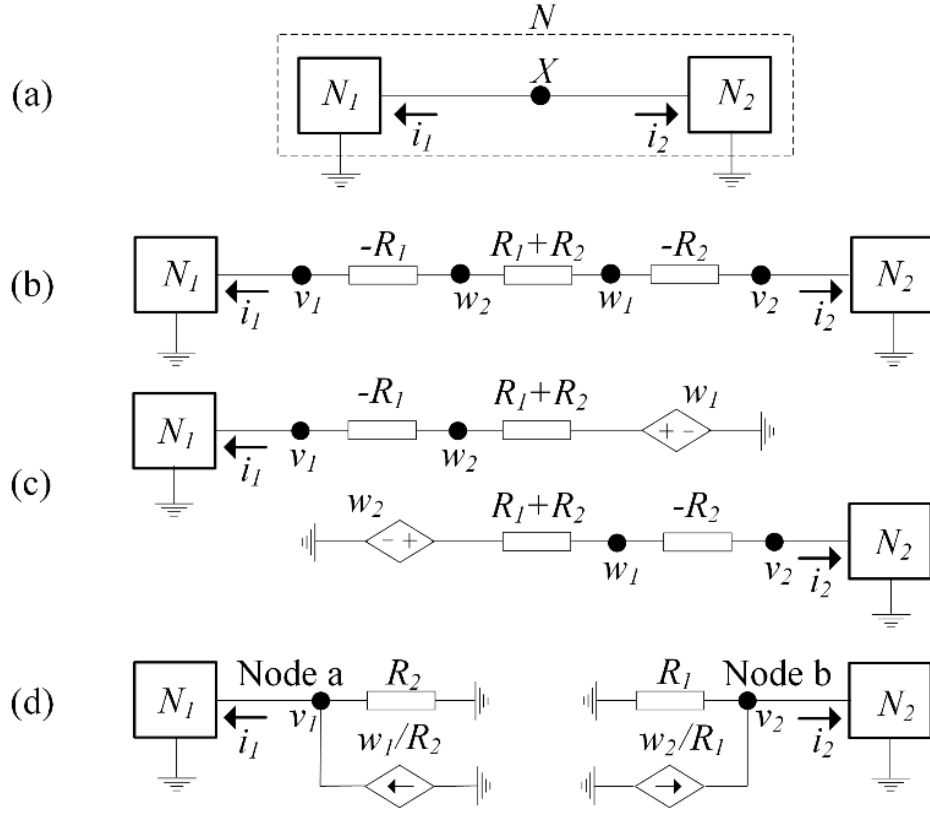


**Figure 2.1: Partitioning of system  $N$ . (a) Localization of splitting node  $X$ . (b) Insertion of a series connection of three resistances  $-R_1$ ,  $(R_1 + R_2)$  and  $-R_2$  at node  $X$ . (c) Creation of an overlap partitioning for  $N$  into  $N_1$  and  $N_2$  (d) Resulting two-subsystem partition of  $N$  with corresponding Norton interface.**

$$i_1(t)^{(k)} = -i_2(t)^{(k-1)} \text{ and } i_2(t)^{(k)} = -i_1(t)^{(k-\delta)} \quad (2.1)$$

$t \in [0, T]$ ,  $k$  represents the iteration count, and  $\delta$  is a parameter which takes value 1 for GJ relaxation and value 0 for the GS case. A more convenient way to perform WR iterations is through successive updates of the current sources  $w_1/R_2$  and  $w_2/R_1$  at the Norton interface between  $N_1$  and  $N_2$  (Figure 2.1(d)). An equivalent form of TC (2.1) is obtained if currents  $i_2^{(k-1)}$ ,  $i_1^{(k)}$ ,  $i_1^{(k-\delta)}$  and  $i_2^{(k)}$  are replaced with their expressions given in

$$\begin{aligned}
i_2^{(k-1)} &= (w_2^{(k-1)} - v_2^{(k-1)})/R_1, \\
i_1^{(k)} &= (w_1^{(k)} - w_2^{(k-1)})/(R_1 + R_2), \\
i_1^{(k-\delta)} &= (w_1^{(k-\delta)} - v_1^{(k-\delta)})/R_2, \\
i_2^{(k)} &= (w_2^{(k)} - w_1^{(k-\delta)})/(R_1 + R_2)
\end{aligned} \tag{2.2}$$

Equations (2.2) are directly derived from Figure 2.1©. The following equivalent TC is adopted

$$\begin{aligned}
w_1^{(k)} &= v_2^{(k-1)}(1 + R_2/R_1) - w_2^{(k-1)}(R_2/R_1) \\
w_2^{(k)} &= v_1^{(k-\delta)}(1 + R_1/R_2) - w_1^{(k-\delta)}(R_1/R_2)
\end{aligned} \tag{2.3}$$

Tables 2.1 and 2.2 present the main steps in the application of WR algorithm on the two-subsystem partition of  $N$ , see Figure 2.1(d), with a GJ then a GS relaxation. The proposed Norton interface in Figure 2.1(d) can be used to partition a system into multiple subsystems. It suffices to identify all pairs of non-overlapping subsystems that are in an open loop serial connection. The next section discusses local convergence properties of the proposed WR algorithm.

**Table 2.1: Pseudocode. WR algorithm for a two-subsystem partition. GJ relaxation**

- 
1. Generate initial guess  $w_1^{(0)}$  and  $w_2^{(0)}$
  2. Set iteration count  $k = 0$
  3. Set maximum tolerance  $\varepsilon$
  4. **Repeat**
  5. Solve  $N_1$  using  $w_1^{(k)}$  and get  $v_1^{(k)}$
  6. Solve  $N_2$  using  $w_2^{(k)}$  and get  $v_2^{(k)}$
  7. Compute  $w_1^{(k+1)}$  and  $w_2^{(k+1)}$  using TC (3)
  8. Compute error
  9. Set  $k = k + 1$

10. **Until** error  $\leq \varepsilon$

---

**Table 2.2: Pseudocode. WR algorithm for a two-subsystem partition. GS relaxation**

---

1. Generate initial guess  $w_1^{(0)}$
  2. Set iteration count  $k = 0$
  3. Set maximum tolerance  $\varepsilon$
  4. **Repeat**
  5. Solve  $N_1$  using  $w_1^{(k)}$  and get  $v_1^{(k)}$
  6. Compute  $w_2^{(k)}$  using TC (3)
  7. Solve  $N_2$  using  $w_2^{(k)}$  and get  $v_2^{(k)}$
  8. Compute  $w_1^{(k+1)}$  using TC (3)
  9. Compute error
  10. Set  $k = k + 1$
  11. **Until** error  $\leq \varepsilon$
- 

### 2.1.2 Local convergence analysis of WR algorithm

The application of Kirchhoff's current law at nodes a and b, see Figure 2.1(d), results in the following two equations

$$w_1/R_2 = v_1/R_2 + i_1, \quad w_2/R_1 = v_2/R_1 + i_2 \quad (2.4)$$

In the Laplace domain, linear subsystems  $N_1$  and  $N_2$  are replaced with their Thevenin generators  $(V_{N_1}(s), Z_1(s))$  and  $(V_{N_2}(s), Z_2(s))$ .  $V_{N_1}$  and  $V_{N_2}$  are the Thevenin source terms while  $Z_1$  and  $Z_2$  represent the Thevenin impedances, they are also the input impedances of  $N_1$  and  $N_2$  seen at node  $X$  in Figure 2.1(a).  $s = \sigma + j\omega$  denotes the complex frequency and  $j^2 = -1$ . Let  $\hat{v}_1$ ,  $\hat{v}_2$ ,  $\hat{w}_1$ ,  $\hat{w}_2$ ,  $\hat{i}_1$ , and  $\hat{i}_2$  be the Laplace transform variables of  $v_1$ ,  $v_2$ ,  $w_1$ ,  $w_2$ ,  $i_1$  and  $i_2$  respectively. Replacing  $\hat{i}_1 = (V_{N_1} - \hat{v}_1)/Z_1$  and  $\hat{i}_2 = (V_{N_2} - \hat{v}_2)/Z_2$  in (2.4) results in



$$\hat{w}_1 = \hat{v}_1(1 + R_2/Z_1) - V_{N_1}(1 + R_2/Z_1) \quad (2.5)$$

$$\hat{w}_2 = \hat{v}_2(1 + R_1/Z_2) - V_{N_2}(1 + R_1/Z_2) \quad (2.6)$$

To study the convergence of WR algorithm, the source terms  $V_{N_1}$  and  $V_{N_2}$  in (2.5) and (2.6) are set to zero. This amounts to considering only the homogenous ordinary differential equation systems of  $N_1$  and  $N_2$  obtained from the modified nodal analysis equation formulation in the time domain. Taking the  $k$ -iterates of  $\hat{w}_1$  and  $\hat{w}_2$  in (2.5) and (2.6) after setting  $V_{N_1} = V_{N_2} = 0$ , and replacing  $\hat{v}_1^{(k)}$  and  $\hat{v}_2^{(k)}$  by their expressions from TC equations (2.3) results in the following two recursive expressions for the relaxation variables

$$\hat{w}_1^{(k)} = \hat{w}_2^{(k-1)}(Z_2 - R_2)/(Z_2 + R_1) \quad (2.7)$$

$$\hat{w}_2^{(k)} = \hat{w}_1^{(k-\delta)}(Z_1 - R_1)/(Z_1 + R_2) \quad (2.8)$$

A relation for  $\hat{w}_1^{(k)}$  and  $\hat{w}_2^{(k)}$  over two WR iterations in the GJ relaxation, and over one WR iteration in the GS case, is obtained

$$[\hat{w}_1 \hat{w}_2]^{(k+1)} = \rho[\hat{w}_1 \hat{w}_2]^{(k-\delta)} \quad (2.9)$$

where  $\rho$  is the WR local convergence rate at the interface between  $N_1$  and  $N_2$ , defined as

$$\rho = [(Z_1 - R_1)(Z_2 - R_2)]/[(Z_1 + R_2)(Z_2 + R_1)] \quad (2.10)$$

By induction, it is found that  $[\hat{w}_1 \hat{w}_2]^{(2k)} = \rho^k[\hat{w}_1 \hat{w}_2]^{(0)}$  and  $[\hat{w}_1 \hat{w}_2]^{(2k+1)} = \rho^k[\hat{w}_1 \hat{w}_2]^{(1)}$  for the GJ relaxation, and  $[\hat{w}_1 \hat{w}_2]^{(k)} = \rho^k[\hat{w}_1 \hat{w}_2]^{(0)}$  for the GS case. Convergence occurs when  $|\rho(Z_1, Z_2, R_1, R_2)| < 1$  for  $\Re(s) > 0$ , and for fast convergence, the magnitude of  $\rho$  must be much smaller than one,  $|\rho(Z_1, Z_2, R_1, R_2)| \ll 1$ .

In partitions of  $M$  subsystems,  $M > 2$ , let  $I$  refer to the set of all Norton interfaces  $(l, m)$  between subsystems  $N_l$  and  $N_m$ ,  $l, m \in [1, M]$ . Every interface  $(l, m)$  consists of two current sources  $(w_l^{l,m}/R_m^{l,m}, R_m^{l,m})$  and  $(w_m^{l,m}/R_l^{l,m}, R_l^{l,m})$  connected to  $N_l$  and  $N_m$

respectively.  $w_l^{l,m}$  and  $w_m^{l,m}$  are the relaxation variables of WR algorithm while  $R_l^{l,m}$  and  $R_m^{l,m}$  represent the relaxation or decoupling resistances. At every interface  $(l, m)$ , WR uses same TCs as in the two-subsystem partition. If the electromagnetic coupling between TLs is weak and can be neglected, then local convergence rate  $\rho_{l,m}$  of WR algorithm at interface  $(l, m)$  is defined as

$$\rho_{l,m} = \frac{(Z_l^{l,m} - R_l^{l,m})(Z_m^{l,m} - R_m^{l,m})}{(Z_l^{l,m} + R_m^{l,m})(Z_m^{l,m} + R_l^{l,m})} \quad (2.11)$$

$Z_l^{l,m}$  and  $Z_m^{l,m}$  are the input impedances of  $N_l$  and  $N_m$  respectively. A general form of the recursive equation (2.9), applicable to a  $M$ -subsystem partition, is produced

$$\widehat{\mathbf{w}}^{(k+1)} = \mathbf{P}\widehat{\mathbf{w}}^{(k-\delta)} \quad (2.12)$$

where vector  $\widehat{\mathbf{w}} = [\widehat{w}_1^{1,2} \widehat{w}_2^{1,2} \dots \widehat{w}_l^{l,m} \widehat{w}_m^{l,m} \dots]^T \in \mathbb{C}^{2\text{card}(I) \times 1}$  contains all relaxation variables of WR for the partition, and  $\mathbf{P} = \text{diag}(\rho_{1,2}, \rho_{1,2}, \dots, \rho_{l,m}, \rho_{l,m}, \dots) \in \mathbb{C}^{2\text{card}(I) \times 2\text{card}(I)}$  is a diagonal matrix with local convergence coefficients at its diagonal entries,  $\text{card}(I)$  is the number of interfaces present in the partition, and  $T$  refers to the non-conjugate transpose operator. WR algorithm applied on a  $M$ -subsystem partition, converges if the corresponding matrix  $\mathbf{P}$  is convergent whenever  $s \in \mathbb{C}$  and  $\Re(s) \geq 0$ .

Next, an efficient method to calculate the decoupling resistances at each interface is presented, first in the elementary case of two subsystems then for the more general case of  $M$  subsystems.

### 2.1.3 Two-subsystem problem

To achieve fast convergence, classical WR algorithm uses two adjustable parameters; the decoupling resistances  $R_1$  and  $R_2$ , to make its local convergence rate  $|\rho|$  in (2.10) small and uniform with respect to frequency. Such values for  $R_1$  and  $R_2$  represent the solution to the following optimization problem

$$\min_{R_1, R_2 > 0} \left( \max_{\Re(s) \geq 0} |\rho(Z_1(s), Z_2(s), R_1, R_2)| \right) \quad (2.13)$$

Impedances  $Z_1(s)$  and  $Z_2(s)$  are positive real functions of complex frequency  $s$ ,  $\Re(s) \geq 0$ . Subsystems  $N_1$  and  $N_2$  are passive when Thevenin sources  $V_{N_1}$  and  $V_{N_2}$  are set to zero. A property which prevents  $\rho$  from having any poles in the right half-plane and makes it analytic.  $|\rho|$  possesses a maximum on the boundary at  $\sigma = 0$  by the maximum principle for analytic functions [92].  $|\rho(j\omega)|$  is also an even function of angular frequency  $\omega$ . With these arguments, the optimization problem (13) simplifies to

$$\min_{R_1, R_2 > 0} \left( \max_{0 \leq \omega \leq \omega_{\max}} |\rho(Z_1(j\omega), Z_2(j\omega), R_1, R_2)| \right) \quad (2.14)$$

where  $\omega$  is truncated at the largest practically relevant frequency value  $\omega_{\max}$  for the problem. In this work,  $\omega_{\max}$  is equal to the bandwidth of the primary input signal.  $\omega_{\max}$  can be made input-independent if  $\omega$  is truncated at a much higher value taken at the maximum frequency supported by the time discretization [74]-[80].

A direct solution of (2.14) is problem dependent and presents the following difficulties; an analytical solution necessitates an in-depth study of the variation of function  $|\rho|$ . A task which becomes quickly tedious and impractical especially for partitions of more than two subsystems. On the other hand, a numerical solution of (2.14) requires a priori knowledge of the frequency points where  $|\rho|$  is large, and therefore needs insight into the variation of  $|\rho|$ . *A practical approach for automating the numerical solution of (2.14) would be to provide optimization instances without having to study the variations of the objective function  $|\rho|$ . This approach leads to a suboptimal solution of (2.14).*

In this work, the proposed suboptimal solution is obtained by solving a nearby min-max problem to (2.14). The new objective function; the magnitude of a function  $r$  which will be defined next, has the following characteristics:  $r$  takes all values of  $\rho$  on any interval  $[0, \omega_{\max}]$ ,  $\max|r| \geq \max|\rho|$ , and most importantly function  $r$  possesses a priori known maxima. The values of input impedances  $Z_1$  and  $Z_2$  at these a priori known extremum points are used as instances for the replacing optimization problem of (2.14).

Let  $\Gamma_1$  and  $\Gamma_2$  be the sets of values of impedances  $Z_1$  and  $Z_2$  for all points  $\omega$  in  $[0, \omega_{\max}]$ . Sets  $\Gamma_1$  and  $\Gamma_2$  are bounded in  $\mathbb{C}$  for lossy circuits. In other words, frequency points  $\omega_1^{\min}$ ,  $\omega_1^{\max}$ ,  $\omega_2^{\min}$ , and  $\omega_2^{\max}$  are found in  $[0, \omega_{\max}]$  where  $|Z_1(j\omega_1^{\min})| \leq |Z_1| \leq$

$|Z_1(j\omega_1^{\max})|$  and  $|Z_2(j\omega_2^{\min})| \leq |Z_2| \leq |Z_2(j\omega_2^{\max})|$ . The extremum values are referred to as  $Z_1(j\omega_1^{\min}) = Z_1^{\min}$  and  $Z_1(j\omega_1^{\max}) = Z_1^{\max}$  for impedance  $Z_1$ . Same thing holds for  $Z_2$ . If impedances  $Z_1$  and  $Z_2$  are allowed to take their values in  $\Gamma_1$  and  $\Gamma_2$  independently of each other, then a larger set  $D$  of points  $(Z_1, Z_2)$  is constructed. The following function  $r$  is defined on set  $D$  by  $r(Z_1, Z_2) = \rho(Z_1, Z_2)$ . Function  $r$  is the analytic continuation of  $\rho$  on  $D$ . It has a maximum amplitude  $\max|r| \geq \max|\rho|$ , and its maximum is on the boundary of  $D$  by the maximum modulus principle on bounded domains [92]. It can be shown that the maximum is on  $\Re(Z_1) = \Re(Z_2) = 0$  at  $(Z_1^{\max}, Z_2^{\min})$  when  $R_1 < R_2$  and on  $\Re(Z_1) = \Re(Z_2) = 0$  at  $(Z_1^{\min}, Z_2^{\max})$  when  $R_1 > R_2$ . Finally,  $|r|$  reaches a maximum amplitude of  $|r| = 1$  on all points of  $D$  where  $\Re(Z_1) = \Re(Z_2) = 0$  for  $R_1 = R_2$ . Based on these observations, a suboptimal solution of problem (2.14) is proposed by solving the following min-max problem

$$\min_{R_1, R_2 > 0} \left( \max_{(Z_1, Z_2) \in P} |r(Z_1, Z_2, R_1, R_2)| \right) \quad (2.15)$$

The objective function  $|r|$  is evaluated at the following set  $P$  of four points

$$\{(Z_1^{\max}, Z_2^{\min}), (Z_1^{\min}, Z_2^{\max}), (Z_1^{\max}, Z_2^{\max}), (Z_1^{\min}, Z_2^{\min})\} \quad (2.16)$$

where  $Z_1^{\max}$ ,  $Z_1^{\min}$ ,  $Z_2^{\max}$  and  $Z_2^{\min}$  are taken with the smallest real part. The replacing optimization problem (2.15) aims to minimize  $\max|r|$  by balancing its values on set  $P$ . This ensures that  $\max|\rho|$  stays within the same range of values as  $\max|r|$ . The computation of instances (2.16) will be addressed in 2.1.5. Section 2.1.4 extends the present result to multi-subsystem partitions.

#### 2.1.4 Multi-subsystem problem

To achieve fast convergence for circuit partitions of  $M$  subsystems, the WR algorithm uses its  $2\text{card}(I)$  adjustable parameters; all pairs  $(R_l^{l,m}, R_m^{l,m})$  of decoupling resistances, to make all its local convergence rates  $|\rho_{l,m}|$  in (2.11) small and fairly uniform with respect to frequency. This requirement is formulated in the following min-max problem

$$\min_{\mathbf{R} > \mathbf{0}} \left( \max_{\substack{\Re(s) \geq 0 \\ (l,m) \in I}} \text{all } |\rho_{l,m}(Z_l^{l,m}(s, \mathbf{R}), Z_m^{l,m}(s, \mathbf{R}), \mathbf{R})| \right) \quad (2.17)$$

where  $\mathbf{R} = [R_1^{1,2} R_2^{1,2} \dots R_l^{l,m} R_m^{l,m} \dots]^{tr} \in (\mathbb{R}^+)^{2\text{card}(I) \times 1}$  is the vector of all decoupling resistances in the partition. As in the case of two-subsystem partitions, the positive definiteness of all input impedances  $Z_l^{l,m}$  and  $Z_m^{l,m}$ , and the analyticity of all  $\rho_{l,m}$  restrict the optimization of coefficients  $|\rho_{l,m}|$  to a bounded frequency interval. Problem (2.17) reduces to

$$\min_{\mathbf{R} > \mathbf{0}} \left( \max_{\substack{0 \leq \omega \leq \omega_{\max} \\ (l,m) \in I}} \text{all } |\rho_{l,m}(Z_l^{l,m}(j\omega, \mathbf{R}), Z_m^{l,m}(j\omega, \mathbf{R}), \mathbf{R})| \right) \quad (2.18)$$

The multi-subsystem problem is a collection of interdependent two-subsystem problems. At every interface  $(l, m)$ , input impedance  $Z_l^{l,m}$  or  $Z_m^{l,m}$  or both depend on the decoupling resistances from other interfaces involving subsystems  $N_l$  or  $N_m$ . The result obtained for the two-subsystem case generalizes naturally to the multi-subsystem problem. Despite this fact, it cannot be used to reach a suboptimal solution to problem (2.18) since it is not possible to obtain set P (2.16) for all interfaces. In a multi-subsystem partition, any two neighboring subsystems  $N_l$  and  $N_m$  are either part of a chain connection (Figure 2.2) or a branch (Figure 2.3). In a chain,  $N_l$  possesses two input impedances—upstream and downstream. Same thing holds for  $N_m$  if neither  $N_l$  nor  $N_m$  are located at any extremity of the partition. The downstream impedance of  $N_l$  is expressed by

$$Z_l^{l,m} = (Z_{11}Z_{22} - Z_{12}^2 + Z_{22}R_{\text{series}})/(Z_{11} + R_{\text{series}}) \quad (2.19)$$

in terms of the Z-parameter triplet  $(Z_{11}, Z_{12}, Z_{22})_l$  of  $N_l$  where  $\Re(Z_{11}), \Re(Z_{22}) > 0$ , and a series relaxation resistance  $R_{\text{series}}$  connected to  $N_l$  on its upstream side, see Figure 2.2(c).

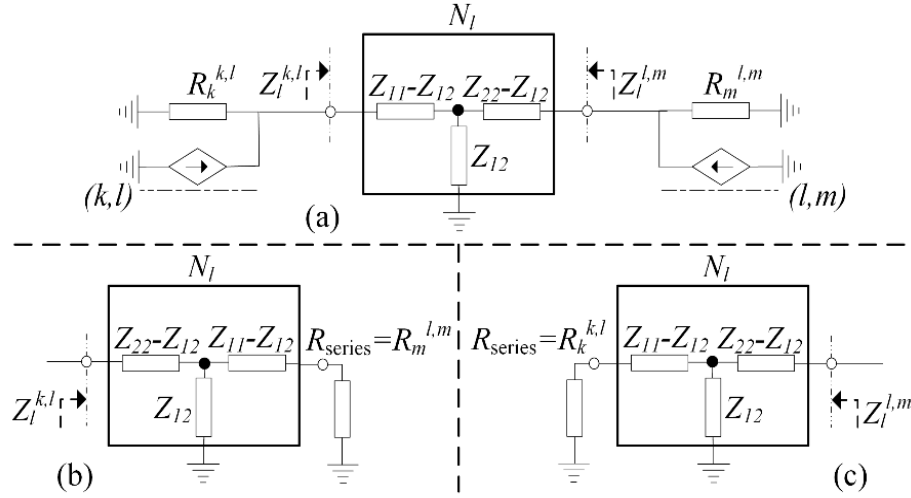


**Figure 2.2: (a) Cascade connection. (b) Upstream input impedance of  $N_l$  at interface  $(k, l)$ . (c) Downstream input impedance of  $N_l$  at interface  $(l, m)$ .**

Similarly, the upstream impedance of  $N_l$  is expressed using (2.19) after permuting  $Z_{11}$  and  $Z_{22}$  and letting  $R_{series}$  represent the series relaxation resistance connected to  $N_l$ , this time on its downstream side (Figure 2.2(b)). Same approach leads to defining the upstream impedance  $Z_m^{l,m}$  of  $N_m$  as well as its downstream one. Now, if the neighboring subsystems  $N_l$  and  $N_m$  are involved in a branch, impedance  $Z_l^{l,m}$  is not given by (2.19) alone. This is due to the presence of a shunt resistance  $R_{shunt}$  which lumps all the relaxation resistances from other branch connections present on the downstream side of  $N_l$  and involving  $N_l$  with subsystems other than  $N_m$  in Figure 2.3(a). In this case, impedance  $Z_l^{l,m}$  of  $N_l$  at interface  $(l, m)$  is the parallel combination of its downstream input impedance from the chain connection configuration, given by (2.19), and resistance  $R_{shunt}$ , see Figure 2.3(b). Same considerations apply to the upstream impedance of  $N_m$ .

The following two key observations are made. First, distributed circuits have input impedances whose values vary considerably with respect to frequency in general, ranging from small values, in the sense of the amplitude, to very large values. This is due mainly to the dominant reactive nature of interconnects. Quantitatively speaking, the presence of a series decoupling resistance  $R_{series}$  at one side of a subsystem clamps the minimum

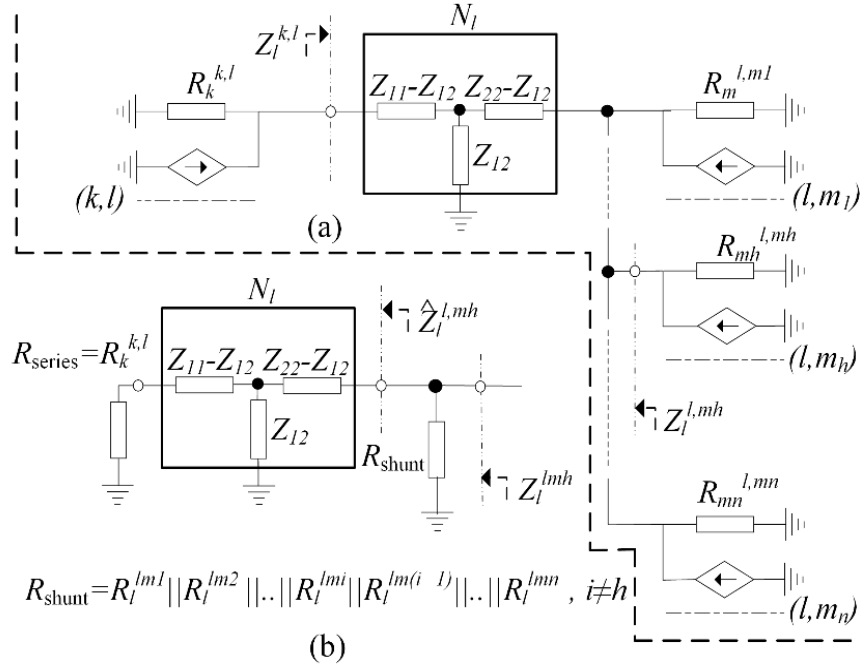


**Figure 2.3: (a) Branch connection. (b) Input impedance of  $N_l$  at interface  $(l, m_h)$ .**

value of its input impedance seen from the other side. The maximum value of this later is also clipped if a shunt decoupling resistance  $R_{\text{shunt}}$  is present. Second, local convergence rate  $|\rho_{l,m}|$ , attains large values when ratios  $\Re(Z_l^{l,m})/|Z_l^{l,m}|$  and  $\Re(Z_m^{l,m})/|Z_m^{l,m}|$  are small positive numbers. It is worth noticing that the proposed set P (2.16) satisfies these algebraic conditions. Based on these observations, the criterion for selecting the points of set P can be relaxed. Instead of targeting points where the input impedances are extremum, the new optimization instances produce sufficiently small and sufficiently large impedances with small real parts for the chain connection configuration. The new optimization instances are totally expressed in terms of  $Z$ -parameters of  $N_l$  and  $N_m$  if both subsystems have unknown impedances or partially if only one of them does. As in section 2.1.3, the number of these instances at every interface is constant, independently of the problem.

Let  $\Gamma_{11}$ ,  $\Gamma_{12}$  and  $\Gamma_{22}$  be the sets of values of  $Z$ -parameters  $Z_{11}(j\omega)$ ,  $Z_{12}(j\omega)$  and  $Z_{22}(j\omega)$  of subsystem  $N_l$  for all points  $\omega$  in  $[0, \omega_{\text{max}}]$  respectively. For lossy circuits,  $\Gamma_{11}$ ,

$\Gamma_{12}$  and  $\Gamma_{22}$  are bounded in  $\mathbb{C}$ . In other words, frequency points  $\omega_{11}^{\min}$ ,  $\omega_{11}^{\max}$  are found in  $[0, \omega_{\max}]$  where  $|Z_{11}(j\omega_{11}^{\min})| \leq |Z_{11}| \leq |Z_{11}(j\omega_{11}^{\max})|$ . The extremum values are referred to as  $Z_{11}(j\omega_{11}^{\min}) = Z_{11}^{\min}$  and  $Z_{11}(j\omega_{11}^{\max}) = Z_{11}^{\max}$  for  $Z_{11}$ . Same thing holds for  $Z_{12}$  and  $Z_{22}$ . If  $Z$ -parameters  $Z_{11}$ ,  $Z_{12}$  and  $Z_{22}$  are allowed to take their values in  $\Gamma_{11}$ ,  $\Gamma_{12}$  and  $\Gamma_{22}$  independently of each other, then a larger set  $D'$  of points  $(Z_{11}, Z_{12}, Z_{22})$  is constructed. The following function  $\tilde{Z}_i^{l,m}$  is defined on set  $D'$  by  $\hat{Z}_i^{l,m}(Z_{11}, Z_{12}, Z_{22}) = Z_i^{l,m}(Z_{11}, Z_{12}, Z_{22})$ , given in (19).  $\hat{Z}_i^{l,m}$  is analytic on  $D'$ , it takes all values of impedance  $Z_i^{l,m}$ . Moreover,  $Z_i^{l,m}$  takes the same set of values on the boundary  $\partial D'$  of  $D'$  as in the whole set  $D'$  [93]. With this property,  $|\hat{Z}_i^{l,m}|$  and  $\Re(\hat{Z}_i^{l,m})$  are investigated on the boundary  $\partial D'$  only. Numerical experiments show that points  $(Z_{11}^{\max}, Z_{12}^{\max}, Z_{22}^{\max})$  and  $(Z_{11}^{\min}, Z_{12}^{\min}, Z_{22}^{\min})$  lead in general to small and large values of  $|\hat{Z}_i^{l,m}|$  with small values for ratio  $\Re(\hat{Z}_i^{l,m})/|\hat{Z}_i^{l,m}|$ .

As in the case of a two-subsystem partition, a suboptimal solution to (2.18) is proposed by solving a nearby optimization problem. The new objective function is constructed as follows: At every interface  $(l, m)$  between subsystems  $N_l$  and  $N_m$ , a function  $\tilde{r}_{l,m}$  is defined by  $\tilde{r}_{l,m}(\tilde{Z}_l^{l,m}, \tilde{Z}_m^{l,m}) = \rho(\tilde{Z}_l^{l,m}, \tilde{Z}_m^{l,m})$  where  $\tilde{Z}_i^{l,m}$  is given as

Case1:  $\tilde{Z}_i^{l,m}(Z_{11}, Z_{12}, Z_{22}) = Z_i^{l,m}(Z_{11}, Z_{12}, Z_{22})$  with  $Z$ -parameters  $Z_{11}$ ,  $Z_{12}$ , and  $Z_{22}$  of  $N_m$  taken as independent variables if  $Z_i^{l,m}$  depends on the decoupling resistances from the neighboring interfaces.

Case2:  $\tilde{Z}_i^{l,m} = Z_i^{l,m}$  if input impedance  $Z_i^{l,m}$  does not depend on any decoupling resistance, and therefore its numerical value is known a priori.

Same arguments apply to  $\tilde{Z}_m^{l,m}$  considering  $Z_m^{l,m}$ . Given these considerations, any function  $\tilde{r}_{l,m}$  takes all values of coefficient  $\rho_{l,m}$ , its maximum value satisfies the inequality  $\max|\tilde{r}_{l,m}| \geq \max|\rho_{l,m}|$ , and  $\tilde{r}_{l,m}$  is the analytic continuation of  $\rho_{l,m}$ . The suboptimal solution to (2.18) is obtained by solving the following nearby problem.

$$\min_{\mathbf{R} > \mathbf{0}} \left( \max_{\substack{(x,y) \in \mathbb{P}^{l,m} \text{ or } \mathbb{Q}^{l,m} \\ (k,l) \in I}} |\tilde{r}_{l,m}(\tilde{Z}_l^{l,m}(x, \mathbf{R}), \tilde{Z}_m^{l,m}(y, \mathbf{R}), \mathbf{R})| \right) \quad (2.20)$$



$P^{l,m}$  and  $Q^{l,m}$  represent the sets of instances at every interface  $(l, m)$ . They are given by

$$\begin{aligned}
P^{l,m} = & \left\{ \left( (Z_{l(\text{or } m)}^{l,m})^{\max}, (Z_{11}^{\max}, Z_{12}^{\max}, Z_{22}^{\max})_{m(\text{or } l)} \right), \right. \\
& \left( (Z_{l(\text{or } m)}^{l,m})^{\max}, (Z_{11}^{\min}, Z_{12}^{\min}, Z_{22}^{\min})_{m(\text{or } l)} \right), \\
& \left( (Z_{l(\text{or } m)}^{l,m})^{\min}, (Z_{11}^{\max}, Z_{12}^{\max}, Z_{22}^{\max})_{m(\text{or } l)} \right), \\
& \left. \left( (Z_{l(\text{or } m)}^{l,m})^{\min}, (Z_{11}^{\min}, Z_{12}^{\min}, Z_{22}^{\min})_{m(\text{or } l)} \right) \right\} \quad (2.21)
\end{aligned}$$

when subsystem  $N_l(\text{or } N_m)$  has a known input impedance and

$$\begin{aligned}
Q^{l,m} = & \left\{ \left( (Z_{11}^{\max}, Z_{12}^{\max}, Z_{22}^{\max})_l, (Z_{11}^{\max}, Z_{12}^{\max}, Z_{22}^{\max})_m \right), \right. \\
& \left( (Z_{11}^{\max}, Z_{12}^{\max}, Z_{22}^{\max})_l, (Z_{11}^{\min}, Z_{12}^{\min}, Z_{22}^{\min})_m \right), \\
& \left( (Z_{11}^{\min}, Z_{12}^{\min}, Z_{22}^{\min})_l, (Z_{11}^{\max}, Z_{12}^{\max}, Z_{22}^{\max})_m \right), \\
& \left. \left( (Z_{11}^{\min}, Z_{12}^{\min}, Z_{22}^{\min})_l, (Z_{11}^{\min}, Z_{12}^{\min}, Z_{22}^{\min})_m \right) \right\} \quad (2.22)
\end{aligned}$$

when both subsystems have unknown input impedances. The minimization of all  $\max|\tilde{r}_{l,m}|$  on points (2.21),(2.22) by balancing these values on the entire partition, aims to maintain all  $\max|\rho_{l,m}|$  within the same range of all  $\max|\tilde{r}_{l,m}|$ .

### 2.1.5 Construction of the optimization problem

Coefficient  $|\rho_{k,l}|$  at interface  $(k, l)$  is given by

$$|\rho_{k,l}|^2 = \frac{|Z_k^{k,l}|^2 - 2\Re(Z_k^{k,l})R_k^{k,l} + (R_k^{k,l})^2}{|Z_k^{k,l}|^2 + 2\Re(Z_k^{k,l})R_k^{k,l} + (R_k^{k,l})^2} \frac{|Z_l^{k,l}|^2 - 2\Re(Z_l^{k,l})R_l^{k,l} + (R_l^{k,l})^2}{|Z_l^{k,l}|^2 + 2\Re(Z_l^{k,l})R_l^{k,l} + (R_l^{k,l})^2} \quad (2.23)$$

The objective function  $|\tilde{r}_{k,l}|$  can be constructed with an automated procedure implemented with Matlab [105] or any other scripting language. Real part and magnitude

of  $\tilde{Z}_k^{k,l}$  and  $\tilde{Z}_l^{k,l}$  are calculated in terms of the  $Z$ -parameters of subsystems  $N_k$  and  $N_l$  and the neighboring relaxation resistances. This dependency is defined here for two configurations; chain and branch connections.

### 2.1.5.1 Chain connection

The cascade connection of three subsystems  $N_k$ ,  $N_l$ , and  $N_m$  and is presented in Figure 2.2(a).  $Z_l^{k,l}$  and  $Z_l^{l,m}$  are input impedances of  $N_l$  at interfaces  $(k, l)$  and  $(l, m)$ . Real part and magnitude of the upstream input impedance  $Z_l^{k,l}$ , see Figure 2.2(b), are given by

$$2\Re(Z_l^{k,l}) = \frac{a_0 + a_1 R_{\text{series}} + a_2 R_{\text{series}}^2}{c_0 + c_1 R_{\text{series}} + R_{\text{series}}^2}$$

$$|Z_l^{k,l}|^2 = \frac{b_0 + b_1 R_{\text{series}} + b_2 R_{\text{series}}^2}{c_0 + c_1 R_{\text{series}} + R_{\text{series}}^2} \quad (2.24)$$

Coefficients  $a_0$ ,  $a_1$ ,  $a_2$ ,  $b_0$ ,  $b_1$ ,  $b_2$ ,  $c_0$ , and  $c_1$  for the upstream case, are expressed in terms of  $(Z_{11}, Z_{12}, Z_{22})$  as

$$a_0 = 2|Z_{22}|^2 \Re(Z_{11}) - 2\Re(Z_{12}^2 \overline{Z_{22}})$$

$$a_1 = 4\Re(Z_{11})\Re(Z_{22}) - 2\Re(Z_{12}^2)$$

$$a_2 = 2\Re(Z_{11})$$

$$b_0 = |Z_{11}Z_{22} - Z_{12}^2|^2$$

$$b_1 = 2\Re((Z_{11}Z_{22} - Z_{12}^2)\overline{Z_{11}})$$

$$b_2 = |Z_{11}|^2$$

$$c_0 = |Z_{22}|^2$$

$$c_1 = 2\Re(Z_{22}) \quad (2.25)$$

and  $R_{\text{series}} = R_m^{l,m}$ . Real part and magnitude of the downstream input impedance  $Z_l^{l,m}$ , see Figure 2.2(c) are also computed using (2.24) after permuting  $Z_{11}$  and  $Z_{22}$  in equations (2.25) and letting  $R_{\text{series}} = R_k^{k,l}$  in (2.24).

### 2.1.5.2 Branch

In Figure 2.3(a), subsystem  $N_l$  branches to  $n$  subsystems  $N_{m_1}, N_{m_2}, \dots, N_{m_n}$ . Input impedance  $Z_l^{l,m_h}$  of  $N_l$  at  $(l, m_h)$ ,  $h \in [1, n]$ , is the parallel combination of  $\hat{Z}_l^{l,m_h}$  (2.19) with resistance  $R_{\text{shunt}}$ . This later is the parallel combination of all decoupling resistances  $R_{m_i}^{l,m_i}$ ,  $i \in [1, n]$  and  $i \neq h$ , see Figure. 2.3. Real part and magnitude of  $\hat{Z}_l^{l,m_h}$  are determined using relations (2.24),(2.25) after permuting  $Z_{11}$  and  $Z_{22}$  in (2.25) and taking  $R_{\text{series}} = R_k^{k,l}$  in (2.24). Next, real part and magnitude of  $Z_l^{l,m_h}$  are calculated using

$$2\Re(Z_l^{l,m_h}) = \frac{2e_1 R_{\text{shunt}} + e_2 R_{\text{shunt}}^2}{e_1 + e_2 R_{\text{shunt}} + R_{\text{shunt}}^2}$$

$$|Z_l^{l,m_h}|^2 = \frac{e_1 R_{\text{shunt}}^2}{e_1 + e_2 R_{\text{shunt}} + R_{\text{shunt}}^2} \quad (2.26)$$

where  $e_1 = |\hat{Z}_l^{l,m_h}|^2$  and  $e_2 = 2\Re(\hat{Z}_l^{l,m_h})$ . Real part and magnitude of  $Z_l^{k,l}$  in Figure 2.3(a) are computed using (2.24),(2.25) with  $R_{\text{series}}$  equal to the parallel combination of all resistances from the branch in (2.24).

The objective function  $|\tilde{r}_{k,l}|$  is constructed at every interface  $(k, l)$  between two adjacent subnetworks  $N_k$  and  $N_l$ . It generates a four by one vector. Table 2.3 summarizes the steps needed to construct the companion objective function of a partition.

### 2.1.5.3 Optimization instances

Every subsystem  $N_k$  is analyzed in the frequency domain. The stamp, a  $Y$  –parameters  $2 \times 2$  matrix, of single transmission lines in the TEM mode are used in the formulation of the modified nodal analysis equations [94]. The resulting system is solved in SPICE on a set of discrete frequency points on the interval  $[0, \omega_{\text{max}}]$ . In example 1 of section 2.3, it is shown that instances (2.16) and (2.21),(2.22) do not need to be precisely calculated since they do not significantly affect the optimization results if key frequencies are spotted.

**Table 2.3: Formulation of the objective function.**


---

**Input:-** Adjacency matrix for  $M$  –subsystem partition of  $N$ .

- Max and min. amplitude input impedances or max and min. amplitude  $Z$ -parameters of subnetworks.

**Output:** Source file of  $|\tilde{r}(\mathbf{R})|$

---

1. **Procedure** objective\_function\_generator
  2. **If**  $M = 2$  **Then**
  3.     Construct  $|r_{1,2}|$  on set P (2.16)
  4. **Else**
  5.     **For** every interface  $(k, l)$  **Do**
  6.         **If**  $N_k$  **or**  $N_l$  is of known input impedance **Then**
  7.             Construct  $|\tilde{r}_{k,l}|$  on set  $P^{k,l}$  (2.21)
  8.             **Else**
  9.             Construct  $|\tilde{r}_{k,l}|$  on set  $Q^{k,l}$  (2.22)
  10.         **EndIf**
  11.     **EndFor**
  12. **EndIf**
  13.     Return (source file of  $|\tilde{r}(\mathbf{R})|$ )
  14. **EndProcedure.**
- 

*Remarks*

- 1) Careful examination of subsystems can give an idea on the location of key frequencies and help reduce the number of points. For example, in interconnect dominated circuits with capacitive loads, the input impedance values of maximum and minimum amplitude occur at DC and at high frequencies, respectively. A small number of frequency points is sufficient to capture these values.
- 2) The applicability of WR is subject to satisfying the convergence conditions ( $|\rho_{k,l}| < 1$ ), which can be verified by frequency sampling between 0 and  $\omega_{\max}$ , once the decoupling resistance are calculated. Numerical experiments showed that

for lossy TL circuits, the optimization leads to very low values for all coefficients  $|\tilde{r}_{k,l}|$ , and the larger values of all  $|\rho_{k,l}|$  will remain low ( $|\rho_{k,l}| \ll 1$ ).

- 3) As the losses in the circuits decrease, coefficients  $|\rho_{k,l}|$  approaches one and the proposed method requires increased number of iterations to converge. It is important to note that all resistive decoupling based WR methods are inefficient for highly reactive low loss circuits [70].

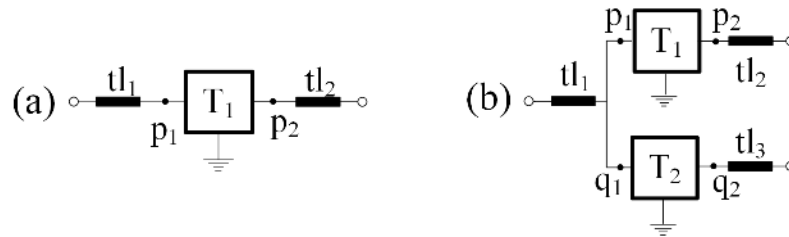


**Figure 2.4: Potential locations for partitioning. (a) Series. (b) Branch.**

### 2.1.6 LP-WR

For cascaded chain and tree circuits composed of two-conductor transmission lines and lumped circuit elements, every TL is treated as an indivisible part and is allocated to only one subcircuit. The number of subcircuits is equal to the number of TLs in the circuit. Every subcircuit can be solved independently with its own largest time step generally determined by its distributed part. Figure 2.4(a) shows two transmission lines  $tl_1$  and  $tl_2$  connected in series, a Norton interface can be inserted at points  $p_1$ ,  $p_2$  or any internal node of lumped circuit  $T_1$ . In the case of a branch connection of three TLs  $tl_1$ ,  $tl_2$  and  $tl_3$ , see Figure 2.4(b), two Norton interfaces are inserted. First one decouples  $tl_1$  and  $tl_2$  at points  $p_1$ ,  $p_2$  or any internal node of lumped circuit  $T_1$  and second one decouples  $tl_1$  and  $tl_3$  at  $q_1$ ,  $q_2$  or any internal node of  $T_2$ .

Logic signal flow [53] is used to order subcircuits for transient analysis by grouping them into enumerated levels. Level 1 groups all subcircuits that are directly connected to sources. The set of their adjacent subcircuits forms level 2 and so on until all subcircuits

are grouped. Subcircuits of same level are not adjacent and are solved concurrently on a parallel machine. A basic schedule [53] is used for the application of WR. Levels are scheduled for analysis alternatively in the forward and backward directions. Starting with level one for the direct sweep and level with the highest index for the backward sweep. The iterative process continues until all relative errors fall below a set tolerance  $\varepsilon$ . Global error at round  $n$ —one round corresponds to one forward sweep followed by one backward sweep, or at iteration  $n$  (the two—subsystem case), is computed by

$$\text{error} = \max_{\substack{(k,l) \in I \\ m \in \{k,l\}}} \left( \frac{\| (w_m^{k,l})^{(n)} - (w_m^{k,l})^{(n-1)} \|_2}{\| (w_m^{k,l})^{(n)} \|_2} \right) \quad (2.27)$$

Table 2.4 summarizes the main steps of the proposed parallel GS WR algorithm

**Table 2.4: Summary of steps for the proposed parallel GS-WR algorithm.**

- 
- Step 1:** 1) Partition circuit into enumerated sub—circuits.  
2) Group these subcircuits into levels.  
3) Define  $\varepsilon$  =the tolerance error for the convergence of waveform relaxation iterations.
- Step 2:** Set all relaxation sources  $w(t)$  to zero DC.
- Step 3:** Set the number of rounds  $r = 1$
- Step 4:** Set the queue of work tasks to be executed, ordering levels in forward and backward directions.
- Step 5:** **FOR** every level **DO** the following in parallel using  $p$  processors  
1) Simulate all current subcircuits for the entire time interval of interest.  
2) Update all upstream (downstream) relaxation sources  $w(t)$  using (2.3) in the forward (backward) direction.
- Step 6:** At the end of every round, compute error using (2.27)
- Step 7:** **IF** error  $\leq \varepsilon$ , exit **ELSE GO TO** step 4
-

### 2.1.6.1 Computational cost analysis

To simplify the analysis, the system is partitioned into  $M$  balanced subcircuits that are grouped in  $m$  levels, where  $m < M$ . Balanced subcircuits exhibit the same computational cost for time-domain analysis. The cost of solving the original circuit is  $\phi_o = O(\beta^\alpha M^\alpha)$ , where  $\beta$  denotes the size of one subcircuit and  $\alpha$  typically varies from 1.1 to 2.4 depending on the sparsity of circuit matrices [95]. Let  $n_1, n_2, \dots, n_m$  denote the numbers of subcircuits present in levels 1, 2, ...,  $m$  respectively,  $n_1 + n_2 + \dots + n_m = M$ . Typically, the number of subcircuits increases as the level index gets higher due to branching (Figure 2.3(b)). WR algorithm is run on a  $p$ -processor machine, it takes  $r$  rounds to converge. If overhead due to memory latencies, waveform interpolations and relaxation variables updates is ignored; last point is justified since the cost of updating one relaxation source uses a first order polynomial expression, see (2.3), plus one waveform interpolation. The computational cost  $\phi_{WR}$  of waveform relaxation is approximated by

$$\phi_{WR} = r \left( \lceil n_1/p \rceil + 2 \sum_{k=2}^{k=m-1} \lceil n_k/p \rceil + \lceil n_m/p \rceil \right) O(\beta^\alpha) \quad (2.28)$$

where  $\lceil \cdot \rceil$  is the ceiling operator. To get an idea of the CPU time efficiency of WR algorithm, cost ratio  $\phi_o/\phi_{WR}$  is considered. It is given by

$$O(M^\alpha) / \left( r \left( \lceil n_1/p \rceil + 2 \sum_{k=2}^{k=m-1} \lceil n_k/p \rceil + \lceil n_m/p \rceil \right) \right) \quad (2.29)$$

WR performance (2.29) depends on the size of the problem, the number of subsystems, the adjacency pattern (the distribution of subcircuits among levels), the number of rounds, and the number of processors. Ideally, the cost of solving a  $M$ -subsystem partition with  $m$  levels can be brought down to  $2r(m-1)O(\beta^\alpha)$  with a number of processors  $p = \max(n_k)$ ,  $k \in [1, m]$ . In other words, the cost  $\phi_{WR}$  cannot be less than that of  $m$  serial subcircuits. The efficiency limit value is  $O(M^\alpha)/2r(m-1)$ . In practice however the number of subcircuits  $n_k > p$  for some levels  $k$ ,  $k \in [1, m]$ . In regular

partitions where the numbers of subcircuits per level  $n_1, n_2, \dots, n_m$  are multiple of same number except may be the early levels, WR has a CPU performance of  $(p/r)O(M^{\alpha-1})$  when the number of processors is a perfect divisor of all numbers  $n_1, n_2, \dots, n_m$  with the exception of those less than  $p$ . In such cases there is no CPU idling within levels for all levels  $k$  where  $n_k > p$ . For non-regular partitions, WR performance is diminished due to idling and a more aggressive scheduling is needed.

## 2.2 Numerical Examples

Five examples are presented to validate the accuracy and efficiency of the proposed WR method. Examples one and two treat the two–subsystem case. The pertinence of solution (2.15) is demonstrated and its sensitivity with respect to the number of frequency points used to capture instances (2.16) is examined. Next, the multi–subsystem case is treated in examples three, four and five. Starting with a chain connection in example three where the pertinence of solution (2.20) is again demonstrated. Examples four and five apply LP-WR to TL tree structures. This class of circuits leads to partitions with multiple subcircuits per level. Performance and scalability of WR with respect to the number of CPUs and the size of the partition are presented. The objective function’s source file is generated and solved in MATLAB [105].

A custom circuit simulator is implemented in MATLAB on a dual quad-core Xeon-Phi 2630 (1.6Ghz) machine with 64GB RAM. In all examples, maximum truncation frequency  $\omega_{\max}$  corresponds to the inverse rise/fall time of the input signal [104]. TLs are macromodeled using DEPACT algorithm [102] to preserve passivity in the time domain. GS-WR iterative analysis is started with all relaxations sources set to a zero DC waveform. Convergence is obtained within a maximum tolerance  $\varepsilon \leq 10^{-3}$ , see eq. (2.27). HSPICE [106] simulation results are provided to illustrate the correctness of WR results.

### 2.2.1 Example One-Proof of concept

The effect of the proposed solution on local convergence rate is examined for the simple circuit of Figure 2.5(a) The per-unit-length parameters (PUL)–Line1(Line2):  $R = 69(217)\Omega/m$ ,  $L = 278(293)nH/m$ ,  $C = 159(151)pF/m$ ,  $G = 18.00(18.00)nS/m$  and



length = 1.0(6.0)cm. The input signal is a 1V trapezoidal voltage pulse with 0.05ns rise/fall time and 2.10ns pulse width. The circuit is split into two parts at node P (Figure 2.5(b)).

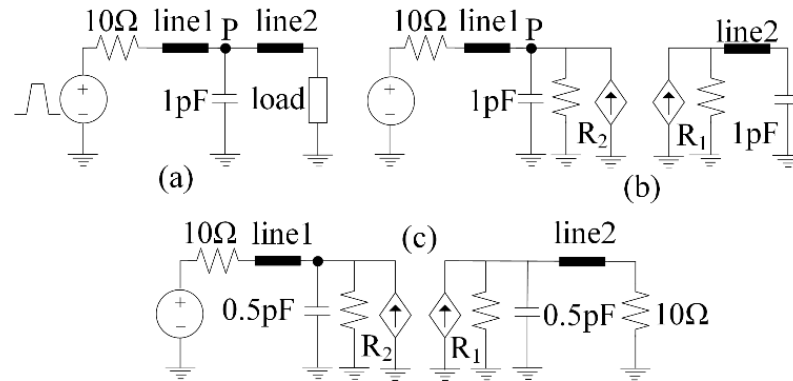


**Figure 2.5: Circuit of Example One. (a) Original circuit. (b) Partitioned circuit—capacitive load (c) Partitioned circuit—resistive load.**

Input impedances of the two subnetworks are evaluated on 1024 equidistant frequency points on  $[0,20\text{GHz}]$ . Solving (15) yields  $R_1 = 28.74\Omega$  and  $R_2 = 41.73\Omega$ . It is found that  $\max|r| \cong 0.573$  at the four instances, while  $\max|\rho| \cong 0.687$  (Figure 2.6).

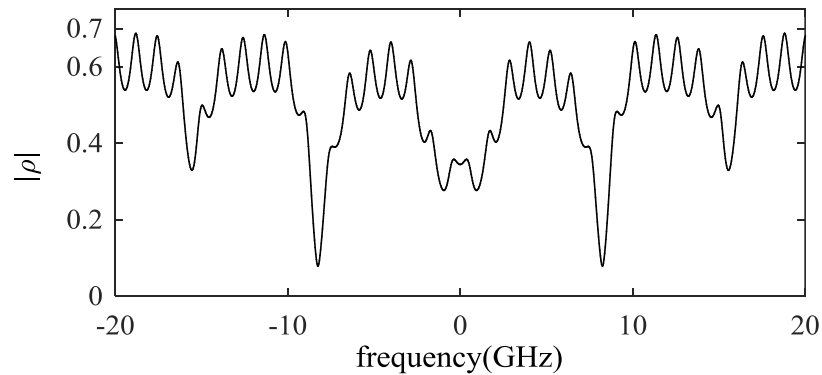


**Figure 2.6: Magnitude of convergence coefficient  $\rho$ . Example One.**

Transient analysis is performed up to 4.5ns. WR takes six iterations to converge. Voltage waveforms at the farend of line 1, near end of line 2 and the farend of line 2 for iterations one, three and five are presented in Figures 2.7, 2.8 and 2.9.

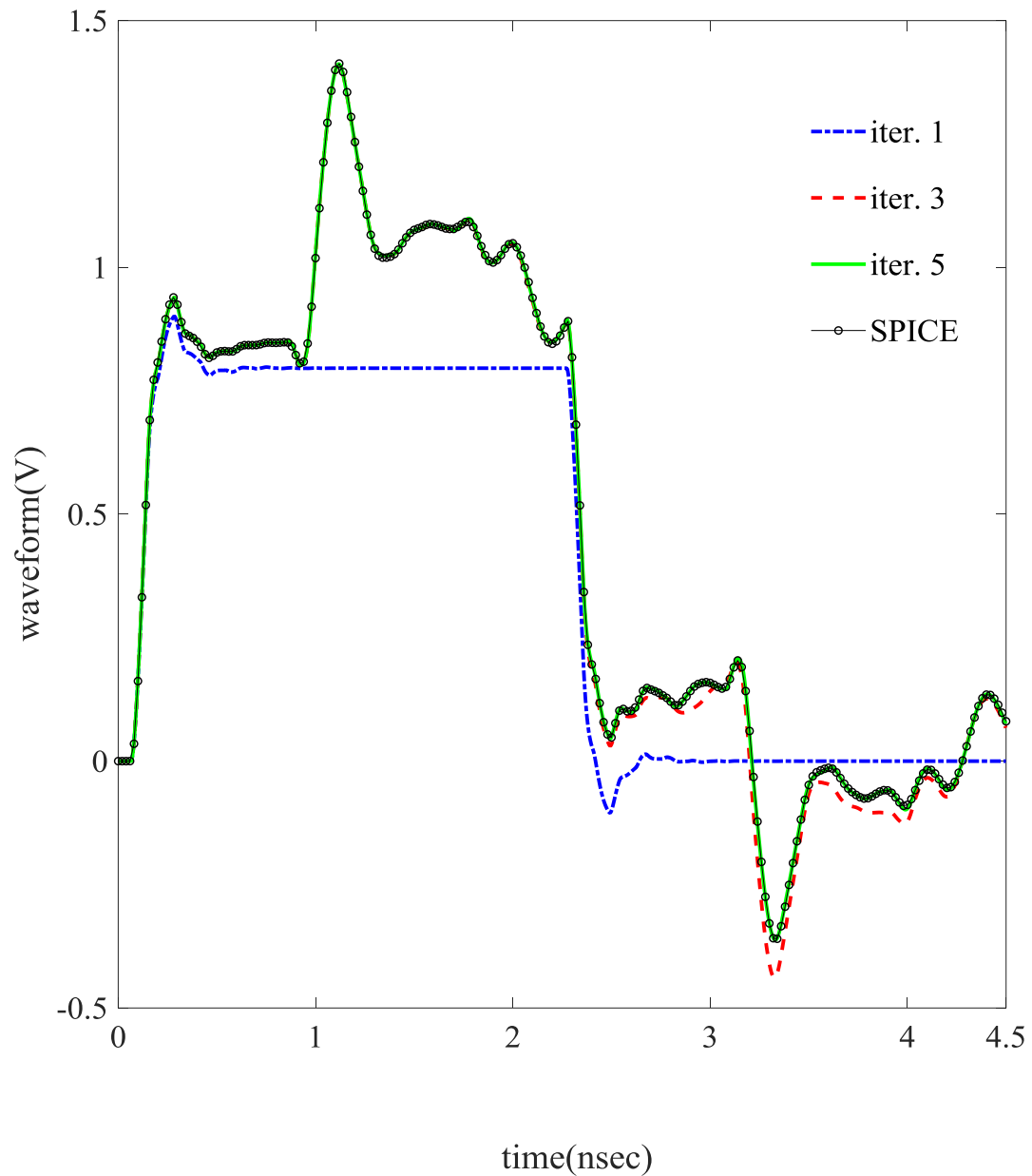


**Figure 2.7: Iteration waveform. (a) Far-end line 1. Example One.**

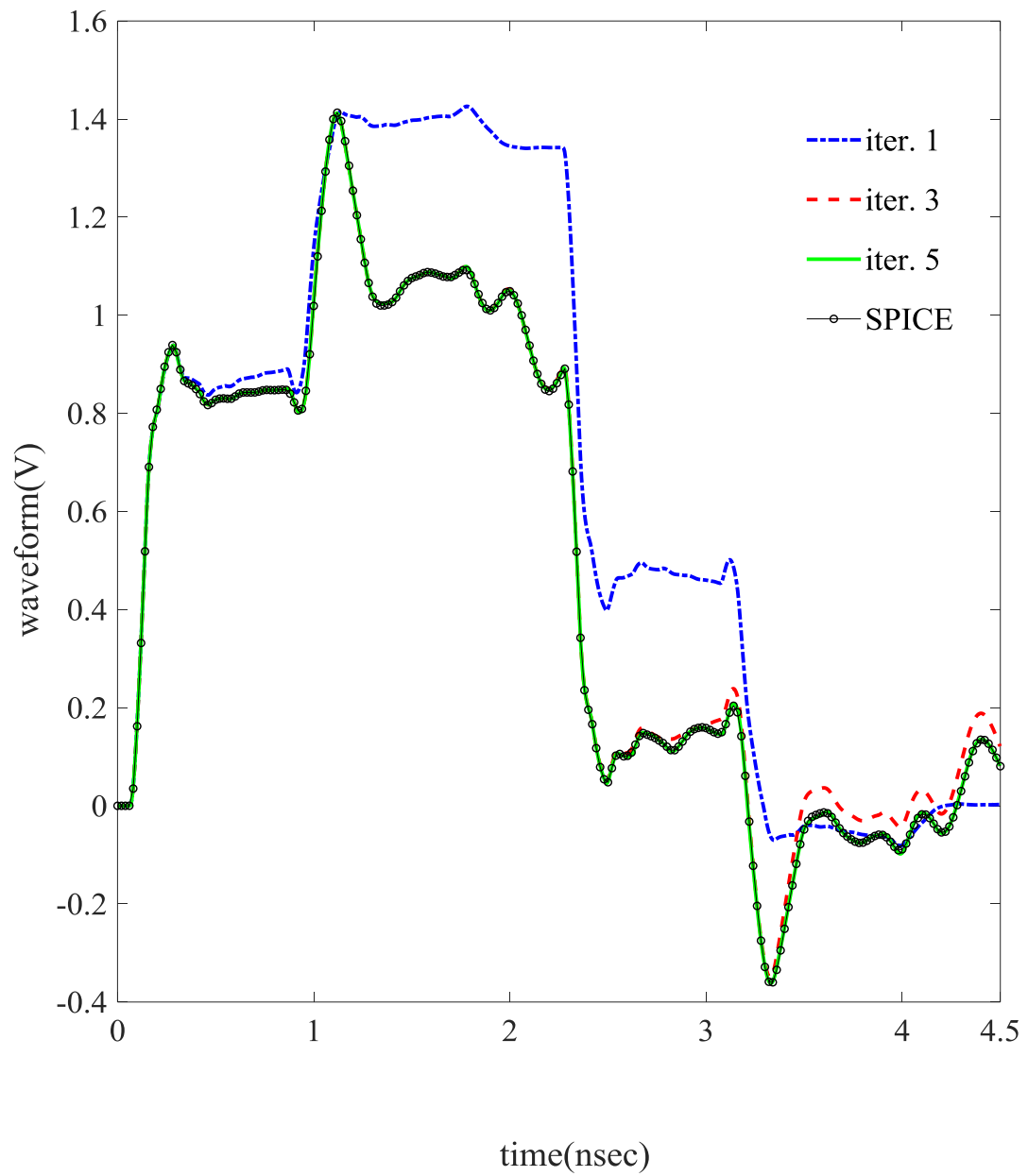


**Figure 2.8: Iteration waveform. (a) Near-end line 1. Example One.**

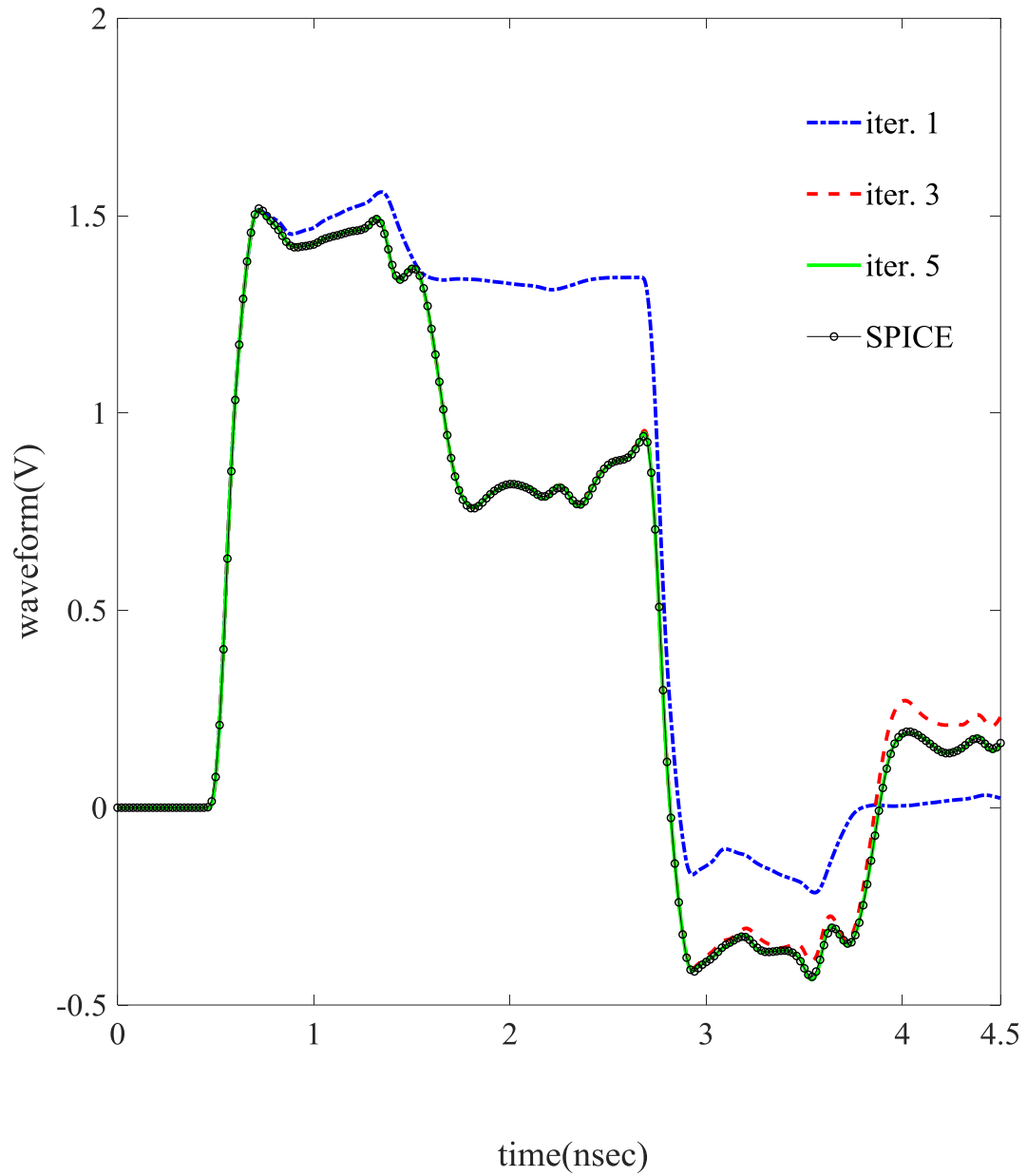


**Figure 2.9: Iteration waveform. (a) Far-end line 2. Example One.**

Next a sweep is realized by varying the decoupling resistances from  $1\Omega$  to  $100\Omega$  in steps of  $0.5\Omega$ . At every point  $(R_1, R_2)$ , WR is performed for seven iterations, the resulting relative error is recorded. The sensitivity of the suboptimal solution with respect to the value of instances (16) is examined. For this, 16, 32, 128, 256 and 512 equidistant frequency points on  $[0, 20\text{GHz}]$  are used to determine instances (2.16) and the optimization problem (2.15) is solved for each case. The solutions are found to be close to the island with the lowest error in Figure 2.10.

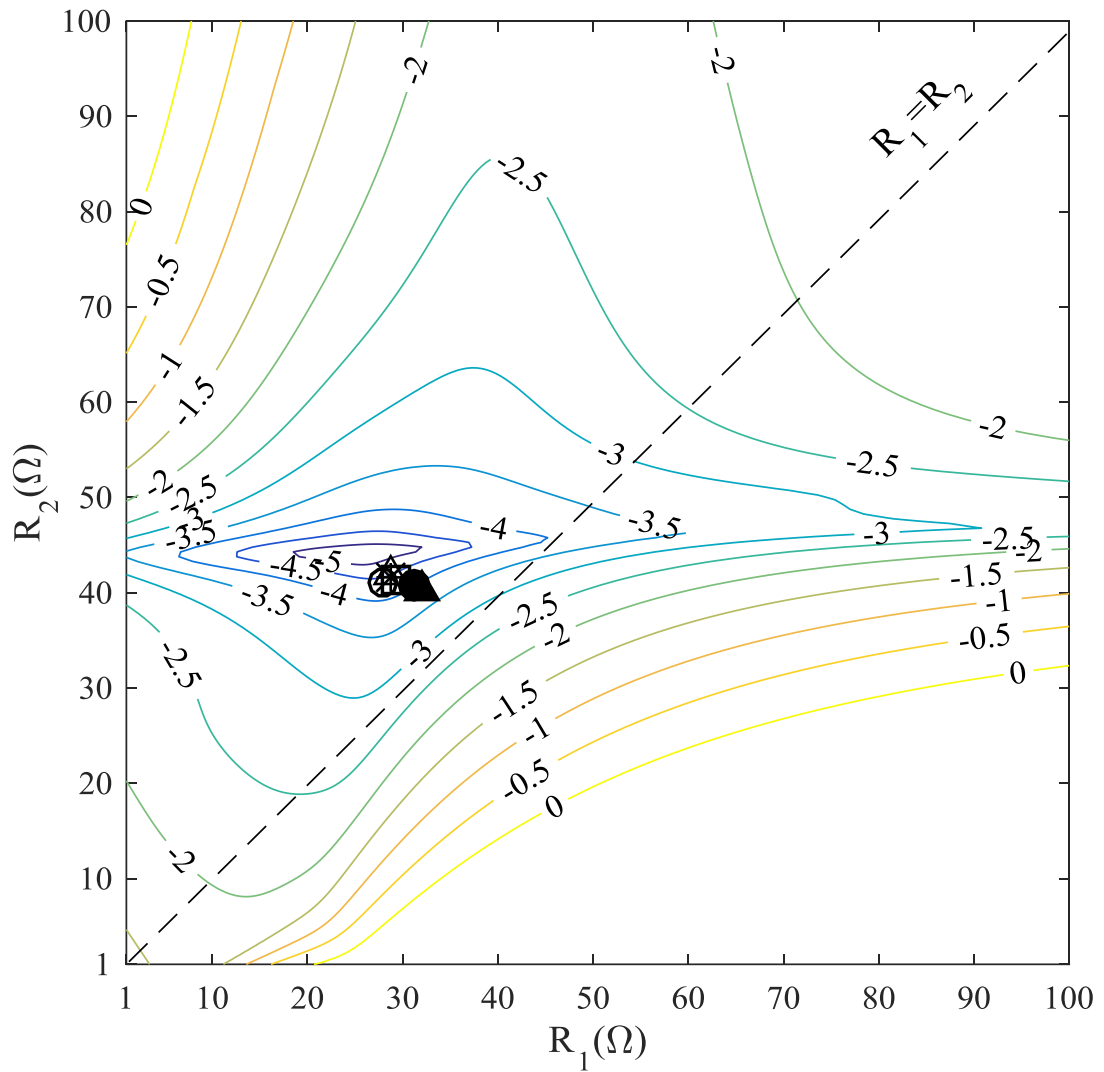


**Figure 2.10: Logarithm of error after seven WR iterations. Example One (b).**

The reason is that values  $Z_1^{\max}$  and  $Z_2^{\max}$  are located at DC and are captured by all frequency discretization. This occurrence happens each time a subsystem is terminated with a capacitive load and few frequency points can be used as long as DC is included. Finally, the position of the error islands with respect to the diagonal line  $R_1 = R_2$  (Figure 2.10) shows that faster convergence is achieved by taking  $R_1$  and  $R_2$  independent especially for adjacent subcircuits with different input impedances.

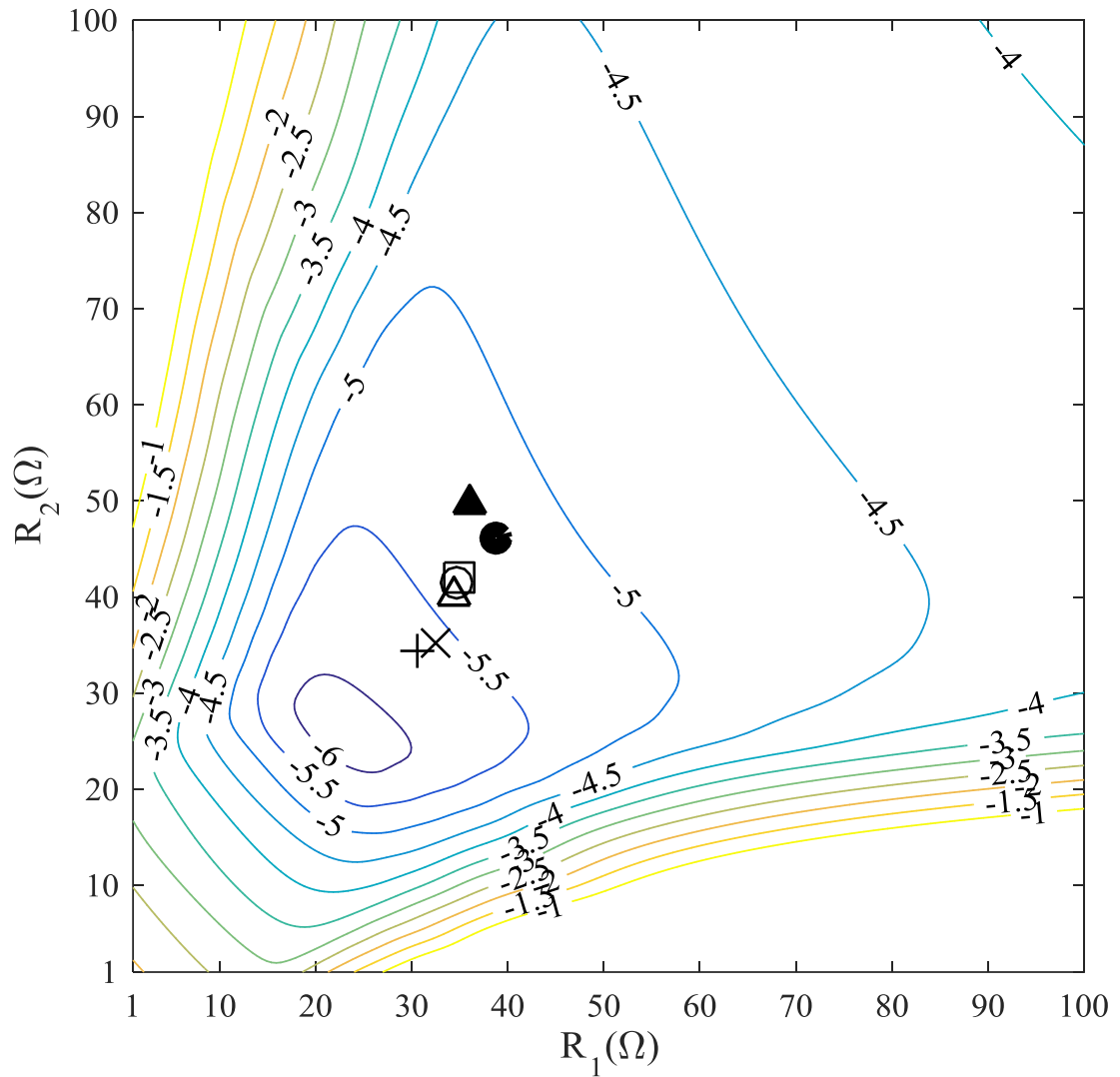


**Figure 2.11: Logarithm of error after seven WR iterations. Example One (c).**

A second partitioning is performed on the circuit of Figure 2.5(a) this time with a  $10\Omega$  –load resistance at the far-end (Figure 2.5(c)). The exact values of instances (2.16) are located at frequency points inside  $[0,20\text{GHz}]$ . The same sets of frequency points are used to capture instances (2.16). For every value, problem (2.15) is solved. Solutions are found inside the same island of error value  $10^{-5}$  (Figure 2.11). It is possible to obtain good values for the relaxation resistances quickly without having to precisely determine the extremum values of the input impedances.

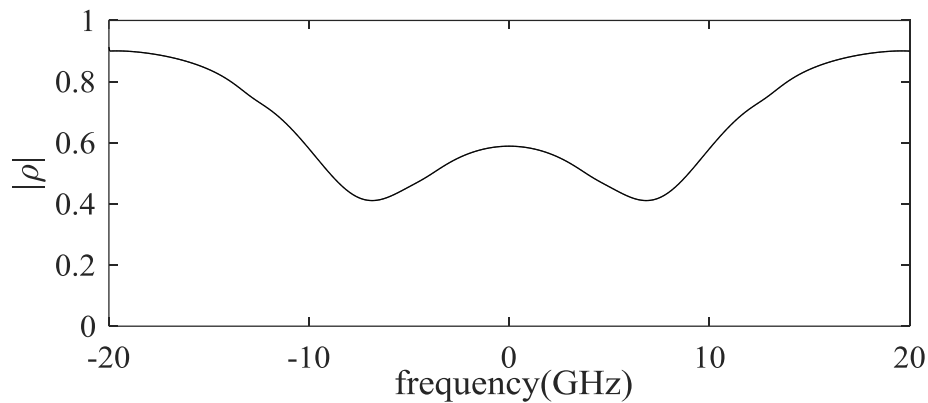


**Figure 2.12: Magnitude of convergence coefficient  $|\rho|$ . Example Two.**

### 2.2.2 Example Two-Low loss distributed circuit-perfect dielectric.

The circuit of Figure 2.5(a) is reconsidered with a  $1\text{pF}$  –load capacitance and two low loss lines with the following PUL–Line1(Line2):  $R = 15(11)\Omega/\text{m}$ ,  $L = 28(50)\text{nH}/\text{m}$ ,  $C = 100(170)\text{pF}/\text{m}$ ,  $G = 0(0)\text{S}/\text{m}$  and length =  $1.0(2.0)\text{cm}$ . This circuit is split into two parts, see Figure 2.5(b). The right-hand side subcircuit does not provide a DC path to ground and has infinite input impedance at DC. The objective function  $|r|$  of problem (2.15) is reformulated as follow:  $|r(R_1, R_2)| = \rho|R_1, R_2|$  at the instances  $(Z_1^{\min}, Z_2^{\min})$  and  $(Z_1^{\max}, Z_2^{\min})$ , and  $|r(R_1, R_2)| = |(Z_1 - R_1)/(Z_1 + R_2)|$  at the instances  $(Z_1^{\min}, \infty)$  and  $(Z_1^{\max}, \infty)$  The solution of (15) yields  $R_1 \cong 20.26\Omega$  and  $R_2 \cong 45.53\Omega$ . It is found that  $\max|r| \cong 0.642$  and  $\max|\rho| \cong 0.901$  on the interval  $[0,20\text{GHz}]$  (Figure 2.12. WR requires fourteen iterations to converge, against six in Example One. For low

loss circuits  $|\rho|$  gets closer to one, which increases the number of iterations to converge and reduces the performance of the WR algorithm.

### 2.2.3 Example Three-Chain connection.

This example examines the relevance of the proposed method for multi-subsystem partitions. A chain of twenty-one cascaded blocks  $B_i$ ,  $1 \leq i \leq 21$ , is proposed (Figure 2.13). Every block  $B_i$  is composed of a TL and a  $0.1\text{pF}$  –grounded capacitor. Blocks  $B_i$  with indices  $i$  of same parity are identical. PUL are  $R = 15(10)\Omega/\text{m}$ ,  $L = 0.28(0.29)\mu\text{H}/\text{m}$ ,  $C = 160(1550)\text{pF}/\text{m}$ ,  $G = 18(25)\text{nS}/\text{m}$ , and length =  $1.0(2.0)\text{cm}$  when index  $i$  is odd(even). A  $1\text{V}$  –trapezoidal pulse source of  $0.1\text{ns}$  – rise/fall time and  $2.0\text{ns}$  –pulse width with a  $10\Omega$  –internal resistance is connected to block  $B_1$  at node  $a_1$ . A  $1.0\text{pF}$  –load capacitor is connected to  $B_{21}$  at node  $b_{21}$ . Every block  $B_i$  stands as a subcircuit, this leads to twenty-one subcircuits grouped in twenty-one levels.  $B_1$  being in level 1 and  $B_{21}$  in level 21. The  $Z$  –parameters of subcircuits  $B_i$ ,  $2 \leq i \leq 20$  and the input impedances of  $B_1$  and  $B_{21}$  are evaluated at 512 and 256 equidistant frequency points on  $[0,10\text{GHz}]$  respectively. The objective function  $|\tilde{r}|$  is constructed on instances

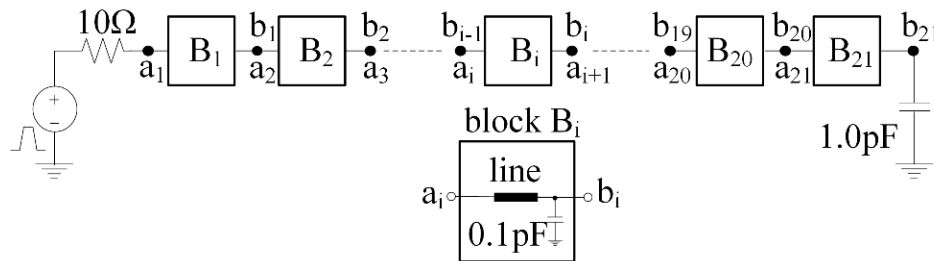


**Figure 2.13: Circuit of Example Three.**



(2.21),(2.22). The optimization problem (2.20) is solved on  $4 \times 20$  points and local convergence coefficients are shown in Figure 2.14. In this example, all  $\max|\rho_{k,l}(j\omega)|$  are slightly higher than their corresponding  $\max|\tilde{r}_{k,l}|$  in Figure 2.15.

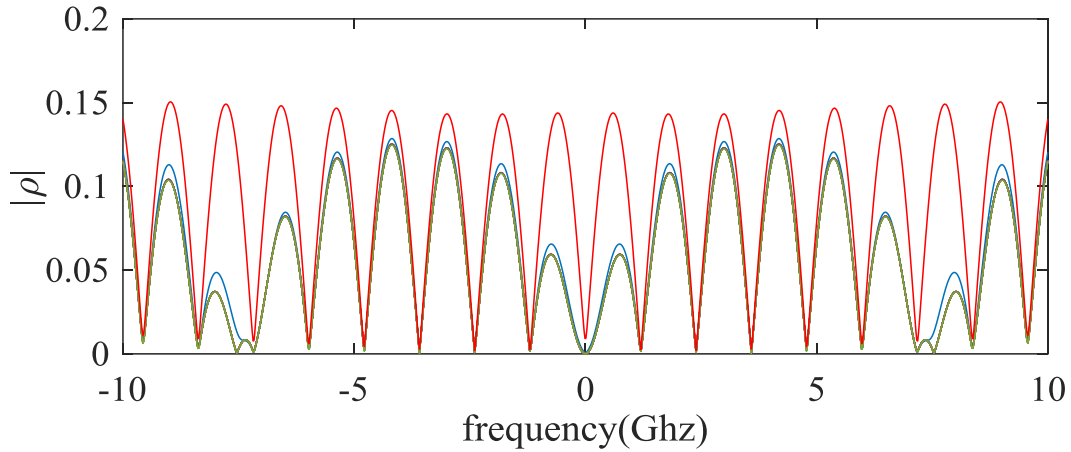


**Figure 2.14: Magnitude of local convergence coefficients  $\rho_{k,l}$ . Example Three.**

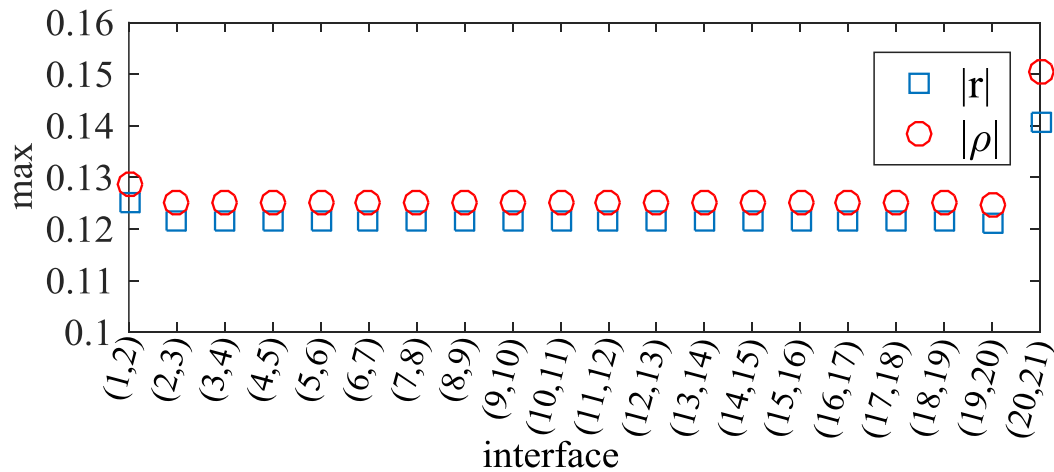


**Figure 2.15: Maximum values of  $|\tilde{r}_{k,l}|$  vs  $|\rho_{k,l}|$ . Example Three.**

WR takes twelve rounds to converge. Figures 2.16, 2.17 and 2.18 show sample transient responses at nodes  $b_{11}$ ,  $a_{12}$  and  $b_{21}$ . Note that the iterate waveforms of nodes  $b_{11}$  and  $a_{12}$  are similar to each other due to a low  $|\rho_{11,12}|$  on  $[0,10\text{GHz}]$ .

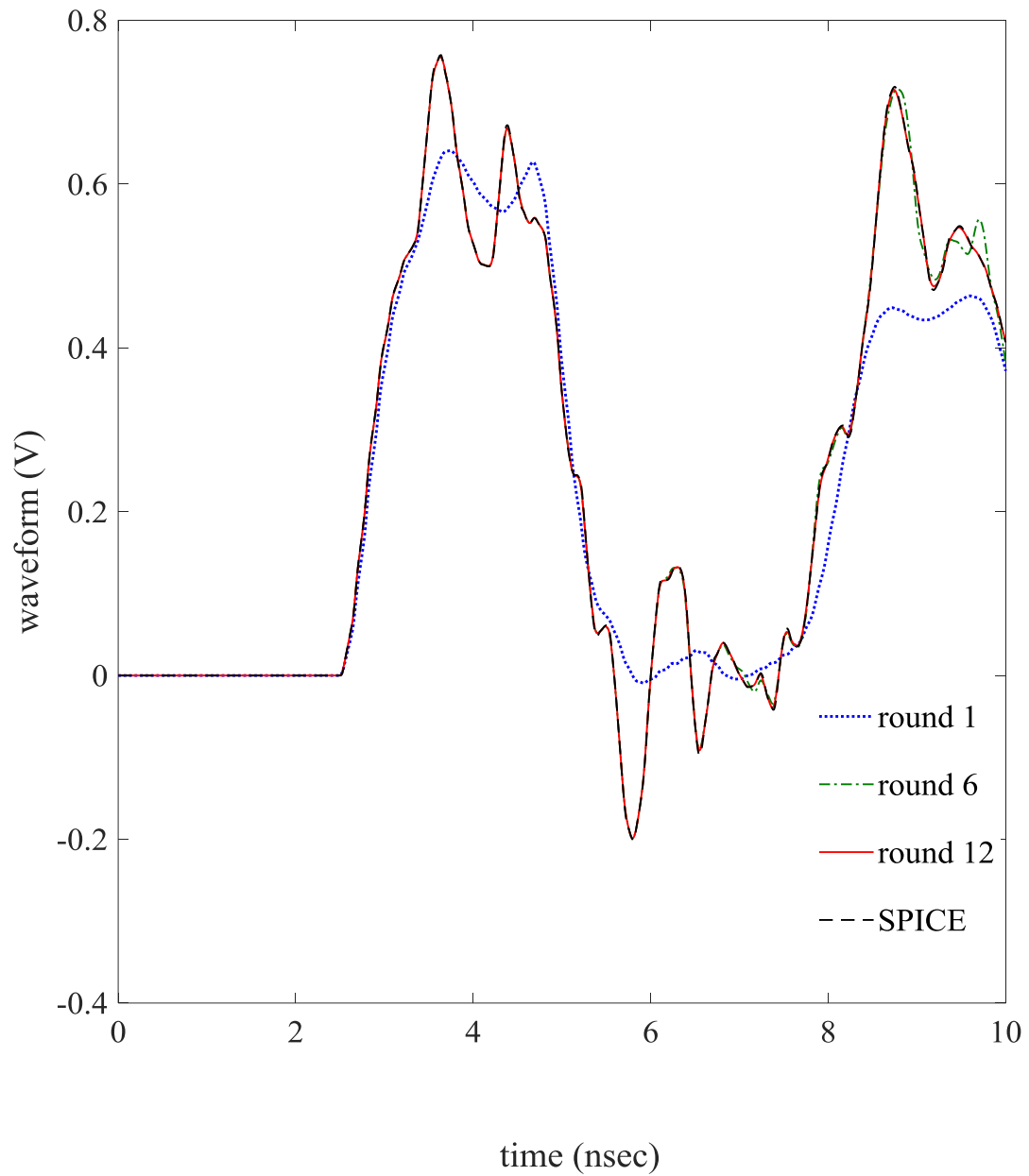


**Figure 2.16: Iteration waveforms, Node b11. Example Three.**

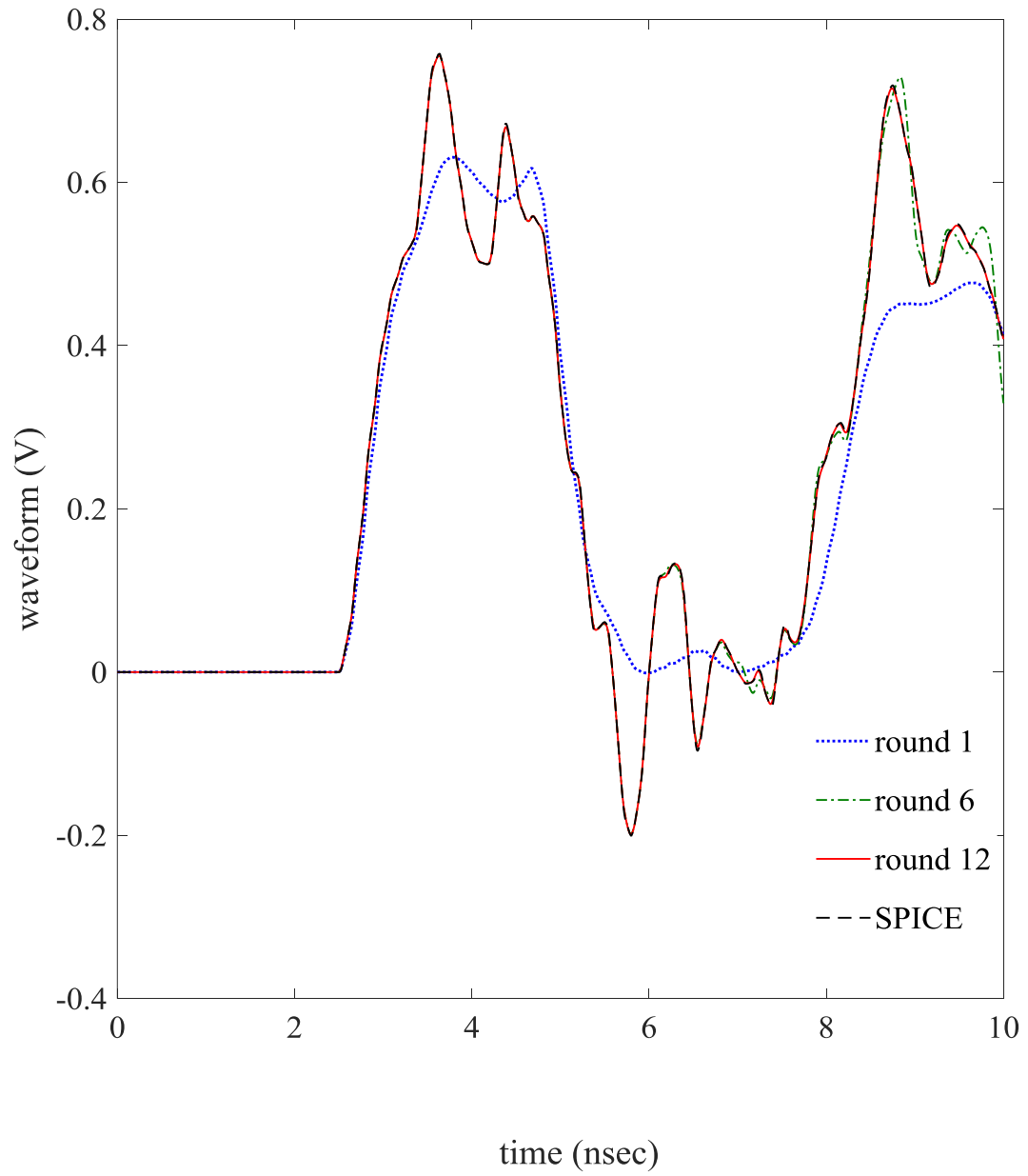


**Figure 2.17: Iteration waveforms. Node a12. Example Three.**

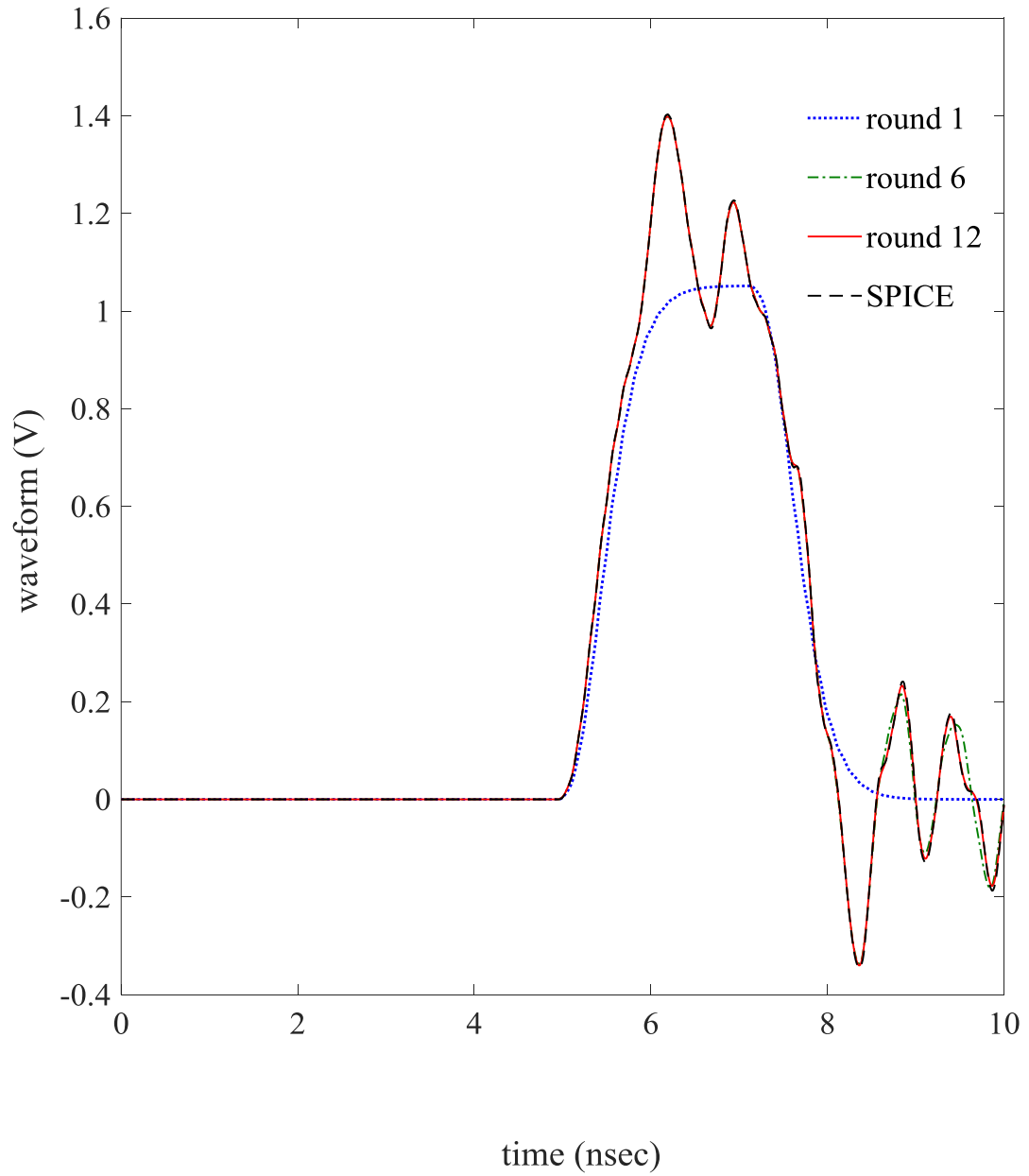


**Figure 2.18: Iteration waveforms. Node b21. Example Three.**

To assess the pertinence of solution (2.25), all decoupling resistances are swept together from  $1\Omega$  to  $200\Omega$  in steps of  $1\Omega$ . At each point, WR algorithm is executed until convergence. WR needs at least fifteen rounds to converge when all decoupling resistances are equal to  $14\Omega$ , see Figure 2.19.

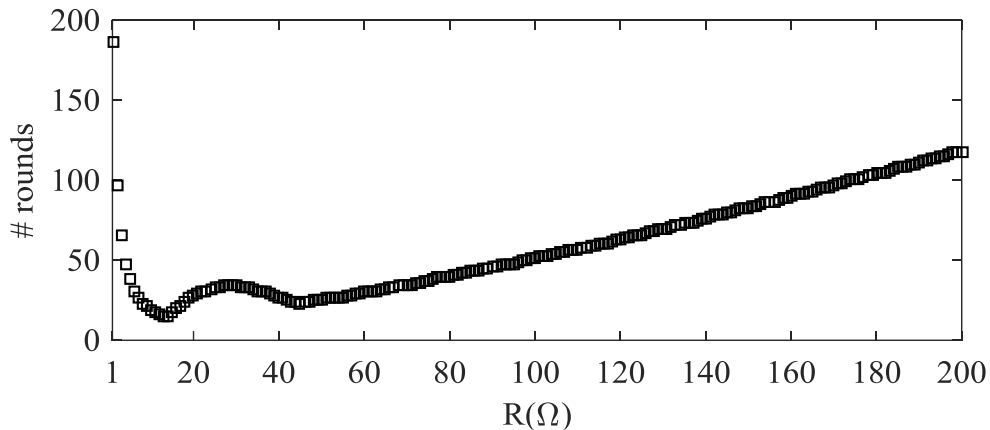


**Figure 2.19: Number of rounds to converge. Sweep on the diagonal. Example Three.**

#### 2.2.4 Example Four Tree structure-scalability with respect to number of CPUs.

In this example, a thirty-three TL circuit (Figure 2.20) is considered. PUL parameters, line lengths and the description of the lumped elements are also provided on Figure 2.20. The input signal is a 1V –trapezoidal pulse of 0.1ns –rise/fall time and 2.1ns –pulse width. This circuit is partitioned into thirty-three subcircuits labeled  $L_1$  to  $L_{33}$  and grouped in five levels (Figure 2.20).

The optimization problem is performed on  $4 \times 32$  points. The values of all  $|\rho_{k,l}|$  are shown in Figure 2.21. For this example,  $\max \text{all } |\tilde{r}_{k,l}| \cong 0.144$ , while  $\max \text{all } |\rho_{k,l}| \cong 0.254$ . Each subcircuit is solved on interval  $[0, T]$ ,  $T = 10\text{ns}$ . WR converges in four rounds.

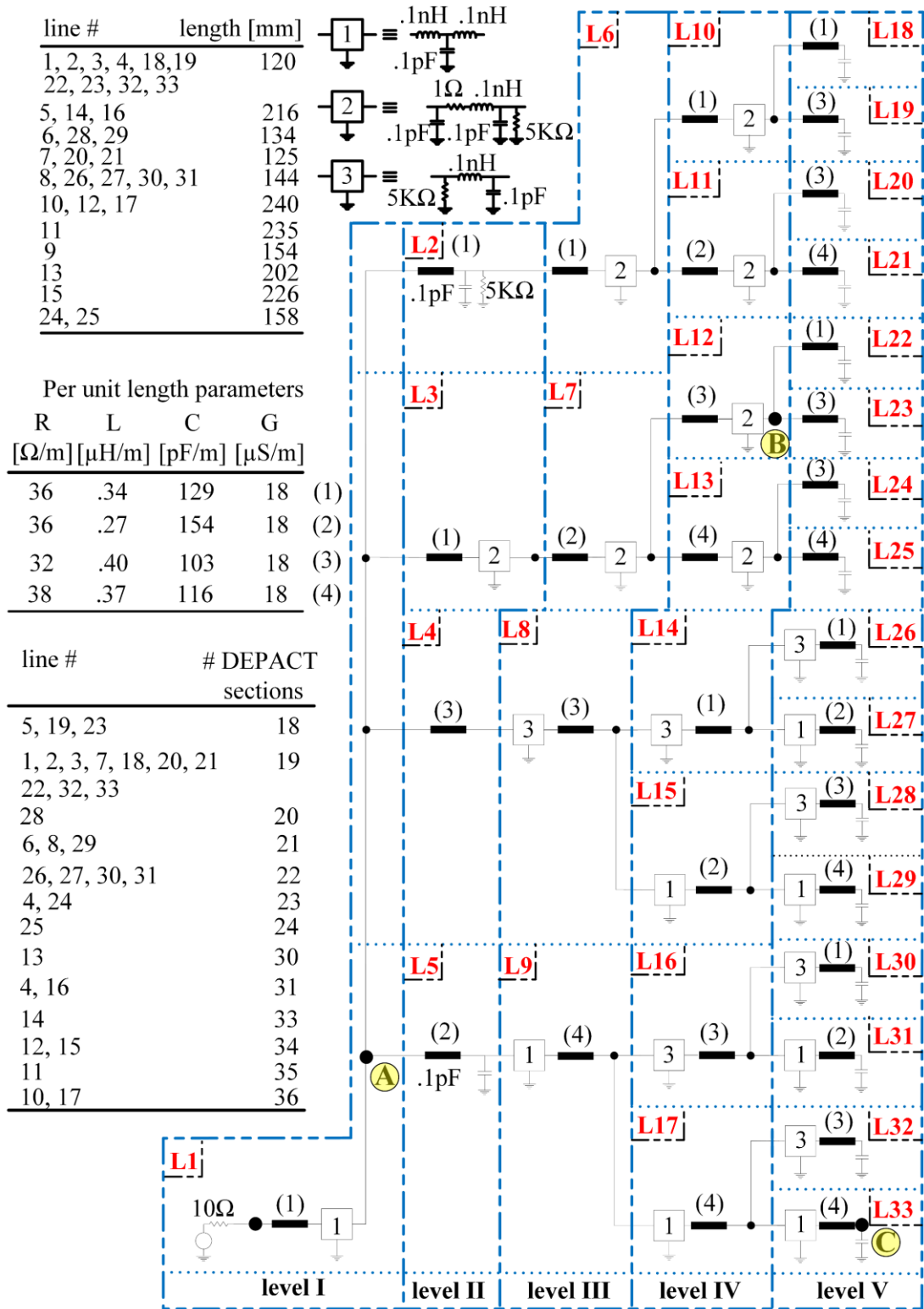
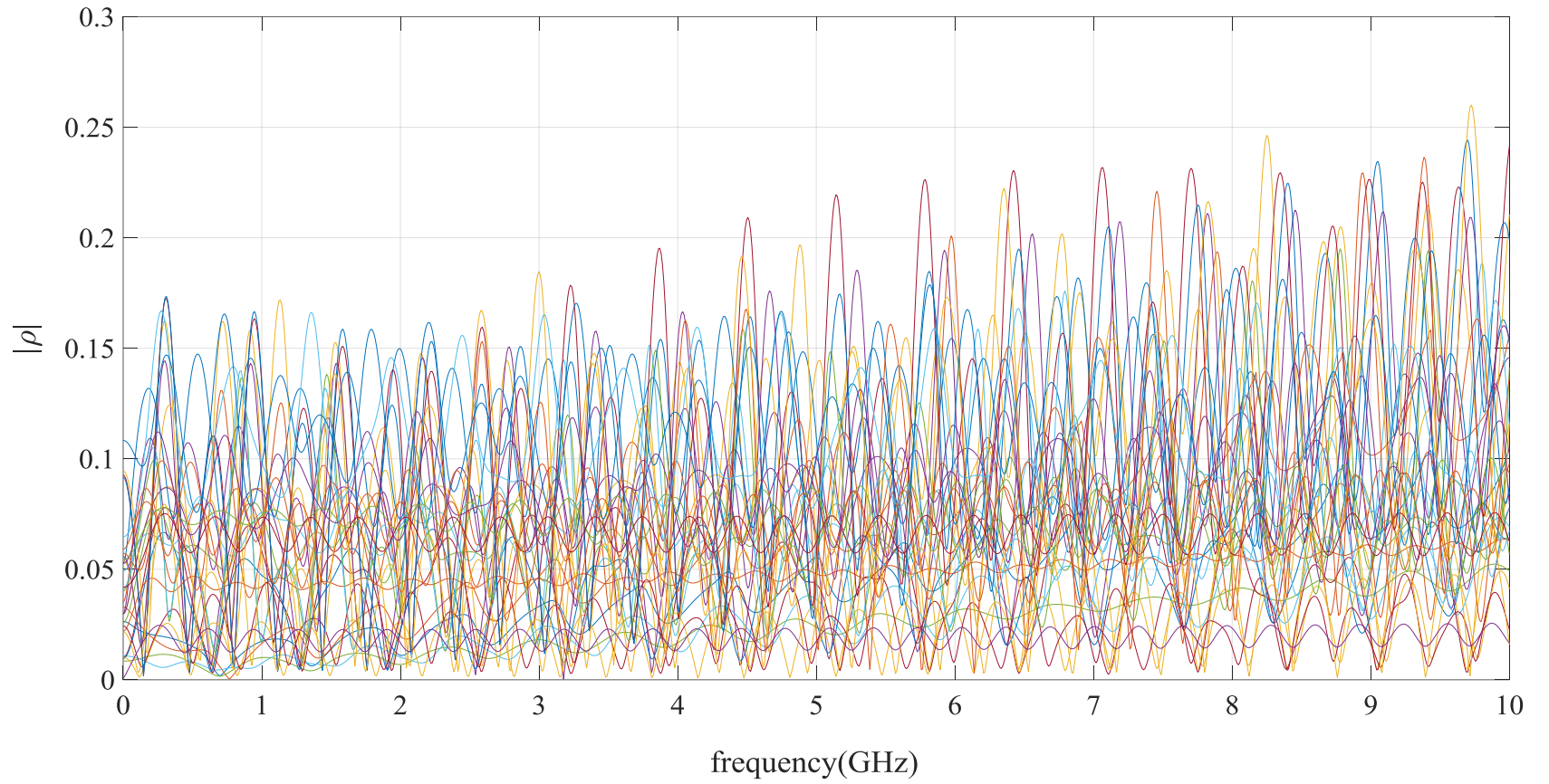
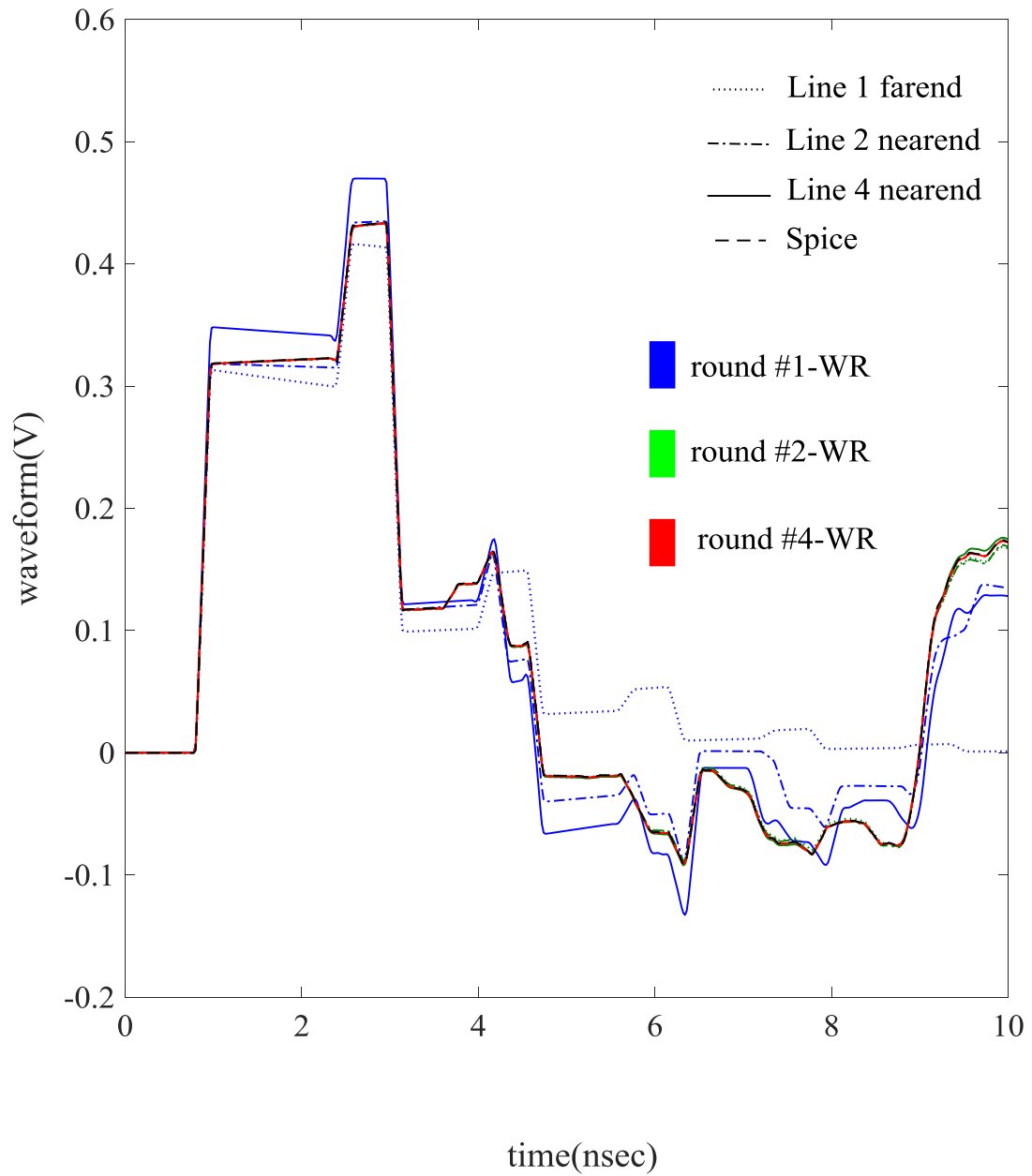


Figure 2.20: Circuit of Example Four.



**Figure 2.21: Local convergence coefficients  $|\rho_{k,l}|$ . Example Four.**

The iterate waveforms at nodes A, B and C for round one, two and four are shown in Figures 2.22, 2.23 and 2.24.



**Figure 2.22: Iteration waveform. Node A. Example Four.**



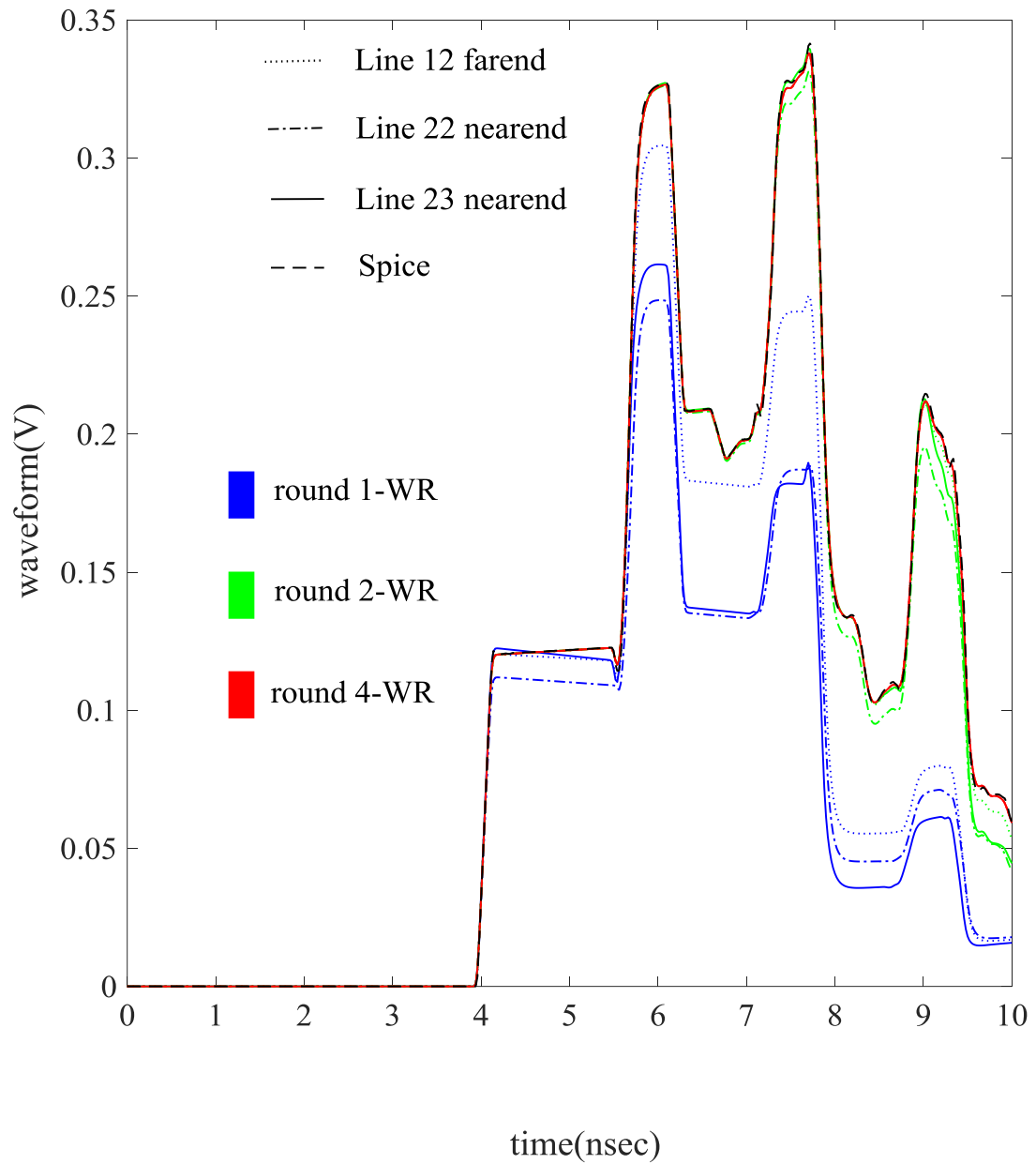


**Figure 2.23: Iteration waveform. Node B. Example Four.**

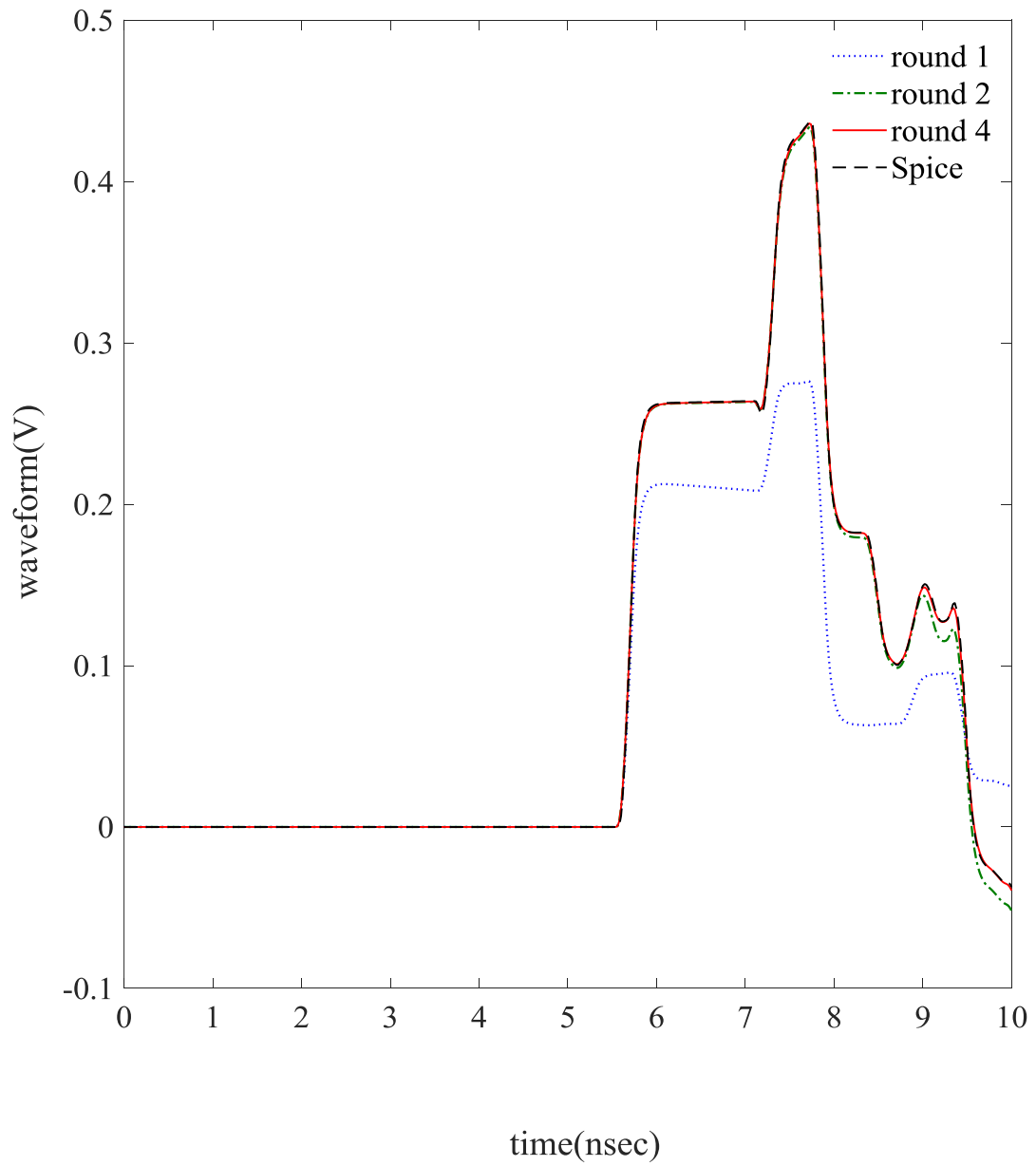


**Figure 2.24: Iteration waveform. Node C. Example Four.**

Next, the performance of the proposed waveform relaxation algorithm is examined. The CPU time to solve the optimization problem is 2.0s. The number of CPUs used to run the proposed method is increased from one to eight CPUs and the corresponding times are compared against full-circuit analysis in Table 2.5.

**Table 2.5: Performance of proposed algorithm. Example Four.**

# CPU	WR time (s)	Full analysis time (s)	Optimization cost (s)	WR speed up	Method speed up
1	29.4			0.85	0.82
2	17.0			1.47	1.31
4	10.2	25.0	2.0	2.43	2.05
6	8.7			2.87	2.58
8	5.8			4.31	3.20

For this circuit, a speedup of 4.3 is obtained with eight CPUs without the optimization overhead. The speedup decreases to 3.2 with the optimization overhead. The performance scalability with respect to the number of CPUs is compared against the estimated values of (2.29) in Figure 2.25.

It was previously mentioned that due to the fact that instances (2.16) and (2.21),(2.22) are approximately located with a discrete frequency sampling, there exist frequency points where  $|\rho|$  or  $|\rho_{k,l}|$  is higher than the maximum value of its corresponding  $|r|$  or  $|\tilde{r}_{k,l}|$  as depicted in Figure 2.26(a). To investigate the effect of these points on the WR rate of convergence, the optimization problem (2.20) is repeatedly solved on a larger set of instances. The instances at frequency points where the generated coefficients  $\rho_{k,l}$

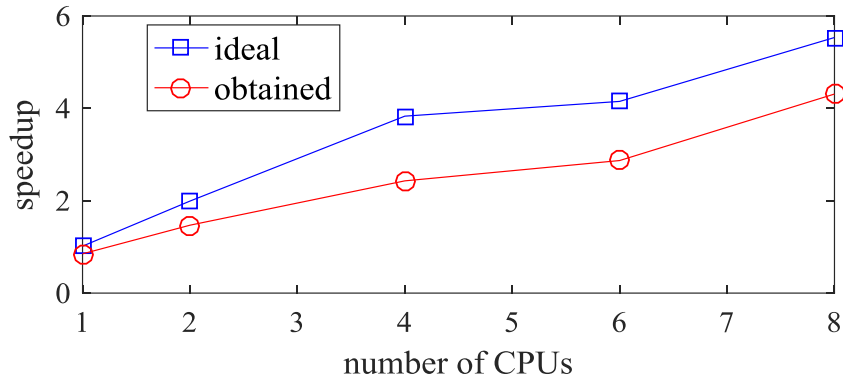
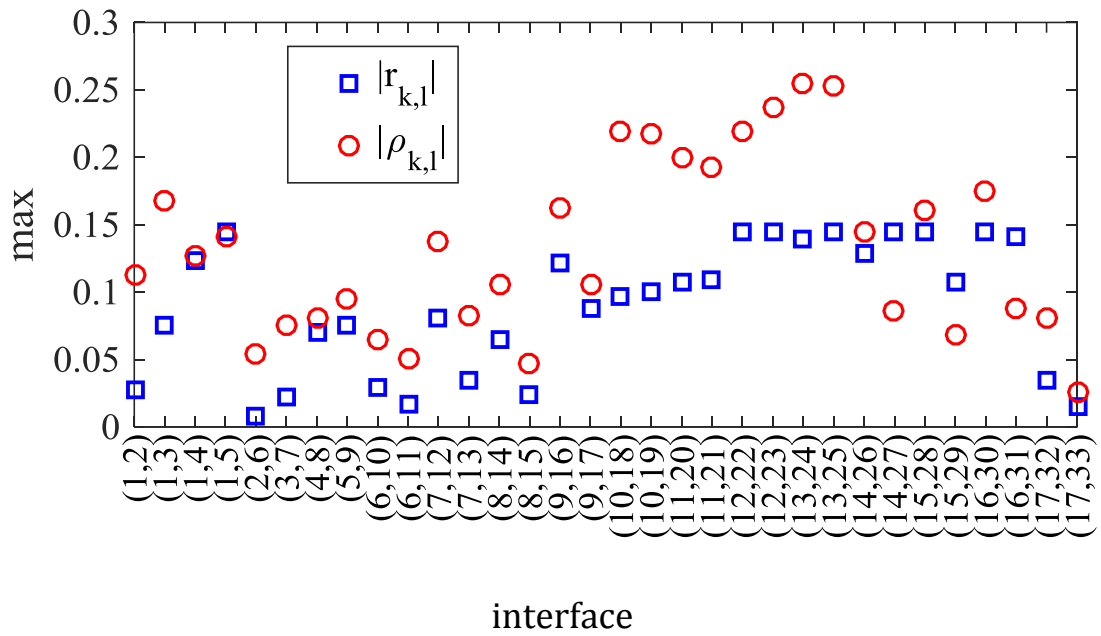
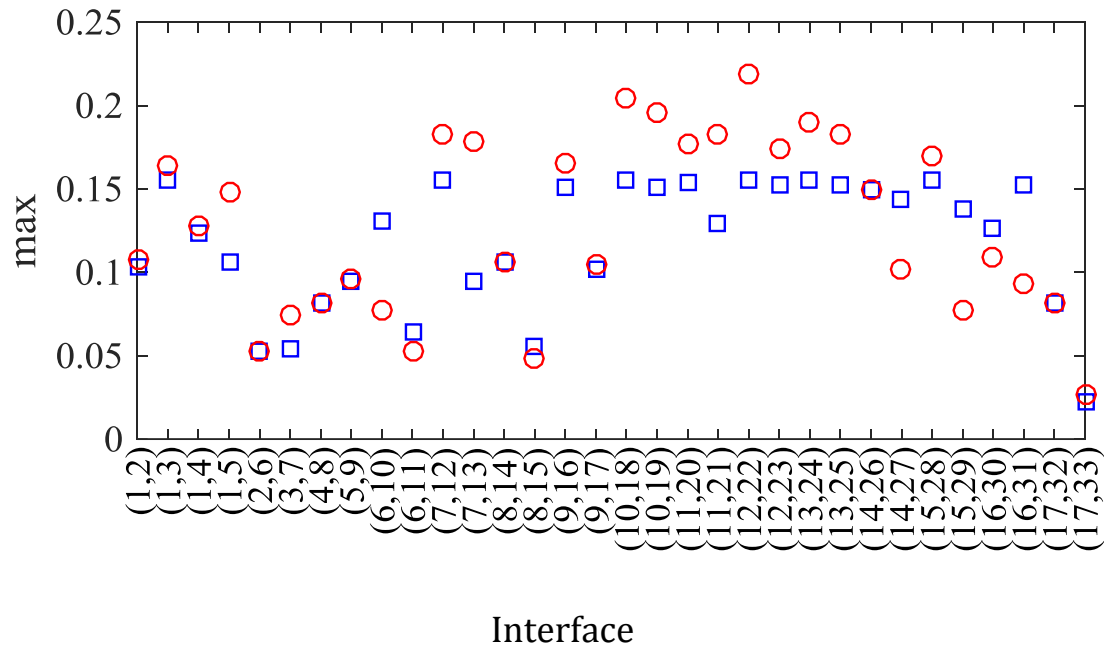


**Figure 2.25: Speedup. Example Four.**

satisfy  $\max|\rho_{k,l}| > \max|\tilde{r}_{k,l}|$  are added to regular instances in (2.21),(2.22) and the optimization is performed again. This procedure is repeated twice. Adding these instances reduced the points where  $\max|\rho_{k,l}| > \max|\tilde{r}_{k,l}|$  and led to more uniform  $|\rho_{k,l}|$  on  $[0,10\text{GHz}]$  as depicted in Figure 2.26(b). Overall, the additional instances did not significantly decrease the range of values of  $|\rho_{k,l}|$  in Figure 2.27. The WR algorithm is run with the new set of relaxation resistances. The error at the end of each round is compared with the one yielded by the regular solution in Figure 2.28. Adding new instances did not improve the overall rate of convergence. In this example, the original optimization resulted in a slightly faster convergence rate due to the lower values of  $|\rho_{k,l}|$  near DC.



(a)



(b)

**Figure 2.26:  $\max |\tilde{r}_{k,l}|$  vs.  $\max |\rho_{k,l}|$ . (a) 128 points. (b) 164 points. Example Four.**

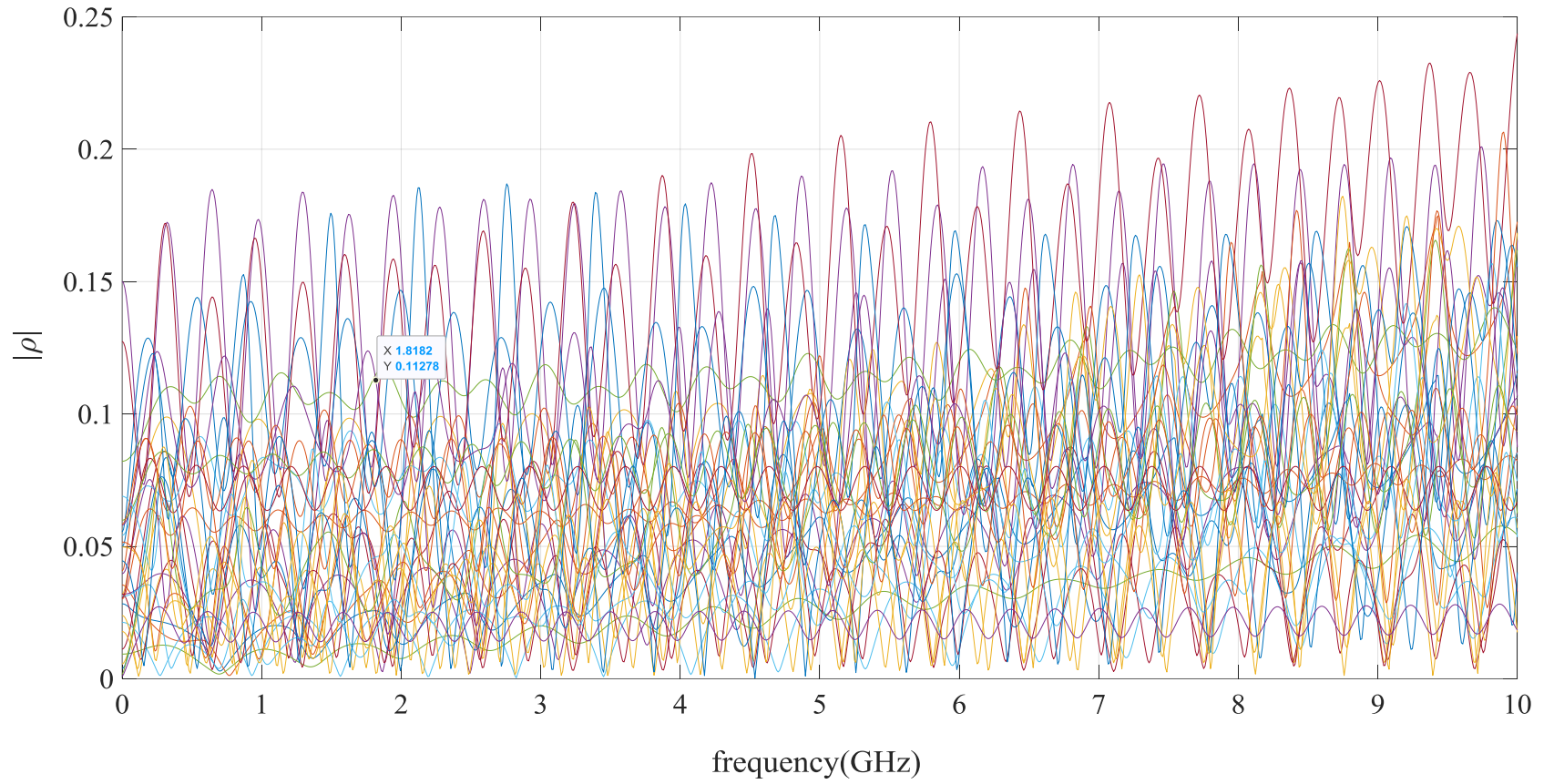


**Figure 2.27: Local convergence coefficients  $|\rho_{k,l}|$  after adding instances (164 points). Example Four.**

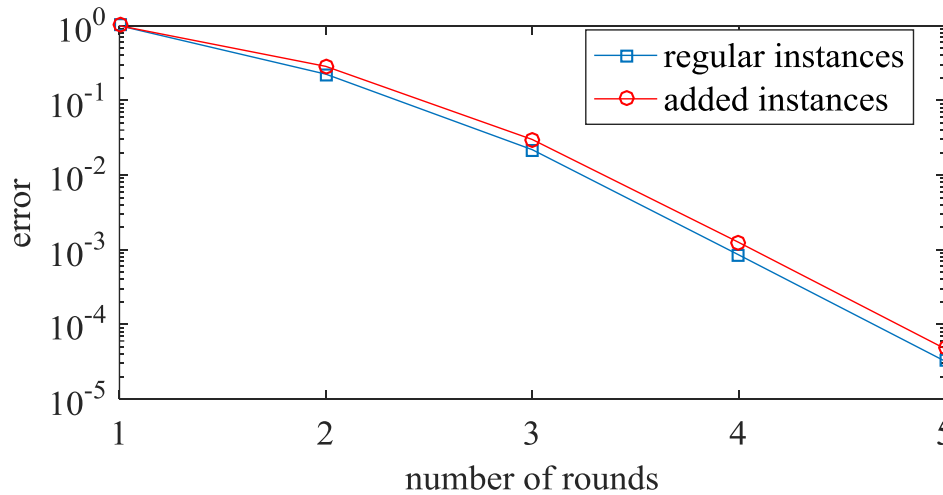


**Figure 2.28: Error evolution. Example Four.**

### 2.2.5 Example Five-Tree structure-scalability with respect to the partition size.

In this example, the scalability of the proposed algorithm is investigated. The circuit of Figure 2.29 is considered. All building blocks B are composed of one fan-out of two TLs line1 and line2, both terminated with a  $0.1\text{pF}$  –capacitor to ground. PUL parameters are—line1(line2)  $R = 60(45)\Omega/\text{m}$ ,  $L = 3.4(4.7)\mu\text{H}/\text{m}$ ,  $C = 130(110)\text{pF}/\text{m}$ ,  $G = 6.0(6.0)\mu\text{S}/\text{m}$ , and length =  $11.0(12.0)\text{cm}$ . A  $1\text{V}$  –trapezoidal pulse source of  $0.1\text{ns}$  rise/fall time and  $2.0\text{ns}$  pulse width with a  $10\Omega$  internal resistance, is connected to node  $a_0$ . Blocks B at the level with the highest index  $K$  are terminated with  $0.9\text{pF}$  –capacitors to ground. Every TL together with its far-end capacitor forms a subcircuit. Eight CPUs are used to execute this example. Blocks B are used to build three circuits with  $= 5, 6,$  and  $7$  levels, resulting in a total  $31, 63,$  and  $127$  TLs, respectively. The CPU cost to solve the optimization problem for the three circuits is provided in Table 2.6. The three networks are solved on interval  $[0, T]$ , where  $T = 12\text{ns}$ . For all three circuits, convergence is achieved within four rounds. Iteration waveforms at the far-end terminations of line 127 (node A) for the 127-TL circuit are shown in Figure 2.30. The

corresponding CPU run times are compared against full-circuit analysis in Table 2.6 with the resulting speedup ranging from 3.5 to 5.1 without the optimization overhead and from 2.4 to 3.2 with the optimization overhead.

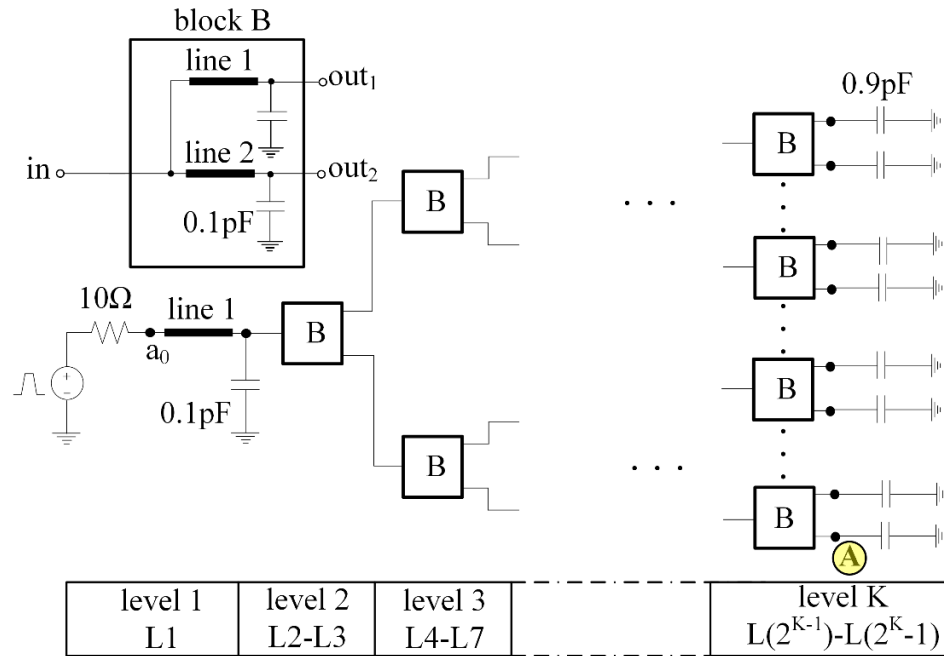


**Figure 2.29: Circuit of Example Five.**

**Table 2.6: Scaling with respect to the number of transmission lines. Example Five.**

# lines	WR time (s)	CPU Full analysis time (s)	Optimization cost	WR speedup	Method speedup
31	4.11	14.46	2.00	3.5	2.4
63	7.09	29.78	4.09	4.2	2.7
127	11.91	61.04	7.40	5.1	3.2



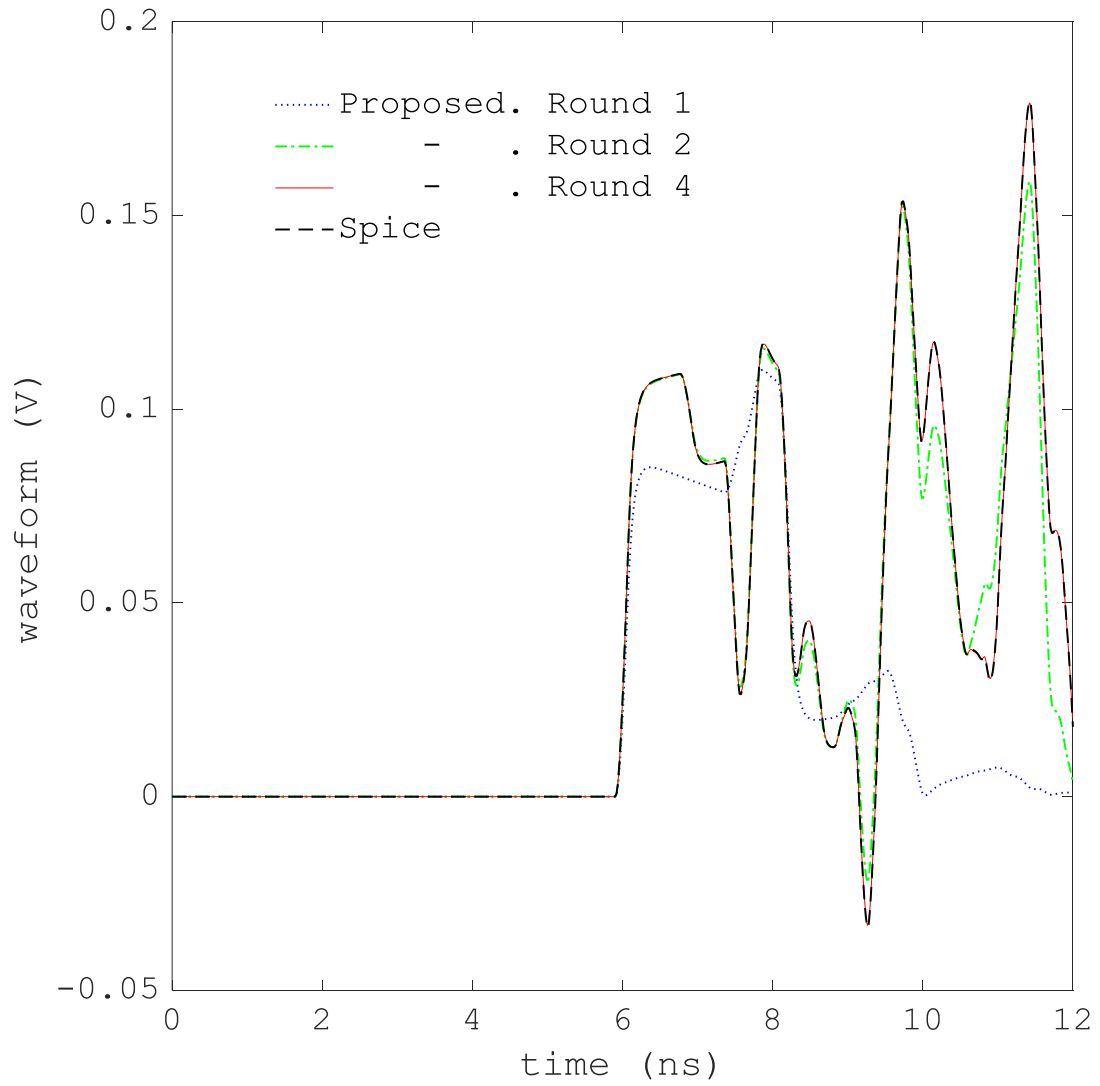


**Figure 2.30: Iteration waveform. Node A. Example Five.**

## 2.3 Conclusion

In this chapter, a new resistive coupling-based LP-WR algorithm is presented for the analysis of transmission line dominated circuits. The proposed longitudinal partitioning scheme subdivides these circuits and leads to multi-level partitions. The adjacent subcircuits are decoupled with a Norton interface. The decoupling resistances of every Norton interface are determined for improved WR local convergence rates. A step-by-step method is provided to construct the companion optimization problem for any given partition, and the decoupling resistances are determined by a suboptimal solution to this problem. Numerical examples illustrate that the parallel LP-WR algorithms outperforms SPICE in the analysis of lossy TL trees. For highly reactive low loss or lossless circuits, LP-WR is slow or fail to converge. Future work will include extending this algorithm to multi-conductor transmission lines with nonlinear loads.

## Chapter 3

### 3 Using Strictly Dissipative Impedance Coupling in the Waveform Relaxation Method for the Analysis of Interconnect Circuits

Strictly dissipative impedance coupling is introduced in the waveform relaxation algorithm with longitudinal partitioning to address the slow convergence of standard resistive coupling in the analysis of low-loss highly reactive circuits. The pertinence, feasibility, and consistency of the proposed WR algorithm are demonstrated. Its convergence is examined for any passive linear time-invariant (LTI) system. Rational-with-delay impedances are presented to decouple general transmission line circuits. The proposed coupling strategy uses coarse macromodeling of the transmission lines to construct the coupling impedances directly as passive distributed auxiliary circuits. Numerical examples show a superior speed of convergence and further runtime savings.

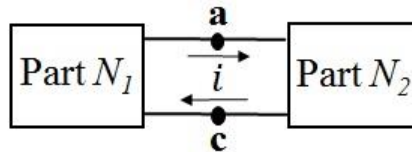


**Figure 3.1:** Parts  $N_1$  and  $N_2$  are connected directly.

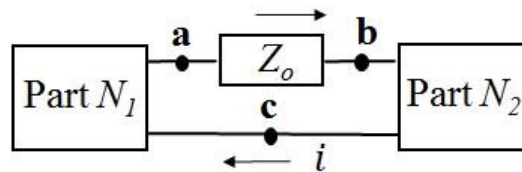


**Figure 3.2:** Parts  $N_1$  and  $N_2$  are connected via a strictly dissipative element  $Z_o$ .

#### 3.1 Strictly dissipative impedance coupling

Standard resistive coupling is extended to strictly dissipative impedance coupling. Insertion  $\{-R_1, R_1 + R_2, -R_2\}$ ,  $R_1, R_2 > 0$  in Figure 2.1(b) is replaced by a neutral series connection of three impedances  $\{-\zeta_1(s), \zeta_2(s), -\zeta_2(s)\}$ . Coupling impedances

$\zeta_1(s)$  and  $\zeta_2(s)$  are strictly positive-real functions for all  $s \in \mathbb{C}$  and  $\Re(s) \geq 0$  [96]. They are driving-point impedances of lossy passive circuits whereas  $\zeta_\Sigma$  represents the driving-point impedance of the created circuit overlap. The strict positive realness condition must be imposed to ensure the subsequent WR is consistent and to make the overall system stable by construction as discussed in section 3.3.3.

As with resistive coupling [63],[64],[97], the proposed WR also applies on general circuits. It decouples any two parts  $N_1$  and  $N_2$  in a decomposed circuit when these are directly connected (Figure 3.1), and creates an overlap  $\zeta_\Sigma(s) = \zeta_1(s) + \zeta_2(s)$  to guarantee the neutrality of insertion  $\{-\zeta_1(s), \zeta_\Sigma(s), -\zeta_2(s)\}$ . If there is an element  $Z_o(s)$  in the decomposed system that connects  $N_1$  to  $N_2$  (Figure 3.2), then  $Z_o(s)$  can be included in overlap  $\zeta_\Sigma(s)$  provided it too is strictly dissipative as discussed in 3.2.1, making  $\zeta_\Sigma(s) = \zeta_1(s) + \zeta_2(s) + Z_o(s)$ .

Despite the presence of opposite impedances  $(-\zeta_1(s))$  and  $(-\zeta_2(s))$ , instability is not introduced since total insertions  $(\zeta_\Sigma(s) - \zeta_1(s))$  and  $(\zeta_\Sigma(s) - \zeta_2(s))$  to both the left and right parts are still positive-real impedances, see Figure 3.3.

Insertions  $\{-R_1, R_1 + R_2, -R_2\}$  and  $\{-\zeta_1(s), \zeta_\Sigma(s), -\zeta_2(s)\}$  create overlaps  $(R_1 + R_2)$  and  $\zeta_\Sigma(s)$  between  $N_1$  and  $N_2$ . As a result, the subsequent WR iterations are carried out through successive updates of same nodal voltage waveforms  $u_2(t)$  and  $w_{-2}(t)$  implemented as voltage sources in Figure 3.3.

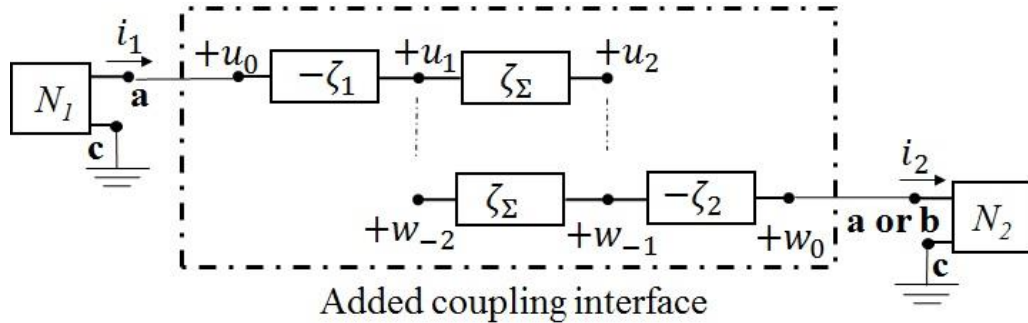


**Figure 3.3: Dissipative coupling of parts  $N_1$  and  $N_2$ . Node c is put to Ground.**

$$u_2^{(k+1)}(t) = w_{-1}^{(k)}(t) \quad (3.1)$$

$$w_{-2}^{(k+1)}(t) = u_1^{(k+\nu)}(t) \quad (3.2)$$

Integer  $k$  refers to the iteration count and parameter  $\nu = 1$  for Gauss-Seidel (GS) relaxation and  $\nu = 0$  for Gauss-Jacobi (GJ) one. The effect of replacing resistances by impedances on WR is explained in section 3.2.1 to justify the pertinence of the proposed generalization.

A Norton interface was presented in Figure 2.1(d) to divide a circuit into several parts. It consists of positive coupling resistances  $R_1$  and  $R_2$  from insertion  $\{-R_1, R_1 + R_2, -R_2\}$ , and uses an all-voltages relationship to update the two relaxation sources  $u_2$  and  $w_{-2}$  of the WR in the time-domain, see eq. (2.3).

$$u_2^{(k+1)}(t) = w_0^{(k)}(t) (1 + R_2/R_1) - w_{-2}^{(k)}(t) R_2/R_1 \quad (3.3)$$

$$w_{-2}^{(k+1)} = u_0^{(k)}(t) (1 + R_1/R_2) - u_2^{(k)}(t) R_1/R_2 \quad (3.4)$$

A similar Norton interface is readily built for  $\{-\zeta_1(s), \zeta_\Sigma(s), -\zeta_2(s)\}$ . It too consists of only  $\zeta_1(s)$  and  $\zeta_2(s)$  and updates its relaxation sources  $u_2(t)$  and  $w_{-2}(t)$  using relations

$$u_2^{(k+1)}(t) = w_0^{(k)}(t) * \left( \mathcal{L}^{-1} \left( \frac{\zeta_\Sigma}{\zeta_\Sigma - \zeta_2} \right) \right) (t) - w_{-2}^{(k)}(t) * \left( \mathcal{L}^{-1} \left( \frac{\zeta_2}{\zeta_\Sigma - \zeta_2} \right) \right) (t) \quad (3.5)$$

$$w_{-2}^{(k+1)}(t) = u_0^{(k+\nu)}(t) * \left( \mathcal{L}^{-1} \left( \frac{\zeta_\Sigma}{\zeta_\Sigma - \zeta_1} \right) \right) (t) - u_2^{(k+\nu)}(t) * \left( \mathcal{L}^{-1} \left( \frac{\zeta_1}{\zeta_\Sigma - \zeta_1} \right) \right) (t) \quad (3.6)$$

where  $\mathcal{L}^{-1}$  is the inverse Laplace transform and  $*$  refers to the convolution integral. When every insertion  $\{-\zeta_1(s), \zeta_\Sigma(s), -\zeta_2(s)\}$  is implemented as a Norton interface, the WR solution is obtained by solving enlarged subcircuits (including the realization of

$\zeta_1(s)$  and  $\zeta_2(s)$ ) in addition to resorting to nonlocal operators in time in the update of the relaxation sources whenever  $\zeta_1(s)$  or  $\zeta_2(s)$  is a rational or a rational-with-delay complex function of the complex frequency  $s$  according to (3.5) and (3.6). The expensive update must be executed outside a classic circuit simulator environment in general before every part is scheduled next for analysis. Such serial overhead renders the WR solution inefficient for sparse problems like single line circuits where coupling between lines is ignored. To avoid the expensive update, every insertion  $\{-\zeta_1(s), \zeta_\Sigma(s), -\zeta_2(s)\}$  must be realized as in Figure 3.3. If the one-time cost of these circuit realizations is low, then it is possible to cluster the method's overhead in the repetitive time-domain analysis of the enlarged parts. A parallel execution of the algorithm can naturally absorb the repetitive overhead and results in possible runtime saving if it achieves a right balance between fast convergence and the cost of the iteration.

The rest of the chapter is organized as follows: First the relevance of dissipative impedance coupling is demonstrated in 3.2.1, and its feasibility is addressed in section 3.2.2. Second, the consistency of the subsequent WR algorithm is shown and its convergence is examined for any passive LTI system in section 3.2.3. Third, the proposed coupling strategy is presented for the analysis of single transmission line circuits in section 3.2.4. Finally, numerical examples illustrate the efficiency of the proposed impedance coupling and compare its performance against resistive coupling [31] for general single line circuits and against the optimized WR for RLCG type circuits [36]-[39] in section 3.3.

## 3.2 Proposed WR algorithm

### 3.2.1 Relevance of strictly dissipative impedance coupling

First consider the system of Figure 3.1. The objective is to determine what action does insertion  $\{-\zeta_1(s), \zeta_\Sigma(s), -\zeta_2(s)\}$  exert on the voltage waveforms  $u_0(t)$  and  $w_0(t)$  and on currents  $i_1(t)$  and  $i_2(t)$  at the split node between parts  $N_1$  and  $N_2$  in Figure 3.4.

Let  $\tilde{u}_0(s)$ ,  $\tilde{u}_1(s)$ ,  $\tilde{u}_2(s)$ ,  $\tilde{w}_{-2}(s)$ ,  $\tilde{w}_{-1}(s)$ ,  $\tilde{w}_0(s)$ ,  $\tilde{i}_1(s)$  and  $\tilde{i}_2(s)$  be the Laplace transforms of voltage waveforms  $u_0(t)$ ,  $u_1(t)$ ,  $u_2(t)$ ,  $w_{-2}(t)$ ,  $w_{-1}(t)$ ,  $w_0(t)$  and

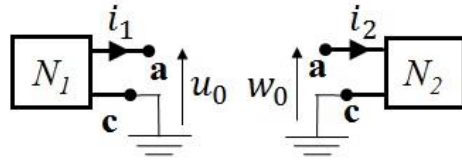


**Figure 3.4: Circuit partitioning. No circuit overlap.**

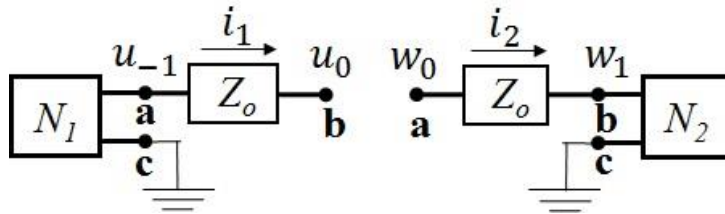


**Figure 3.5: Circuit partitioning. Overlap  $Z_o$  is strictly dissipative. Node  $c$  is put to Ground.**

currents  $i_1(t)$ ,  $i_2(t)$  in Figure 3.3. The application of Kirchhoff's voltage law (KVL) results in the following equations for the four node voltages involved in the exchange (1),(2)

$$\tilde{u}_1(s) = \tilde{u}_0(s) + \zeta_1(s) \tilde{i}_1(s) \quad (3.7) \quad \tilde{w}_{-1}(s) = \tilde{w}_0(s) - \zeta_2(s) \tilde{i}_2(s) \quad (3.9)$$

$$\tilde{u}_2(s) = \tilde{u}_0(s) - \zeta_2(s) \tilde{i}_1(s) \quad (3.8) \quad \tilde{w}_{-2}(s) = \tilde{w}_0(s) + \zeta_1(s) \tilde{i}_2(s) \quad (3.10)$$

Using (3.7)-(3.10), equations (3.1) and (3.2) are written as

$$u_0^{(k+1)}(t) - (\mathcal{L}^{-1}(\zeta_2))(t) * i_1^{(k+1)}(t) = w_0^{(k)}(t) - (\mathcal{L}^{-1}(\zeta_2))(t) * i_2^{(k)}(t) \quad (3.11)$$

$$w_0^{(k+1)}(t) + (\mathcal{L}^{-1}(\zeta_1))(t) * i_2^{(k+1)}(t) = u_0^{(k+v)}(t) + (\mathcal{L}^{-1}(\zeta_1))(t) * i_1^{(k+v)}(t) \quad (3.12)$$

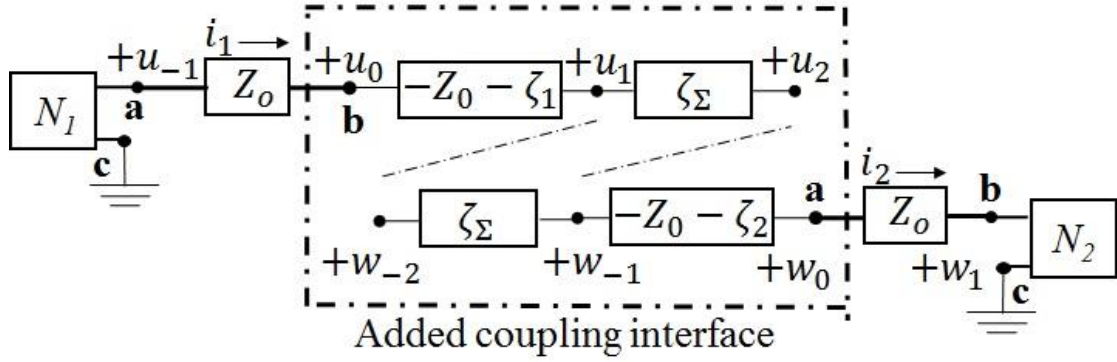


**Figure 3.6: Decoupled parts  $N_1$  and  $N_2$ .  $Z_o$  is visible. Node  $c$  is put to Ground.**

in the time domain. Next, let us see how equations (3.11) and (3.12) are altered when element  $Z_o(s)$  connects  $N_1$  to  $N_2$  in the decomposed system of Figure 3.2, and is used as a natural circuit overlap in the partitioning of Figure 3.5. To keep  $Z_o(s)$  visible on both sides of the insertion, the coupling of Figure 3.3 is described in an equivalent manner in Figure 3.6 for  $\zeta_\Sigma(s) = \zeta_1(s) + \zeta_2(s) + Z_o(s)$ . In the frequency-domain, nodal voltages  $u_0(t)$ ,  $u_1(t)$ ,  $u_2(t)$ , and  $u_3(t)$  on the side of  $N_1$  and  $w_{-1}(t)$ ,  $w_{-2}(t)$  and  $w_{-3}(t)$  on the side of  $N_2$  can be expressed by the following KVL equations

$$\tilde{u}_2(s) = \tilde{u}_0(s) + \frac{\zeta_2(s)}{Z_o(s)} (\tilde{u}_0(s) - \tilde{u}_{-1}(s)) \quad (3.13)$$

$$\tilde{w}_{-1}(s) = \tilde{w}_1(s) + \frac{\zeta_2(s)}{Z_o(s)} (\tilde{w}_1(s) - \tilde{w}_0(s)) \quad (3.14)$$

$$\tilde{w}_{-2}(s) = \tilde{w}_0(s) + \frac{\zeta_1(s)}{Z_o(s)} (\tilde{w}_0(s) - \tilde{w}_1(s)) \quad (3.15)$$

$$\tilde{u}_1(s) = \tilde{u}_{-1}(s) + \frac{\zeta_1(s)}{Z_o(s)} (\tilde{u}_{-1}(s) - \tilde{u}_0(s)) \quad (3.16)$$

currents  $\tilde{i}_1(s) = (\tilde{u}_{-1}(s) - \tilde{u}_0(s))/Z_o(s)$ , and  $\tilde{i}_2(s) = (\tilde{w}_0(s) - \tilde{w}_1(s))/Z_o(s)$  on both sides are finite, which requires  $Z_o(s)$  to be strictly dissipative. Now, voltage exchange (3.1),(3.2) can be put as



$$u_0^{(k+1)}(t) + \left( \mathcal{L}^{-1} \left( \frac{\zeta_2}{Z_o} \right) \right) (t) * \left( u_0^{(k+1)}(t) - u_{-1}^{(k+1)}(t) \right) =$$
(3.17)

$$w_1^{(k)}(t) + \left( \mathcal{L}^{-1} \left( \frac{\zeta_2}{Z_o} \right) \right) (t) * \left( w_1^{(k)}(t) - w_0^{(k)}(t) \right)$$

$$w_0^{(k+1)}(t) + \left( \mathcal{L}^{-1} \left( \frac{\zeta_1}{Z_o} \right) \right) (t) * \left( w_0^{(k+1)}(t) - w_1^{(k+1)}(t) \right) =$$
(3.18)

$$u_{-1}^{(k+v)}(t) + \left( \mathcal{L}^{-1} \left( \frac{\zeta_1}{Z_o} \right) \right) (t) * \left( u_{-1}^{(k+v)}(t) - u_0^{(k+v)}(t) \right)$$

in the time domain. Equations (3.11),(3.12) and (3.17),(3.18) show that dissipative impedance coupling exchanges a combination of currents and nodal voltages at the teared nodes at both ends of insertion  $\{-\zeta_1(s), \zeta_\Sigma(s), -\zeta_2(s)\}$ . Each combination represents a sum of a voltage waveform and a convoluted waveform representing the electric current. The weight coefficients in these sums are convolution integral transforms whose kernels are the inverse Laplace transforms of  $\zeta_1(s)$ ,  $\zeta_2(s)$ ,  $\zeta_1(s)/Z_o(s)$  and  $\zeta_2(s)/Z_o(s)$ . Replacing resistances by impedances amounts to replacing a simple multiplication by a constant positive value in the weight coefficients by integral operators. Equations (3.11),(3.12) and (3.17),(3.18) are examples of the general transmission coupling conditions introduced in the work of Gander et al. on the optimized WR applied to circuit problems [74, eq. (2.9)] [74, eq. (2.5)]. A careful choice of these coupling impedances or kernels will enhance the convergence of WR over resistive coupling.

### 3.2.2 Feasibility

Opposite impedances  $(-\zeta_1(s))$  and  $(-\zeta_2(s))$  must have a time-domain realization to directly implement insertion  $\{-\zeta_1(s), \zeta_\Sigma(s), -\zeta_2(s)\}$ . It can be demonstrated that if the one-port circuit  $M$  is a realization of  $\zeta$ , composed of lumped resistances  $R$ , lumped inductances  $L$ , lumped capacitances  $C$  and lossless elements  $(Z_c, \tau)$  with a delay then, the replacement in  $M$  of every  $R$  by  $(-R)$ , of every  $L$  by  $(-L)$ , of every  $C$  by  $(-C)$ , and of

every  $(Z_c, \tau)$  by  $(-Z_c, \tau)$ , results in a realization for  $(-\zeta)$ . Here,  $Z_c$  and  $\tau$  represent the characteristic impedance and delay of a lossless transmission line or line segment [98].

Now that it has been established that dissipative impedance coupling WR is a general algorithm, its consistency and optimal convergence are examined.

### 3.2.3 Properties of impedance coupling based WR

#### 3.2.3.1 Consistency

If the proposed WR algorithm converges, then it is essential to know whether the WR solution is indeed the correct system solution. A requirement which is satisfied according to the following lemma.

*Lemma 3.1 (consistency).* If a dissipative impedance coupling-based WR algorithm converges, then it always converges to the correct system solution.

*Proof.* Transmission condition equations (3.11) and (3.12) can be written in the frequency domain under the following form

$$\begin{aligned} [\tilde{u}_0(s) - \tilde{w}_0(s)] - \zeta_2(s)[\tilde{i}_1(s) - \tilde{i}_2(s)] &= 0 \\ [\tilde{u}_0(s) - \tilde{w}_0(s)] + \zeta_1(s)[\tilde{i}_1(s) - \tilde{i}_2(s)] &= 0 \end{aligned} \quad (3.19)$$

The WR algorithm converges to the correct system response if and only if the homogeneous system (3.19) of the two equations with respect to unknowns  $[\tilde{u}_0(s) - \tilde{w}_0(s)]$  and  $[\tilde{i}_1(s) - \tilde{i}_2(s)]$  accepts the zero solution. That is its determinant  $\zeta_\Sigma(s) := \zeta_1(s) + \zeta_2(s) \neq 0$  for all  $\Re(s) \geq 0$ . A condition which is satisfied since  $\Re(\zeta_\Sigma(s)) > 0$  for all  $\Re(s) \geq 0$ . Now, let us consider transmission conditions equations (3.17) and (3.18). They can be put under the following form in the frequency domain

$$\begin{aligned} \left(1 + \frac{\zeta_2(s)}{Z_o(s)}\right) [\tilde{u}_0(s) - \tilde{w}_1(s)] - \frac{\zeta_2(s)}{Z_o(s)} [\tilde{u}_{-1}(s) - \tilde{w}_0(s)] &= 0 \\ -\frac{\zeta_1(s)}{Z_o(s)} [\tilde{u}_0(s) - \tilde{w}_1(s)] + \left(1 + \frac{\zeta_1(s)}{Z_o(s)}\right) [\tilde{u}_{-1}(s) - \tilde{w}_0(s)] &= 0 \end{aligned} \quad (3.20)$$

Again, the WR method converges to the correct system response if and only if the homogeneous system (3.20) of the two equations with respect to unknowns  $[\tilde{u}_0(s) -$

$\tilde{w}_1(s)]$  and  $[\tilde{u}_{-1}(s) - \tilde{w}_0(s)]$  accepts the zero solution. That is its determinant  $\zeta_\Sigma(s) := \zeta_1(s) + \zeta_2(s) + Z_o(s) \neq 0$  for all  $\Re(s) \geq 0$ . A condition which is satisfied since  $\Re(\zeta_\Sigma(s)) > 0$  for all  $\Re(s) \geq 0$ . ■

It is worth mentioning that condition  $\zeta_\Sigma(s) \neq 0$  for eqs. (3.17) and (3.18), represents consistency condition  $\beta^{-1}(s) \neq \alpha^{-1}(s) + 1$  [75, (2.10)] after taking  $\alpha(s) = Z_o(s)/\zeta_2(s)$  and  $\beta(s) = -Z_o(s)/\zeta_1(s)$  for the case where strictly dissipative element  $Z_o$  connects  $N_1$  and  $N_2$ . Second, same condition  $\zeta_\Sigma(s) \neq 0$  this time for eqs. (3.11) and (3.12), corresponds to consistency condition  $\alpha(s) \neq \beta(s)$  [74, Sec. 2.2] after taking  $\alpha^{-1}(s) = -\zeta_2(s)$  and  $\beta^{-1}(s) = \zeta_1(s)$  for the case where these parts are directly connected.

Note that the strict positive-realness condition imposed on  $\zeta_1(s)$  and  $\zeta_2(s)$  is stronger than the consistency condition derived in the oWR [74],[75]. This is to also guarantee realizability and stability of the expanded system [99]. The next section studies the convergence of the WR algorithm.

### 3.2.3.2 Convergence

Convergence is examined here for any passive LTI circuit [96] using GJ relaxation. Similar analysis is carried out for the GS case. It is supposed that source signals are continuously zero for  $t < 0$ . Their time-domain waveforms are represented by piecewise continuous functions on any closed interval along the positive real line. They are absolutely and square absolutely integrable functions. In LTI passive circuits, input signals of  $L^1$  type ensure the existence of the Laplace integral for any current or voltage waveform on region  $\Re(s) \geq 0$ . The  $L^2$  type characterizes a signal of finite energy in time and represents a key assumption that helps describe the convergence condition in the sense of a weighted Lebesgue  $L^2$  norm in the time-domain. Let  $Z_{in1}(s)$  and  $Z_{in2}(s)$  be the input impedances of  $N_1$  and  $N_2$  taken both between nodes **a** and **c** when the two parts are directly connected (Figure 3.4), or between nodes **a** and **c** for  $N_1$  and **b** and **c** for  $N_2$  in the presence of element  $Z_o(s)$  (Figure 3.5). The condition of convergence is given by the next theorem

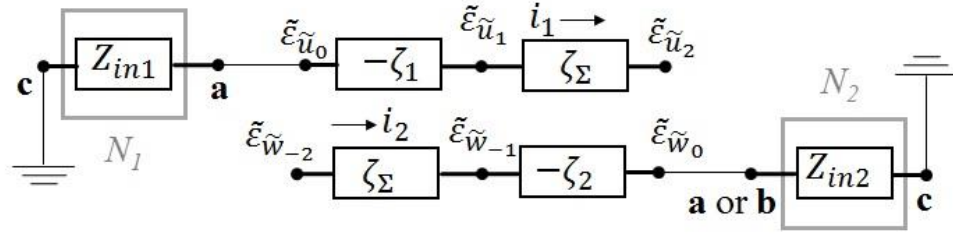


**Figure 3.5: Convergence analysis circuit.**

*Theorem 3.2. (condition of convergence).* The dissipative impedance coupling-based WR admits a convergence factor  $\rho(s)$  defined as

$$\rho(s) = \frac{(Z_{in1}(s) - \zeta_1(s))(Z_{in2}(s) - \zeta_2(s))}{(Z_{in1}(s) - \zeta_1(s) + \zeta_\Sigma(s))(Z_{in2}(s) - \zeta_2(s) + \zeta_\Sigma(s))} \quad (3.21)$$

It converges for all time  $t \geq 0$  if and only if  $|\rho(s)| < 1$  for all  $s \in \mathbb{C}$  and  $\Re(s) \geq 0$ .

*Proof.* In the time-domain, modified nodal analysis (MNA) formulation of circuit equations leads in general to systems of linear differential algebraic equations (DAE) or delay differential algebraic equations (DDAE) with discrete constant delays and constant coefficients. Let  $\mathbf{x}(t)$  be the vector of all current and voltage variables in the MNA equations. If  $\boldsymbol{\varepsilon}_x^{(k)}(t)$  represents the difference between the exact solution  $\mathbf{x}(t)$  and its  $k^{th}$  iterate  $\mathbf{x}^{(k)}(t)$  at iteration  $k$ :  $\boldsymbol{\varepsilon}_x^{(k)}(t) = \mathbf{x}(t) - \mathbf{x}^{(k)}(t)$  then, error  $\boldsymbol{\varepsilon}_x^{(k)}(t)$  is a solution of the subsequent homogeneous linear DAE or DDAE with homogeneous initial conditions. The Laplace transform  $\tilde{\boldsymbol{\varepsilon}}_x^{(k)}(s) = \tilde{\mathbf{x}}(s) - \tilde{\mathbf{x}}^{(k)}(s)$  of error  $\boldsymbol{\varepsilon}_x^{(k)}(t)$ , satisfies the frequency-domain formulation of the homogeneous system obtained after replacing subcircuits  $N_1$  and  $N_2$  with their input impedances  $Z_{in1}(s)$  and  $Z_{in2}(s)$  in Figure 3.7.

First, recursive equations (3.1) and (3.2) are expressed in terms of the iteration errors  $\varepsilon_{u_1}(t)$ ,  $\varepsilon_{u_2}(t)$ ,  $\varepsilon_{w_{-1}}(t)$  and  $\varepsilon_{w_{-2}}(t)$  in voltages  $u_1(t)$ ,  $u_2(t)$ ,  $w_{-1}(t)$  and  $w_{-2}(t)$  as follows

$$\tilde{\varepsilon}_{u_2}^{(k+1)}(s) = \tilde{\varepsilon}_{w_{-1}}^{(k)}(s) \quad (3.22)$$

$$\tilde{\varepsilon}_{\tilde{w}_{-2}}^{(k+1)}(s) = \tilde{\varepsilon}_{\tilde{u}_1}^{(k+v)}(s) \quad (3.23)$$

in the frequency domain. Next, replacing  $\tilde{\varepsilon}_{\tilde{u}_1}(s)$  and  $\tilde{\varepsilon}_{\tilde{w}_{-1}}(s)$  by their expressions

$$\tilde{\varepsilon}_{\tilde{u}_1}(s) = \rho_{1/2}(s) \tilde{\varepsilon}_{\tilde{u}_2}(s) \quad (3.24)$$

$$\tilde{\varepsilon}_{\tilde{w}_{-1}}(s) = \rho_{2/1}(s) \tilde{\varepsilon}_{\tilde{w}_{-2}}(s) \quad (3.25)$$

$$\rho_{1/2}(s) = (Z_{in1}(s) - \zeta_1(s)) / (Z_{in1}(s) - \zeta_1(s) + \zeta_\Sigma(s)) \quad (3.26)$$

$$\rho_{2/1}(s) = (Z_{in2}(s) - \zeta_2(s)) / (Z_{in2}(s) - \zeta_2(s) + \zeta_\Sigma(s)) \quad (3.27)$$

obtained with voltage divider formula in (3.22) and (3.23) at iteration  $(k + 2)$  leads to

$\tilde{\varepsilon}_{\tilde{u}_2}^{(k+2)}(s) = \rho_{2/1}(s) \tilde{\varepsilon}_{\tilde{u}_1}^{(k)}(s)$  and  $\tilde{\varepsilon}_{\tilde{w}_{-2}}^{(k+2)}(s) = \rho_{1/2}(s) \tilde{\varepsilon}_{\tilde{w}_{-1}}^{(k)}(s)$ . Applying eqs. (3.24) and (3.25) a second time leads to  $\tilde{\varepsilon}_{\tilde{u}_2}^{(k+2)}(s) = \rho_{1/2}(s) \rho_{2/1}(s) \tilde{\varepsilon}_{\tilde{u}_1}^{(k)}(s)$  and  $\tilde{\varepsilon}_{\tilde{w}_{-2}}^{(k+2)}(s) = \rho_{1/2}(s) \rho_{2/1}(s) \tilde{\varepsilon}_{\tilde{w}_{-1}}^{(k)}(s)$ , and to the following general expressions

$$\tilde{\varepsilon}_{\tilde{u}_2}^{(2k)}(s) = \left( \rho_{1/2}(s) \rho_{2/1}(s) \right)^k \tilde{\varepsilon}_{\tilde{u}_2}^{(0)}(s) \quad (3.28)$$

$$\tilde{\varepsilon}_{\tilde{w}_{-2}}^{(2k)}(s) = \left( \rho_{1/2}(s) \rho_{2/1}(s) \right)^k \tilde{\varepsilon}_{\tilde{w}_{-2}}^{(0)}(s) \quad (3.29)$$

Error sequences  $\left( \tilde{\varepsilon}_{\tilde{u}_2}^{(2k)} \right)_{k \in \mathbb{N}}$   $\left( \tilde{\varepsilon}_{\tilde{w}_{-2}}^{(2k)} \right)_{k \in \mathbb{N}}$  converge to zero if and only if  $|\rho_{1/2} \rho_{2/1}| < 1$  for all  $s \in \mathbb{C}$  and  $\Re(s) \geq 0$ . Coefficient  $\rho(s) = \rho_{1/2}(s) \rho_{2/1}(s)$  represents the convergence factor of the proposed WR algorithm.

Next, the implication of condition  $|\rho(s)| < 1$  for  $s \in \mathbb{C}$  and  $\Re(s) \geq 0$ , must be sought for what concerns time-domain errors. Since a LTI system that is passive is also causal [100] and because all signals are continuously zero for  $t < 0$ , unilateral Laplace transform  $\tilde{\varepsilon}_{\tilde{u}_2}(s)$  of  $\varepsilon_{u_2}(t)$  and Fourier transform  $\hat{E}_{\tilde{u}_2}(i\omega)$  of function  $E_{u_2}(t) = e^{-\sigma t} \varepsilon_{u_2}(t)$  are related by:

$$\tilde{\varepsilon}_{\hat{u}_2}(\sigma + i\omega) = \hat{E}_{\hat{u}_2}(i\omega)$$

$$s = \sigma + i\omega, \sigma \geq 0, \omega \in \mathbb{R}, \text{ and } i^2 = -1 \quad (3.30)$$

A similar relation is also derived for error  $\varepsilon_{w_{-2}}(t)$ . Replacing  $\tilde{\varepsilon}_{\hat{u}_2}^{(2k)}(s)$  and  $\tilde{\varepsilon}_{\hat{u}_2}^{(0)}(s)$  in (3.28) by their corresponding Fourier transforms in (3.30), then taking the square of their absolute values leads to

$$\left| \hat{E}_{\hat{u}_2}^{(2k)}(i\omega) \right|^2 \leq \left( \sup_{\substack{\sigma \geq 0 \\ \omega \in \mathbb{R}}} |\rho(\sigma + i\omega)| \right)^{2k} \left| \hat{E}_{\hat{u}_2}^{(0)}(i\omega) \right|^2 \quad (3.31)$$

Rate  $\rho(s)$  in (3.21) is analytic on region  $\sigma \geq 0$  by the properties of strictly positive-real functions [92],[96]. Hence, its modulus  $|\rho(s)|$  possesses a maximum by the maximum principal of complex analytic functions [92] and inequality (3.31) is therefore justified. Next, integrating both sides in inequality (3.31) on the real line leads to

$$\int_{-\infty}^{+\infty} \left| \hat{E}_{\hat{u}_2}^{(2k)}(i\omega) \right|^2 d\omega \leq \left( \sup_{\substack{\sigma \geq 0 \\ \omega \in \mathbb{R}}} |\rho(\sigma + i\omega)| \right)^{2k} \int_{-\infty}^{+\infty} \left| \hat{E}_{\hat{u}_2}^{(0)}(i\omega) \right|^2 d\omega \quad (3.32)$$

since  $\varepsilon_{u_2} \in L^1(\mathbb{R}) \cap L^2(\mathbb{R})$ . Finally, The application of Parseval formula [101] results in the following interpretation of (3.32) in the time-domain

$$\left\| e^{-\sigma t} \varepsilon_{u_2}^{(2k)}(t) \right\|_{L^2} \leq \left( \sup_{\omega \in \mathbb{R}} |\rho(\sigma + i\omega)| \right)^k \left\| e^{-\sigma t} \varepsilon_{u_2}^{(0)}(t) \right\|_{L^2} \quad (3.33)$$

Condition  $|\rho(s)| < 1$  ensures WR converge for all time  $t \geq 0$  in the sense of a weighted  $\|e^{-\sigma t} \cdot\|_{L^2}$  norm when  $\sigma > 0$  and in the sense of  $L^2$  norm when  $\sigma = 0$ . ■

Next, the optimal impedances  $\zeta_1(s)$  and  $\zeta_2(s)$  are derived from the expression of the local convergence rate  $\rho(s)$  in (3.21).

*Theorem 3.3. (optimal convergence for two subsystems).* Dissipative coupling WR algorithm converges in two iterations if  $\zeta_1(s) = Z_{in1}(s)$  or  $\zeta_2(s) = Z_{in2}(s)$  independently of initial waveforms.

*Proof.* It suffices to notice that  $\zeta_1(s) = Z_{in1}(s)$  or  $\zeta_2(s) = Z_{in2}(s)$  makes  $\rho(s)$  vanish and results in  $\tilde{\varepsilon}_{\tilde{u}_2}^{(2)}(s) = \tilde{\varepsilon}_{\tilde{u}_2}^{(3)}(s) = \tilde{\varepsilon}_{\tilde{u}_2}^{(4)}(s) = \dots = 0$ . Convergence occurs after two iterations. ■

Transmission condition equations (3.11),(3.12) and (3.17),(3.18) are optimal when  $\zeta_1(s) = Z_{in1}(s)$  and  $\zeta_2(s) = Z_{in2}(s)$  for a two-subsystem partition. According to [75, Thm. 4.1], WR method converges in exactly  $N$  GJ iterations for  $N$  cascaded sub-systems when all its transmission conditions are optimal. The following theorem presents a circuit interpretation of such optimal result.

*Theorem 3.4. (optimal convergence for  $N$  cascaded subsystems).* Dissipative impedance coupling-based WR algorithm converges in  $N$  GJ iterations for  $N$  cascaded parts, if every two consecutive parts  $P_l$  and  $P_{l+1}$ ,  $1 \leq l \leq N - 1$  are decoupled with  $\zeta_l(s)$  and  $\zeta_{l+1}(s)$  taken exactly equal to their input impedances at the interface between them.

Rate  $\rho(s)$  in (3.21) is an analytic complex function of frequency  $s$  [92],[96]. It attains its maximum on the boundary of its domain of definition  $\Re(s) = \sigma \geq 0$  according to the maximum principle [92]. The results of Theorems 3.3 and 3.4 allow an informed choice on the type of approximations to consider for a given circuit partition. Any approximation  $\zeta(s)$  must be of lower order than  $Z(s)$  to expect a cost-efficient WR algorithm. In transmission line circuits, the interconnect dominated subcircuit behaves as a low pass filter due to the dielectric shunt distributive capacitance of its lines. When  $\sigma \rightarrow \infty$  or  $\omega \rightarrow \infty$  ie  $|s| \rightarrow \infty$ , the interconnect becomes a resistance after the reactive part of its input impedance  $Z(s)$  dies out. Any valid approximation  $\zeta(s)$  is expected to produce a similar low-pass filter behavior or at least stay constant, which makes  $|\rho(s)| < 1$ . The presence of overlap  $Z_o$  between two interconnect parts in the circuit will further lower the limit value of  $|\rho(s)|$  at high frequencies (3.21). For  $\sigma = 0$  and  $\omega \rightarrow 0$ , the input impedance  $Z(s)$  of an interconnect dominated subcircuit increases rapidly due its reactive part. A

valid approximation  $\zeta(s)$  must also have the same behavior or at least stay constant. Since the order of  $\zeta(s)$  is less than the order of  $Z(s)$ , kernel  $\zeta(s)$  is not expected to increase as quickly as  $Z(s)$ , which will increase  $|\rho(s)|$  and makes it close to one. The analytic function  $\rho(s)$  attains its maximum values on the part  $\sigma = 0$  of the boundary of its domain of definition. Condition (3.33) is considered for  $L^2$  norm, and convergence analysis is performed in Fourier domain. Moreover,  $\rho(i\omega)$  in (3.21) satisfies  $|\rho(i\omega)| = |\rho(-i\omega)|$  for all  $\omega \in \mathbb{R}$  [96, Chap. 1]. The time-domain condition of convergence (3.33) can be simplified to

$$\|\varepsilon_{u_2}^{(2k)}(t)\|_{L^2} \leq \left( \sup_{\omega \geq 0} |\rho(i\omega)| \right)^k \|\varepsilon_{u_2}^{(0)}(t)\|_{L^2} \quad (3.34)$$

The proof of *Theorem 3.2* concerns a continuous WR algorithm where exact solution  $\mathbf{x}(t)$  is known. In practice,  $\mathbf{x}(t)$  is a priori unavailable to compute errors  $\varepsilon_{u_2}^{(k)}(t)$  and  $\varepsilon_{w_{-2}}^{(k)}(t)$  after every iteration  $k$ . To monitor convergence, the relaxation algorithm instead calculates differences  $e_{u_2}^{(k+1)}(t) = u_2^{(k+1)}(t) - u_2^{(k)}(t)$  and  $e_{w_{-2}}^{(k+1)}(t) = w_{-2}^{(k+1)}(t) - w_{-2}^{(k)}(t)$ ,  $k \in \mathbb{N}$ , from the last two iterates of its external variables  $u_2(t)$  and  $w_{-2}(t)$  at the end of every iteration  $(k + 1)$ . Similarly, it is found that errors  $e_{u_2}(t)$  and  $e_{w_{-2}}(t)$  satisfy same recurrent relations  $\tilde{e}_{\tilde{u}_2}^{(k+2)}(s) = \rho(s) \tilde{e}_{\tilde{u}_2}^{(k)}(s)$  and  $\tilde{e}_{w_{-2}}^{(k+2)}(s) = \rho(s) \tilde{e}_{w_{-2}}^{(k)}(s)$  in the frequency-domain and also show convergence for the same condition  $|\rho(i\omega)| < 1$ ,  $\omega \geq 0$ . The practical WR iteratively approaches the solution on discrete time instants. The Euclidian norm naturally replaces the  $L^2$  norm. However, any other norm can also be used in the discretized WR since the solution space is of finite dimension where all norms are equivalent.

Next, a coupling strategy is presented for the WR analysis of transmission line circuits. The assignment-partitioning step of the proposed method concerns the one-node overlap case (Figure 3.1). Coupling impedances  $\zeta_1(i\omega)$  and  $\zeta_2(i\omega)$  in every neutral insertion  $\{-\zeta_1(i\omega), \zeta_\Sigma(i\omega), -\zeta_2(i\omega)\}$ , which represent the operators' kernels in the companion transmission condition equations (3.11),(3.12) are constant and rational-with-delay functions in the frequency-domain.



### 3.2.4 Coupling strategy

The partitioning scheme described in section 2.1.6 of this thesis or in [97, Sec. II.F], is used to locate potential nodes where insertions  $\{-\zeta_1(i\omega), \zeta_\Sigma(i\omega), -\zeta_2(i\omega)\}$  are added in the circuit. Every subcircuit contains one transmission line. Every added insertion  $(-\zeta_k^{k,l}(i\omega), \zeta_\Sigma^{k,l}(i\omega), -\zeta_l^{k,l}(i\omega))$  at a split node between subcircuit  $N_k$  and a neighbor  $N_l$ , appends  $N_k$  with two series impedances  $(-\zeta_k^{k,l}(i\omega))$  and  $\zeta_\Sigma^{k,l}(i\omega)$  whose equivalent impedance  $\zeta_l^{k,l}(i\omega) = -\zeta_k^{k,l}(i\omega) + \zeta_\Sigma^{k,l}(i\omega)$ . Every input impedance  $Z_k^{k,l}(i\omega)$  of the enlarged subcircuit of  $N_k$  is taken at the split node between  $N_k$  and its neighbor  $N_l$ . An efficient rational-with-delay approximation  $\zeta_k^{k,l}(i\omega)$  of the optimal kernel  $Z_k^{k,l}(i\omega)$  must capture the system delay of the enlarged subcircuit  $N_k$ . To avoid this complication,  $\zeta_k^{k,l}(i\omega)$  is set to capture the delay of the transmission line in  $N_l$  only by taking all  $\zeta_l^{k,l'}(i\omega)$ ,  $l' \neq l$ , from other insertions  $(-\zeta_k^{k,l'}(i\omega), \zeta_\Sigma^{k,l'}(i\omega), -\zeta_l^{k,l'}(i\omega))$  as resistances of apriori *ad hoc* known values. The objective is to simplify the approximation procedure, lower the number of rational-with-delay approximations, and keep the size of the enlarged parts minimum. The following points emanate from this discussion, they help decide whether a coupling impedance should be simply a constant or a rational-with-delay function.

1. Every two adjacent subcircuits are decoupled with a resistance and a rational-with-delay impedance.
2. Coupling impedances associated with the same subcircuit must be of same kind; all resistances or all rational-with-delay impedances.

The next point sets the values of the coupling resistances.

3. Every coupling resistance takes the value  $\min\{\sqrt{R/G}, \sqrt{L/C}, Z_{in}(j0)\}$  where  $R, L, C, G$  are the PUL parameters of the line in its associated subcircuit and  $Z_{in}(j0)$  is its input impedance at DC whenever available.

Once every two added serial impedances  $\left(-\zeta_k^{k,l'}(i\omega)\right)$  and  $\zeta_\Sigma^{k,l'}(i\omega)$ ,  $l' \neq l$ , are replaced with their equivalent  $\zeta_{l'}^{k,l'}(i\omega) = -\zeta_k^{k,l'}(i\omega) + \zeta_\Sigma^{k,l'}(i\omega)$  in the appended subcircuit of  $N_k$ , the resulting subcircuit possesses a well-defined structure: a serial connection of one single transmission line and two lumped and passive RLC circuits, one at each end. This circuit will represent a realization of the rational-with-delay approximation  $\zeta_k^{k,l}(i\omega)$  of  $Z_k^{k,l}(i\omega)$  after its unique transmission line is represented in the time-domain with a very coarse DEFACT macromodel [102],[103]. The main reason of using a coarse macromodel is not to capture the losses in the line but to capture a major part of its delay by means of the delay-extraction step of the DEFACT. An approach which gets more relevant when lines are long and low loss. The duplication of the passive lumped RLC circuits helps get approximation  $\zeta_k^{k,l}(i\omega)$  very close to  $Z_k^{k,l}(i\omega)$  at very low frequencies. The following analysis elaborates on this idea.

Using the exact transverse description of a single line [94], input impedance  $Z_k^{k,l}(i\omega)$  of the enlarged subcircuit  $N_k$  is estimated by

$$Z_k^{k,l}(i\omega) = V_Z(i\omega)/I_Z(i\omega) \quad (3.35)$$

$$\begin{bmatrix} V_Z(i\omega) \\ I_Z(i\omega) \end{bmatrix} = \left( \mathbf{a}(i\omega) e^{A+i\omega B} \mathbf{b}(i\omega) \right) \begin{bmatrix} 1 \\ 0 \end{bmatrix} \quad (3.36)$$

$$\mathbf{A} = \begin{bmatrix} 0 & -R \\ -G & 0 \end{bmatrix} d, \quad \mathbf{B} = \begin{bmatrix} 0 & -L \\ -C & 0 \end{bmatrix} d$$

where  $\mathbf{a}(i\omega) \in \mathbb{C}^{2 \times 2}$  is the chain parameter matrix of the RLC circuit located on the side where  $Z(i\omega)$  is measured. The second RLC circuit at the other end possesses a chain parameter matrix  $\mathbf{b}(i\omega) \in \mathbb{C}^{2 \times 2}$ . Term  $e^{A+i\omega B}$  is the matrix exponential stamp of the single line, and  $R$ ,  $L$ ,  $C$ ,  $G$  and  $d$  are its per unit length (PUL) parameters and physical length respectively [94]. The approximating impedance  $\zeta_k^{k,l}(i\omega)$  is expressed as follows

$$\zeta_k^{k,l}(i\omega) = V_\zeta(i\omega)/I_\zeta(i\omega) \quad (3.37)$$

$$\begin{bmatrix} V_\zeta(i\omega) \\ I_\zeta(i\omega) \end{bmatrix} = \left( \mathbf{a}(i\omega) \left( \prod_{r=1}^m e^{\frac{A}{2m}} e^{i\omega \frac{B}{m}} e^{\frac{A}{2m}} \right) \mathbf{b}(i\omega) \right) \begin{bmatrix} 1 \\ 0 \end{bmatrix} \quad (3.38)$$

By forcing  $I_Z = I_\zeta = 1A$  in (3.36) and (3.38), difference  $(Z_k^{k,l}(i\omega) - \zeta_k^{k,l}(i\omega))$  satisfies

$$\|Z_k^{k,l}(i\omega) - \zeta_k^{k,l}(i\omega)\| < \left\| \mathbf{a} \left( e^{A+j\omega B} - \prod_{r=1}^m e^{\frac{A}{2m}} e^{j\omega \frac{B}{m}} e^{\frac{A}{2m}} \right) \mathbf{b} \right\| \quad (3.39)$$

for  $\omega \geq 0$  in any sub-multiplicative norm. Difference  $(e^{A+i\omega B} - \prod_{r=1}^m e^{\frac{A}{2m}} e^{i\omega \frac{B}{m}} e^{\frac{A}{2m}})$  represents the macromodeling error [102]. It converges to zero when  $m \rightarrow \infty$ . In the search of the minimal order  $m$ , impedance mismatch  $\left| \frac{(Z_k^{k,l}(i\omega) - \zeta_k^{k,l}(i\omega))}{Z_k^{k,l}(i\omega)} \right|$  is computed iteratively and is used as an estimate for rate  $|\rho(i\omega)|$ . Order  $m$  is taken at the smallest value that yields  $\left| \frac{(Z_k^{k,l}(i\omega) - \zeta_k^{k,l}(i\omega))}{Z_k^{k,l}(i\omega)} \right| < 1$  for  $0 \leq \omega \leq \omega_{max}$  according to the pseudocode of Figure 3.6. Value  $\omega_{max}$  is the largest practically relevant frequency for TL problems [104].

---

**Input:** -Frequency sampling  $J$  of  $[0, f_{max}]$ .  
 -Matrices  $\mathbf{a}$  and  $\mathbf{b}$   
 -p.u.l parameters and length of TL of  $N_k$   
**Output:** DEPACT coarse model order  $m$

---

**Procedure** *Coarse\_Model\_Order*

1. **Begin**
  2. calculate  $Z_k^{k,l}(i\omega)$  using (21),(22)
  3. initialize  $m = 0$
  4. **Repeat**
  5. take  $m = m + 1$
  6. calculate  $\zeta_k^{k,l}(i\omega)$  using (23),(24)
  7. calculate  $\left| \frac{(Z_k^{k,l}(i\omega) - \zeta_k^{k,l}(i\omega))}{Z_k^{k,l}(i\omega)} \right|$
  8. **Until**  $\left| \frac{(Z_k^{k,l}(i\omega) - \zeta_k^{k,l}(i\omega))}{Z_k^{k,l}(i\omega)} \right| < 1$  on  $J$
  9. **Return**  $m$
  10. **End**
- 

**Figure 3.6: Computation of order  $m$  of coarse DEPACT model.**

Note that directives 1 and 2 do not produce a unique assignment for a given multi-subcircuit partition. They serve mainly to ensure all rational-with-delay approximations are constructed only for subcircuits where transmission lines are their only passive circuit elements with delay. Finally, the main steps in the application of the proposed method are summarized in Figure 3.7.

- 
1. Apply the partitioning scheme, see section 2.1.6, on a TL circuit  $N$  and obtain the set of  $M$  subcircuits  $N_k$ ,  $1 \leq k \leq M$ .
  2. Use directives 1 and 2 to set a type for every WR parameter in the partition.
  3. Use directive 3 to attribute a value to all coupling resistances.
  4. Construct all realizations of rational- with-delay approximations and their opposites.
  5. Augment all subcircuits.
  6. Group subcircuits into levels.
  7. Set all relaxation sources to zero DC.
  8. Set the number of rounds  $r = 1$
  9. Set the queue of work tasks to be executed, ordering levels in forward and backward directions.
  10. **FOR** every level **DO** the following in parallel using  $p$  processors
    - 10.1. Simulate all current sub-circuits for the entire time interval of interest.
    - 10.2. Update all upstream (downstream) relaxation sources  $w(t)$  using (4) in the forward (backward) direction.
  11. At the end of every round, compute error using [32, eq. (27)]
  12. **IF** error  $\leq$  tolerance, exit **ELSE GO TO** step 9.
- 

**Figure 3.7: Main steps in the application of the WR-LP algorithm.**

### 3.2.5 Computational cost analysis

The study concerns an arborescent TL circuit which contains  $n$  transmission lines. It is partitioned into  $n$  subcircuits grouped in  $m$  levels,  $m < n$ . Every level  $k$ ,  $k = 1, 2, \dots, m$  contains  $n_k$  non-adjacent subcircuits where  $n_1 \leq n_2 \leq \dots \leq n_m$  because of branching. A

cost analysis of a WR solution is challenging in the general case. To simplify the analysis, it is assumed that: 1) All subcircuits exhibit the same computational cost for time-domain analysis, which results in a balanced partition. 2) Every subcircuit in level  $k = 1, 2, \dots, m - 1$  branches out to  $q_k$  subcircuits in level  $k + 1$ , which necessitates  $n_{k+1}$  be a multiple of  $n_k$ . 3) For every level, the allocated coupling impedances to its subcircuits are either all resistances or all rational-with-delay functions built around DEFACT models of same order. The resulting enlarged subcircuits that belong to the same level have the same computational cost. This will eliminate any threads overlap due to differences in the cost analysis between these subcircuits. For a fixed number  $p$  of available processors, assumptions 1), 2) and 3) describe in fact a partition which yields a minimum-cost solution per level and per round.

The cost of solving the original circuit is  $\phi_o = O(\beta^\alpha n^\alpha)$ , where  $\beta$  denotes the size of one subcircuit and  $\alpha$  typically varies from 1.1 to 2.4 depending on the sparsity of circuit matrices [109]. If overhead due to memory latencies and sources update, is ignored; last point is justified since it is a basic exchange of nodal voltages, then the computational cost  $\phi_{WR}$  of a WR solution is approximated by

$$\phi_{WR} = r \varphi O(\beta^\alpha) \quad (3.40)$$

$$\varphi = \sum_{k=1}^m a_k \lceil n_k/p \rceil O((1 + b_k \Delta\beta/\beta)^\alpha)$$

$a_1 = a_m = 1$ , and  $a_k = 2$  otherwise.

where  $\lceil . \rceil$  is the ceiling operator,  $r$  is the number of rounds. and  $\Delta\beta$  represents the increase in the size  $\beta$  of a subcircuit caused by appending it with the realization of one rational-with-delay approximation. Coefficients  $b_k$  in (3.40) represent the increase in size  $\beta$  of subcircuits caused by the impedance coupling scheme. They are functions of fan-outs  $q_k$ . They also depend on the parities of number  $m$  and the enumeration  $k$  of the level whose subcircuits received rational-with-delay impedances, as reported in Table 3.1. Note that all subcircuits in levels  $k = 2, \dots, m - 1$  are solved twice per round, once in every direction, hence  $a_k = 2$ . Whereas subcircuits in levels 1 and  $m$  are solved once,

**Table 3.1: Coefficients. Computational cost analysis**

	m is even		m is odd	
	<b>A</b>	<b>B</b>	<b>A</b>	<b>B</b>
$b_1 =$	$2q_1$	$q_1$	$2q_1$	$q_1$
$b_{2k'} =$	$1 + q_{2k'}$	$2(1 + q_{2k'})$	$1 + q_{2k'}$	$2(1 + q_{2k'})$
$b_{2k+1} =$	$2(1 + q_{2k'+1})$	$1 + q_{2k'+1}$	$2(1 + q_{2k'+1})$	$1 + q_{2k'+1}$
$b_m =$	1	2	2	1

**A** (or **B**): Allocate rational-with-delay approximations to all subcircuits in odd (or

which amounts to  $a_1 = a_m = 1$ . To get an idea of the CPU time efficiency of the WR algorithm, cost ratio is considered

$$\phi_o/\phi_{WR} = O(n^\alpha)/(r\varphi) \quad (3.41)$$

Ideally, the cost of solving a n-subsystem partition with m levels can be brought down to  $r \sum_{k=1}^m a_k O((\beta + b_k \Delta\beta)^\alpha)$  with a number of processors  $p = \max(n_k)$ ,  $k \in [1, m]$ . In other words, the cost  $\phi_{WR}$  cannot be less than that of m cascaded subcircuits of sizes  $(\beta + b_k \Delta\beta)$ ,  $1 \leq k \leq m$  and of same complexity  $\alpha$ . The WR efficiency has a maximum theoretical value  $O(n^\alpha)/(r \sum_{k=1}^m a_k O((1 + b_k \Delta\beta/\beta)^\alpha))$ .

### 3.2.6 Concluding remarks

Several relevant points regarding the theory and implementation of the proposed algorithm are worth noting.

- 1) When optimization is used to determine the best approximations of the optimal parameters, the set of constraints of the corresponding min-max problem represents

the conditions which ensure the positive realness of the approximating functions themselves.

- 2) The pseudocode of Figure 3.6 can be implemented in Matlab [105] or any other high-level language. The iterative process involves direct  $2 \times 2$  matrix operations and concerns low values of order  $m$ . The cost of the search is very low and does not have a significant impact on the efficiency of the method.
- 3) Main steps 4, 5 and 6 in the application of WR (Figure 3.7) can be automated using a DEPACT parameters generator with a circuit netlist generator to obtain the complete netlist of every extended subcircuit, or directly using a DEPACT matrices generator with selector matrices to construct the system matrices of every extended subcircuit
- 4) Numerical experiments showed that condition  $|(Z(i\omega) - \zeta(i\omega))/Z(i\omega)| < 1$  on  $[0, \omega_{max}]$  is conservative in the sense that the mismatch can exceed one on the high-frequency end of  $[0, \omega_{max}]$  and still yields local rate  $|\rho(i\omega)| < 1$ . The applicability of WR is subject to satisfying the convergence condition  $|\rho(i\omega)| < 1$  which can be verified on a frequency sampling of  $[0, \omega_{max}]$ . If the condition is violated at some frequency points, then order  $m$  can be increased.

### 3.3 Numerical Examples

Four transverse-electromagnetic-mode type TL circuits are produced and simulated using a custom circuit simulator which is implemented in MATLAB on a dual quad-core Xeon-Phi 2630 (1.6Ghz) machine with 64GB RAM. The first example shows the very fast convergence of impedance coupling for a two-line circuit. The second example illustrates the convergence scalability with the simulation window length for a cascade connection of transmission lines. In the third example, the solution of an arborescent TL circuit on a parallel machine shows further runtime saving. The fourth example compares impedance coupling with the optimized explicit result derived for RLCG type line [77]. In examples one, two and three, a comparison with resistive coupling [97] is also produced. In all examples, maximum truncation frequency  $f_{max}$  corresponds to the inverse rise/fall time of the input signal [104]. In examples one, two and three, TLs are represented with DEPACT model [102],[103]. All relaxations sources are set initially to a zero DC waveform unless stated otherwise. Convergence is obtained within a maximum

tolerance  $\varepsilon \leq 10^{-3}$ , see eq. (2.27). HSPICE [106] simulation waveforms are also provided to illustrate the correctness of WR results.

### 3.3.1 Example One-Proof of Concept

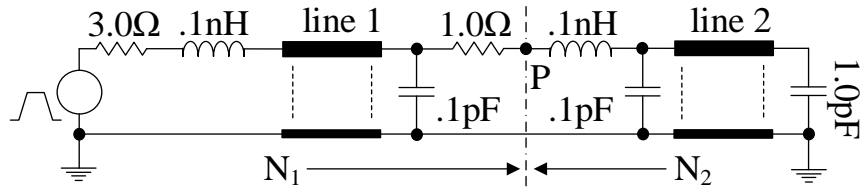


**Figure 3.8: Circuit of Example One.**

**Table 3.2: P.U.L parameters. Example One.**

	Low loss case		Lossy case	
	Line1	Line2	Line 1	Line 2
R[Ω/m]	2	5	10	12
L[H/m]	$5 \times 10^{-a}$	$3 \times 10^{-a}$	$5 \times 10^{-a}$	$3 \times 10^{-a}$
C[F/m]	$60 \times 10^{-b}$	$10 \times 10^{-b}$	$60 \times 10^{-b}$	$10 \times 10^{-b}$
G[S/m]	$10^{-9}$	$10^{-9}$	$5 \times 10^{-8}$	$5 \times 10^{-8}$
Length [m]	$10^{-2}$	$4 \times 10^{-2}$	$8 \times 10^{-2}$	$7 \times 10^{-2}$

$$a \in \{6,7\} \text{ and } b \in \{10,11,12\}$$

The circuit of Figure 3.8 is considered. It is driven by a 1V<sub>peak</sub> trapezoidal voltage pulse of 0.05ns rise/fall time and 2.10ns width through a 3Ω-resistance. The maximum practical frequency relevant to this problem is  $f_{max} = 1/0.05\text{ns} = 20\text{Ghz}$ . Every line in Figure 3.8 is represented with six sets of PUL parameters in Table II for the lossy and



low-loss cases, which makes it to a total of twelve combinations. Every combination is referred to by the word low-loss or lossy followed by value  $(a, b)$  where  $(a, b) \in \{6, 7\} \times \{10, 11, 12\}$ . The circuit is split at node P into two parts  $N_1$  and  $N_2$ . To implement the resistive coupling WR[97] (chapter 2), the min-max problem (eq. (2.15)) is solved on its four instances (eq. (2.16)) for every combination, and coupling resistances  $R_1$  and  $R_2$  are calculated. In low-loss (7,12) for example,  $R_1 = 100\Omega$  and  $R_2 = 103\Omega$  at objective function  $r = 0.925$  on the four instances. To implement the proposed algorithm, parts  $N_1$  and  $N_2$  are decoupled with impedance  $\zeta_1(i\omega)$  and resistance  $\zeta_2$  in arrangement Z-R, then with resistance  $\zeta_1$  and impedance  $\zeta_2(i\omega)$  in arrangement R-Z. Figure 3.10 presents the resulting two-subcircuit partition for arrangement R-Z of combination low-loss (7,12). Coupling impedance  $\zeta_1 = \sqrt{5.0 \times 10^{-7} / (6 \times 10^{-11})} = 91.3\Omega$  and the circuit realization of  $\zeta_2(i\omega)$  and its opposite  $(-\zeta_2(i\omega))$  are shown in Figure 3.10 for order  $m = 1$  after inspecting mismatch  $|(Z(i\omega) - \zeta(i\omega))/Z(i\omega)|$ , see Figure 3.9. The sparsity pattern of the MNA matrices of  $N_2$  and its enlarged subcircuit in Figure 3.11, show the effect of adding insertion  $(-\zeta_1, \zeta_1 + \zeta_2)$  to  $N_1$  and  $(-\zeta_2, \zeta_1 + \zeta_2)$  to  $N_2$  in the proposed method compared to no node addition in the resistive coupling scheme [97]. The total MNA space size of the partition increases from 21 in the resistive coupling method [97] to 40 in the R-Z arrangement of the proposed method. To perform the analysis in the two methods, the relaxation source of  $N_1$  is initialized with twenty DC waveforms. Their amplitudes are taken from a set of eighteen random values in interval  $]0, 1[$  plus values 0 and 1. For every initial guess, the two-subcircuit partitions are solved on  $[0, T]$ ,  $T = 50\text{ns}$ . In the case low-loss (7,12), the resistive coupling based WR [97] takes *at least* 72 iterations to converge at a cost of 169.53s. The proposed algorithm on the other hand, takes *at most* 2 iterations at a cost of 2.78s for its Z-R arrangement, and *at most* 4 iterations at a cost of 5.21s for its R-Z arrangement.

The above-mentioned steps are repeated for the remaining combinations and for both methods: resistive coupling based WR [97] vs proposed, and same data is collected and reported in Table III. In all combinations, it is found that a coarse DEPACT macromodel of order  $m = 1$  leads to a mismatch of magnitude less than one on  $[0, f_{max}]$ . In low-loss cases, the proposed method takes at most 2 to 4 iterations to converge against 11 to 72

iterations at least for [97]. In lossy cases, it is 2 to 4 iterations again against 4 to 45 iterations. Figure 3.12 and Figure 3.13 show the error decay as a function of the iteration in the limit cases: lossy(6,10) and low-loss (7,12) which correspond to the smallest and largest cost savings respectively. To contrast the speeds of convergence in the highly reactive case low-loss (7,12), convergence rates are reported on Figure 3.14. The superior convergence of the proposed method makes its iteration waveform approaches the solution in the early iterations as illustrated in Figure 3.15 compared to the iteration waveforms of the resistive coupling based WR in Figure 3.16.

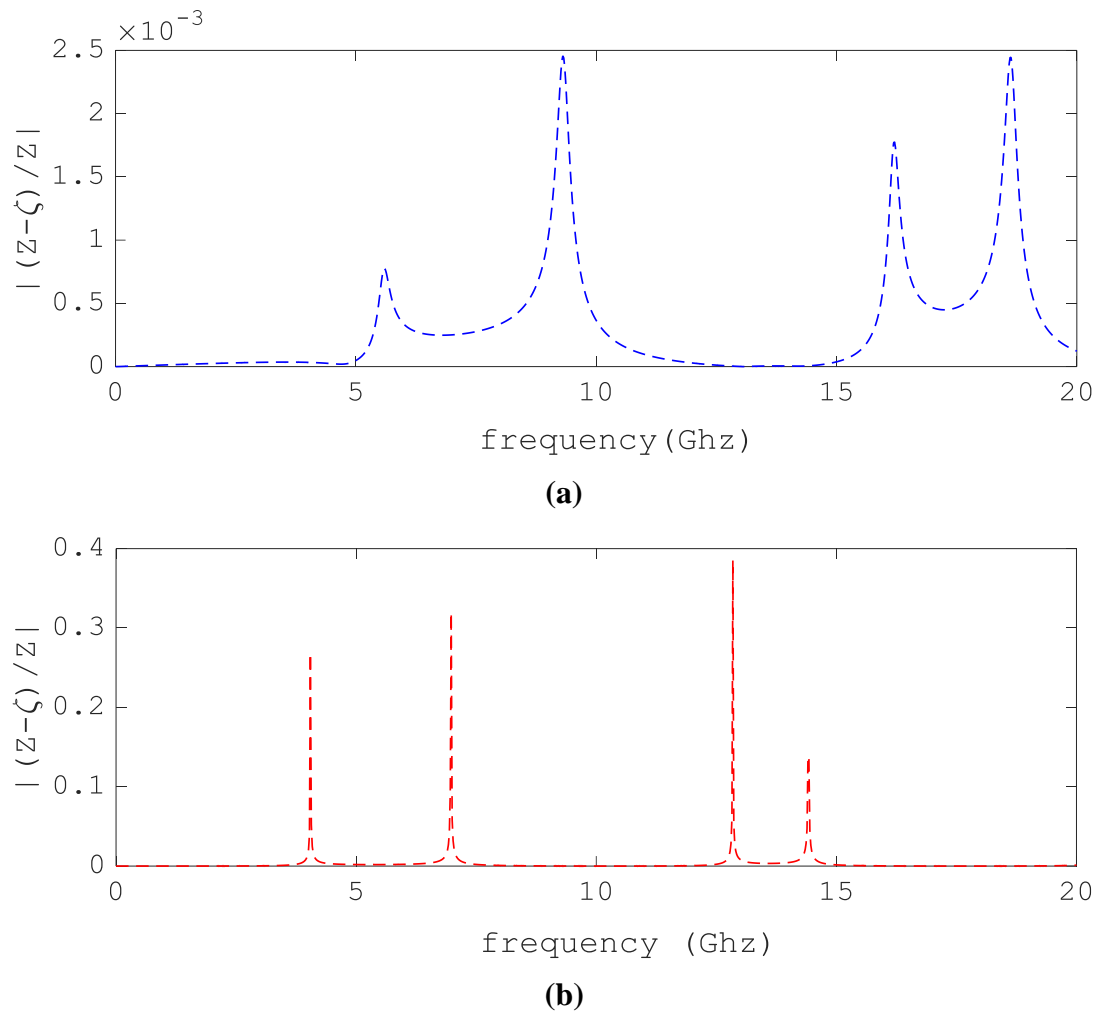


**Figure 3.9: Impedance mismatch for low-loss (7, 12). (a) Z-R disposition (b) R-Z disposition. Example One.**

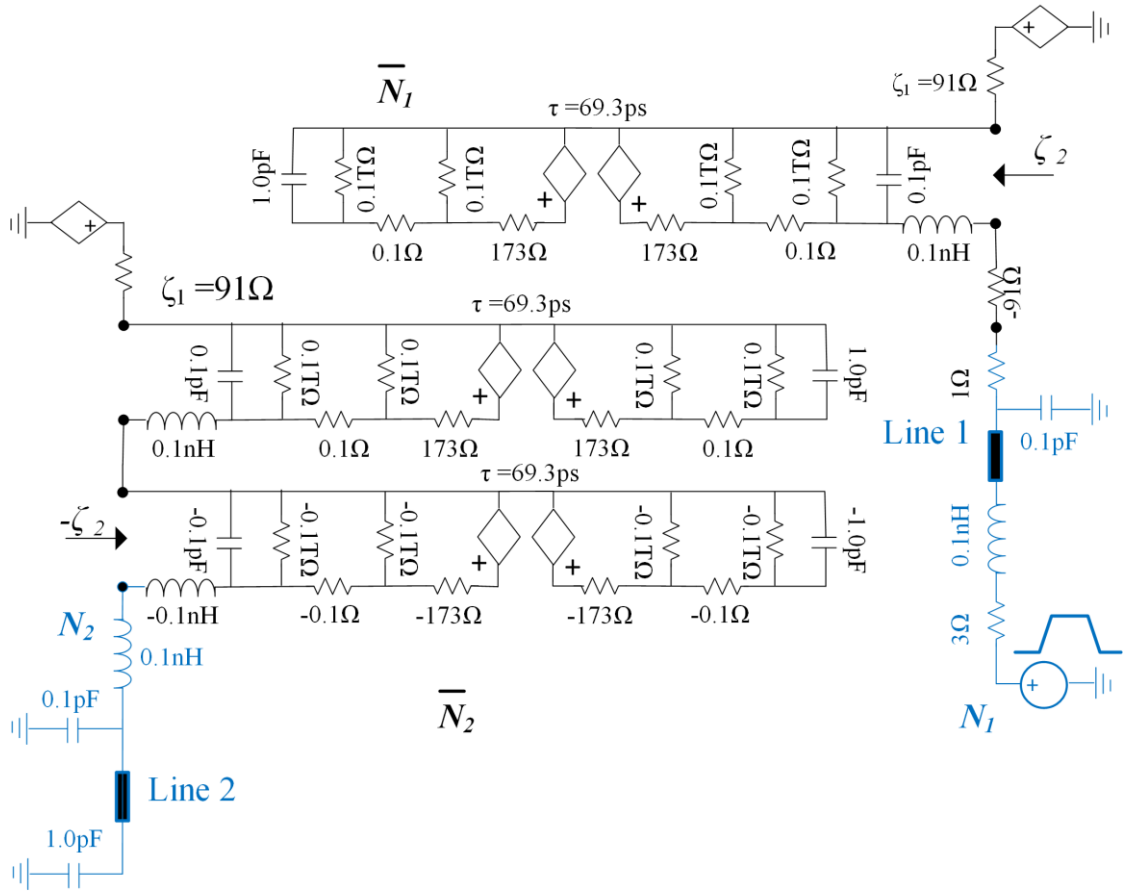


**Figure 3.10: Augmented subcircuits  $\bar{N}_1$  and  $\bar{N}_2$  of  $N_1$  and  $N_2$ . Low-loss (7, 12). Arrangement R-Z. Example One.**

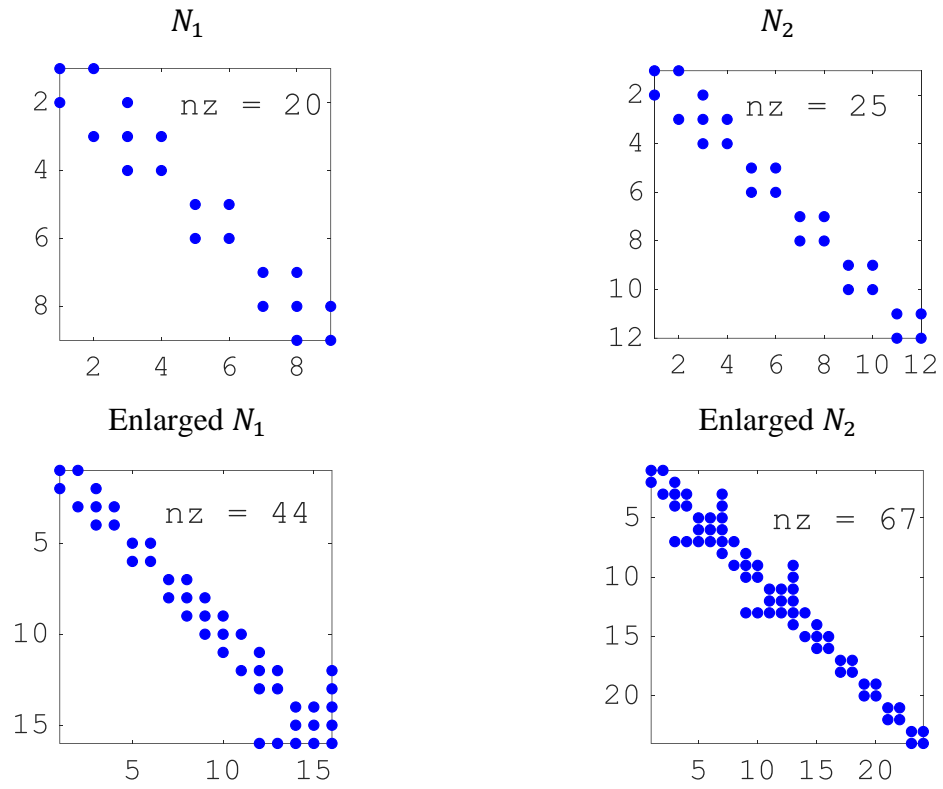


**Figure 3.11: Sparsity pattern of MNA matrices. Low-loss (7, 12). Top: Resistive coupling [97]. Bottom: Proposed R-Z. Example O.**

**Table 3.3: Performance of proposed algorithm. Example One.**

		<b>b</b>																						
		<b>10</b>			<b>11</b>			<b>12</b>			<b>10</b>			<b>11</b>			<b>12</b>							
		Nbr.	MNA	Cost	Nbr.	MNA	Cost	Nbr.	MNA	Cost	Nbr.	MNA	Cost	Nbr.	MNA	Cost	Nbr.	MNA	Cost	Nbr.	MNA	Cost		
		Iter.	Mat.	(s)	Iter.	Mat.	(s)	Iter.	Mat.	(s)	Iter.	Mat.	(s)	Iter.	Mat.	(s)	Iter.	Mat.	(s)	Iter.	Mat.	(s)		
			Sze.			Sze.			Sze.			Sze.			Sze.			Sze.			Sze.			
<b>a</b>	<b>6</b>	11	55	7.31	27	29	21.28	70	19	61.85	4	509	17.52	8	163	12.90	21	71	17.63				<b>[97]</b>	
		2	77	1.78	2	51	2.46	2	41	2.78	3	531	14.44	3	185	6.78	3	93	3.98				<b>Z-R</b>	
		3	74	3.29	3	48	3.51	4	38	5.21	3	528	14.24	4	182	8.63	4	90	5.32				<b>R-Z</b>	
	<b>7</b>	12	71	10.96	29	33	35.07	72	21	169.53	7	467	82.09	16	157	24.60	42	59	65.07				<b>[97]</b>	
		02	93	2.37	2	55	3.51	2	43	6.14	3	489	38.27	3	179	5.81	3	81	7.11				<b>Z-R</b>	
		4	90	4.61	3	52	5.80	4	40	12.11	4	486	51.10	4	176	7.76	4	78	9.40				<b>R-Z</b>	
Low-loss											Lossy													

Number of WR iterations to converge (Nbr. Iter.), MNA matrix size (MNA Mat. Sze.), CPU runtime of transient analysis in seconds (Cost).

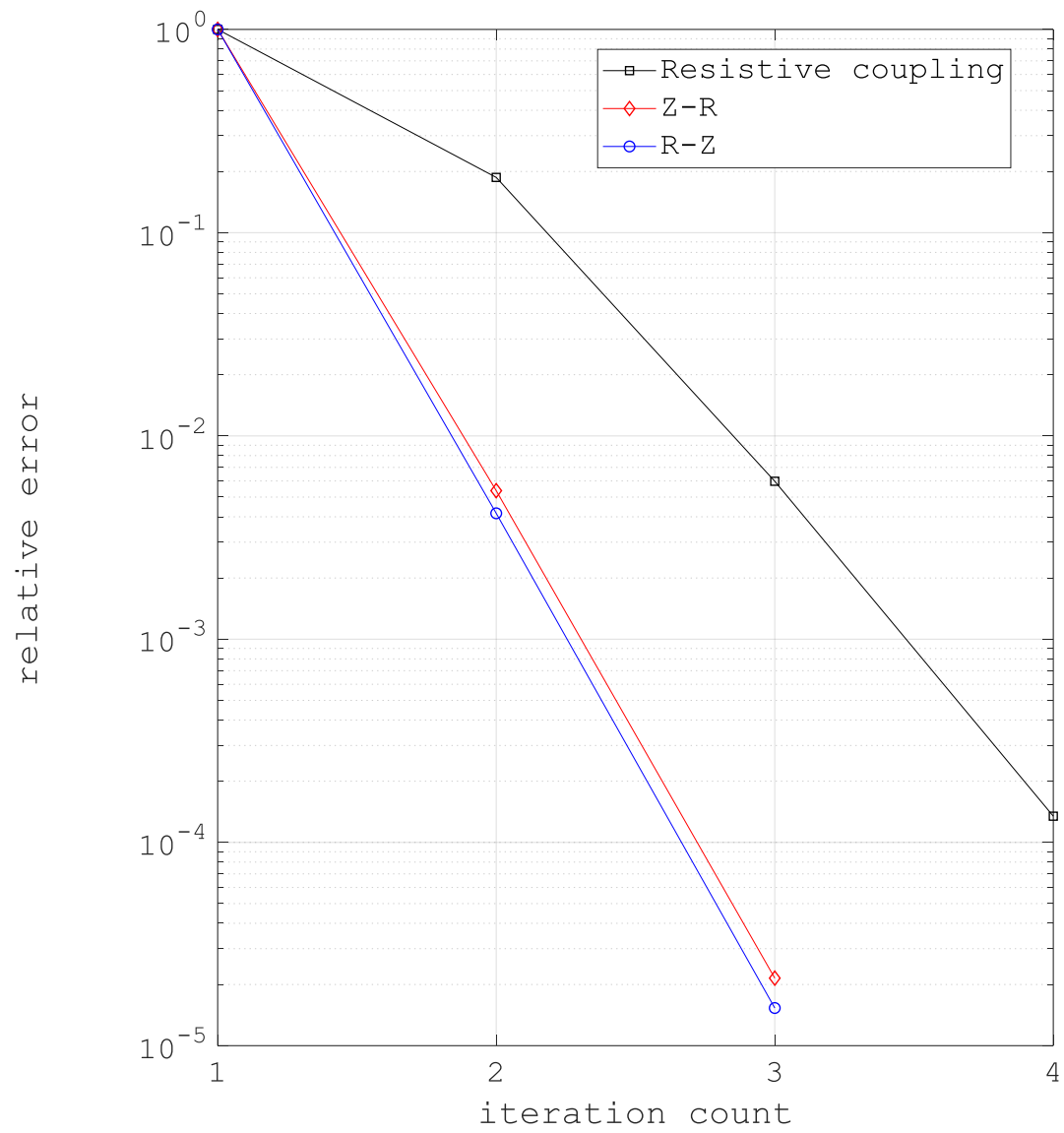


**Figure 3.12: Error decay. Lossy (6, 10). Example One.**

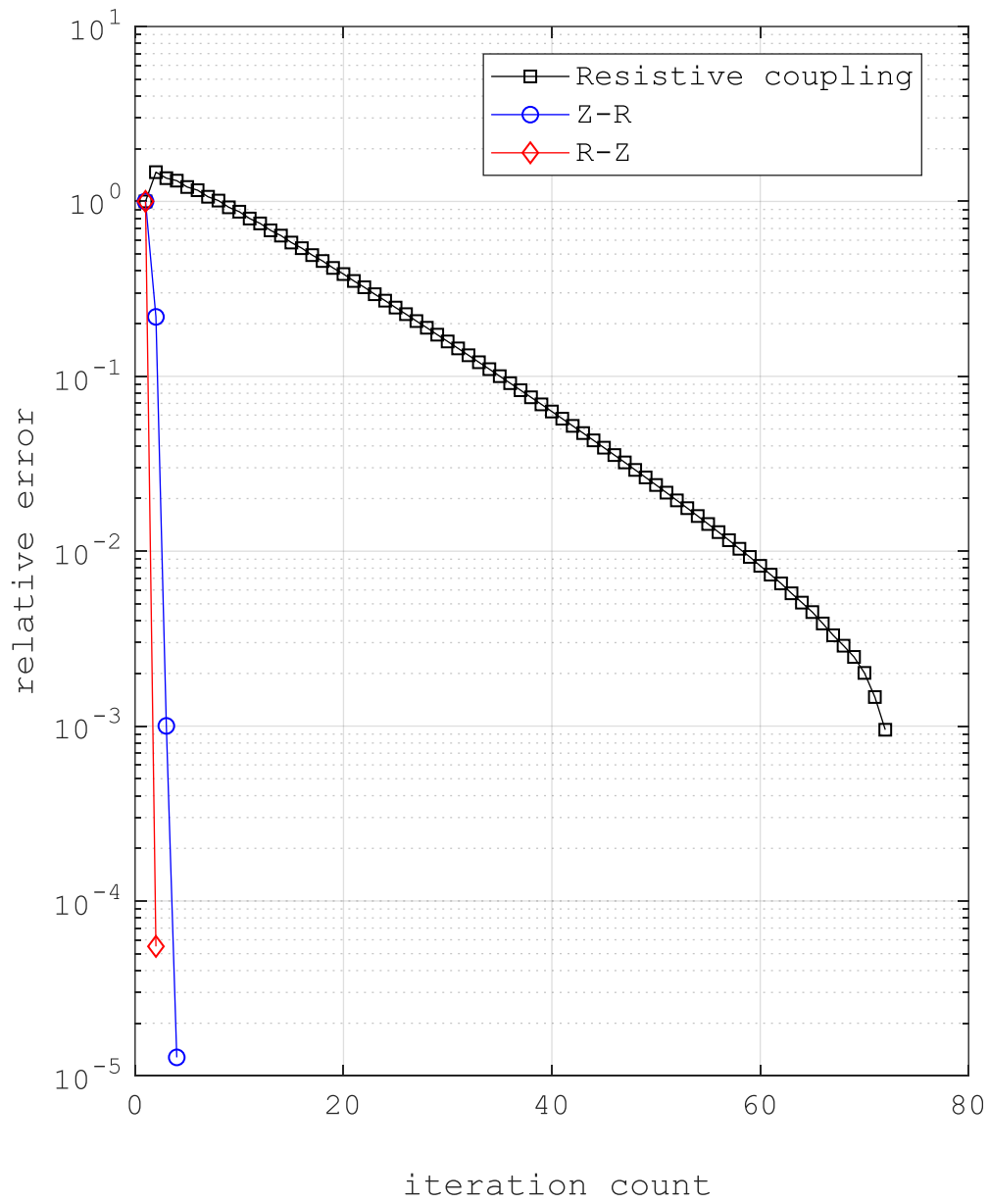


**Figure 3.13: Error decay. Low-loss (7, 12). Example One.**

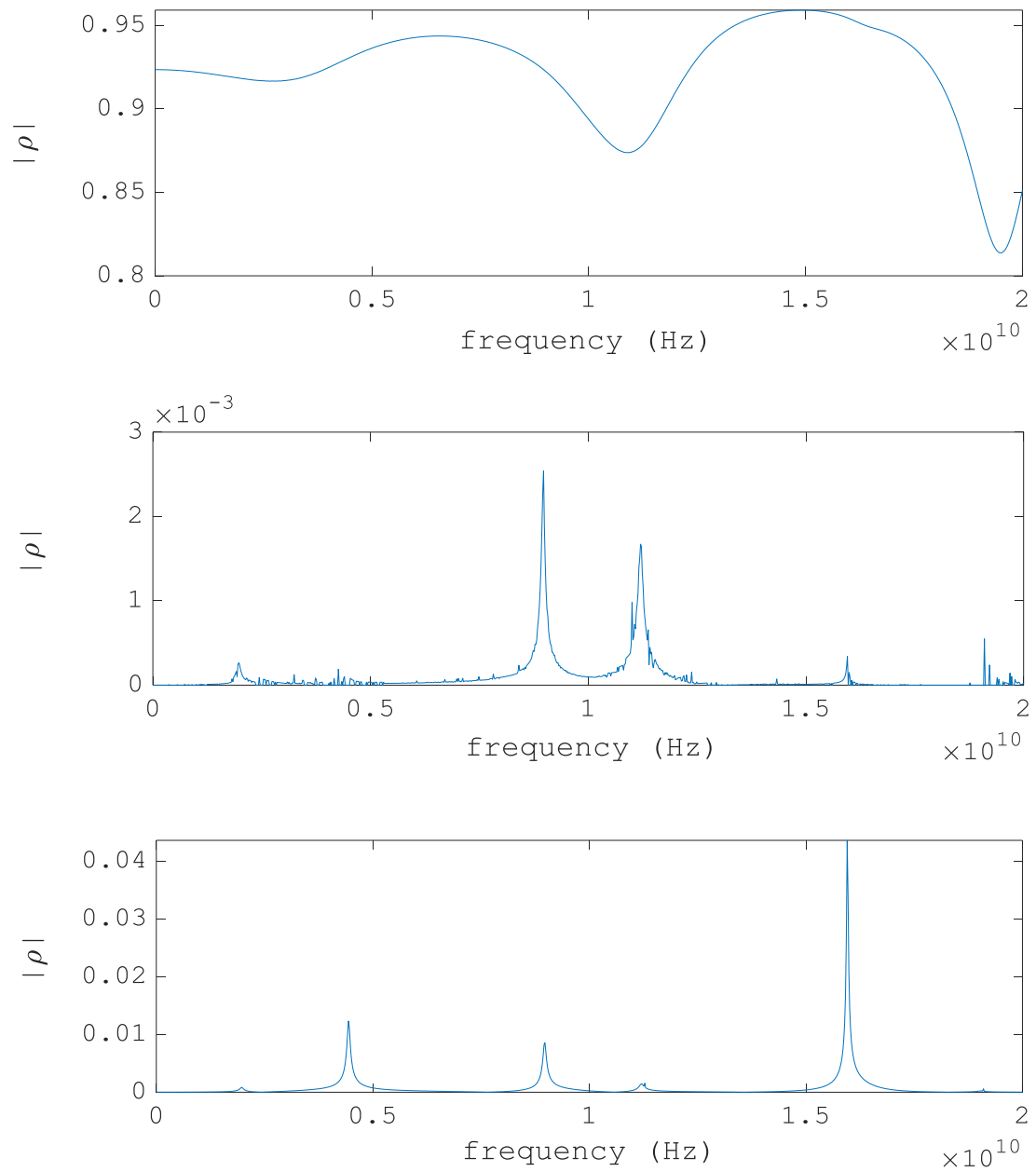


**Figure 3.14: Rate of convergence. Low-loss (7, 12). Top: Resistive coupling [97]. Middle: Proposed Z-R. Bottom: \_\_ R-Z. Example One.**



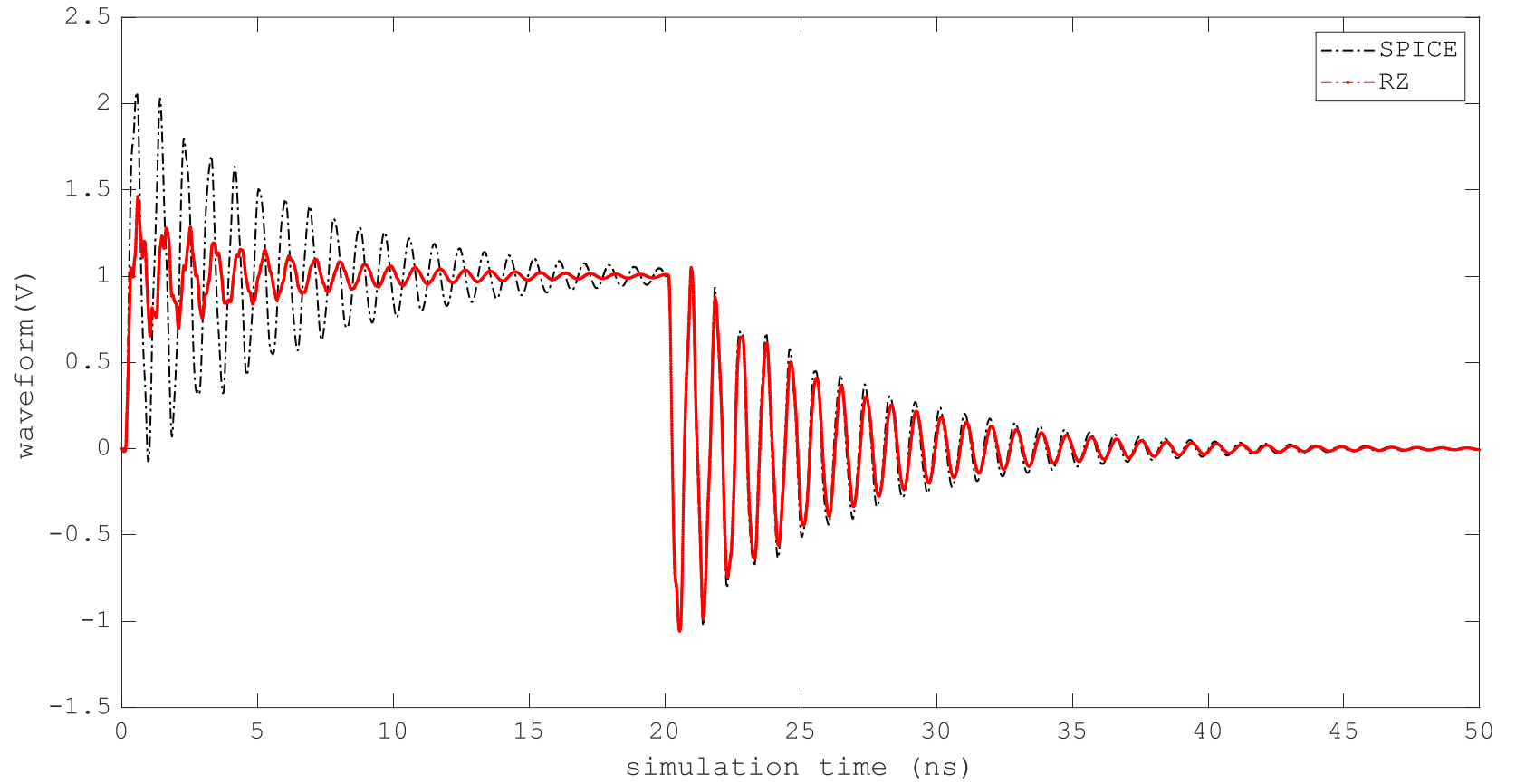


**Figure 3.15: Farend iteration waveform. Low-loss (7, 12). (b) Proposed (R-Z). Iteration one. Example One.**

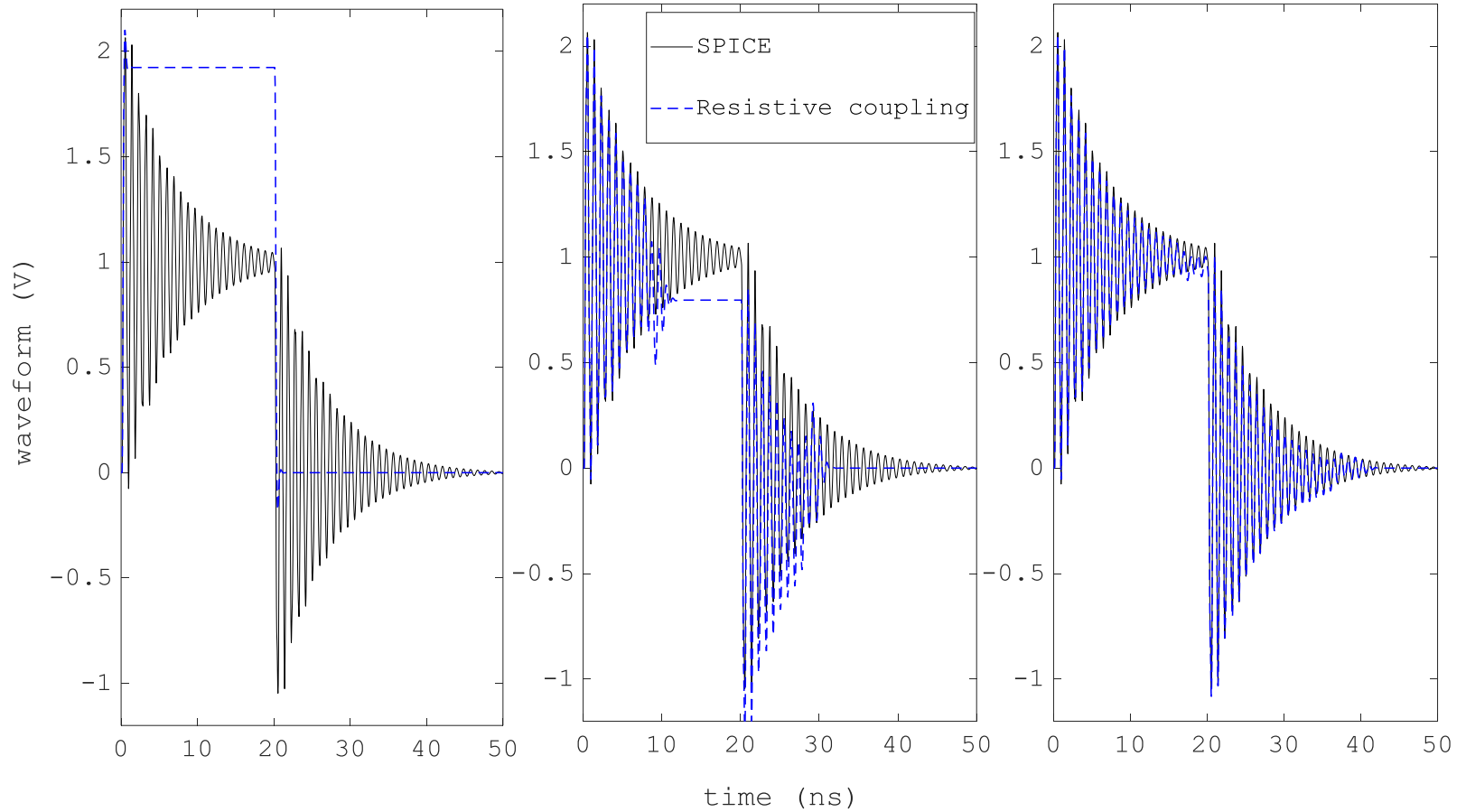


**Figure 3.16: Farend iteration waveform. Low-loss (7, 12). (a) Resistive coupling [97]. Left: Iteration one. Middle: iteration twenty. Right: Iteration forty. Example One.**

### 3.3.2 Example Two-Chain connection.

To illustrate the convergence behavior of the proposed method in the challenging case of a damped oscillatory alternating response, a cascade connection of ten blocks  $B_i$ ,  $1 \leq i \leq 10$ , is examined in Figure 3.17. Each block  $B_i$  represents a subcircuit and consists of one single line terminated with a grounded capacitor. The value of the capacitor is 0.1pF for blocks  $B_i$ ,  $1 \leq i \leq 9$ , and 1.0pF for block  $B_{10}$ . A 1Vpeak trapezoidal pulse source of 0.05ns-rise/fall time and 1.0ns-width drives the chain through a 10 $\Omega$ -internal resistance. PUL parameters are  $R = 5.0(2.0) \Omega/\text{m}$ ,  $L = 0.25(0.7) \mu\text{H}/\text{m}$ ,  $C = 7.0(60.0) \text{pF}/\text{m}$ ,  $G = 10.0(1.0) \text{nS}/\text{m}$  and length  $l = 10.0(3.0) \text{cm}$  for odd (even) block indices. In arrangement A, rational-with-delay impedances are constructed for blocks  $B_i$ ,  $i \in \{1,3,5,7,9\}$ , and use a coarse model of order  $m = 2$ , see Figure 3.18(a). In arrangement B, rational-with-delay impedances are constructed for blocks  $B_i$ ,  $i \in \{2,4,6,8,10\}$ , and use order  $m = 1$  for their coarse models, see Figure 3.18(b).

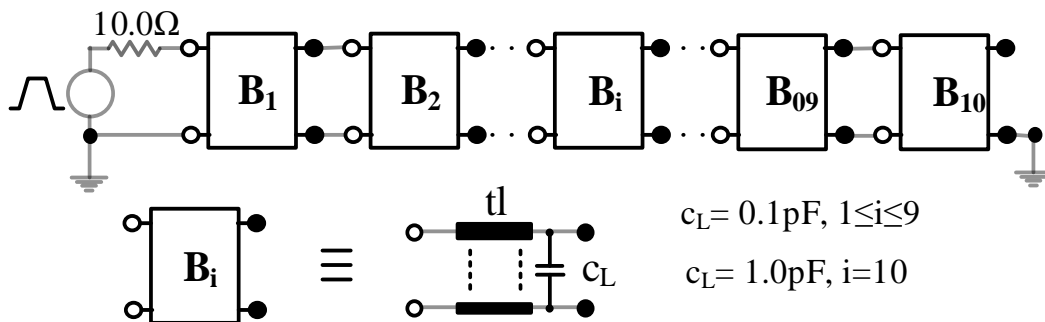


**Figure 3.17: Circuit of Example Two.**

The total MNA size of the partition is 361 in arrangement A and 307 in arrangement B, compared to 190 in the resistive coupling [97]. The two algorithms solve the two partitions on intervals  $[0, T]$  where  $T = 10\text{ns}$ ,  $15\text{ns}$ ,  $20\text{ns}$ ,  $25\text{ns}$  and  $30\text{ns}$ . The resulting numbers of rounds to converge and their costs are reported on Table 3.4. In comparison with resistive coupling WR [97], the proposed method achieves a speed-up which increases from almost  $4 \times$  for  $T = 10\text{ns}$  to more than  $5 \times$  for  $T = 30\text{ns}$  in arrangement A and from  $2 \times$  for  $T = 10\text{ns}$  to  $2.7 \times$  for  $T = 30\text{ns}$  in arrangement B.

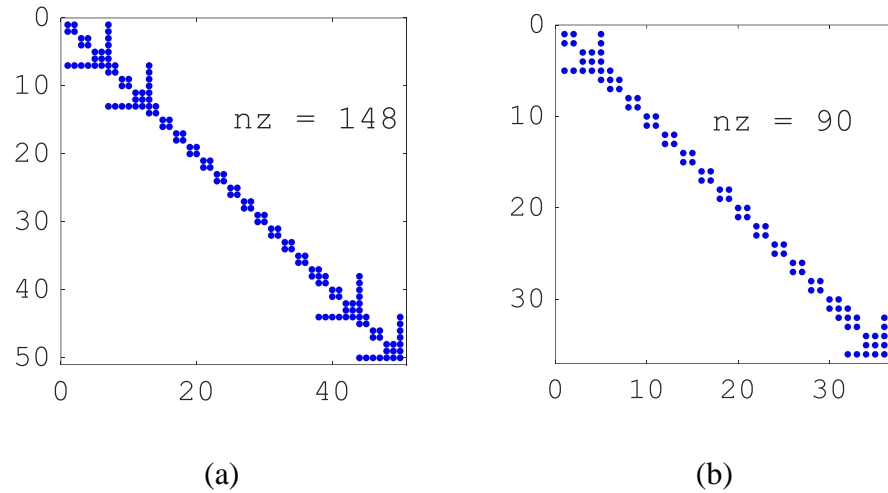


**Figure 3.18: Sparsity pattern of MNA matrices. Interior odd numbered subcircuit. Left: in arrangement A. Right: in arrangement B. Example Two.**

The proposed method scales better with length  $T$  of the simulation window than the resistive coupling based WR [97]. To contrast the difference in performance between the algorithms, Figure 3.19 shows the global error as a function of the round for  $T = 30$ ns, and Figures 3.20-3.22 illustrate the improvement in the magnitude of local convergence factors.

**Table 3.4: Performance of proposed algorithm. Example Two.**

Duration $T$ (ns)										
10		15		20		25		30		
Nbr.	Tran.	Nbr.	Tran.	Nbr.	Tran.	Nbr.	Tran.	Nbr.	Tran.	
Rds.	Cost	Rds.	Cost	Rds.	Cost	Rds.	Cost	Rds.	Cost	
265	775.1	412	1157.4	560	1541.9	708	1911.3	857	2795.1	<b>[97]</b>
15	78.8	22	116.6	29	158.2	35	197.4	42	285.1	<b>A</b>
13	63.1	19	93.8	24	125.9	30	157.8	35	219.7	<b>B</b>

Number of rounds to converge (Nbr. Rds.), CPU runtime of transient analysis in Seconds (Tran. Cost).

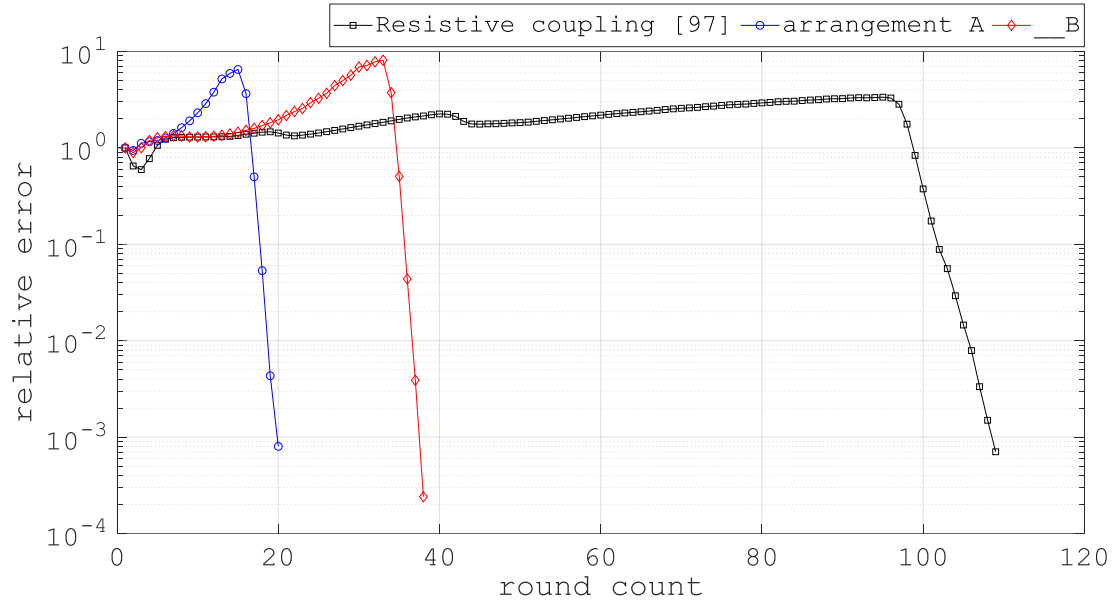


**Figure 3.19: Global error.  $T = 30\text{ns}$ . Example Two.**

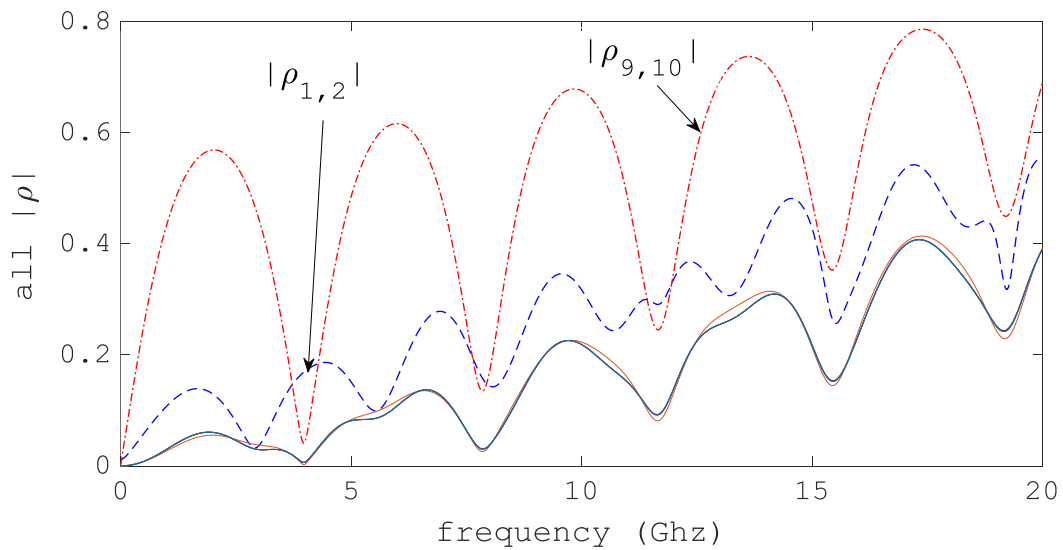


**Figure 3.20: Local convergence factors. Resistive coupling based WR [97]. Example Two.**

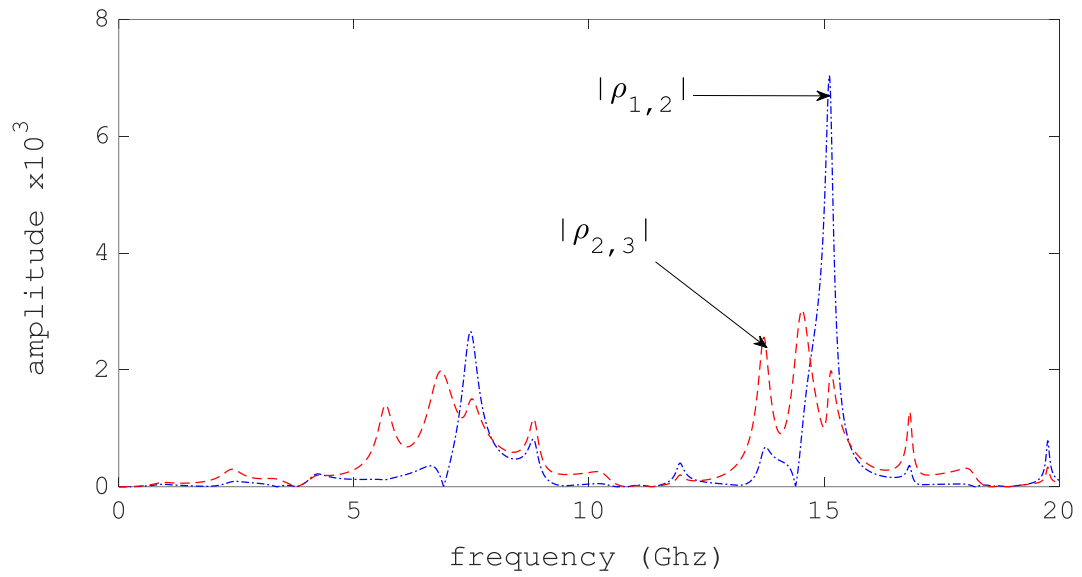


**Figure 3.22: Local convergence factors-I. Proposed, arrangement A. Example Two.**

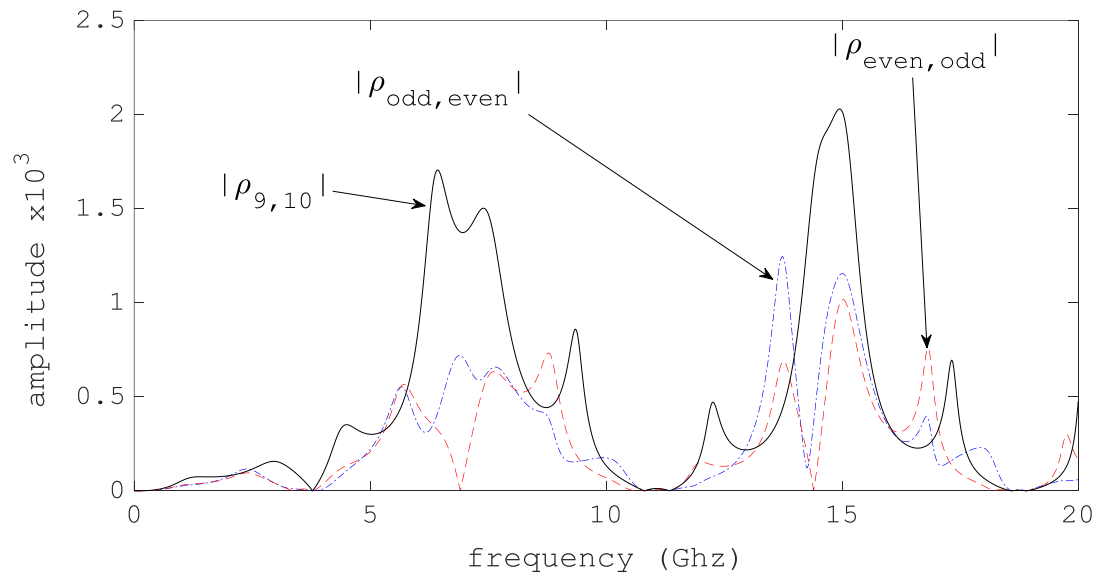


**Figure 3.21: Local convergence factors-II. Proposed, arrangement A. Example Two.**

The difference in convergence is also illustrated by the iteration waveforms in Figures 3.23-3.26. To show clearly the extent of the achieved convergence along the iteration waveforms, a zoom in was performed by clipping the parts of the waveforms outside interval  $[-3, +3]$  at round 10 for both methods in Figure 3.25 and in round 17 for the resistive coupling WR [97] alone in Figure 3.26(Left). Saving in the number of rounds offsets the increase in the cost of the round and makes impedance coupling run up to  $3 \times$  and  $2 \times$  faster for arrangements A and B respectively.

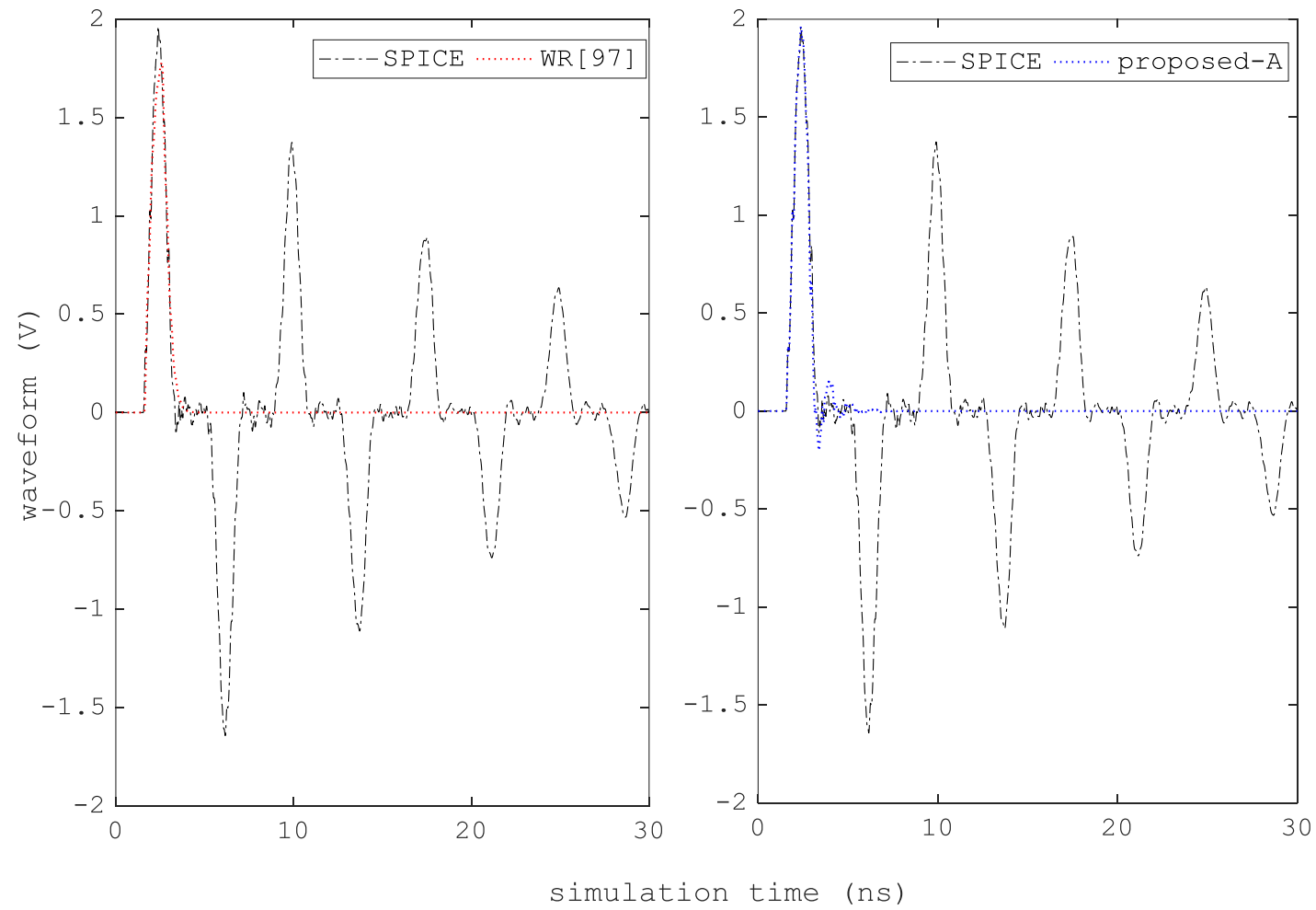


**Figure 3.23: Farend. Left: Resistive coupling [97]. Right: Proposed (B). Round 1. Example Two.**



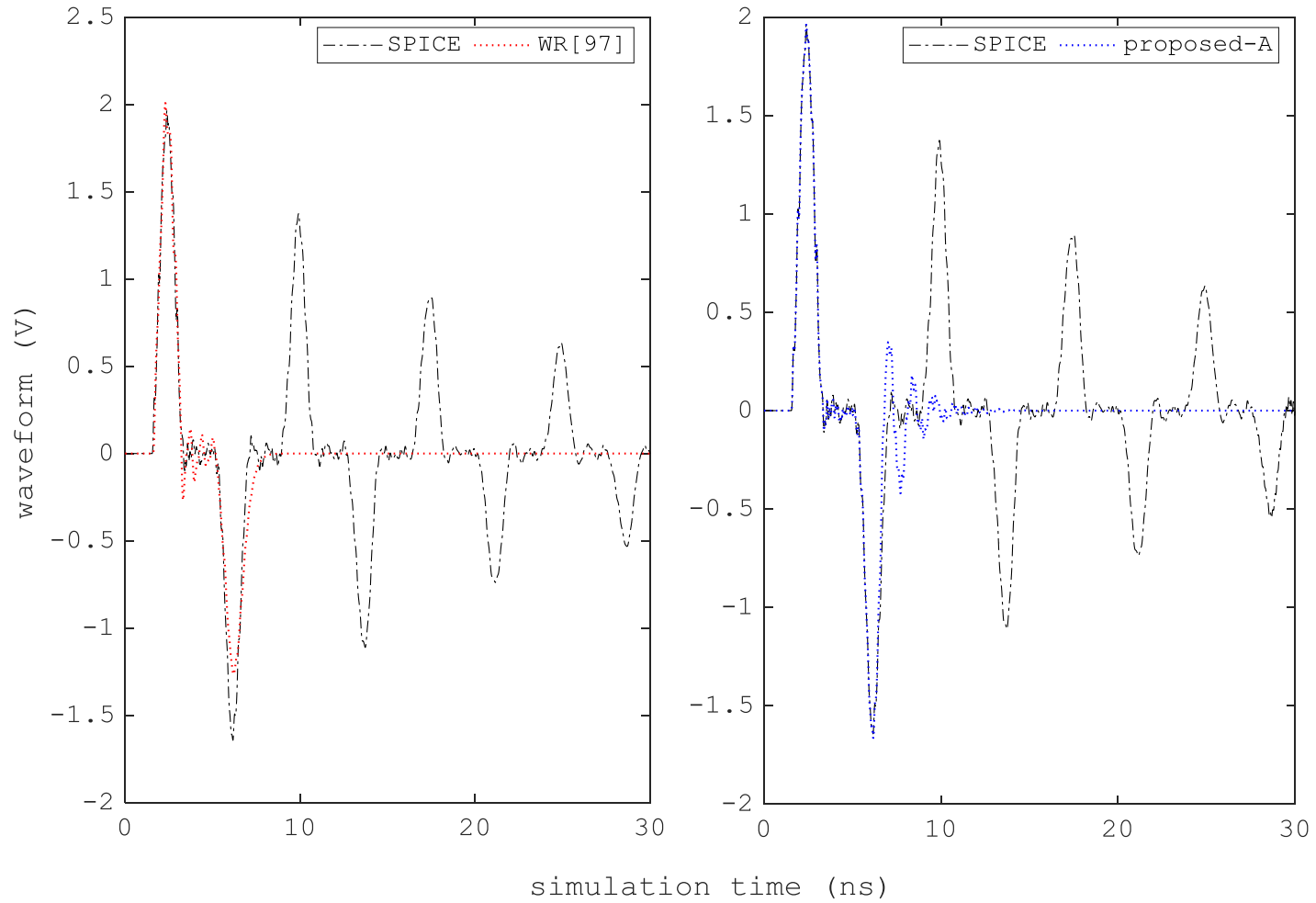


**Figure 3.24: Resistive coupling [97]. Right: Proposed (B). Round 2. Example Two.**

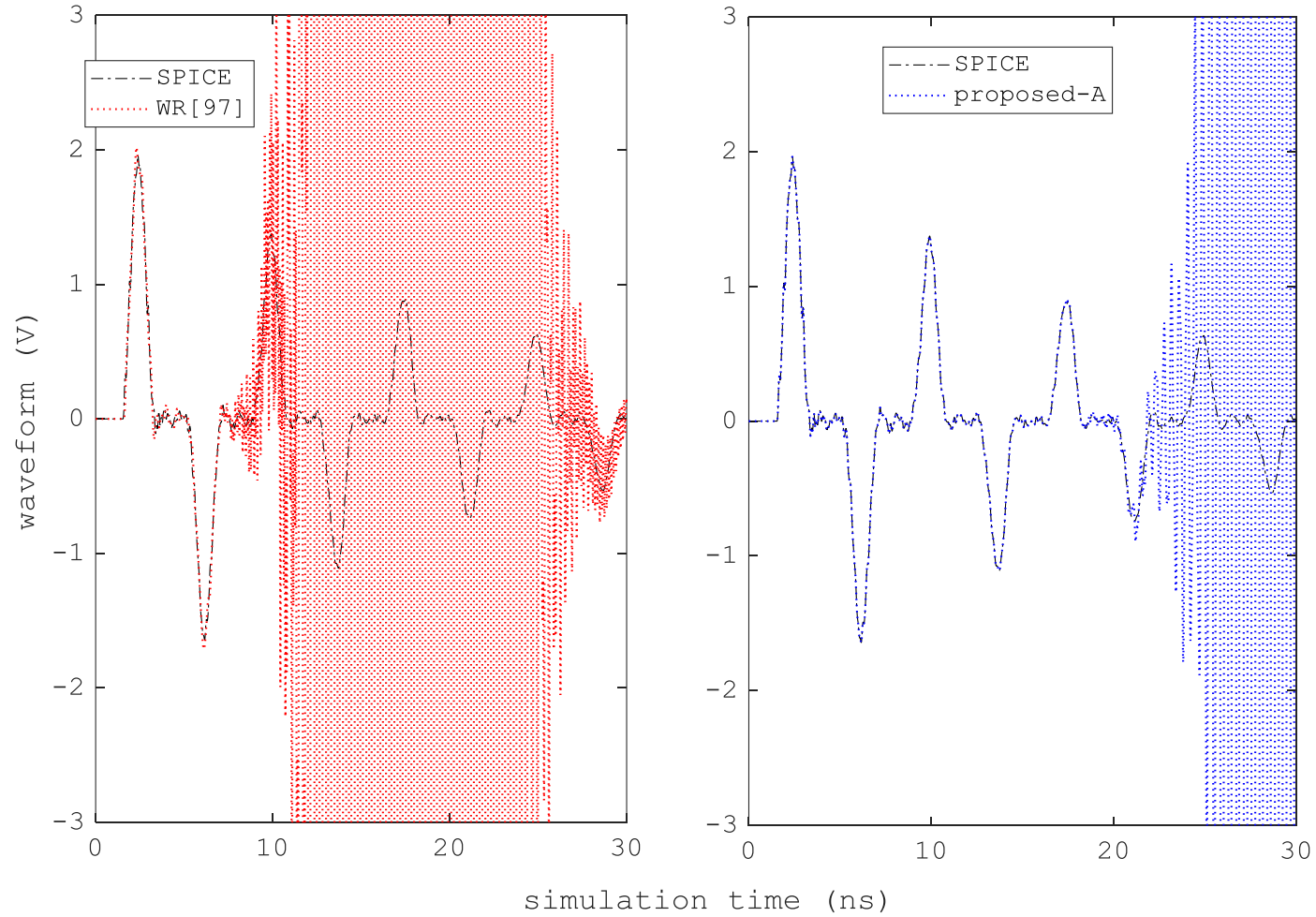


**Figure 3.25: Farend. Left: Resistive coupling [97]. Right: Proposed (B). Round 10. Example Two.**

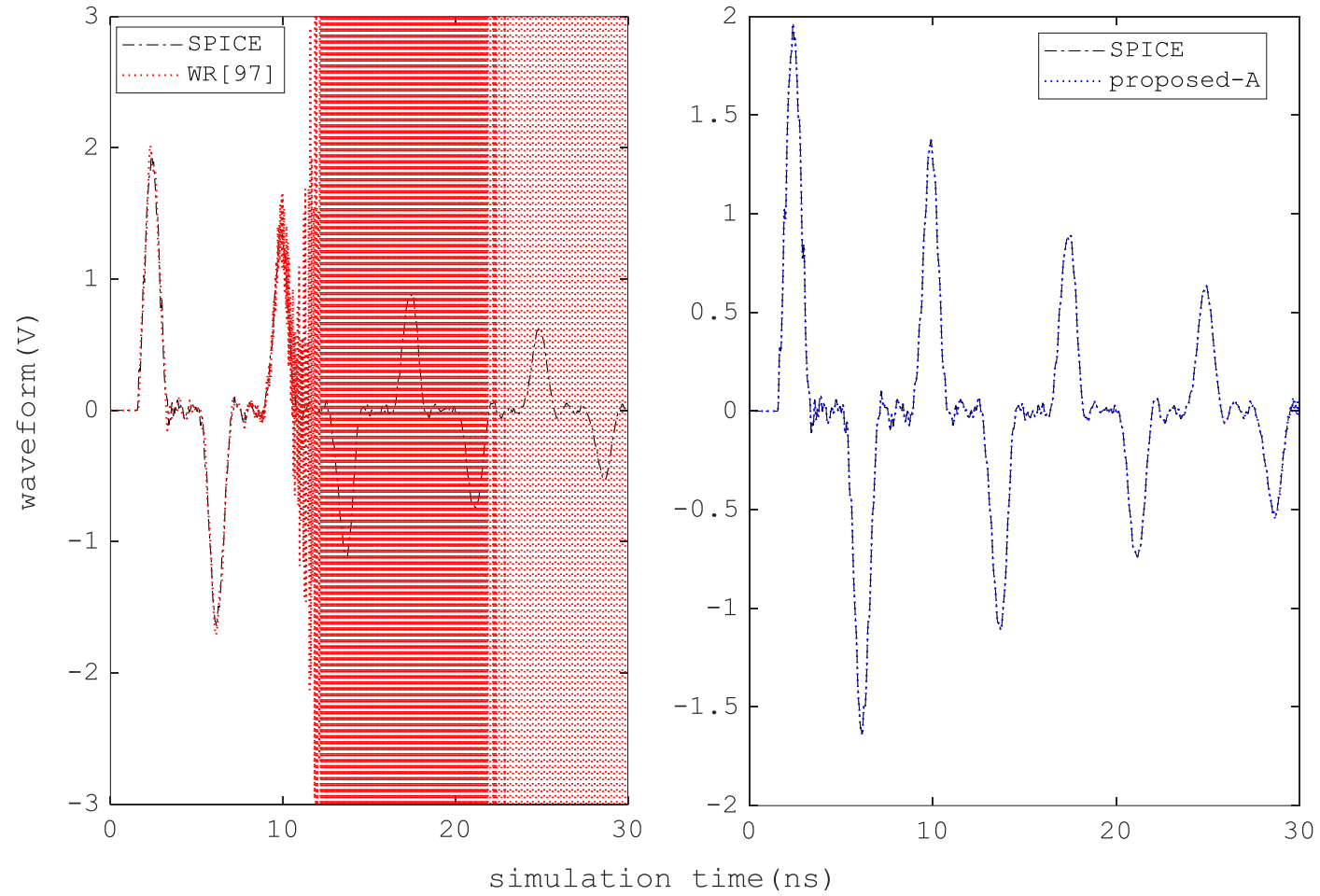


**Figure 3.26: Farend. Left: Resistive coupling [97]. Right: Proposed (B). Round 17. Example Two.**

### 3.3.3 Example Three-Tree structure.

In this example, the circuit in Figure 3.27 is considered. The input is a 1V<sub>peak</sub> trapezoidal pulse of 0.05ns rise/fall time and 2.0ns width, fed through a 1 $\Omega$ -resistance. The MNA formulation lead to system matrices of size 757  $\times$  757. The sparsity pattern of the MNA matrix in this problem, is shown in Figure 3.28. To implement the WR solution, the circuit is partitioned into thirty-three subcircuits labeled L<sub>1</sub> to L<sub>33</sub> and grouped into five ordered levels for analysis (Figure 3.27). Level I have the highest precedence and its subcircuits are scheduled first for analysis. Level V gets the lowest precedence and its subcircuits are solved last. Subcircuits in same level are solved in parallel. First, resistive coupling is considered, and the companion min-max problem is solved on 32  $\times$  4 instances to determine the 32  $\times$  2 relaxation resistances, see eqs. 2.20-2.22. The total MNA space size of the partition is 789 when resistive coupling is used. Figure 3.29(top) shows the sparsity pattern of the MNA matrices of subcircuits L1 and L6. Impedance coupling is considered next, and rational-with-delay functions are constructed for all subcircuits in levels I, III and V. All approximations use coarse models of order one, which leads to an average increase  $\Delta\beta/\beta$  between 1/6 and 1/4 (section 3.2.5). The total MNA space size of the partition becomes 1433. The sparsity pattern of the MNA matrices of augmented subcircuits L<sub>1</sub> and L<sub>6</sub>, is shown in Figure 3.29(bottom). Finally, Figure 3.30 represents the circuit of the augmented subsystem L<sub>6</sub>.

The resistive coupling WR [97] and the proposed algorithms solve the circuit on interval  $[0, T]$ ,  $T = 30\text{ns}$ . The number of rounds to converge and theirs cost are reported in Table 3.5. Impedance coupling takes 05 rounds to converge against 20 for resistive coupling [97]. The iteration waveform at node A in Figures 3.31-3.33 and the evolution of the global error in Figure 3.34 contrast the difference in performance. Eight CPUs are available to execute the parallel WR algorithms. Impedance coupling achieves a maximum speedup of 4.5 compared to 2.18 in the resistive coupling WR [97] when the cost of solving the min-max problem is included (Table 3.4). The performance scalability with respect to the number of CPUs is compared against the maximum theoretical value (26),(27) at the limit values  $\Delta\beta/\beta = 1/4$  and  $\Delta\beta/\beta = 1/6$  in Figure 3.35. Even though

impedance coupling lead to practically double the size of the partition, a very fast convergence enables its serial execution to run faster than full-circuit analysis in this example.

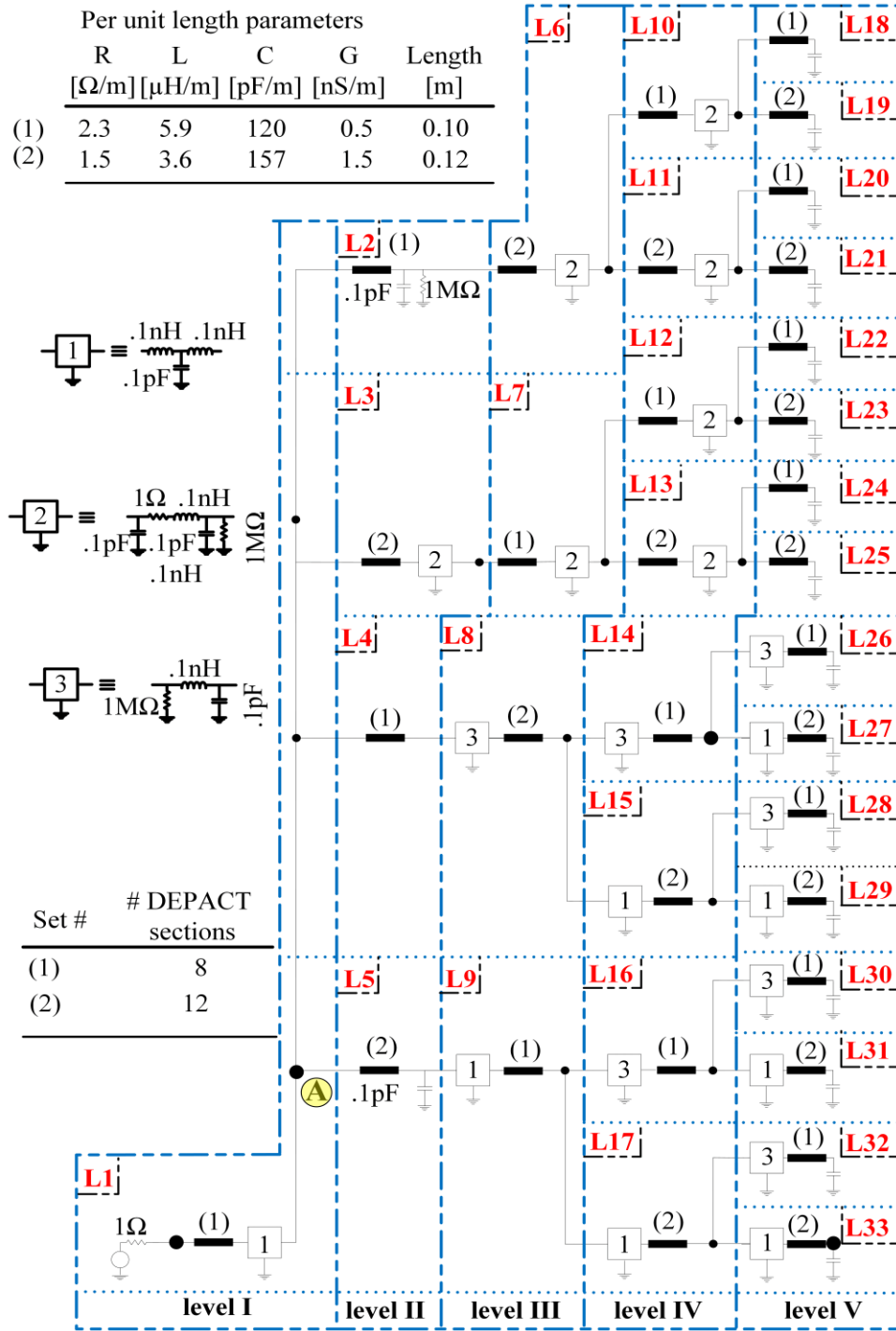
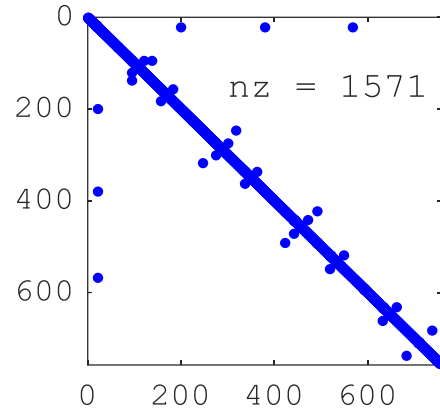
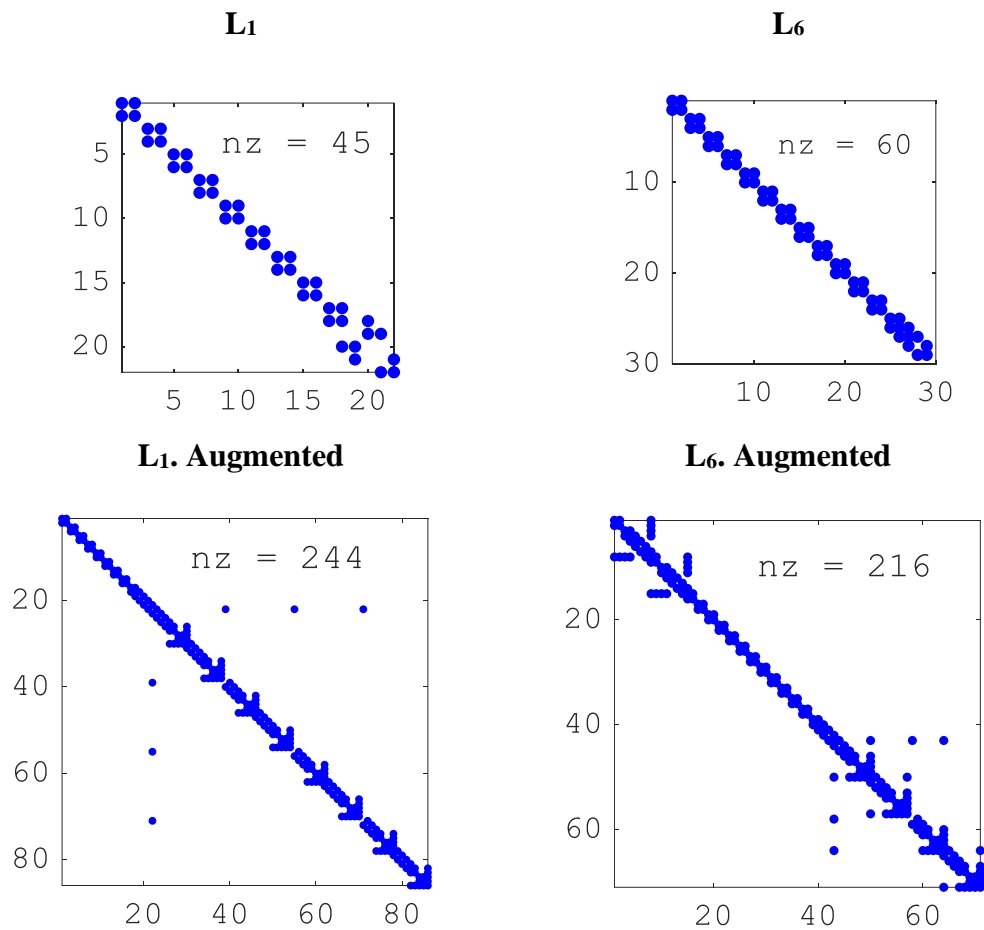


Figure 3.27: Circuit of Example Three.



**Figure 3.28: Sparsity pattern of MNA matrix of entire circuit. Example Three.**



**Figure 3.29: Sparsity pattern of MNA matrices of subcircuits  $L_1$  and  $L_6$ . Top: Resistive coupling [97]. Bottom: Proposed. Example Three.**

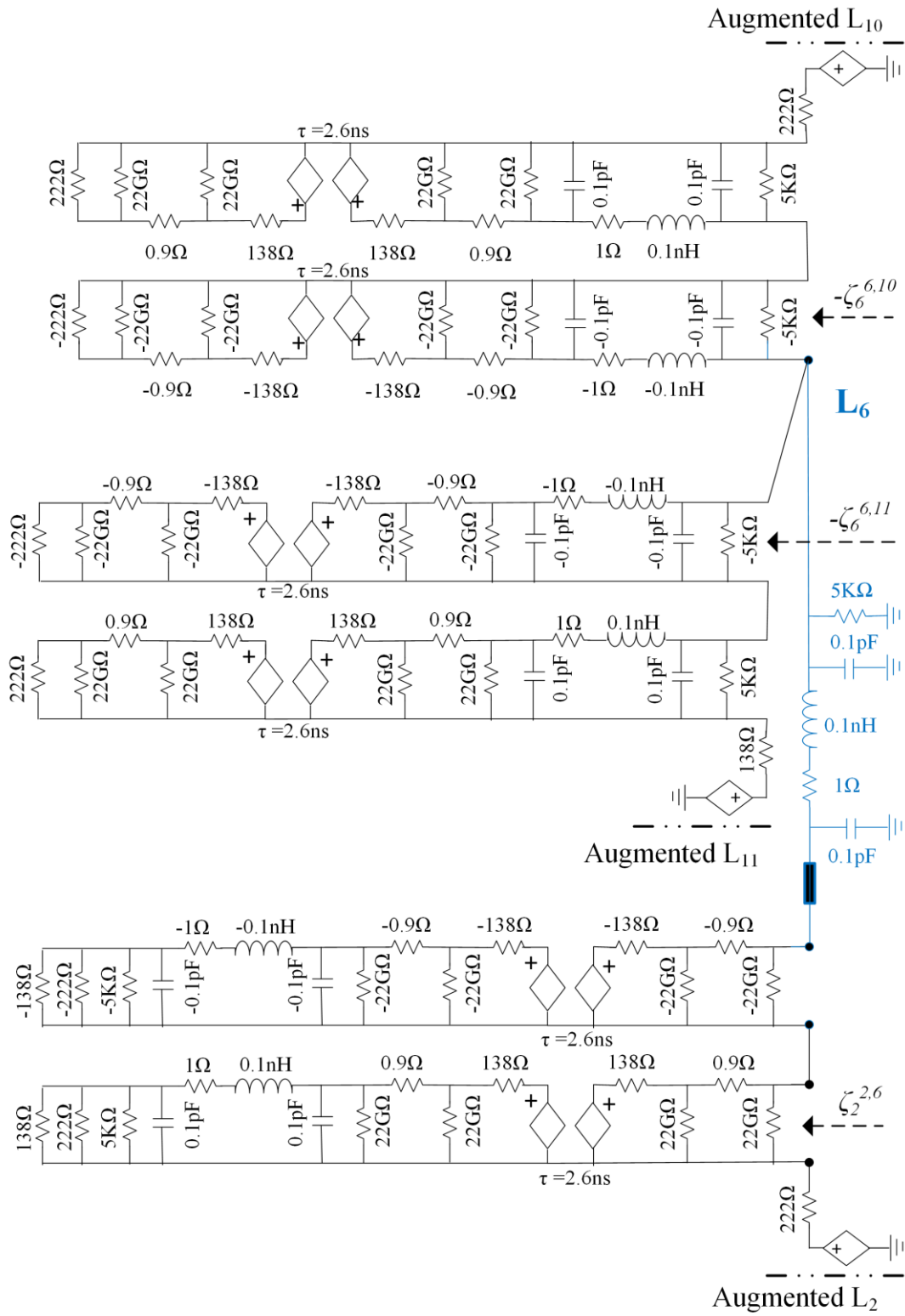
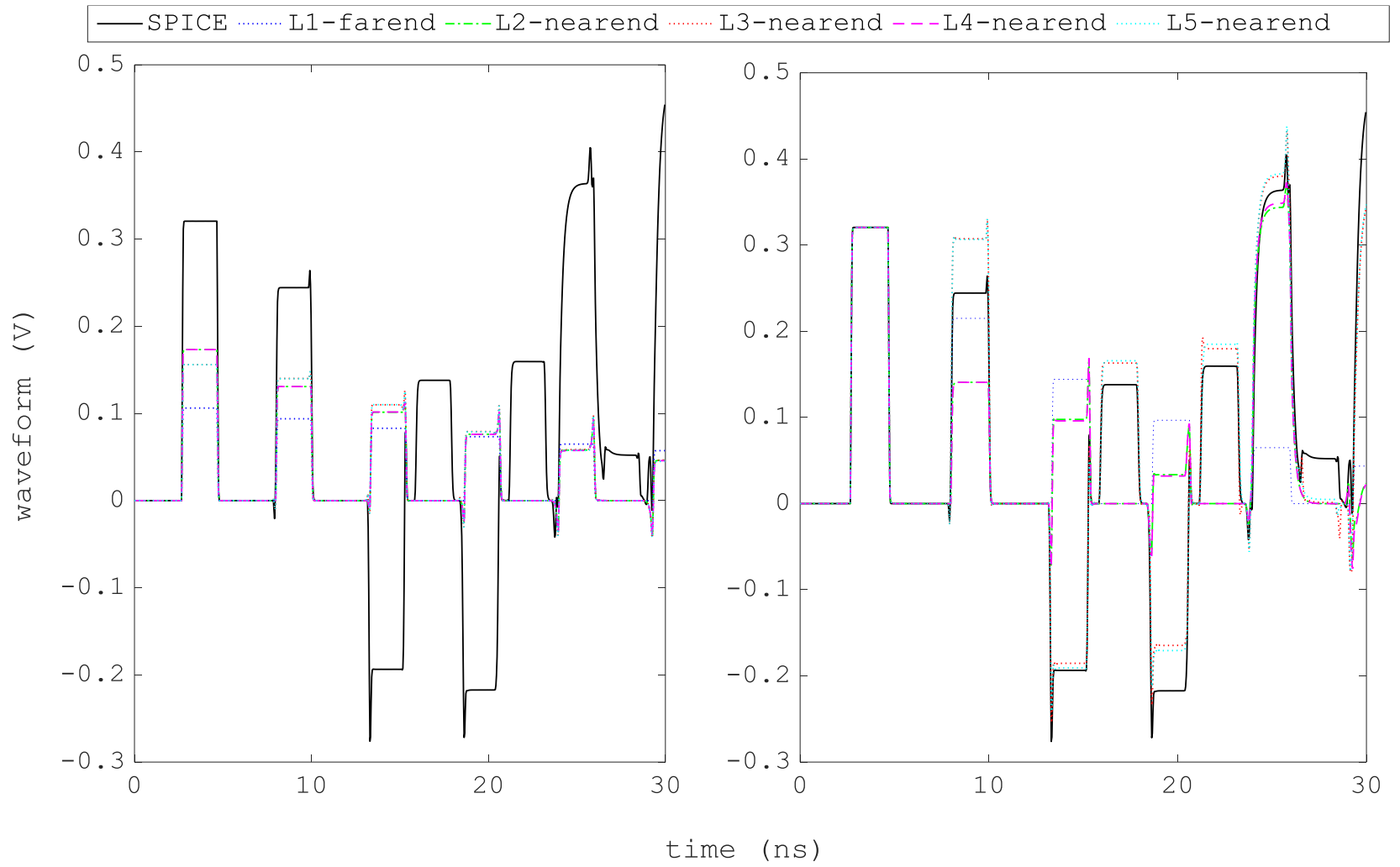


Figure 3.30: Augmented subcircuit  $L_6$ . Example Three.

**Table 3.5: Performance of proposed algorithm. Example Three.**

# CPU	Time (s)				speedup		
	WR [97]	Proposed	Full circuit analysis	Min-max problem [97]	WR Trasient analysis [97]	WR Transient analysis+optimization [97]	Proposed
1	24.10	13.65	17.22	1.62	0.71	0.67	1.26
2	14.60	9.12			1.18	1.06	1.89
4	8.36	5.32			2.06	1.72	3.24
6	7.19	4.65			2.39	1.95	3.70
8	6.27	3.81			2.75	2.18	4.52





**Figure 3.31: Iteration waveform. Left: Resistive coupling [97]. Right: Impedance coupling. Round 1. Example Three.**

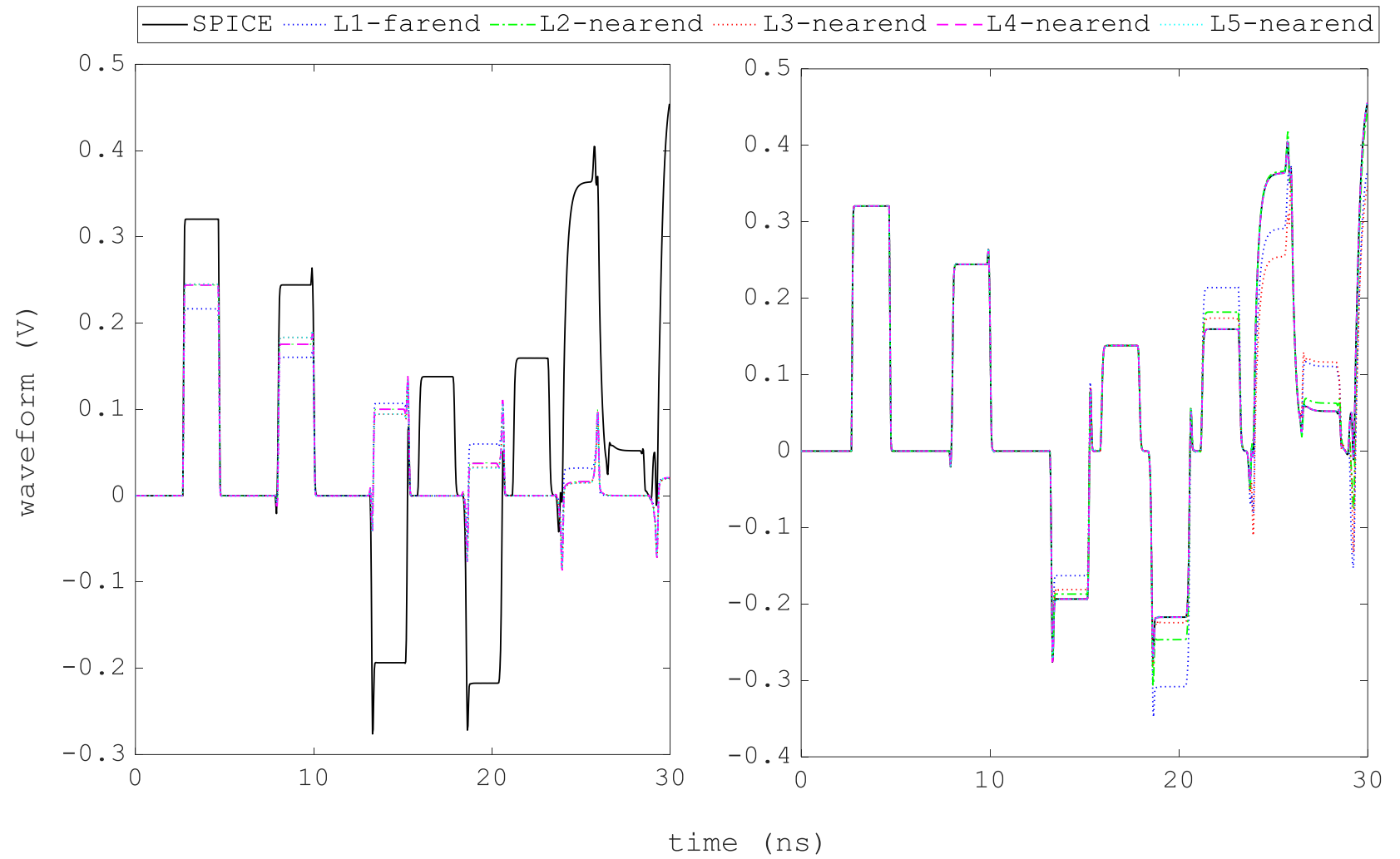


**Figure 3.32: Iteration waveform. Left: Resistive coupling [97]. Right: Impedance coupling. Round 2. Example Three.**

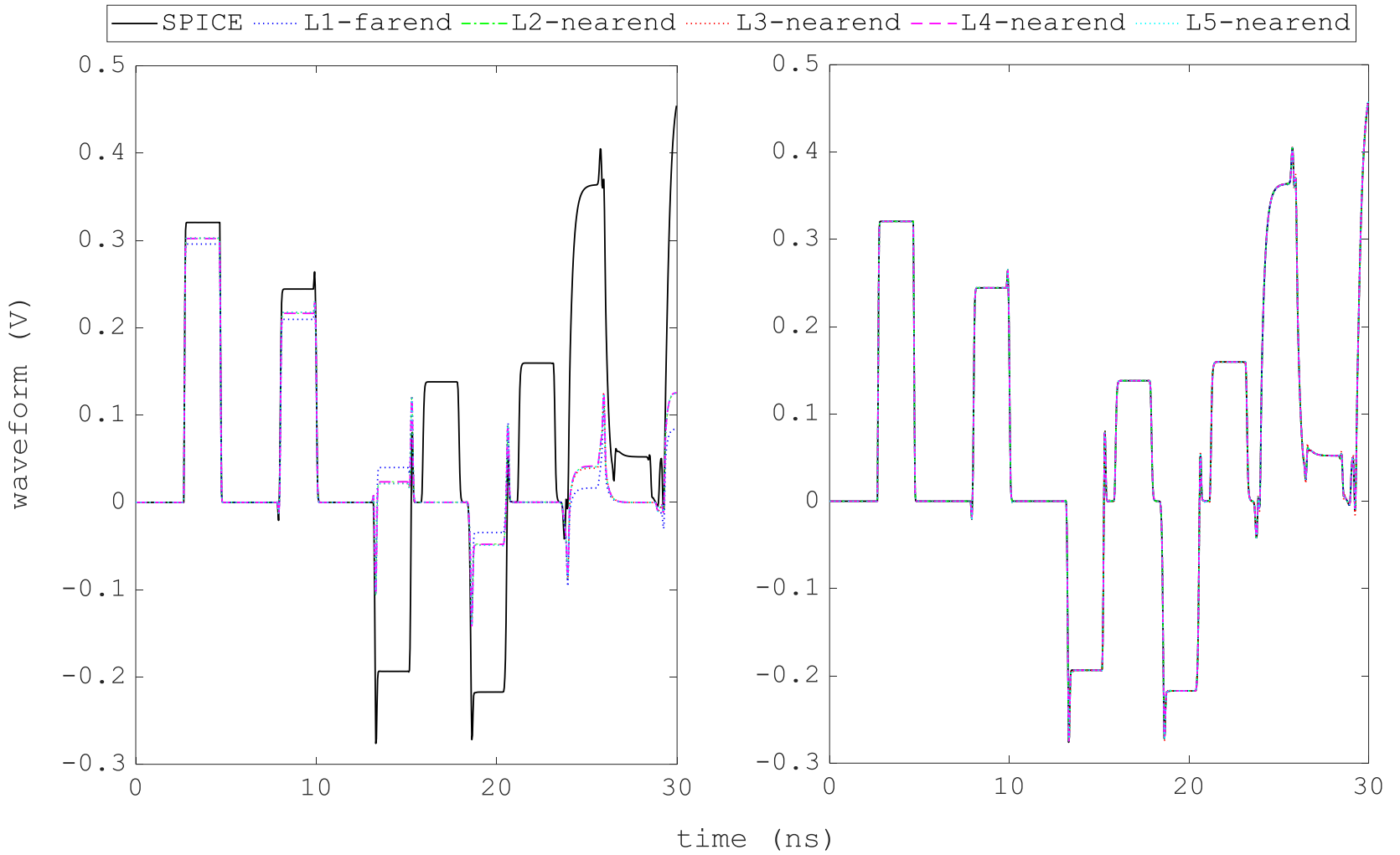


**Figure 3.33: Iteration waveform. Left: Resistive coupling [97]. Right: Impedance coupling. Round 4. Example Three.**

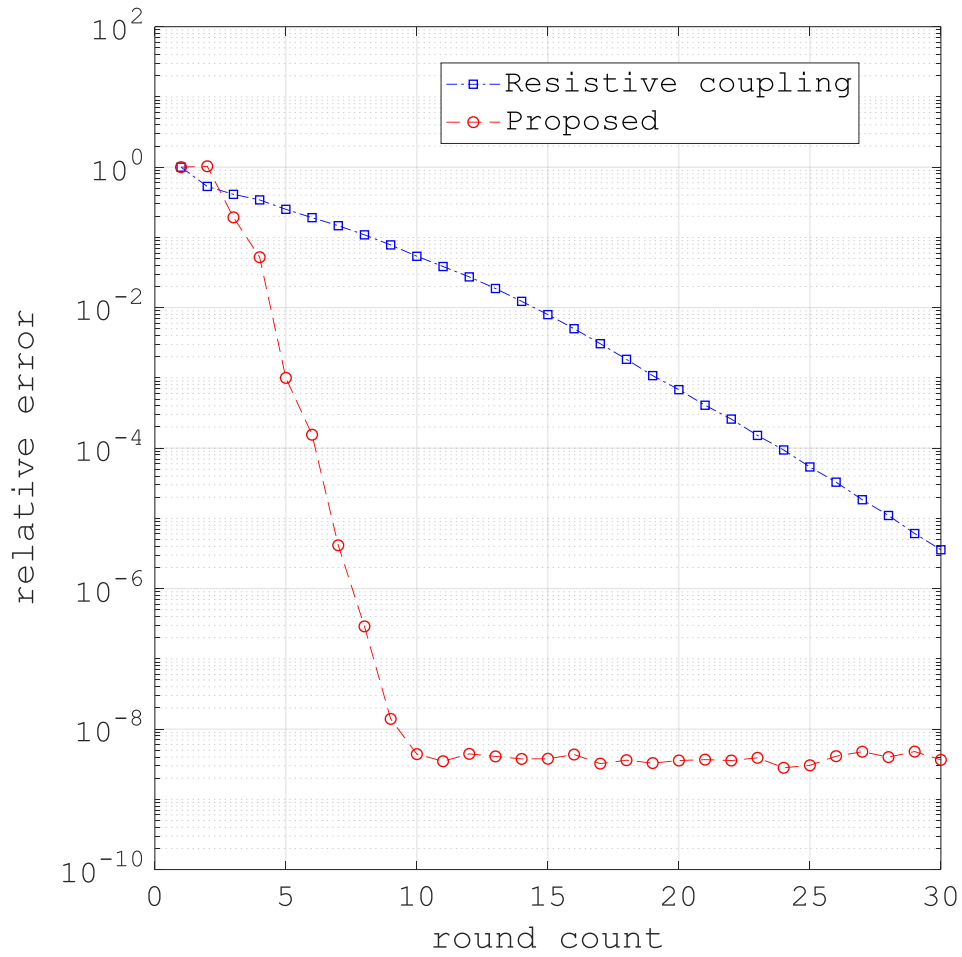


**Figure 3.34: Global error, simulation time  $T = 30\text{ns}$ . Example Three.**

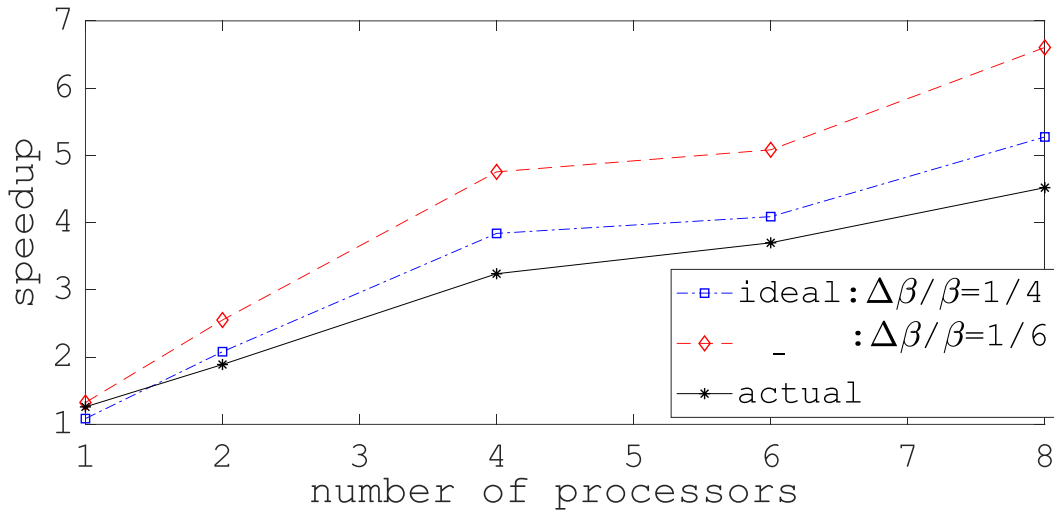


**Figure 3.35: Speedup: Theoretical vs actual. Example Three.**

### 3.3.4 Example Four-RLCG single line problem [77].

The objective is to compare the proposed approximation against the suboptimal constant approximation of the resistive coupling-based WR, see chapter 2 or [97], and against the asymptotically optimized constant parameters of the non overlapping optimized WR algorithm oWR [77] for a single RLCG line problem. The lossy and slightly reactive example in [77] is considered here. The circuit represents a single transmission line driven by a voltage source and loaded with an impedance. The voltage source possesses a  $50\Omega$ -internal resistance and produces a  $1V$  peak trapezoidal pulse of  $t_r = 0.1$  ns-rise/fall time. The width of the input pulse represents 40% of the simulation time  $T$ . The line parameters are  $R = 50 \Omega/m$ ,  $L = 495$  nH/m,  $C = 63$  pF/m,  $G = 0$  S/m [77, (III.29)] and length  $d = 0.15$  m. The load is either a  $50\Omega$ -resistor or a  $1.0$ pF-capacitor. Using the well-known rule of thumb [110, pp. 203], the line is represented with  $\lceil 20d \sqrt{LC}/(t_r) \rceil = 168$  sections in the time-domain, and is split half, which amounts for 84 RLCG sections in both parts. First, the asymptotically optimized constants  $\alpha_m^* = 6.51 \times 10^{-3}$  [77, (III.38)] and  $\alpha_l^* = -3.408 \times 10^{-5} T^{-1/3}$  [77, (III.31)]. Second, the solution of the min-max problem is computed, see eq. 2.15 and 2.16 or [97, eqs. (15),(16)]. The resulting

**Table 3.7: Cost and performance. Load: 50Ω. Example Four.**

		WR[77]				WR [97]		Proposed			
		$\alpha_m$		$\alpha_l$				R-Z		Z-R	
		Nbr. Iter.	Cost (s)	Nbr. Iter.	Cost (s)	Nbr. Iter.	Cost (s)	Nbr. Iter.	Cost (s)	Nbr. Iter.	Cost (s)
$T$ (ns)	<b>100</b>	<b>6</b>	3.63	<b>6</b>	3.67	<b>4</b>	2.49	<b>3</b>	1.79	<b>3</b>	1.84
	<b>500</b>	<b>6</b>	18.37	<b>8</b>	24.77	<b>4</b>	12.25	<b>3</b>	8.95	<b>2</b>	6.14
	<b>100</b>	<b>6</b>	36.05	<b>10</b>	61.85	<b>4</b>	24.36	<b>3</b>	18.05	<b>2</b>	12.41
	<b>5000</b>	<b>6</b>	178.02	<b>15</b>	449.49	<b>4</b>	119.81	<b>3</b>	90.21	<b>2</b>	62.00

**Table 3.6: Cost and performance. Load: 1pF. Example Four.**

		WR[77]				WR [97]		Proposed			
		$\alpha_m$		$\alpha_l$				R-Z		Z-R	
		Nbr. Iter.	Cost (s)	Nbr. Iter.	Cost (s)	Nbr. Iter.	Cost (s)	Nbr. Iter.	Cost (s)	Nbr. Iter.	Cost (s)
$T$ (ns)	<b>100</b>	<b>11</b>	6.67	<b>10</b>	6.17	<b>7</b>	4.31	<b>4</b>	2.35	<b>3</b>	1.82
	<b>500</b>	<b>11</b>	33.40	<b>17</b>	52.29	<b>7</b>	21.04	<b>4</b>	12.02	<b>3</b>	8.86
	<b>100</b>	<b>11</b>	67.45	<b>22</b>	133.18	<b>7</b>	42.62	<b>4</b>	23.89	<b>3</b>	17.98
	<b>5000</b>	<b>11</b>	369.39	<b>36</b>	1101.70	<b>7</b>	211.08	<b>4</b>	119.70	<b>2</b>	61.45

coupling resistances are  $(88.66\Omega, 88.66\Omega)$  with objective function  $r = 0.071$  at the four instances in the  $50\Omega$ -load case, and  $(88.50\Omega, 90.55\Omega)$  with  $r = 0.265$  for the  $1.0\text{pF}$ -load one. The costs of these two min-max solutions are 14ms and 17ms respectively and are

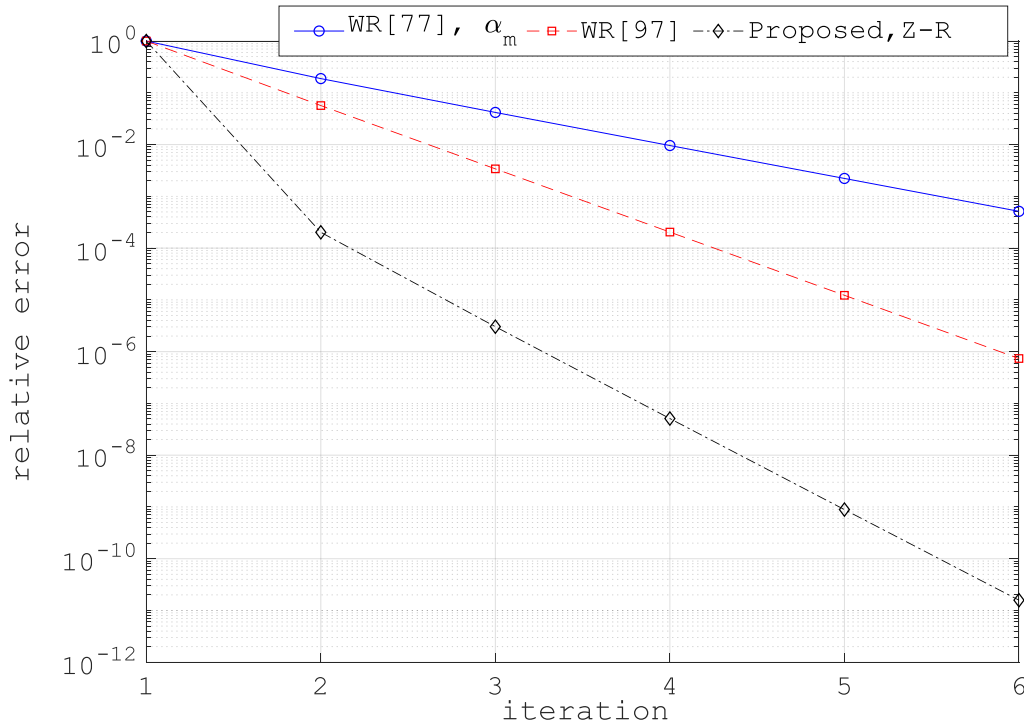


**Figure 3.36: 25 Error decay.  $T = 5000\text{ns}$ . Load  $50\Omega$ . Example Four.**

neglected as they represent less than 1% of the total cost. Note that the coupling resistances [97] are close to the characteristic impedance  $\sqrt{495 \times 10^{-9} / 63 \times 10^{-12}} = 88.64\Omega$  of the lossless transmission line, a value which was chosen in [63],[64] to speed up the convergence of WR. Third, a rational-with-delay approximation is constructed for one part in the circuit, it uses a coarse model of order one for the half-line. Whereas a resistance of value  $88.64\Omega$  is allocated to the other part. The MNA space size of both subcircuits in [97] and [77] is 253, which makes it to a total size of 506. In both dispositions Z-R and R-Z of the proposed coupling, the MNA space size is 258 for one subcircuit and 261 for the other one, which makes to a total size of 519. The WR solutions are computed on  $T = 100\text{ns}$ ,  $500\text{ns}$ ,  $1000\text{ns}$  and  $5000\text{ns}$ , and the corresponding numbers of iterations and costs are reported on Tables 3.6 and 3.7.

The proposed method produces the fastest solution for the four simulation windows. Disposition Z-R generates the best times in the proposed WR method. It is compared against the resistive coupling-based WR[97], and against oWR[77] for parameter  $\alpha_m^*$ . It

is 2x to 3x faster than oWR[77] and 1.4x to 2x faster than WR[97] for 50 $\Omega$ -load. When the load is a 1pF-capacitor, the proposed algorithm runs 3.7x to 6x faster than [77], and 2.3x to 3.4x faster than [97]. Figure 3.36 contrasts the errors' speed of decay in the first six iterations, and attests of the superior convergence of the proposed method. It is worth mentioning that comparing the proposed WR method with [97] and [77] is in fact a comparison of TC equations of different classes. The delay based TCs of the proposed method against the constant parameters in [97] and [77].

### 3.4 Conclusion

A general dissipative impedance coupling scheme for the WR algorithm with longitudinal partitioning, was presented in this chapter. It demonstrated that replacing resistances by impedances in the well-known resistive coupling scheme leads to faster convergence of the subsequent WR-LP algorithm. However, such improvement came at the price of increasing the cost of the iteration. Therefore, cost would be more adequate to assess the efficiency of the proposed coupling impedance scheme.

The present work also proposed a flexible coupling strategy for the WR analysis of single transmission line circuits. Customized rational-with-delay impedance and resistance were proposed to decouple every two adjacent subcircuits, and a step-by-step procedure was presented to apply the proposed coupling to arborescent TL partitions. Numerical examples demonstrated the flexibility of this easy-to-apply coupling strategy and illustrated its performance especially when circuits are low-loss and highly reactive.



## Chapter 4

### 4 Some Convergence Results on Waveform Relaxation for Chains of Circuits

A nilpotent WR operator converges in a finite number of steps, and thus is equivalent to a direct solver. Even though a nilpotent WR algorithm can be inefficient e.g., the optimal WR algorithm, judicious approximations of its nilpotency conditions can produce cost effective methods such as the resistive and the hybrid rational-with-delay impedance/resistance coupling-based WR algorithms (chapters 2 and 3). In the present chapter, the conditions that lead to a nilpotent dissipative coupling-based WR algorithm are examined for chains of general linear time-invariant circuits. Iteration matrices are derived for GJ and GS relaxations, and their nilpotency is examined in the Fourier space for positive real frequencies,  $\omega \geq 0$  (section 3.2.3.2)

In the present chapter, the convergence of WR for chains of identical symmetric circuits is also studied when resistive coupling is applied. It is asserted that WR should converge independently of the number  $N$  of cascaded parts in a chain by proving that the spectral radius of its GJ and GS iteration matrices is bounded by a function that does not depend on length  $N$ . This case stands out from the usual convergence degradation of WR for increasingly long chains [107].

#### 4.1 Nilpotency of Strictly Dissipative Impedance Coupling based Waveform Relaxation Algorithm

Consider a circuit that can be decomposed into a cascade of  $N$ ,  $N \geq 3$ , reciprocal passive parts as illustrated in Figure 4.1. Each part  $P_n$ ,  $1 \leq n \leq N$ , is represented by its  $Z$ -parameters  $Z_{11}^n(i\omega)$ ,  $Z_{12}^n(i\omega)$ ,  $Z_{21}^n(i\omega)$  and  $Z_{22}^n(i\omega)$  with  $Z_{12}^n = Z_{21}^n$ ,  $\omega \geq 0$  and  $i^2 = -1$ . For the sake of generality, a Thevenin generator is connected at each end of the chain;  $(V_{TL}, Z_{TL})$  at the left side and  $(V_{TR}, Z_{TR})$  at the right side.

Every two consecutive parts  $P_n$  and  $P_{n+1}$ ,  $1 \leq n \leq N - 1$  are decoupled with insertion  $\{-\zeta_{n,n+1}^n, \zeta_{n,n+1}^n + \zeta_{n,n+1}^{n+1}, -\zeta_{n,n+1}^{n+1}\}$  which is implemented as a Thévenin generator. Total

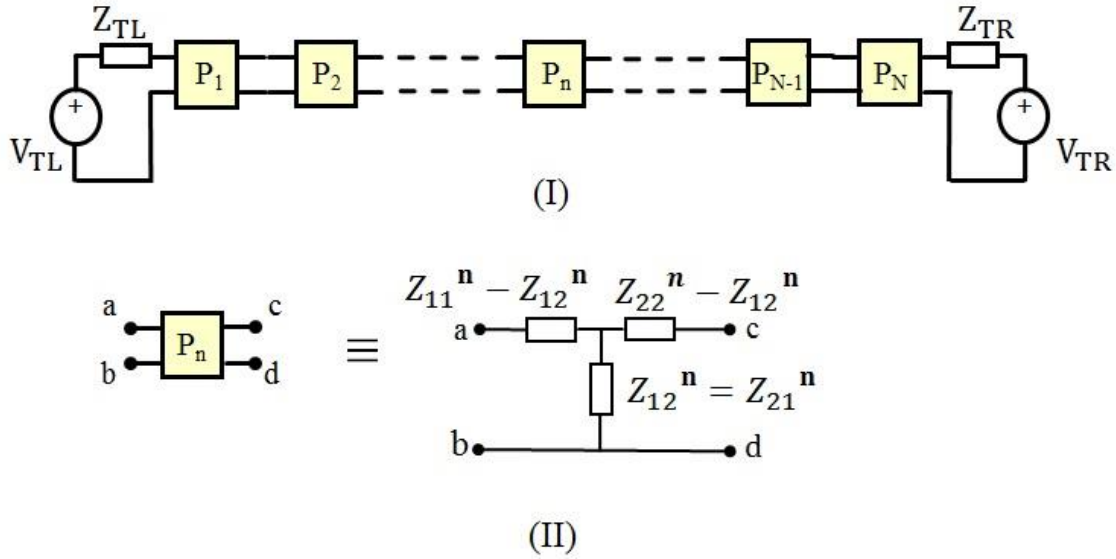


**Figure 4.1: (I) Cascade connection of  $N$  parts  $P_n$ ,  $1 \leq n \leq N$ . (II) Frequency-domain representation of part  $P_n$ .**

insertions on the sides of  $P_n$  and  $P_{n+1}$  are  $\zeta_{n,n+1}^{n+1}$  and  $\zeta_{n,n+1}^n$  respectively while the WR external variables  $w_{n,n+1}^n$  and  $w_{n,n+1}^{n+1}$  are represented with voltage sources in Figure 4.2. The enumeration of parts and thereafter relaxation sources starts for left to right. Part  $P_1$  is connected to primary input  $(V_{TL}, Z_{TL})$  and  $P_N$  to primary input  $(V_{TR}, Z_{TR})$ . It is also natural to enumerate parts along the opposite direction. In both cases, the enumeration intuitively maps the signal flow in this bidirectional circuit [53]. In fact, for the GJ and GS relaxations, all possible orders are equivalent since they produce similar iteration matrices, which in addition of having same spectral radius also possess same 1-norm and  $\infty$ -norm. Mapping the signal flow leads to the natural order of the relaxation sources in the  $2(N-1) \times 1$  vector

$$\mathbf{w}_1 = (w_{1,2}^2, w_{1,2}^1, w_{2,3}^3, w_{2,3}^2, \dots, w_{n-1,n}^n, w_{n-1,n}^{n-1}, \dots, w_{N-1,N}^N, w_{N-1,N}^{N-1})^T \quad (4.1)$$

for the GJ relaxation, and in the  $2(N-1) \times 1$  vector

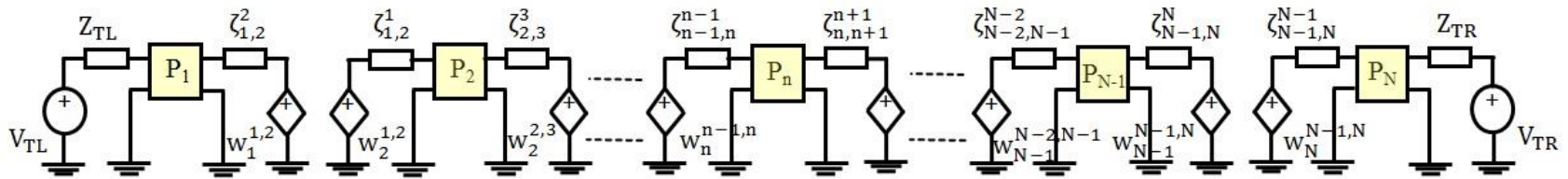


Figure 4.2: Dissipative coupling of the chain.

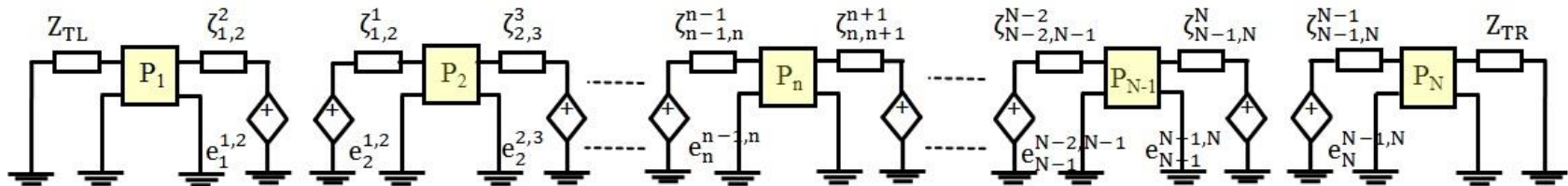


Figure 4.3: WR converge analysis circuit. The homogeneous problem.

$$\mathbf{w}_2 = (w_{1,2}^1, w_{2,3}^3, w_{3,4}^3, w_{4,5}^5, w_{5,6}^5, \dots, w_{1,2}^2, w_{2,3}^2, w_{3,4}^4, w_{4,5}^4, w_{5,6}^6, w_{6,7}^6, \dots)^T \quad (4.2)$$

for the GS relaxation. The evolution of the error in vectors  $\mathbf{w}_1$  and  $\mathbf{w}_2$ , as a function of the iteration count  $k$ ,  $k \in \mathbb{N}$ , is examined. Let  $e_{1,2}^{1(k)}$ ,  $e_{n-1,n}^{n(k)}$ ,  $e_{n,n+1}^{n(k)}$  and  $e_{N-1,N}^{N(k)}$  be the differences between relaxation waveforms  $w_{1,2}^{1(k)}$ ,  $w_{n-1,n}^{n(k)}$ ,  $w_{n,n+1}^{n(k)}$  and  $w_{N-1,N}^{N(k)}$ ,  $2 \leq n \leq N-1$ , calculated at iteration  $k$  and their final values. The error vectors at iteration  $k$  are

$$\mathbf{e}_1^{(k)} = \left( (e_{1,2}^2, e_{1,2}^1, e_{2,3}^3, e_{2,3}^2, \dots, e_{n-1,n}^n, e_{n-1,n}^{n-1}, \dots, e_{N-1,N}^N, e_{N-1,N}^{N-1})^{(k)} \right)^T \quad (4.3)$$

in  $\mathbf{w}_1^{(k)}$ , and

$$\mathbf{e}_2^{(k)} = \left( (e_{1,2}^1, e_{2,3}^3, e_{3,4}^3, e_{4,5}^5, e_{5,6}^5, \dots, e_{1,2}^2, e_{2,3}^2, e_{3,4}^4, e_{4,5}^4, e_{5,6}^6, e_{6,7}^6, \dots)^{(k)} \right)^T \quad (4.4)$$

in  $\mathbf{w}_2^{(k)}$ . Since the system is linear, errors  $\mathbf{e}_1$  and  $\mathbf{e}_2$  satisfy the subsequent homogeneous problem for the zero solution in the circuit of Figure 4.3.

First, we produce the WR iteration matrix  $J_N$  for GJ relaxation over one iteration. Vector  $\mathbf{e}_1^{(k)}$ ,  $k \geq 0$ , satisfies the following recurrent relation

$$\mathbf{e}_1^{(k+1)} = J_N \mathbf{e}_1^{(k)} \quad (4.5)$$

where  $J_N \in \mathbb{C}^{2(N-1) \times 2(N-1)}$  is given by

$$J_N = \left[ \begin{array}{cc|cc|cc|cc} 0 & a_1^+ & 0 & 0 & & & & \\ a_2^- & 0 & 0 & b_2^- & & & & \\ \hline b_2^+ & 0 & 0 & a_2^+ & 0 & 0 & & \\ 0 & 0 & a_3^- & 0 & 0 & b_3^- & & \\ \hline & \ddots & \ddots & & \ddots & \ddots & \ddots & \ddots \\ & \ddots & \ddots & & \ddots & \ddots & & \\ \hline & & & & b_{N-2}^+ & 0 & 0 & a_{N-2}^+ & 0 & 0 \\ & & & & 0 & 0 & a_{N-1}^- & 0 & 0 & b_{N-1}^- \\ \hline & & & & & & & & b_{N-1}^+ & 0 & 0 & a_{N-1}^+ \\ & & & & & & & & 0 & 0 & a_N^- & 0 \end{array} \right] \quad (4.6)$$

and

$$\begin{aligned} a_1^+ &= \frac{Z_{1,2}^1 - \zeta_{1,2}^1}{Z_{1,2}^1 + \zeta_{1,2}^1} \\ a_2^- &= \frac{Z_{1,2}^2 - \zeta_{1,2}^2}{Z_{1,2}^2 + \zeta_{1,2}^1} \\ b_2^- &= \frac{(\zeta_{1,2}^1 + \zeta_{1,2}^2)Z_{12}^2}{(Z_{2,3}^2 + \zeta_{2,3}^3)(Z_{11}^2 + \zeta_{1,2}^1)} \\ a_2^+ &= \frac{Z_{2,3}^2 - \zeta_{2,3}^2}{Z_{2,3}^2 + \zeta_{2,3}^3} \\ b_2^+ &= \frac{(\zeta_{2,3}^2 + \zeta_{2,3}^3)Z_{12}^2}{(Z_{1,2}^2 + \zeta_{1,2}^1)(Z_{22}^2 + \zeta_{2,3}^3)} \end{aligned} \quad (4.7)$$

$$\begin{aligned}
& \vdots \\
& \vdots \\
a_n^- &= \frac{Z_{n-1,n}^n - \zeta_{n-1,n}^n}{Z_{n-1,n}^n + \zeta_{n-1,n}^{n-1}} \\
b_n^- &= \frac{(\zeta_{n-1,n}^{n-1} + \zeta_{n-1,n}^n) Z_{12}^n}{(Z_{n,n+1}^n + \zeta_{n,n+1}^{n+1})(Z_{11}^n + \zeta_{n-1,n}^{n-1})} \\
a_n^+ &= \frac{Z_{n,n+1}^n - \zeta_{n,n+1}^n}{Z_{n,n+1}^n + \zeta_{n,n+1}^{n+1}} \\
b_n^+ &= \frac{(\zeta_{n,n+1}^n + \zeta_{n,n+1}^{n+1}) Z_{12}^n}{(Z_{n-1,n}^n + \zeta_{n-1,n}^{n-1})(Z_{22}^n + \zeta_{n,n+1}^{n+1})} \\
& \vdots \\
& \vdots \\
a_{N-1}^- &= \frac{Z_{N-2,N-1}^{N-1} - \zeta_{N-2,N-1}^{N-1}}{Z_{N-2,N-1}^{N-1} + \zeta_{N-2,N-1}^{N-2}} \\
b_{N-1}^- &= \frac{(\zeta_{N-2,N-1}^{N-2} + \zeta_{N-2,N-1}^{N-1}) Z_{12}^{N-1}}{(Z_{N-1,N}^{N-1} + \zeta_{N-1,N}^N)(Z_{11}^{N-1} + \zeta_{N-2,N-1}^{N-2})} \\
a_{N-1}^+ &= \frac{Z_{N-1,N}^{N-1} - \zeta_{N-1,N}^{N-1}}{Z_{N-1,N}^{N-1} + \zeta_{N-1,N}^N} \\
b_{N-1}^+ &= \frac{(\zeta_{N-1,N}^{N-1} + \zeta_{N-1,N}^N) Z_{12}^{N-1}}{(Z_{N-2,N-1}^{N-1} + \zeta_{N-2,N-1}^{N-2})(Z_{22}^{N-1} + \zeta_{N-1,N}^N)} \\
a_N^- &= \frac{Z_{N-1,N}^N - \zeta_{N-1,N}^N}{Z_{N-1,N}^N + \zeta_{N-1,N}^{N-1}}
\end{aligned}$$

$Z_{n-1,n}^n$  and  $Z_{n,n+1}^n$ ,  $2 \leq n \leq N-1$ , represent the input impedances of interior part  $P_n$  at its interfaces with its neighbors  $P_{n-1}$  and  $P_{n+1}$ , whereas  $Z_{1,2}^1$  and  $Z_{N-1,N}^N$  are the input impedances of parts  $P_1$  and  $P_N$  at the extremities.

Products  $a_n^+(i\omega)a_{n+1}^-(i\omega)$ ,  $1 \leq n \leq N - 1$ , represent local convergence rates of the WR at the interface between any two consecutive parts  $P_n$  and  $P_{n+1}$ . A detailed derivation of matrix  $\mathbf{J}_N$  is found in section 4.3.1.

A recursive relationship is obtained for every local error  $(e_{n-1,n}^n, e_{n-1,n}^{n-1})$  at the interface between  $P_{n-1}$  and  $P_n$  over two GJ iterations by taking

$$\mathbf{e}_1^{(k+2)} = (\mathbf{J}_N)^2 \mathbf{e}_1^{(k)} \quad (4.8)$$

where matrix  $(\mathbf{J}_N)^2$  is the GJ iteration matrix over two iterations. Its expression is given in equation (4.9).

$a_1^+ a_2^-$	0	0	$a_1^+ b_2^-$	0	0								
0	$a_1^+ a_2^-$	$b_2^- a_3^-$	0	0	$b_2^- b_3^-$								
0	$a_1^+ b_2^+$	$a_2^+ a_3^-$	0	0	$a_2^+ b_3^-$	0	0						
$b_2^+ a_3^-$	0	0	$a_2^+ a_3^-$	$b_3^- a_4^-$	0	0	$b_3^- b_4^-$						
$b_2^+ b_3^+$	0	0	$a_2^+ b_3^+$	$a_3^+ a_4^-$	0	0	$a_3^+ b_4^-$	0	0				
0	0	$b_3^+ a_4^-$	0	0	$a_3^+ a_4^-$	$b_4^- a_5^-$	0	0	$b_4^- b_5^-$				
	$\ddots$	$\ddots$		$\ddots$	$\ddots$	$\ddots$	$\ddots$	$\ddots$	$\ddots$	$\ddots$			
				$\ddots$	$\ddots$	$\ddots$	$\ddots$	$\ddots$	$\ddots$	$\ddots$			
				$b_{N-4}^+ b_{N-3}^+$	0	0	$a_{N-4}^+ b_{N-3}^+$	$a_{N-3}^+ a_{N-2}^-$	0	0	$a_{N-3}^+ b_{N-2}^-$	0	0
				0	0	$b_{N-3}^+ a_{N-2}^-$	0	0	$a_{N-3}^+ a_{N-2}^-$	$b_{N-2}^- a_{N-1}^-$	0	0	$b_{N-2}^- b_{N-1}^-$
						$b_{N-3}^+ b_{N-2}^+$	0	0	$a_{N-3}^+ b_{N-2}^+$	$a_{N-2}^+ a_{N-1}^-$	0	0	$a_{N-2}^+ b_{N-1}^-$
						0	0	$b_{N-2}^+ a_{N-1}^-$	0	0	$a_{N-2}^+ a_{N-1}^-$	$b_{N-1}^- a_N^-$	0
								$b_{N-2}^+ b_{N-1}^+$	0	0	$a_{N-2}^+ b_{N-1}^+$	$a_{N-1}^+ a_N^-$	0
								0	0	$b_{N-1}^+ a_N^-$	0	0	$a_{N-1}^+ a_N^-$

(4.9)



Next, the iteration matrix  $\mathbf{S}_N$  for the GS relaxation over one iteration, is produced. Vector  $\mathbf{e}_2^{(k)}$ ,  $k \geq 0$ , satisfies the following recurrent relation over one iteration

$$\mathbf{e}_2^{(k+1)} = \mathbf{S}_N \mathbf{e}_2^{(k)} \quad (4.10)$$

$$\mathbf{S}_N = \begin{bmatrix} \mathbf{A} & \mathbf{0} \\ \mathbf{0} & \mathbf{B} \end{bmatrix} \quad (4.11)$$

where  $\mathbf{A}$  and  $\mathbf{B}$  are two  $(N-1) \times (N-1)$  block matrices defined by

$$\mathbf{A} = \begin{pmatrix} a_1^+ a_2^- & b_2^+ a_3^- & b_2^- b_3^- & 0 & 0 & 0 & & \\ a_1^+ b_2^+ & a_2^+ a_3^- & a_2^+ b_3^- & 0 & 0 & 0 & & \\ 0 & b_3^+ a_4^- & a_3^+ a_4^- & b_4^- a_5^- & b_4^- b_5^- & 0 & & \\ 0 & b_3^+ b_4^+ & a_3^+ b_4^+ & a_4^+ a_5^- & a_4^+ b_5^- & 0 & & \\ & \ddots & \ddots & \ddots & \ddots & \ddots & \ddots & \\ & \ddots & \ddots & \ddots & \ddots & \ddots & \ddots & \\ & & & 0 & b_{N-3}^+ a_{N-2}^- & a_{N-3}^+ a_{N-2}^- & b_{N-2}^- a_{N-1}^- & b_{N-2}^- b_{N-1}^- \\ & & & 0 & b_{N-3}^+ b_{N-2}^+ & a_{N-3}^+ b_{N-2}^+ & a_{N-2}^+ a_{N-1}^- & a_{N-2}^+ b_{N-1}^- \\ & & & & & 0 & b_{N-1}^+ a_N^- & a_{N-1}^+ a_N^- \end{pmatrix} \quad (4.12)$$

and

$B =$ 

$$\left( \begin{array}{cc|cc|cc|cc}
a_1^+ a_2^- & a_1^+ b_2^- & 0 & 0 & 0 & 0 & & \\
b_2^+ a_3^- & a_2^+ a_3^- & b_3^- a_4^- & b_3^- b_4^- & 0 & 0 & & \\
\hline
b_2^+ b_3^+ & a_2^+ b_3^+ & a_3^+ a_4^- & a_3^+ b_4^- & 0 & 0 & & \\
0 & 0 & b_4^+ a_5^- & a_4^+ a_5^- & b_5^- a_6^- & b_5^- b_6^- & & \\
\hline
& & \ddots & \ddots & \ddots & \ddots & \ddots & \ddots \\
& & \ddots & \ddots & \ddots & \ddots & \ddots & \ddots \\
\hline
& & & & b_{N-4}^+ b_{N-3}^+ & a_{N-4}^+ b_{N-3}^+ & a_{N-3}^+ a_{N-2}^- & a_{N-3}^+ b_{N-2}^- & 0 \\
& & & & 0 & 0 & b_{N-2}^+ a_{N-1}^- & a_{N-2}^+ a_{N-1}^- & b_{N-1}^+ a_N^- \\
\hline
& & & & & & b_{N-2}^+ b_{N-1}^+ & a_{N-2}^+ b_{N-1}^+ & a_{N-1}^+ a_N^-
\end{array} \right)$$

(4.13)

for N even, and

 $A =$ 

$$\left( \begin{array}{cc|cc|cc|cc}
a_1^+ a_2^- & b_2^- a_3^- & b_2^- b_3^- & 0 & 0 & 0 & & \\
a_1^+ b_2^+ & a_2^+ a_3^- & a_2^+ b_3^- & 0 & 0 & 0 & & \\
\hline
0 & b_3^+ a_4^- & a_3^+ a_4^- & b_4^- a_5^- & b_4^- b_5^- & 0 & & \\
0 & b_3^+ b_4^+ & a_3^+ b_4^+ & a_4^+ a_5^- & a_4^+ b_5^- & 0 & & \\
\hline
& & \ddots & \ddots & \ddots & \ddots & \ddots & \ddots \\
& & \ddots & \ddots & \ddots & \ddots & \ddots & \ddots \\
\hline
& & & & 0 & b_{N-2}^+ a_{N-1}^- & a_{N-2}^+ a_N^- & b_{N-1}^- a_N^- \\
& & & & 0 & b_{N-2}^+ b_{N-1}^+ & a_{N-2}^+ b_N^+ & a_{N-1}^+ a_N^-
\end{array} \right)$$

(4.14)

and

$$\mathbf{B} = \left( \begin{array}{c|ccc|cc|c|c}
 a_1^+ a_2^- & a_1^+ b_2^- & 0 & 0 & 0 & 0 & & \\
 \hline
 b_2^+ a_3^- & a_2^+ a_3^- & b_3^- a_4^- & b_3^- b_4^- & 0 & 0 & & \\
 b_2^+ b_3^+ & a_2^+ b_3^+ & a_3^+ a_4^- & a_3^+ b_4^- & 0 & 0 & & \\
 \hline
 & \ddots & \ddots & \ddots & \ddots & \ddots & \ddots & \\
 & \ddots & \ddots & \ddots & \ddots & \ddots & \ddots & \\
 \hline
 & & & 0 & b_{N-3}^+ a_{N-2}^- & a_{N-3}^+ a_N^- & b_{N-2}^- a_{N-1}^- & b_{N-2}^- b_{N-1}^- \\
 & & & 0 & b_{N-3}^+ b_{N-2}^+ & a_{N-3}^+ b_N^+ & a_{N-2}^+ a_{N-1}^- & a_{N-2}^+ b_{N-1}^- \\
 \hline
 & & & & 0 & 0 & b_{N-1}^+ a_N^- & a_{N-1}^+ a_N^-
 \end{array} \right)$$

(4.15)

for  $N$  odd. A detailed derivation of matrix  $\mathbf{S}_N$  can be found in section 4.3.2.

Next, some results about the nilpotent WR algorithm are presented. The proof of these results is provided in section 4.4.

**Proposition 4.1** *Necessary condition of nilpotency.* A nilpotent WR algorithm has null local convergence factors.

**Proof.** If complex matrix  $(\mathbf{J}_N)^2$  is nilpotent, then its trace  $\sum_{j=1}^{N-1} a_j^+(i\omega) a_{j+1}^-(i\omega) = 0$  at every frequency point  $\omega \geq 0$  [108]. A requirement which is fulfilled when  $a_j^+ a_{j+1}^- = 0$  for all  $1 \leq j \leq N - 1$ . Any nilpotent WR must have zero local convergence rates for GJ and GS relaxations. ■

The search for nilpotent WR algorithms is restricted to the case where all local convergence rates are zero.

**Proposition 4.2** *Optimal WR for  $N \geq 3$ .* If all coefficients  $a_n^+(i\omega) = a_{n+1}^-(i\omega) = 0$ ,  $1 \leq n \leq N - 1$ , on  $\omega \geq 0$ , then the WR algorithm converges exactly in  $N$  iterations for the GJ relaxation and in  $\left(\left\lceil \frac{N}{2} \right\rceil + 1\right)$  iterations for the GS relaxation, independently of any initial guess.

**Proof.** Reasoning by induction is used here. The GJ iteration matrix  $J_N$  defined over one iteration in (4.6), satisfies  $(J_3)^2 = \mathbf{0}$  when  $a_1^+ = a_2^- = a_2^+ = a_3^- = 0$ . When all coefficients  $a_1^+ = a_2^- = a_2^+ = a_3^- = \dots = 0$  for any number  $N \geq 3$ , it is possible to express the  $2N \times 2N$  matrix  $J_{N+1}$  as

$$J_{N+1} = \left[ \begin{array}{cccc|cc} & & & & 0 & 0 \\ & & & & \vdots & \vdots \\ & & & & \vdots & \vdots \\ & & & & 0 & 0 \\ & & & & 0 & b_N^- \\ \hline 0 & \dots & \dots & 0 & b_N^+ & 0 & 0 \\ 0 & \dots & \dots & 0 & 0 & 0 & 0 \end{array} \right] \quad (4.16)$$

and demonstrate that its  $m^{\text{th}}$  power,  $m \in \mathbb{N}$  and  $m \geq 1$ , satisfies

$$(\mathbf{J}_{N+1})^m = \left[ \begin{array}{ccc|cc} & & & 0 & \\ & & & \vdots & \mathbf{B}_{N,m} \\ & & & 0 & \\ \hline & & \mathbf{B}_{N,m}^T & 0 & 0 \\ \hline 0 & \dots & 0 & 0 & 0 \end{array} \right] \quad (4.17)$$

The  $2(N-1) \times 1$  vector  $\mathbf{B}_{N,m}$  is given as

$$\mathbf{B}_{N,m} = b_N^- (\mathbf{J}_N)^{m-1} \mathbf{u}_{2(N-1)} \quad (4.18)$$

where  $\mathbf{u}_j$  is the  $j^{\text{th}}$  vector in the canonical basis of  $\mathbb{R}^{2(N-1)}$  with its  $j^{\text{th}}$  coordinate equal to one. According to (4.17),(4.18), if  $\mathbf{J}_N$  is nilpotent of index  $(N-1)$ , then  $\mathbf{J}_{N+1}$  is also nilpotent with index  $N$ . If there exists an integer  $N_0$  such that  $\mathbf{J}_{N_0}$  were nilpotent of index less than  $(N_0-1)$ , then this would have meant that  $\mathbf{J}_3$  must be zero according to (4.17),(4.18) when counting backward; a result which is not correct. This concludes our demonstration that the GJ iteration matrix  $\mathbf{J}_N$ , defined over one iteration, is nilpotent with index  $(N-1)$ .

Now, it is easy to see that matrix  $(\mathbf{J}_N)^2$  is also nilpotent with index  $\left\lfloor \frac{N}{2} \right\rfloor$ , where  $[\cdot]$  represents the integer part of a real number. Since  $(\mathbf{J}_N)^2$  and  $\mathbf{S}_N$  are similar, then the GS iteration matrix is also nilpotent with same index  $\left\lfloor \frac{N}{2} \right\rfloor$ .

At the end of iteration  $(N-1)$  in the GJ relaxation, all relaxation sources reach together their final zero value for the first time. Still, another iteration is needed to solve the system/circuit and bring all its variables to the zero solution of the homogeneous problem

with homogeneous initial conditions. The subsequent WR algorithm therefore converges in  $N$  GJ iterations. Same reasoning shows that WR takes  $\left(\left\lfloor \frac{N}{2} \right\rfloor + 1\right)$  iterations to converge when GS relaxation is adopted. This result is optimal in the sense that faster convergence is not possible. ■

The result of proposition 4.2 is optimal in the sense that faster convergence is not possible. Another way of making WR converge in a finite number of iterations yet not minimum, is introduced in the next proposition

**Proposition 4.3** *Zeroing all local convergence factors  $a_n^+(i\omega)a_{n+1}^-(i\omega)$  along (+) direction only or along (-) direction only. If all coefficients  $a_n^+(i\omega) = 0$  or if all  $a_{n+1}^-(i\omega) = 0$ ,  $1 \leq n \leq N - 1$  on  $\omega \geq 0$ , then the WR algorithm converges exactly in  $(2N - 1)$  iterations for the GJ relaxation and in  $N$  iterations for the GS relaxation, independently of any initial guess.*

**Proof.** Reasoning by induction is used here. Let us consider the case where only coefficients  $a_2^- = a_3^- = a_4^- = \dots = a_N^- = 0$ . A similar approach can be used for the other case where only  $a_1^+ = a_2^+ = a_3^+ = \dots = a_{N-1}^+ = 0$ .

First, we verify that  $(J_3)^4 = \mathbf{0}$  when  $a_2^- = a_3^- = 0$ . When  $a_2^- = a_3^- = a_4^- = \dots = a_N^- = a_{N+1}^- = 0$ , it can be demonstrated that the first  $2(N - 1)^{\text{th}}$  powers  $(J_{N+1})^m$ ,  $1 \leq m \leq 2(N - 1)$ , of matrix  $J_{N+1}$  satisfy

$$(\mathbf{J}_{N+1})^m = \left[ \begin{array}{ccc|cc} & & & 0 & \\ & & & \vdots & \mathbf{B}_{N,m} \\ & \mathbf{J}_N^m & & 0 & \\ \hline & & & 0 & \\ \mathbf{B}_{N,m}^T & & & 0 & c_m \\ \hline 0 & \dots & 0 & 0 & 0 \end{array} \right] \quad (4.19)$$

$$1 \leq m \leq 2(N - 1).$$

Element  $c_m$  at the  $(2N - 1, 2N)$  entry of matrix product  $(\mathbf{J}_{N+1})^m$  is given by

$$c_{2m'+1} = a_{N-1-m'}^+ \prod_{l=N-m'}^{N-1} (b_l^+ b_l^-) \quad \text{when } m = 2m' + 1$$

and (4.20)

$$c_{2m'} = 0 \quad \text{when } m = 2m'$$

According to equations (4.19) and (4.20), matrix product  $(\mathbf{J}_{N+1})^{2N} = \mathbf{0}$  if  $(\mathbf{J}_N)^{2(N-1)} = \mathbf{0}$ . The GJ iteration matrix  $\mathbf{J}_N$  is therefore nilpotent with index  $2(N - 1)$  when all its coefficients  $a_2^- = a_3^- = a_4^- = \dots = a_N^- = 0$ . Using the same reasoning as in property 4.2, we find that the GS iteration matrix  $\mathbf{S}_N$  is also nilpotent with index  $(N - 1)$ . The subsequent WR algorithm therefore converges in  $(2N - 1)$  GJ iterations or in  $N$  GS iterations. ■

The next result concerns a non-nilpotent WR with null convergence factors.

**Proposition 4.4** *Zeroing all local convergence factors along one alternate direction*

- a) If  $a_2^- = a_2^+ = a_4^- = a_4^+ = \dots = a_{2k}^- = a_{2k}^+ = \dots = 0$  while  $a_1^+, a_3^-, a_3^+, a_5^-, \dots, a_{2k+1}^-, a_{2k+1}^+$  are not equal to zero, then the WR is not nilpotent for any chain of at least three subcircuits.
- a) If  $a_1^+ = a_3^- = a_3^+ = a_5^- = a_5^+ = \dots = a_{2k+1}^- = a_{2k+1}^+ = \dots = 0$  while  $a_2^-, a_2^+, a_4^-, a_4^+, \dots, a_{2k}^-, a_{2k}^+$  are not equal to zero, then the WR is not nilpotent for any chain of at least four subcircuits.

**Proof.** This property is demonstrated by observation. A proof for part a) is presented. A similar approach is used for part b). Let us start with matrix  $J_3$  when  $a_2^- = a_2^+ = a_4^- = 0$

$$J_3 = \begin{bmatrix} 0 & a_1^+ & 0 & 0 \\ 0 & 0 & 0 & b_2^- \\ b_2^+ & 0 & 0 & 0 \\ 0 & 0 & a_3^- & 0 \end{bmatrix} \quad (4.21)$$

The column vectors of  $J_3$  are linearly independent in general. Matrix  $J_3$  is nonsingular and cannot be nilpotent. Now, let us look at  $J_4$

$$J_4 = \begin{bmatrix} 0 & a_1^+ & 0 & 0 & 0 & 0 \\ 0 & 0 & 0 & b_2^- & 0 & 0 \\ b_2^+ & 0 & 0 & 0 & 0 & 0 \\ 0 & 0 & a_3^- & 0 & 0 & b_3^- \\ 0 & 0 & b_3^- & 0 & 0 & a_3^+ \\ 0 & 0 & 0 & 0 & 0 & 0 \end{bmatrix} \quad (4.22)$$



If  $P_{J_3}(X)$  and  $P_{J_4}(X)$  denote the characteristic polynomials of matrices  $J_3$  and  $J_4$ , then  $P_{J_4}(X) = X^2 P_{J_3}(X)$ . Hence, matrix  $J_4$  is not nilpotent since it has non-zero eigenvalues. In fact, it can be shown that any two characteristic polynomials  $P_{J_{2m+1}}(X)$  and  $P_{J_{2m+2}}(X)$  of matrices  $J_{2m+1}$  and  $J_{2m+2}$ ,  $m \geq 1$ , are related by  $P_{J_{2m+2}}(X) = X^2 P_{J_{2m+1}}(X)$ . Matrix  $J_{2m+1}$  ( $m \geq 1$ ) is nonsingular in general since  $a_l^- a_l^+ - b_l^- b_l^- \neq 0$ ,  $l \geq 2$ , on  $\omega \geq 0$ . Matrix  $J_{2m+1}$  is consequently not nilpotent. Therefore, matrix  $J_{2m+2}$  has non-zero eigenvalues and therefore cannot be nilpotent too. ■

To achieve nilpotency, setting all local convergence factors to zero is necessary yet not sufficient. The way in which local convergence factors are set to zero affects the degree of nilpotency (propositions 4.2 and 4.3) and can even destroy it (proposition 4.4).

WR converges exactly in three GJ iterations and in two GS iterations for  $N = 3$  if  $a_1^+ = a_2^- = a_2^+ = a_3^- = 0$  according to proposition 4.2. It turns out that such condition is too strong for  $N = 3$ . The following proposition presents a relaxed optimality requirement for this outlier case. Its demonstration is straightforward.

**Proposition 4.5** *Optimal WR for  $N = 3$ . If  $a_1^+ = a_3^- = 0$ , then WR converges in three iterations for GJ relaxation and in two iterations for GS relaxation.*

Finally, it is brought to the reader's attention that propositions 4.1, 4.3, 4.4 and 4.5 present new results. The optimal result for the GJ relaxation in proposition 4.2 has been first demonstrated by Gander et al. [75] for circuit problems using optimal transmission coupling conditions. In this work, this result is again found using a different approach where the iteration matrix is constructed and its nilpotency is demonstrated in section 4.4. However, the optimal result part of the GS relaxation in proposition 4.2 is novel.

The next analysis concerns the resistive coupling based WR algorithm and its convergence for chains made of identical and symmetric parts.

## 4.2 Convergence of Resistive Coupling-based Waveform Relaxation for Chains of Identical Symmetric Parts

The analysis concerns a chain of  $N$  identical symmetric parts at the exception may be of the two parts at the extremities. Each part is represented in the frequency-domain by its  $Z$ -parameters  $Z_{11}(i\omega)$ ,  $Z_{12}(i\omega)$ ,  $Z_{21}(i\omega)$  and  $Z_{22}(i\omega)$  with  $Z_{12} = Z_{21}$ ,  $Z_{11} = Z_{22}$ ,  $\omega \geq 0$ , and  $i^2 = -1$ . Insertion  $\{-R, 2R, -R\}$  is used to decouple every two consecutive parts and is realized as a Thévenin source in Figure 4.4. To keep the enlarged parts symmetric and identical, all relaxation resistances are set at same value in the partition of Figure 4.4. This way, all interior parts have equal left-side and right-side input impedances. The homogenous problem of Figure 4.5 is studied next. After taking  $\zeta_{n,n+1}^n = \zeta_{n,n+1}^{n+1} = R$  for  $1 \leq n \leq N - 1$  and  $Z_{n-1,n}^n = Z_{n,n+1}^n = Z$  for  $2 \leq n \leq N - 1$  in equations set (4.7), the iteration matrices  $\mathbf{J}'_N$  and  $\mathbf{S}'_N$  for the GJ and GS relaxations over one iteration, can be deduced from (4.6) and (4.11)

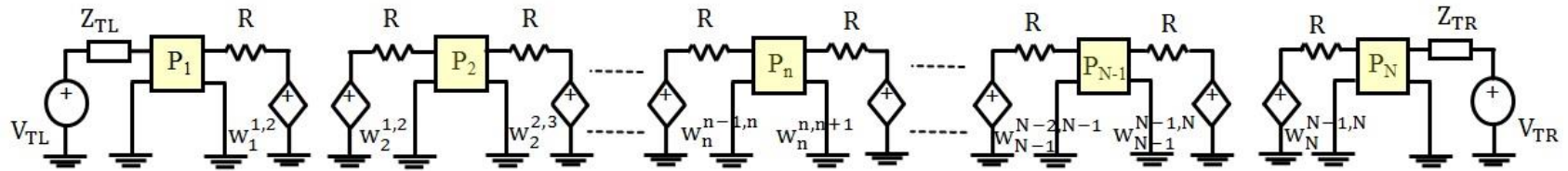


Figure 4.4: Resistive coupling of a chain of identical symmetric parts.

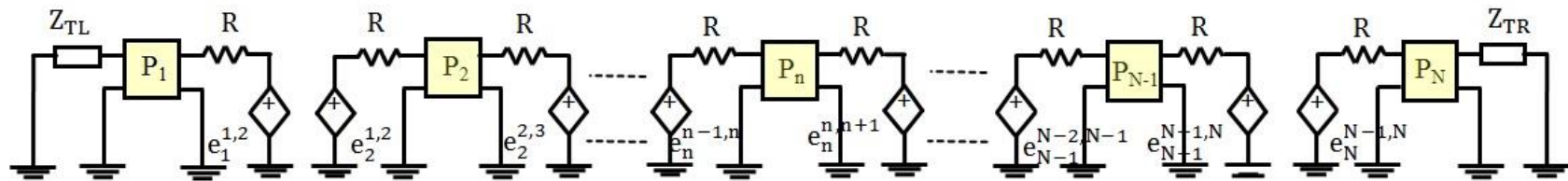


Figure 4.5: WR converge analysis circuit. The homogeneous problem.

$$J'_N = \left[ \begin{array}{cc|cc|c|c|c} 0 & a_1^+ & 0 & 0 & & & \\ a & 0 & 0 & b & & & \\ \hline b & 0 & 0 & a & 0 & 0 & \\ 0 & 0 & a & 0 & 0 & b & \\ \hline & \ddots & \ddots & & \ddots & \ddots & \\ & \ddots & \ddots & & \ddots & \ddots & \\ \hline & & & b & 0 & 0 & a & 0 & 0 \\ & & & 0 & 0 & a & 0 & 0 & b \\ \hline & & & & & & b & 0 & 0 & a \\ & & & & & & 0 & 0 & a_N^- & 0 \end{array} \right] \quad (4.23)$$

where

$$a = a_2^- = a_2^+ = \dots = a_{N-1}^- = a_{N-1}^+ = \frac{Z - R}{Z + R} \quad (4.24)$$

$$b = b_2^- = b_2^+ = \dots = b_{N-1}^- = b_{N-1}^+ = \frac{2RZ_{12}}{(Z + R)(Z_{11} + R)} \quad (4.25)$$

and

$$a_1^+ = \frac{Z_{1,2}^1 - R}{Z_{1,2}^1 + R} \quad (4.26)$$

$$a_N^- = \frac{Z_{N-1,N}^N - R}{Z_{N-1,N}^N + R} \quad (4.26)$$

In the same way, the GJ iteration matrix  $(J'_1)^2$  defined over two iterations, is expressed as follows

$$\mathcal{U}'_{\mathbb{N}})^2 = \left[ \begin{array}{c|c|c|c|c|c|c|c|c|c|c|c}
 a_1^+ a & 0 & 0 & a_1^+ b & 0 & 0 & & & & & & \\
 0 & a_1^+ a & ab & 0 & 0 & b^2 & & & & & & \\
 \hline
 0 & a_1^+ b & a^2 & 0 & 0 & ab & 0 & 0 & & & & \\
 ab & 0 & 0 & a^2 & ab & 0 & 0 & b^2 & & & & \\
 \hline
 b^2 & 0 & 0 & ab & a^2 & 0 & 0 & ab & 0 & 0 & & \\
 0 & 0 & ab & 0 & 0 & a^2 & ab & 0 & 0 & b^2 & & \\
 \hline
 & \ddots & \ddots & \ddots & \ddots & \ddots & \ddots & \ddots & \ddots & \ddots & & \\
 & \ddots & \ddots & \ddots & \ddots & \ddots & \ddots & \ddots & \ddots & \ddots & & \\
 \hline
 & & & b^2 & 0 & 0 & ab & a^2 & 0 & 0 & ab & 0 & 0 \\
 & & & 0 & 0 & ab & 0 & 0 & a^2 & ab & 0 & 0 & b^2 \\
 \hline
 & & & & & b^2 & 0 & 0 & ab & a^2 & 0 & 0 & ab \\
 & & & & & 0 & 0 & ab & 0 & 0 & a^2 & a_{\mathbb{N}}^- b & 0 \\
 \hline
 & & & & & & & b^2 & 0 & 0 & ab & a_{\mathbb{N}}^- a & 0 \\
 & & & & & & & 0 & 0 & a_{\mathbb{N}}^- b & 0 & 0 & a_{\mathbb{N}}^- a
 \end{array} \right] \quad (4.27)$$

Note that:

$$\|(\mathcal{J}'_N)^2\|_1 = \|(\mathcal{J}'_N)^2\|_\infty = \max\{\sigma_1, \sigma_2, \sigma_3, \sigma_4, \sigma_5, \sigma_6, \sigma_7\} \quad (4.28)$$

at every frequency point  $\omega \geq 0$ , where

$$\begin{aligned} \sigma_1 &= |a_1^+|(|a| + |b|) \\ \sigma_2 &= |b|(|a| + |b|) + |a||a_1^+| \\ \sigma_3 &= |a|(|a| + |b|) + |b||a_1^+| \\ \sigma_4 &= (|a| + |b|)^2 \\ \sigma_5 &= |a|(|a| + |b|) + |b||a_N^-| \\ \sigma_6 &= |b|(|a| + |b|) + |a||a_N^-| \\ \sigma_7 &= |a_N^-|(|a| + |b|) \end{aligned} \quad (4.29)$$

Both 1-norm and  $\infty$ -norm take a value which is independent of the size  $N$  of the chain at every frequency point  $\omega \geq 0$  for  $N \geq 5$ . In the following illustrative example, we examine the convergence behavior of WR for the conventional lumped RLCG T model which is realized in the circuit environment with chains made of identical symmetric parts or sections.

### 4.2.1 Illustrative Example

Consider the following PUL parameters:  $R = 25 \Omega/\text{m}$ ,  $L = 0.6 \mu\text{H}/\text{m}$ ,  $C = 121 \text{ pF}/\text{m}$ , and  $G = 20 \text{ GS}/\text{m}$  for a line segment of length  $(0.1/300) \text{ m}$ . This segment is used to build a straight line whose length goes from  $(0.1/300) \text{ m}$  to  $0.1 \text{ m}$  by steps of  $(0.1/300) \text{ m}$ . Every segment is represented in the time-domain by one lumped RLCG T section [94] with the following circuit elements  $R_0 = 4.16 \text{ m}\Omega$ ,  $L_0 = 66.67 \text{ pH}$ ,  $C_0 = 40.33 \text{ fF}$  and  $G_0 = 6.66 \text{ pS}$ . Note that the  $0.1 \text{ m}$  long transmission line is modeled by at least 279 sections. This shows that our segmentation properly models the constructed transmission line at every step. A voltage pulse source of  $1V_{\text{peak}}$  and  $0.05 \text{ ns}$  rise/fall time drives the circuit through a  $10 \Omega$ -resistance while a  $1.0 \text{ pF}$  load is

connected at the far end of our constructed line. Relaxation resistances are set at a value  $R = 20\Omega$ . The GJ iteration matrix  $(\mathbf{J}'_N)^2$  is numerically calculated at every frequency point of the  $2^{11}$  equidistant points on the frequency interval  $0 \leq f \leq 20\text{GHz}$  [104] for chains of lengths 3, 5, 10, 50, 100, 150, 200, 250 and 300 line segments\T sections. The 1-norm and spectral norm are reported on Figures 4.6 and 4.7. The spectral radius is numerically computed on the same frequency sampling and is reported on Figures 4.8-4.10. The numerical results suggest that the spectral norm takes values less than one. They also show that 1-norm and  $\infty$ -norm can be greater than one. The fact that spectral radii  $\rho(\omega)$  of matrices  $(\mathbf{J}'_N)^2$  are less than one on the frequency sampling confirms the observed convergence of WR for chains of circuits when resistive coupling is implemented. Norm inequality  $\rho \leq \left\| (\mathbf{J}'_N)^2 \right\|_2 \leq \sqrt{\left\| (\mathbf{J}'_N)^2 \right\|_1 \left\| (\mathbf{J}'_N)^2 \right\|_\infty} = \left\| (\mathbf{J}'_N)^2 \right\|_1$  however fails to produce an upperbound of  $\left\| (\mathbf{J}'_N)^2 \right\|_2$  and therefore of  $\rho$ , which has values less than one. Hence, it cannot be used to demonstrate the WR convergence for this class of circuit problems despite the fact the 1-norm and  $\infty$ -norm can be readily computed, see (4.28) and (4.29).

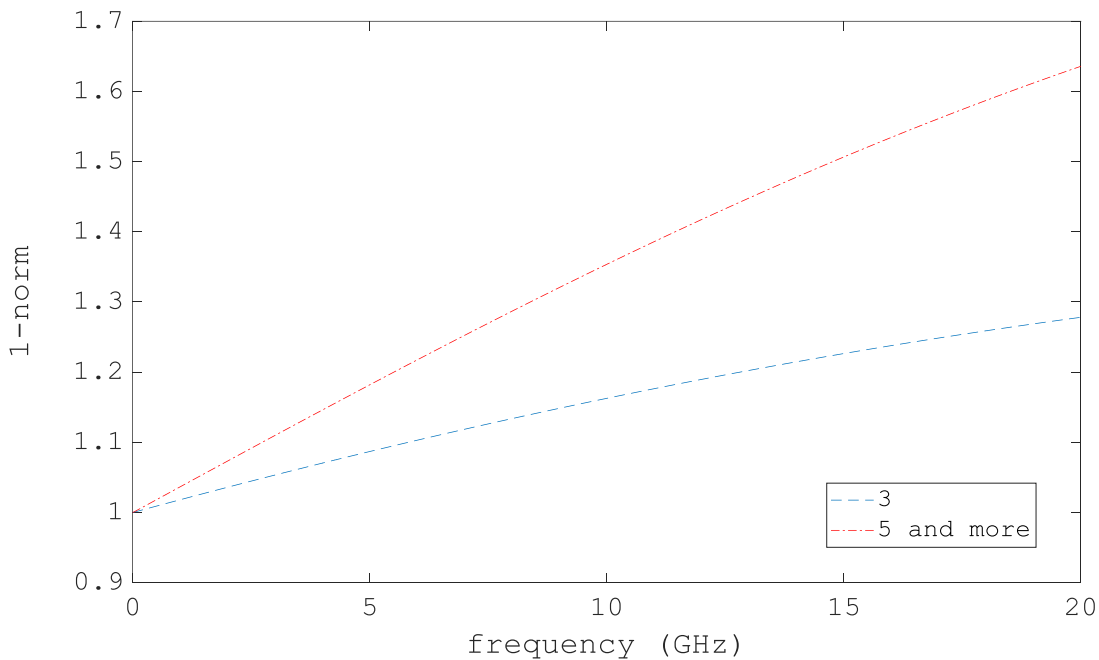


**Figure 4.6: Norms  $\left\| (\mathbf{J}'_N)^2 \right\|_1$ .  $N \in \{3, 5, 10, 50, 100, 150, 200, 250, 300\}$ . Illustrative example.**

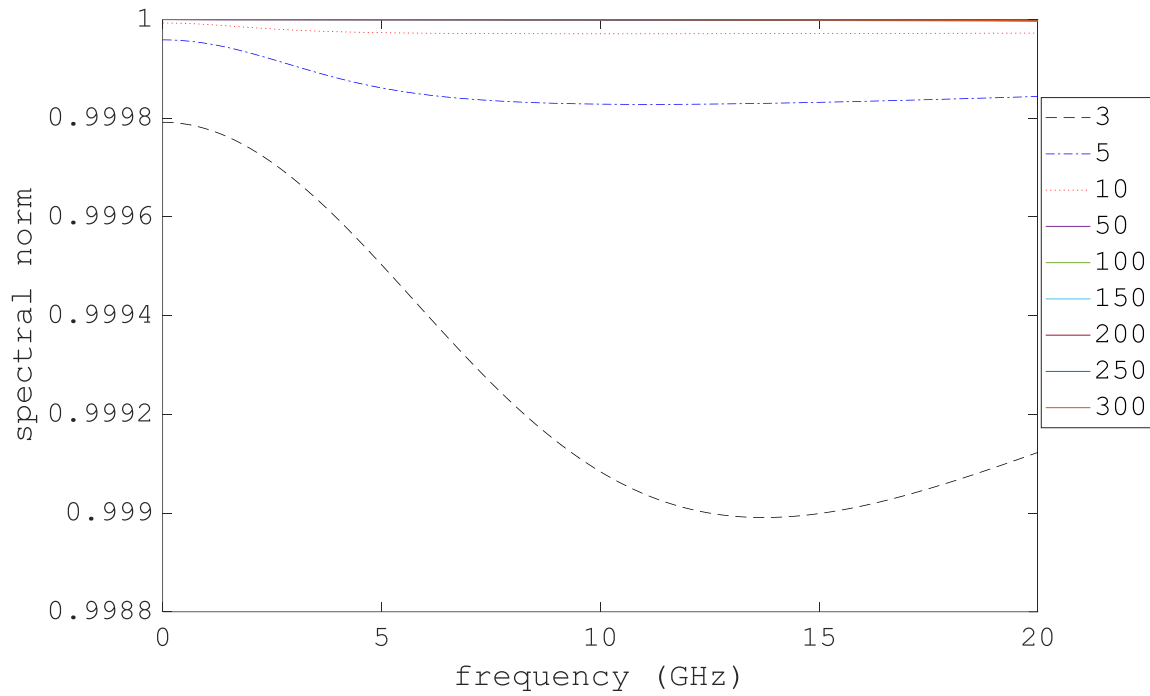


**Figure 4.7: Spectral norms  $\|(J'_N)^2\|_2$ ,  $N \in \{3, 5, 10, 50, 100, 150, 200, 250, 300\}$ .**

**Illustrative example.**

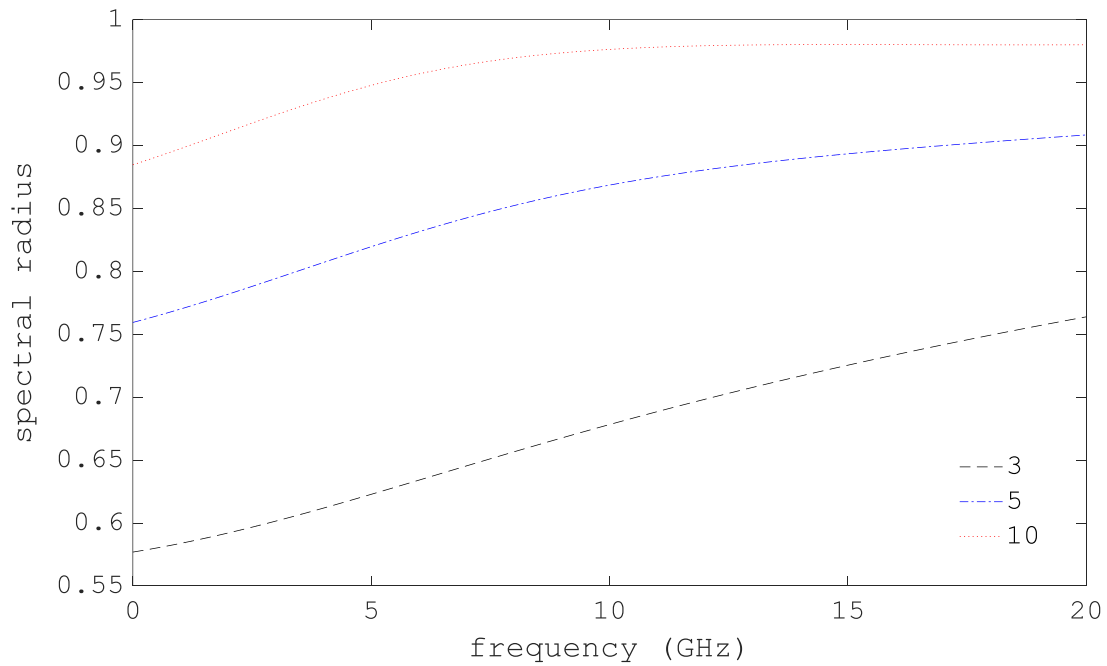


**Figure 4.8: Spectral radii  $\rho((J'_N)^2)$ ,  $N = 3, 5, 10$ . Illustrative example.**



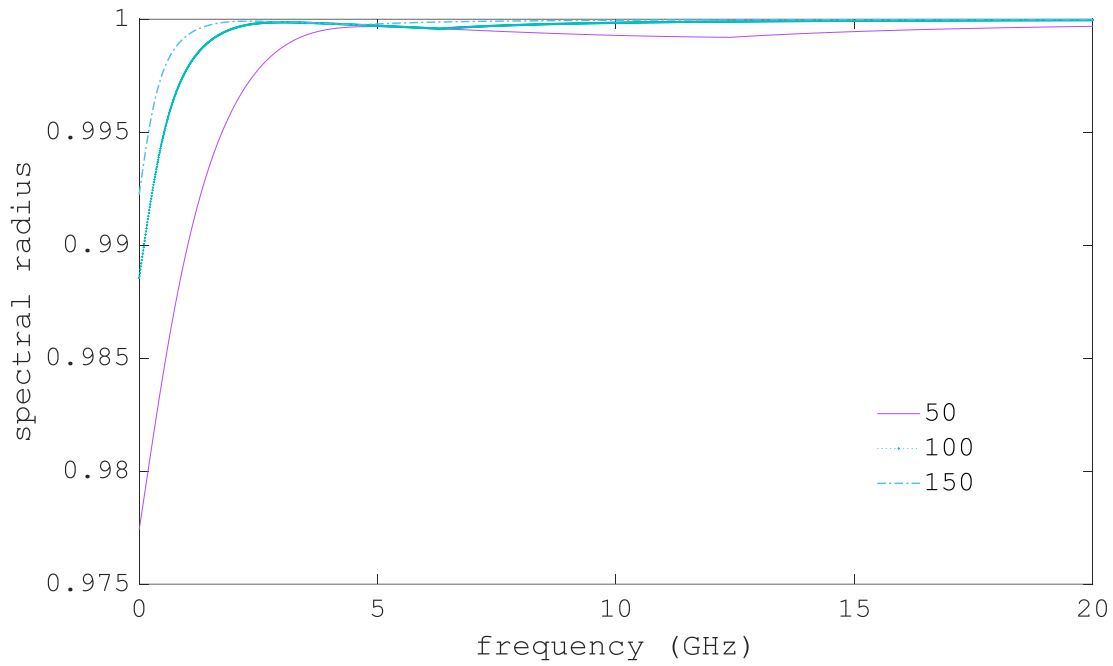


**Figure 4.9: Spectral radii  $\rho((J'_N)^2)$ ,  $N = 50, 100, 150$ . Illustrative example.**

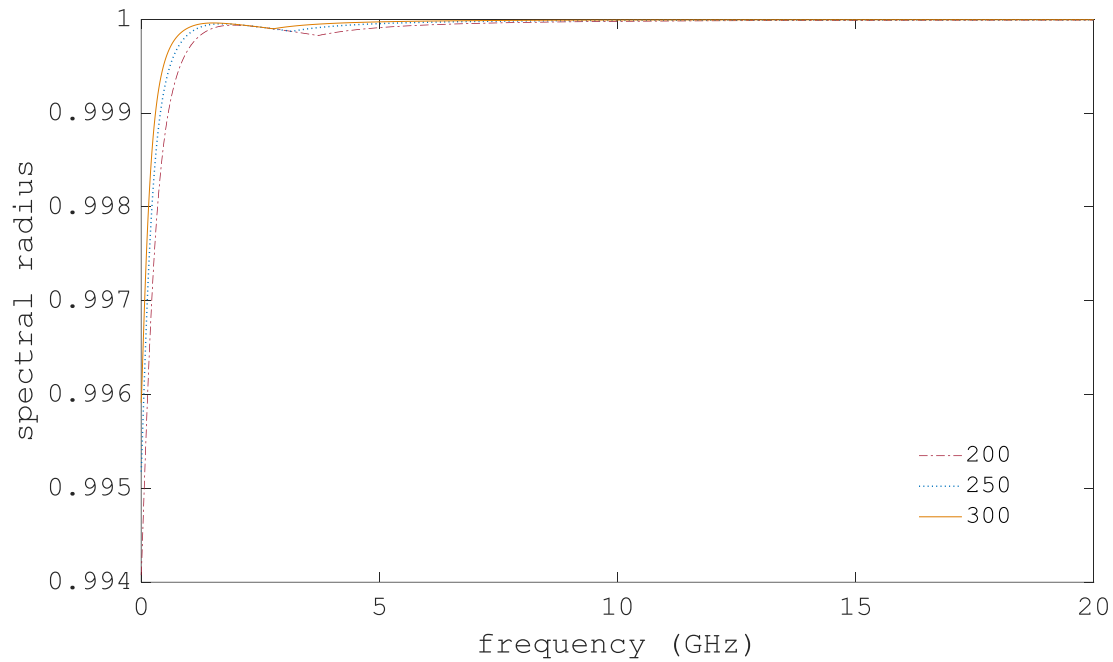


**Figure 4.10: Spectral radii  $\rho((J'_N)^2)$ ,  $N = 200, 250, 300$ . Illustrative example.**

To demonstrate the WR convergence, a valid upperbound, ie of value less than one, is produced for the spectral radius of the GJ and GS iteration matrices. The proposed upperbound does not depend on the number  $N$  of serial parts. It shows that WR converges independently of the chain length  $N$ .

First, a preliminary result is introduced in the following lemma

**Lemma 4.1.** Coefficients  $a(i\omega, R)$  and  $b(i\omega, R)$  defined in equations (4.17) and (4.18), satisfy

$$|a(i\omega, R)|^2 + |b(i\omega, R)|^2 + 2 \left| \Re \left( a(i\omega, R) \bar{b}(i\omega, R) \right) \right| < 1 \quad (4.30)$$

for all angular frequency  $\omega \geq 0$  and coupling resistances  $R > 0$ .

**Proof.** We are going to demonstrate that coefficients  $a = a(i\omega, R)$  and  $b = b(i\omega, R)$  given in eq. (4.17) and in eq. (4.18) respectively, satisfy  $|a - b| < 1$  and  $|a + b| < 1$ . The reason is that  $|a|^2 + |b|^2 + 2|\Re(a\bar{b})| = \max(|a - b|^2, |a + b|^2)$  since  $|a - b|^2 = |a|^2 + |b|^2 - 2\Re(a\bar{b})$  and  $|a + b|^2 = |a|^2 + |b|^2 + 2\Re(a\bar{b})$ .

First, we use the following parameter change;

$$Z_a = Z_{11} - Z_{12} \qquad Z_b = Z_{11} + Z_{12} \quad (4.31)$$

Input impedance  $Z$  and coefficients  $a$  and  $b$  are expressed in terms of  $Z_a$  and  $Z_b$  by

$$Z = \frac{2Z_a Z_b + (Z_a + Z_b)R}{Z_a + Z_b + 2R} \quad (4.32)$$

$$a = \frac{Z_a Z_b - R^2}{Z_a Z_b + (Z_a + Z_b)R + R^2} \quad (4.33)$$

$$b = \frac{(Z_b - Z_a)R}{Z_a Z_b + (Z_a + Z_b)R + R^2} \quad (4.34)$$

Next, we compute  $|a + b|^2 = P(R)/Q(R)$

$$\begin{aligned}
P(R) = & |Z_a|^2|Z_b|^2 + 2[|Z_b|^2\Re(Z_a) + |Z_a|^2\Re(Z_b)]R + (|Z_a|^2+|Z_b|^2 - 4\Re(Z_a)\Re(Z_b))R^2 \\
& + 2(\Re(Z_a) - \Re(Z_b))R^3 + R^4
\end{aligned}$$

(4.35)

and

$$\begin{aligned}
Q(R) = & |Z_a|^2|Z_b|^2 + 2(|Z_a|^2\Re(Z_b) + |Z_b|^2\Re(Z_a))R + 2(|Z_a|^2+|Z_b|^2 + 4\Re(Z_a)\Re(Z_b))R^2 \\
& + (\Re(Z_a) + \Re(Z_b))R^3 + R^4
\end{aligned}$$

(4.36)

we view  $P$  and  $Q$  as two polynomials of unknown  $R$ . Since  $P$  and  $Q$  have same degree four and since  $R > 0$ , then we can compare them by inspecting their coefficients. We use the fact that lattice impedances  $Z_a$  and  $Z_b$ , defined in (4.31), satisfy  $\Re(Z_a(i\omega)) > 0$  and  $\Re(Z_b(i\omega)) > 0$  for all  $\omega \geq 0$  in a dissipative circuit, see [96, Sec. 1.6]. We find that  $P(R) < Q(R)$  and hence  $|a + b|^2 < 1$  for  $\omega \in \mathbb{R}$  and  $R > 0$ .

We follow same steps to show that  $|a - b|^2 < 1$ . Let  $|a - b|^2 = S(R)/Q(R)$ . We only need to compute numerator  $S(R)$  since denominator  $Q(R)$  is already derived in 4.36.

$$\begin{aligned}
S(R) = & |Z_a|^2|Z_b|^2 + 2[|Z_a|^2\Re(Z_b) - |Z_b|^2\Re(Z_a)]R + (|Z_a|^2+|Z_b|^2 - 4\Re(Z_a)\Re(Z_b))R^2 \\
& + 2(\Re(Z_a) - \Re(Z_b))R^3 + R^4
\end{aligned}$$

(4.37)

A comparison of the coefficients of polynomials  $S(R)$  and  $Q(R)$  shows that  $S(R) < Q(R)$ . ■

Next, the proposed upperbound is presented in the following theorem

**Theorem 4.2.** Spectral radius  $\rho(\omega, R)$  of matrices  $(\mathbf{J}'_N)^2$  and  $\mathbf{S}'_N$  for sizes  $N \geq 5$ , has the bound

$$\begin{aligned} \rho(\omega, R) \leq \max & \left( |a_{1t}(i\omega, R)|^2, |a(i\omega, R)|^2 + |b(i\omega, R)|^2 \right. \\ & \left. + 2 \left| \Re \left( a(i\omega, R) \bar{b}(i\omega, R) \right) \right|, |a_{rt}(i\omega, R)|^2 \right) < 1 \end{aligned} \quad (4.38)$$

at any frequency point  $\omega \geq 0$  and for any coupling resistance  $R > 0$ .

**Proof.** We consider the GJ iteration  $(\mathbf{J}'_N)^2$ , defined over two iterations in (4.27). The spectral radius  $\rho((\mathbf{J}'_N)^2)$  of matrix  $(\mathbf{J}'_N)^2$  satisfies the following inequality

$$\rho((\mathbf{J}'_N)^2) \leq \|(\mathbf{J}'_N)^2\|_2 \leq (\mathbf{J}'_N)^2 = \rho((\mathbf{J}'_N)^* \mathbf{J}'_N) = \rho(\mathbf{J}'_N (\mathbf{J}'_N)^*) \quad (4.39)$$

where  $(\mathbf{J}'_N)^*$  is the Hermitian transpose of matrix  $\mathbf{J}'_N$  in (4.23). The positive definite matrix

$$\mathbf{J}'_N (\mathbf{J}'_N)^* = \begin{bmatrix} |a_1^+|^2 & & & & & \\ & |a|^2 + |b|^2 & 2\Re(a\bar{b}) & & & \\ & 2\Re(a\bar{b}) & |a|^2 + |b|^2 & & & \\ & & & \ddots & \ddots & \\ & & & \ddots & \ddots & \\ & & & & & |a|^2 + |b|^2 & 2\Re(a\bar{b}) \\ & & & & & 2\Re(a\bar{b}) & |a|^2 + |b|^2 \\ & & & & & & & |a_N^-|^2 \end{bmatrix}$$

$\mathbf{J}'_N (\mathbf{J}'_N)^*$  is given by

$$(4.40)$$

Matrix  $\mathbf{J}'_N (\mathbf{J}'_N)^*$  possesses the following eigenvalues  $|a_1^+|^2$ ,  $|a|^2 + |b|^2 - 2\Re(a\bar{b})$ ,  $|a|^2 + |b|^2 + 2\Re(a\bar{b})$  and  $|a_N^-|^2$  counted with multiplicity. At every frequency point  $\omega$ , the spectral radius  $\rho_o(\omega)$  of matrix  $\mathbf{J}'_N (\mathbf{J}'_N)^*$  satisfies  $\rho_o(\omega, R) = \max(|a_1^+(i\omega, R)|^2, |a(i\omega, R)|^2 + |b(i\omega, R)|^2 + 2|\Re(a(i\omega, R)\bar{b}(i\omega, R))|, |a_N^-(i\omega, R)|^2)$ . Using the result of Lemma 4.1, we have the bound  $\rho((\mathbf{J}'_N)^2) \leq \rho_o < 1$ . ■

Spectral radius  $\rho$  is bounded by a positive function  $\rho_o$  of variable  $(\omega, R)$  that does not depend on size  $N$ ,  $N \geq 5$ , and whose value is always less than one. The WR always converges independently of the number  $N$  of parts in the chain.

The following section provides a detailed derivation for the iteration matrices of the WR algorithm in both GJ and GS relaxations.

### 4.3 Construction of iteration matrices

A detailed derivation of the expressions of matrices  $(\mathbf{J}_N)^2$  and  $\mathbf{S}_N$  in (4.6)-(4.9) and (4.11)-(4.15). is provided here.

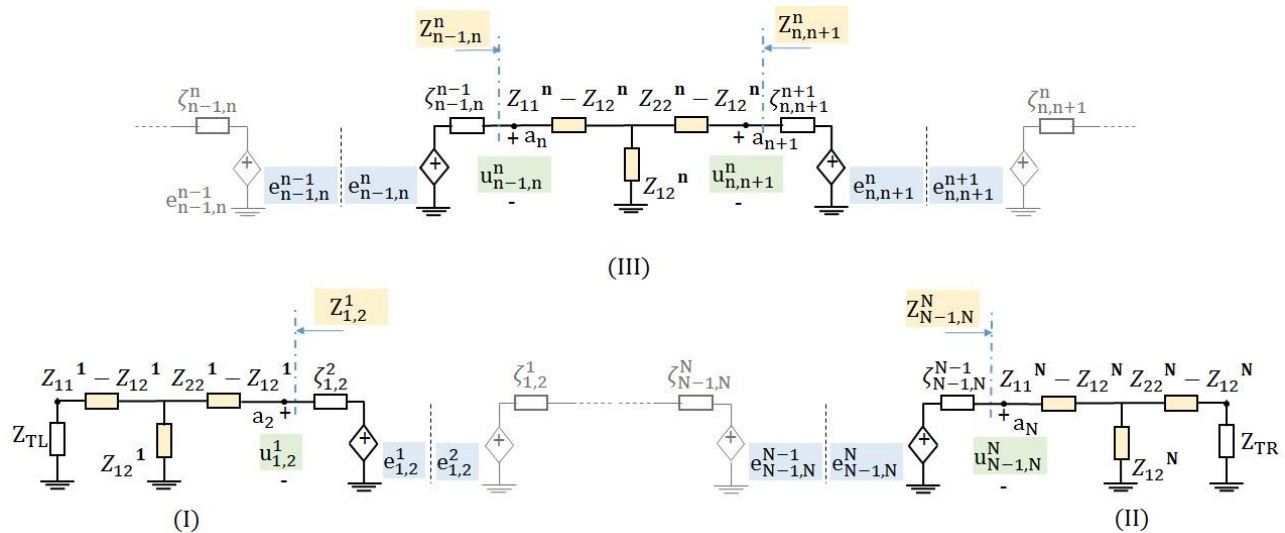


**Figure 4.11: Frequency-domain representation of decoupled parts. (I) Left end. (II) Right end. Interior (III).**

First let us calculate the input impedance of all parts at the artificial interfaces in Figure 4.11.

$$Z_{1,2}^1 = Z_{22}^1 - \frac{(Z_{12}^1)^2}{Z_{11}^1 + Z_{TL}} \quad \text{for part 1 at the left-hand extremity,}$$

$$Z_{N-1,N}^N = Z_{11}^N - \frac{(Z_{12}^N)^2}{Z_{22}^N + Z_{TL}} \quad \text{for part N at the right-hand extremity,} \quad (4.41)$$

For any interior part  $P_n$ , we have

$$Z_{n-1,n}^n = Z_{11}^n - \frac{(Z_{12}^n)^2}{Z_{22}^n + \zeta_{n,n+1}^{n+1}} \quad \text{and}$$

$$Z_{n,n+1}^n = Z_{22}^n - \frac{(Z_{12}^n)^2}{Z_{11}^n + \zeta_{n-1,n}^{n-1}} \quad 2 \leq n \leq N-1$$

Next, the expression of node voltages  $u_{1,2}^1, u_{1,2}^2, \dots, u_{n-1,n}^n, u_{n,n+1}^n, \dots, u_{N-1,N}^N$  in Figure 4.11 must be determined. These expressions will be used in the update of the relaxation sources

$$u_{1,2}^1 = \frac{Z_{1,2}^1}{Z_{1,2}^1 + \zeta_{1,2}^1} e_{1,2}^1$$

for part 1, and

$$\begin{aligned} u_{n-1,n}^n &= \frac{Z_{n-1,n}^n}{Z_{n-1,n}^n + \zeta_{n-1,n}^{n-1}} e_{n-1,n}^n + \frac{Z_{12}^n \zeta_{n-1,n}^{n-1}}{(Z_{11}^n + \zeta_{n-1,n}^{n-1})(Z_{n,n+1}^n + \zeta_{n,n+1}^n)} e_{n,n+1}^n \\ u_{n,n+1}^n &= \frac{Z_{12}^n \zeta_{n,n+1}^{n+1}}{(Z_{22}^n + \zeta_{n,n+1}^{n+1})(Z_{n-1,n}^n + \zeta_{n-1,n}^{n-1})} e_{n-1,n}^n + \frac{Z_{n,n+1}^n}{Z_{n,n+1}^n + \zeta_{n,n+1}^{n+1}} e_{n,n+1}^n \end{aligned} \quad (4.42)$$

for any interior part  $n$  of the chain,  $2 \leq n \leq N-1$ . Finally,

$$u_{N-1,N}^N = \frac{Z_{N-1,N}^N}{Z_{N-1,N}^N + Z_{N-1,N}^{N-1}} e_{N-1,N}^N$$

for part  $N$ .

### 4.3.1 Gauss-Jacobi iteration matrix

Sources update is performed as follows

$$e_{1,2}^{1(k+1)} = \left(1 + \frac{\zeta_{1,2}^2}{\zeta_{1,2}^1}\right) u_{1,2}^{2(k)} - \frac{\zeta_{1,2}^2}{\zeta_{1,2}^1} e_{1,2}^{2(k)}$$

⋮

$$\begin{aligned}
e_{n-1,n}^{n(k+1)} &= \left(1 + \frac{\zeta_{n-1,n}^{n-1}}{\zeta_{n-1,n}^n}\right) u_{n-1,n}^{n-1(k)} - \frac{\zeta_{n-1,n}^{n-1}}{\zeta_{n-1,n}^n} e_{n-1,n}^{n-1(k)} \\
e_{n,n+1}^{n(k+1)} &= \left(1 + \frac{\zeta_{n,n+1}^{n+1}}{\zeta_{n,n+1}^n}\right) u_{n,n+1}^{n+1(k)} - \frac{\zeta_{n,n+1}^{n+1}}{\zeta_{n,n+1}^n} e_{n,n+1}^{n+1(k)}
\end{aligned} \tag{4.43}$$

$$(2 \leq n \leq N-1)$$

$$e_{N-1,N}^{N(k+1)} = \left(1 + \frac{\zeta_{N-1,N}^{N-1}}{\zeta_{N-1,N}^N}\right) u_{N-1,N}^{N-1(k)} - \frac{\zeta_{N-1,N}^{N-1}}{\zeta_{N-1,N}^N} e_{N-1,N}^{N-1(k)}$$

expressions of  $u_{1,2}^1, u_{1,2}^2, \dots, u_{n-1,n}^n, u_{n,n+1}^{n+1}, \dots, u_{N-1,N}^N$  in (4.42) at iteration  $k$  are substituted in the equations set (4.43)

$$\begin{aligned}
e_{1,2}^{1(k+1)} &= a_2^- e_{1,2}^{2(k)} + b_2^- e_{2,3}^{2(k)} \\
e_{1,2}^{2(k+1)} &= a_1^+ e_{1,2}^{1(k)} \\
&\vdots \\
e_{n-1,n}^{n-1(k+1)} &= a_n^- e_{n-1,n}^{n(k)} + b_n^- e_{n,n+1}^{n(k)} \\
e_{n-1,n}^{n(k+1)} &= b_{n-1}^+ e_{n-2,n-1}^{n-1(k)} + a_{n-1}^+ e_{n-1,n}^{n-1(k)} \\
&\vdots
\end{aligned} \tag{4.44}$$

$$\begin{aligned}
e_{N-1,N}^{N-1(k+1)} &= a_N^- e_{N-1,N}^{N(k)} \\
e_{N-1,N}^{N(k+1)} &= b_N^+ e_{N-2,N-1}^{N-1(k)} + a_{N-1}^+ e_{N-1,N}^{N-1(k)}
\end{aligned}$$

where coefficients  $a_1^+, a_2^-, a_2^+, a_2^-, \dots, a_{N-1}^+, a_{N-1}^-,$  and  $a_N^-$  are defined in equations set (4.7). The vector form representation of equations (4.44) with respect to vector  $\mathbf{e}_1 =$

$(e_{1,2}^2, e_{1,2}^1, e_{2,3}^3, e_{2,3}^2, \dots, e_{n-1,n}^n, e_{n-1,n}^{n-1}, \dots, e_{N-1,N}^N, e_{N-1,N}^{N-1})^T$  defined in (4.3), produces the GJ iteration matrix  $J_N$  defined over one iteration in (4.6).

Taking equations set (4.44) at iteration  $(k+2)$ , it is possible to obtain an update over two iterations

$$\begin{aligned}
e_{1,2}^{1(k+2)} &= a_1^+ a_2^- e_{1,2}^{1(k)} + b_2^- a_3^- e_{2,3}^{3(k)} + b_2^- b_3^- e_{3,4}^{3(k)} \\
e_{1,2}^{2(k+2)} &= a_1^+ a_2^- e_{1,2}^{2(k)} + a_1^+ b_2^- e_{2,3}^{2(k)} \\
e_{2,3}^{2(k+2)} &= b_2^+ a_3^- e_{1,2}^{2(k)} + a_2^+ a_3^- e_{2,3}^{2(k)} + b_3^- a_4^- e_{3,4}^{4(k)} + b_3^- b_4^- e_{4,5}^{4(k)} \\
e_{2,3}^{3(k+2)} &= a_1^- b_2^+ e_{1,2}^{1(k)} + a_2^+ a_3^- e_{2,3}^{3(k)} + a_2^+ b_3^- e_{3,4}^{3(k)} \\
&\vdots \\
e_{n-1,n}^{n-1(k+2)} &= a_n^- b_{n-1}^+ e_{n-2,n-1}^{n-1(k)} + a_{n-1}^+ a_n^- e_{n-1,n}^{n-1(k)} + a_n^- b_n^+ e_{n-1,n}^{n(k)} \\
&\quad + b_n^- a_n^+ e_{n,n+1}^{n(k)} \\
e_{n-1,n}^{n(k+2)} &= b_{n-2}^- b_{n-1}^+ e_{n-3,n-2}^{n-2(k)} + b_{n-1}^+ a_{n-2}^+ e_{n-2,n-1}^{n-2(k)} + a_{n-1}^+ a_n^- e_{n-1,n}^{n(k)} \\
&\quad + a_{n-1}^+ b_n^- e_{n,n+1}^{n(k)} \\
&\quad (3 \leq n \leq N-2) \\
&\vdots \\
e_{N-2,N-1}^{N-2(k+2)} &= b_{N-2}^+ a_{N-1}^- e_{N-3,N-2}^{N-2(k)} + a_{N-2}^+ a_{N-1}^- e_{N-2,N-1}^{N-2(k)} + b_{N-1}^- a_N^- e_{N-1,N}^{N(k+2)} \\
e_{N-2,N-1}^{N-1(k+2)} &= b_{N-3}^+ b_{N-2}^+ e_{N-4,N-3}^{N-3} + a_{N-3}^+ b_{N-2}^+ e_{N-3,N-2}^{N-3} + a_{N-2}^+ a_{N-1}^- e_{N-2,N-1}^{N-1} \\
&\quad + a_{N-2}^+ b_{N-1}^- e_{N-1,N}^{N-1}
\end{aligned} \tag{4.45}$$



$$e_{N-1,N}^{N-1(k+2)} = b_{N-1}^+ a_N^- e_{N-2,N-1}^{N-1(k)} + a_{N-1}^+ a_N^- e_{N-1,N}^{N-1(k)}$$

$$e_{N-1,N}^N(k+2) = b_{N-2}^+ b_{N-1}^+ e_{N-3,N-2}^{N-2(k)} + a_{N-2}^+ b_{N-1}^+ e_{N-2,N-1}^{N-2(k)} + a_{N-1}^+ a_N^- e_{N-1,N}^N(k)$$

In vector form representation, equations set (4.45) yields GJ iteration  $(\mathbf{J}_N)^2$  defined over two iterations in (4.9).

Next, we derive iteration matrix  $\mathbf{S}_N$  for the GS relaxation by considering error vector  $\mathbf{e}_2$  (4.4)

### 4.3.2 Gauss-Seidel iteration matrix

One GS iteration is executed in two phases. First, all relaxation sources  $e_{1,2}^1, \dots, e_{2n,2n+1}^{2n+1}$ ,  $e_{2n+1,2n+2}^{2n+1}$ ,  $n \geq 1$ , connected to odd numbered parts are initialized and these parts are solved. Then, the solution of the odd numbered parts is used to update all relaxation sources  $e_{2n-1,2n}^{2n}$ ,  $e_{2n,2n+1}^{2n}$ ,  $n \geq 1$  connected to even numbered parts which are then solved. In the next iteration all sources connected to odd numbered parts are first updated using the solution of the even set from previous iteration and then the odd set is solved again. The even set is solved next after all its sources are updated. The GS iteration is sustained through this two-times update mechanism as opposed to the one-time mechanism in the GJ relaxation. Hence, it is natural to consider error vector  $\mathbf{e}_2 = (e_{1,2}^1, e_{2,3}^3, e_{3,4}^3, e_{4,5}^5, e_{5,6}^5, \dots, e_{1,2}^2, e_{2,3}^2, e_{3,4}^4, e_{4,5}^4, e_{5,6}^6, e_{6,7}^6, \dots)^T$  in (4.4). Relaxation sources are updated according to the following equations

$$e_{1,2}^{1(k+1)} = \left(1 + \frac{\zeta_{1,2}^2}{\zeta_{1,2}^1}\right) u_{1,2}^{2(k)} - \frac{\zeta_{1,2}^2}{\zeta_{1,2}^1} e_{1,2}^{2(k)}$$

⋮

$$e_{2n,2n+1}^{2n+1(k+1)} = \left(1 + \frac{\zeta_{2n,2n+1}^{2n}}{\zeta_{2n,2n+1}^{2n+1}}\right) u_{2n,2n+1}^{2n(k)} - \frac{\zeta_{2n,2n+1}^{2n}}{\zeta_{2n,2n+1}^{2n+1}} e_{2n,2n+1}^{2n(k)}$$

$$e_{2n+1,2n+2}^{2n+1(k+1)} = \left(1 + \frac{\zeta_{2n+1,2n+2}^{2n+2}}{\zeta_{2n+1,2n+2}^{2n+1}}\right) u_{2n+1,2n+2}^{2n+2(k)} - \frac{\zeta_{2n+1,2n+2}^{2n+2}}{\zeta_{2n+1,2n+2}^{2n+1}} e_{2n+1,2n+2}^{2n+2(k)}$$

for odd numbered parts, and

$$e_{2n-1,2n}^{2n(k)} = \left( 1 + \frac{\zeta_{2n-1,2n}^{2n-1}}{\zeta_{2n-1,2n}^{2n}} \right) u_{2n-1,2n}^{2n-1(k)} - \frac{\zeta_{2n-1,2n}^{2n-1}}{\zeta_{2n-1,2n}^{2n}} e_{2n-1,2n}^{2n-1(k)} \quad (4.46)$$

$$e_{2n,2n+1}^{2n(k)} = \left( 1 + \frac{\zeta_{2n,2n+1}^{2n+1}}{\zeta_{2n,2n+1}^{2n}} \right) u_{2n,2n+1}^{2n+1(k)} - \frac{\zeta_{2n,2n+1}^{2n+1}}{\zeta_{2n,2n+1}^{2n}} e_{2n,2n+1}^{2n+1(k)}$$

$$n \geq 1$$

For even numbered parts. Equations (4.46) are represented in vector form by

$$\mathbf{e}_{\text{even}}^{(k)} = \mathbf{M}' \mathbf{e}_{\text{odd}}^{(k)} \quad (4.47)$$

$$\mathbf{e}_{\text{odd}}^{(k+1)} = \mathbf{M} \mathbf{e}_{\text{even}}^{(k)} \quad (4.48)$$

$$k \in \mathbb{N}$$

with respect to  $(N-1) \times 1$  vectors  $\mathbf{e}_{\text{odd}} = (e_{1,2}^1, e_{2,3}^3, e_{3,3}^3, e_{4,5}^5, e_{5,6}^5, \dots)^T$  and  $\mathbf{e}_{\text{even}} = (e_{1,2}^2, e_{2,3}^2, e_{3,4}^4, e_{4,5}^4, \dots)^T$ .  $(N-1) \times (N-1)$  matrices  $\mathbf{M}$  and  $\mathbf{M}'$  are given by

$$\mathbf{M} = \begin{bmatrix} a_2^- & b_2^- & & & & & \\ b_2^+ & a_2^+ & & & & & \\ \hline & & a_4^- & b_4^- & & & \\ & & a_4^+ & b_4^+ & & & \\ \hline & & & & \ddots & \ddots & \\ & & & & \ddots & \ddots & \\ \hline & & & & & & a_{N-2}^- & b_{N-2}^- \\ & & & & & & b_{N-2}^+ & a_{N-2}^+ \\ \hline & & & & & & & a_N^- \end{bmatrix} \quad (4.49)$$

and

$$M' = \begin{bmatrix} a_1^+ & & & & \\ & a_3^- & b_3^- & & \\ & b_3^+ & a_3^+ & & \\ & & & a_5^- & b_5^- \\ & & & a_5^+ & b_5^+ \\ & & & \ddots & \ddots \\ & & & \ddots & \ddots \\ & & & & a_{N-1}^- & b_{N-1}^- \\ & & & & b_{N-1}^+ & a_{N-1}^+ \end{bmatrix} \quad (4.50)$$

when  $N$  is even, and

$$M = \begin{bmatrix} & a_2^- & b_2^- & & \\ & b_2^+ & a_2^+ & & \\ & & & a_4^- & b_4^- \\ & & & b_4^+ & a_4^+ \\ & & & & \ddots & \ddots \\ & & & & \ddots & \ddots \\ & & & & & a_{N-1}^- & b_{N-1}^- \\ & & & & & a_{N-1}^+ & b_{N-1}^+ \end{bmatrix} \quad (4.51)$$

and

$$\mathbf{M}' = \begin{bmatrix} a_1^+ & & & & \\ & a_3^- & b_3^- & & \\ & b_3^+ & a_3^+ & & \\ & & & \ddots & \ddots \\ & & & \ddots & \ddots \\ & & & & a_{N-1}^- & b_{N-1}^- \\ & & & & b_{N-1}^+ & a_{N-1}^+ \\ & & & & & & a_N^- \end{bmatrix} \quad (4.52)$$

when  $N$  is odd. Equations (4.31) and (4.32) lead to recursive relations over one GS iteration

$$\mathbf{e}_{\text{odd}}^{(k+1)} = \mathbf{M}\mathbf{M}'\mathbf{e}_{\text{odd}}^{(k)} \quad (4.53)$$

$$\mathbf{e}_{\text{even}}^{(k+1)} = \mathbf{M}'\mathbf{M}\mathbf{e}_{\text{even}}^{(k)} \quad (4.54)$$

$k \in \mathbb{N}$

Matrix products  $\mathbf{M}\mathbf{M}' = \mathbf{A}$  and  $\mathbf{M}'\mathbf{M} = \mathbf{B}$  introduced earlier in (4.10)-(4.15). It can be easily demonstrated that matrices  $(\mathbf{J}_N)^2$  and  $\mathbf{S}_N$  are similar. The similarity matrix  $\mathbf{P}$  is the permutation defined by  $\mathbf{P}\mathbf{e}_1 = \mathbf{e}_2$ . Matrices  $(\mathbf{J}_N)^2$  and  $\mathbf{S}_N$  have same spectral radius, 1-norm and  $\infty$ -norm. To study the convergence behavior of WR relaxation, the focus was on the GJ case only since it is possible to directly deduce similar results in the GS case with the following fact in mind:  $(\mathbf{J}_N)^2$  is defined over two iterations whereas  $\mathbf{S}_N$  is over one iteration only.

## 4.4 Conclusion

The nilpotency of WR algorithm has been examined for chains of circuits when strictly dissipative impedance coupling is adopted. It was shown that optimal local convergence is a necessary condition yet not sufficient for global convergence. The direction along which local

convergence factors are zeroed, affects the degree of nilpotency and can even produce a non-nilpotent algorithm.

A upperbound estimate was presented for the GJ and GS iteration matrices of the resistive coupling-based waveform relaxation algorithm when it is applied to chains of identical symmetric circuits. It showed that convergence is guaranteed for any number of cascaded circuits.

## Chapter 5

# 5 Conclusion

The contribution of the present thesis is recapitulated, and prospective directions are suggested for future research.

## 5.1 Summary

The focus of the present thesis was on enhancing the speed of convergence of WR algorithm with longitudinal partitioning. Although the proposed algorithms were intended for the solution of general transmission line circuits, their underlying theoretical results apply to any circuit with a linear time-invariant representation.

In chapter 2, an enhanced resistive coupling scheme was presented. Fast convergence was cast as an optimization problem and an automatic solution in the suboptimal sense was provided. Numerical examples illustrated the pertinence of the enhanced resistive coupling and documented the possibility of runtime savings for the analysis of arborescent transmission line circuits.

In chapter 3, a more general coupling scheme was presented and studied. To approximate the optimal convergence conditions of the subsequent algorithm, the presented coupling strategy avoided the difficult problem of optimization and proposed an approximation which captures the delay of the optimal condition. The coupling strategy used coarse macromodeling of the transmission line to construct these high-order approximations directly in circuit form. Numerical examples attested the superior convergence produced by this general coupling.

In chapter 4, new theoretical results were presented. The first part of these results concerns the nilpotent waveform relaxation algorithm for chains of general circuits when dissipative impedance coupling is used. The aim of this study was to identify under what conditions a nilpotent algorithm is reached. This way, it is possible to construct judicious approximations of the nilpotency conditions which can produce cost-efficient algorithms at suboptimal speeds of convergence. The second part demonstrated the global convergence of waveform relaxation for chains of identical symmetric circuits when resistive coupling is applied.

## 5.2 Future work

### 5.2.1 Towards multi-conductor transmission line circuits

The present work can be extended to general multi-conductor transmission line circuits and to power distribution networks. Every neutral series insertion  $\{-R_1, R_1 + R_2, -R_2\}$  made of resistances, is replaced with  $\{-\mathbf{R}_1, \mathbf{R}_1 + \mathbf{R}_2, -\mathbf{R}_2\}$  where  $\mathbf{R}_1$  and  $\mathbf{R}_2$  are matrices whose elements represent coupling resistances. This insertion decouples two adjacent parts which contain multi-conductor transmission lines. In the same way resistive coupling can be generalized to impedance coupling where every neutral series insertion  $\{-\zeta_1, \zeta_\Sigma, -\zeta_2\}$  made of impedances is replaced with  $\{-\boldsymbol{\zeta}_1, \boldsymbol{\zeta}_\Sigma, -\boldsymbol{\zeta}_2\}$  where  $\boldsymbol{\zeta}_1$  and  $\boldsymbol{\zeta}_2$  are matrices whose entries represent impedances.

### 5.2.2 In the presence of nonlinear loads

The present work focused on the application of resistive and impedance coupling to linear circuits where partitioning yields multiple subcircuits or parts. If the circuit contain nonlinear parts that are sandwiched between interconnects, then a multi-subsystem partitioning is required to apply a WR analysis. To reach fast convergence, it is possible to apply the presented results on the linear interconnect circuit to lower the local convergence rate. Of, course the analysis will include the Newton iteration or another suitable method to deal with nonlinear part which can be a line driver, receiver, or source.

## Bibliography

- [1] K. E. Brenan, S. L. Campbell, and L. R. Petzold, *Numerical Solution of Initial-Value problems in Differential-Algebraic Equations*, New York: North Holland, 1989.
- [2] J. M. Ortega and W. C. Rheinbolt, *Iterative Solution of Nonlinear Equations in Several Variables*. Computer Science and Applied Mathematics, New York: Academic press, 1970.
- [3] L. O. Chua and P.-M. Lin, *Computer-Aided Analysis of Electronic Circuits*, Englewood Cliffs, New Jersey: Prentice Hall, 1975.
- [4] J. Vlach and K. Singhal, *Computer Methods for Circuit Analysis and Design*, Berkshire, England: Van Nostrand Reinhold, 1983.
- [5] L. W. Nagel, "SPICE2: A computer program to simulate semiconductor circuits", Berkeley, California: Tech. Rep. REL M520, Electronics Research Laboratory Report, University of California, May 1975.
- [6] W. T. Weeks, A. J. Jimenez, G. W. Mahoney, D. Mehta, H. Quasemzadeh, and T. R. Scott, "Algorithms for ASTAP - A network analysis program," *IEEE Trans. Cir. Theory*, pp. 628-634, November 1973.
- [7] G. Strang, *Linear algebra and Its Applications*, New York: Academic press, 1980.
- [8] G. H. Golub and C. F. Van Loan, *Matrix Computations*. Baltimore, Maryland: The John Hopkins University press, 1983.
- [9] L. S. Duff, A. M. Erisman, and J. K. Reid, *Direct Methods for Sparse Matrices*. Oxford: Clarendon Press, 1986.
- [10] V. Strassen, "Gaussian elimination is not optimal," *Numer. Math.*, vol. 13, pp.354-356, 1968.
- [11] L. F. Richardson, "The approximate arithmetical solution by finite differences of physical problems involving differential equations to the stress in masonry dam," *Philos. Trans. Roy. Soc. London*, vol. Ser. A210, pp. 307-357, 1910.
- [12] R. S. Varga, *Matrix Iterative Analysis*, Automatic Computation Series, Englewood Cliffs, New Jersey: Prentice-Hall Inc, 1962.
- [13] M. R. Hestens and E. Stiefel, "Methods of conjugate gradient for solving linear systems," *Journal of research of the National Bureau of standards*, vol. 49, pp. 409-436, December 1952.
- [14] J. M. Ortega and W. C. Rheinbolt, *Iterative Solution of Nonlinear Equations in Several variables*. Computer Science and Applied Mathematics, New York: Academic Press, 1970.



- [15] O. Axelsson, "Solution of linear systems of equations: Iterative methods," in Sparse Matrix Techniques (V. A. Baker, ed.), pp.1-51, New York: Springer-Verlag, 1976..
- [16] H. C. Helman, *Iterative Methods for Large Sparse Nonsymmetric Systems of Linear Equations*. Ph.D. thesis, Computer Science Dept. Yale University, New haven, CT, 1982.
- [17] Y. Saad and M. Schultz, "GMRES: a generalized minimum residual algorithm for solving nonsymmetric linear systems," *SIAM J. Sci. Statist. Comput.* Vol. 7, pp. 856-869, July 1986.
- [18] P. Sonneveld, "CGS, a fast Lanczos-type solver for nonsymmetric linear systems," *SIAM J. Sci. Statist.*, vol. 10, pp. 36-52, 1989.
- [19] V. Faber and T. Manteuffel, "Necessary and sufficient conditions for the existence of a conjugate gradient method," *SIAM J. Sci. Statist.*, vol. 21, pp. 352-362, 1984.
- [20] R. S. Dembo, S. C. Eisenstat, and T. Steihaug, "Inexact Newton methods," *SIAM J. Sci. Statist.*, vol. 19, pp. 400-408, April 1982.
- [21] C. W. Gear and Y. Saad," Iterative solution of linear equations in ODE codes," *SIAM J. Sci. Statist. Comput.*, vol. 4, pp. 583-601, December 1983.
- [22] P. N. Brown and A. C. Hindmarsh, "Matrix-free methods for stiff systems of ODE's," *SIAM J. Numer. Anal.*, vol. 23, pp. 610-638, June 1986.
- [23] P. N. Brown and A. C. Hindmarsh, "Reduced Storage methods in stiff ODE systems," *J. Appl. Math. Comput.*, vol. 31, pp. 40-91, 1989.
- [24] T. F. Chan and K. R. Jackson, "The use of iterative linear equation solver in codes for large systems of stiff IVP's for ODE's," *SIAM J. Sci. Statist. Comput.*, vol. 7, pp. 378-417,1986
- [25] P. Brown and Y. Saad, "Hybrid Krylov methods for nonlinear systems of equations," *SIAM J. Sci. Statist. Comput.* Vol. 11, pp. 450-481, may 1990.
- [26] C. W. Gear, *Numerical Initial value Problems in Ordinary Differential Equations*. Automatic Computation, Englewood Cliffs, New Jersey: Prentice-Hall, 1971
- [27] P. Maffezzoni and L. Codecasa,"Time-Domain Simulation of Nonlinear Circuits Through Implicit Runge-Kutta Methods," *IEEE Trans. Circ. Syst.* -I: regular paper, vol. 54, no. 02, February 2007
- [28] G. Dahlquist and Å. Björck, *Numerical Methods*. Automatic Computation, Englewood Cliffs, New Jersey: Prentice-Hall, 1974.
- [29] L. V. Kantorovich and G. P. Akilov, *Functional Analysis in Normed Spaces*, Oxford: Pergammon Press, 1964.

- [30] R. Saleh and J. White, "Accelerating relaxation algorithms for circuit simulation using waveform-Newton and step-size refinement," *IEEE Trans. CAD*, vol. 9, no. 9, pp. 951-958, 1990.
- [31] L. M. Silveira, "*Circuit simulation algorithms for massively parallel processors*," Master's thesis, Massachusetts Institute of Technology, Cambridge, MA, May 1990.
- [32] M. Vidyasagar, *Nonlinear Systems Analysis*. Englewood Cliffs, NJ: Prentice-Hall, 1978.
- [33] E. Lelarsmee, A. E. Ruehli, and A. L. Sangiovanni-Vincentelli, "The waveform relaxation method for time domain analysis of large scale integrated circuits," *IEEE Trans. Comp. Aided Design Integr. Circ. Syst.*, vol. 1, pp. 131-145, July 1982
- [34] J. K. White and A. L. Sangiovanni-Vincentelli, *Relaxation Techniques for the Simulation of VLSI Circuits*. Engineering and Computer Science Series, Norwell, Massachusetts: Kluwer Academic Publishers, 1986.
- [35] U. Miekkala and O. Nevanlinna, "Convergence of dynamic iteration methods for initial value problems," *SIAM J. Sci. Stat. Comp.* vol. 8, pp. 459-467, 1987.
- [36] U. Miekkala, "Dynamic iteration methods applied to linear DAE systems," *J. Comput. Appl. Math.*, vol. 25, pp.133-151, 1989.
- [37] E. Z. Xia, "*Parallel waveform-relaxation-Newton for circuit simulation*," Master's thesis, University of Illinois at Urbana-Champaign, 305 Talbot, Urbana-Champaign, IL, 61801-2932, 1988, also University of Illinois Center for Supercomputing research and Development report No. 772.
- [38] A. Lumsdaine, M. Reichelt, and J. White, "Conjugate direction waveform methods for transient two-dimensional simulation of MOS devices," in *International Conference on Computer Aided-design*, (Santa Clara, California), pp. 116-119, November 1991.
- [39] A. Lumsdaine, "*Theoretical and Numerical Aspects of parallel Numerical Algorithms for Initial Value problems, with Applications*," Ph.D. thesis, Massachusetts Institute of Technology, Cambridge, MA 1992.
- [40] R. D. Skeel, "Waveform iteration and the shifted Picard splitting," *SIAM J. Sci. Statist. Comput.*, vol. 10, pp. 756-776, 1989.
- [41] C. Lubich and A. Osterman, "Multigrid dynamic iteration for parabolic problems," *BIT*, vol.27, pp. 216-234, 1987.
- [42] S. Vanderwalle and R. Piessens, "Efficient parallel algorithms for solving initial-boundary value and time-periodic parabolic partial differential equations," *SIAM J. Sci. Statist. Comput.* vol. 13, pp. 1330-1346, 1992.

- [43] C. Lubich, "Chebyshev acceleration of Picard-Lindelöf iteration," *BIT*, vol. 32, pp. 535-538, 1992.
- [44] M. Reichelt, "Accelerated Waveform Relaxation Techniques for Parallel Transient Simulation of Semiconductor Devices," Ph.D. thesis, Massachusetts Institute of Technology, Cambridge, MA, 1993.
- [45] B. Leimkuhler, "Estimating waveform relaxation convergence," *SIAM J. Sci. Comput.* vol. 14, pp. 872-889, 1993.
- [46] O. Nevanlinna, "Linear acceleration of Picard-Lindelöf iteration," *Numer. Math.*, vol. 57, pp. 147-156, 1990.
- [47] M. Reichelt, J. K. White, and J. Allen, "Optimal convolution SOR acceleration of waveform relaxation with application to parallel simulation of semiconductor devices," *SIAM J. Sci. Comput.*, vol. 16, pp. 1137-1158, 1996.
- [48] A. Lumsdaine and D. Wu, "Krylov subspace acceleration of waveform relaxation," *SIAM J. Numer. Anal.*, vol. 41, no. 1, pp. 90-111, 2003.
- [49] E. Lelarasmee, Albert E. Ruehli and A.L Sangiovanni-Vincentelli, "Waveform relaxation decoupling method," *IBM Tech. Disclosure Bull.* vol. 24, no. 7B, pp. 3720-3720, Dec. 1981. 49
- [50] A. E. Ruehli and T. A. Johnson. Circuit Analysis Computing by waveform relaxation, vol. 3. Wiley Encyclopedia of Electrical Electronics Engineering, New York, 1999.
- [51] C. H. Carlin and A. Vachoux, "On partitioning for waveform relaxation time-domain analysis of VLSI circuits," in *Proc. IEEE Int. Symp. Circuits and Systems*, May 1984, pp. 701-705.
- [52] J. White and A. L. Sangiovanni-Vincentelli, "Partitioning algorithms and parallel implementations of waveform relaxation algorithms for circuit simulation," in *Proc. IEEE Int. Symp. Circuits and Systems*, June 1985, pp. 1069-1072.
- [53] A. E. Ruehli, Ed., *Circuit Analysis, Simulation and Design*, New York: Elsevier, 1987.
- [54] K. L. Paap, Y. Han, W. John, B. Klaassen, and G. P. Ploger, "Concurrent circuit simulation schedules by signal flow graphs," in *Proc. Int. Conf. Computing Information*, 1989. 54
- [55] J. K. White and A. Sangiovanni-Vincentelli, "Relaxation Techniques for VLSI Circuits," Kluwer Academic Publishers, 1987.
- [56] F.Y Chang, "The generalized method of characteristics for waveform relaxation analysis of lossy coupled transmission lines," *IEEE Trans. Microw. Theory Tech.* vol. 37, no. 3, pp.2028-2038, Dec. 1989.

- [57] F.Y Chang, "Waveform relaxation analysis of RLGC transmission lines," *IEEE Trans. Cir. Sys.*, vol. 37, no. 11, pp. 1394-1415, Nov. 1990
- [58] F.Y Chang, "Relaxation simulation of transverse electromagnetic wave propagation in coupled transmission lines," *IEEE Trans. Cir. Sys.*, vol. 37, no. 8, pp. 916-926, Aug. 1991
- [59] N. Nakhla, A. Ruehli, M. Nakhla and R. Achar, "Simulation of coupled interconnects using waveform relaxation and transverse partitioning", *IEEE Trans. Adv. Packag.*, vol. 29, no. 1, pp.78-87, Feb. 2006. 58
- [60] M. Farhan, N. Nakhla, M. Nakhla, R. Achar and A. Ruehli, "Overlapping partitioning technique for strongly coupled distributed interconnects ", *IEEE Trans. Comp. Packag. Manufact. Techn.*, vol. 2, no. 7, pp. 1193-1201, July 2012.
- [61] I. M. Elfadel, "Convergence of transverse waveform relaxation", *IEEE Trans. Comp. Aided Design Integ. Circ. Syst.*, vol. 28, no. 8, pp. 1150-1161, Aug. 2009
- [62] D. Paul, N. M. Nakhla, R. Achar and M. S. Nakhla, " Parallel simulation of massive coupled interconnect networks," *IEEE Trans. Adv. Packag.*, vol. 33, no. 1, pp. 115-127, Feb. 2010.
- [63] R. Wang and O. Wing, "Analysis of VLSI multiconductor systems by bi-level waveform relaxation," *IEEE Int. Conf. Dig. Technical Papers*, pp. 166-169, 1990.
- [64] R. Wang and O. Wing, "Transient analysis of Dispersive VLSI interconnects terminated with nonlinear loads", *IEEE Trans. Comp. Aided Design*, vol. 11, no. 10, October 1992
- [65] W. Beyene, "Application of multilinear and waveform relaxation methods for efficient simulation of interconnect-dominated nonlinear networks", *IEEE Trans. Adv. Packag.* vol. 31, no. 3, pp. 637-648, Aug. 2008.
- [66] V. Loggia and S. Grivet-Talocia, "A two-level waveform relaxation approach for fast transient simulation long high-speed interconnects," *Proc IEEE-EPEPS*, pp. 85-88, 2010.
- [67] S. Grivet-Talocia and V. Loggia, "Fast channel simulation via waveform over-relaxation," in *Proc. 15th IEEE Workshop Signal Propagation on Interconnects*, Naples, Italy, pp. 103-106, May 2011.
- [68] S. Grivet-Talocia and V. Loggia, "Signal integrity verification of complex high-speed interconnects via waveform relaxation," *Proc IEEE-EMC*, pp. 328-333, Sept. 2011.
- [69] H. Hu and S. Grivet-Talocia, "Fast iterative simulation of high-speed channels via frequency dependent over-relaxation," in *Proc. IEEE 20th Conf. EPEPS*,

San Jose, CA, USA, pp. 115-118, Oct. 2011.

- [70] V. Loggia, S. Grivet-Talocia and H. Hu, "Transient simulation of complex high-speed channels via waveform relaxation". *IEEE Trans. Compon. Packag. Manufact. Tech.*, vol 1, no. 11, Nov. 2011.
- [71] S. B. Olivadese and S. Grivet-Talocia, "Transient analysis of high-speed channels via Newton-GMRES waveform relaxation," in Proc. IEEE 21st Conf. EPEPS, Tempe, AZ, USA, Oct. 2012, pp. 240-243.
- [72] H. Hu and S. Grivet-Talocia, "A preconditioned waveform relaxation solver for signal integrity analysis of high-speed channels," in *Proc, Int. Sym. Electromagn. Compat. (EMC Europe)*, Rome, Italy, Sept. 2012, pp. 1-6.
- [73] S. B. Olivadese and S. Grivet-Talocia, "Macromodel-based iterative solvers for simulation of high-speed links with nonlinear terminations," *IEEE Trans., Comp., Packag., Manuf., Technol.*, vol. 4, no. 11, pp1847-1861, Nov. 2014.
- [74] M. Gander, M. Al Khaleel and A. Ruehli, "Solution of large transmission line type circuits using a new optimized waveform relaxation partitioning" *Proc. IEEE: EMC*, May 2003, pp.331-647.
- [75] M. J. Gander and A. E. Ruehli, "Optimized waveform relaxation for RC type circuits", *IEEE Trans. Cir. Syst. I*, vol. 51, no. 4, pp.755-768, April 2004.
- [76] M. Gander, M. Al Khaleel and A. Ruehli, "Waveform relaxation technique for longitudinal partitioning of transmission lines", *Proc. IEEE: EPEP*, Oct. 2006, pp.207-210.
- [77] M. Gander, M. Al khaleel and A. Ruehli, "Optimized waveform relaxation methods for longitudinal partitioning of transmission lines", *IEEE Trans. Circ. Syst.* vol. 56, no. 8, pp. 1732-1743, Aug. 2009.
- [78] M. Al Khaleel, M. Gander, A. Ruehli, "Optimized waveform relaxation solution of RLCG transmission line type circuits", *Proc. IEEE: IIT*, pp.136-140, March 2013.
- [79] M. J. Gander and A. E. Ruehli, "Optimized waveform relaxation solution of electromagnetic and circuit problems," *Proc. IEEE-IPEPS*, pp. 65-68, 2010.
- [80] M. D. Al-Khaleel, M. J. Gander and A. E. Ruehli, "Optimization of transmission conditions in waveform relaxation techniques for RC circuits," *SIAM J. Numer. Anal.*, vol. 52, no. 2, pp1076-1101, April 2014.
- [81] SL. Wu and M. Al-Khaleel, "Parameter optimization in waveform relaxation for fractional-order RC circuits," *IEEE Trans. Circuits Syst. I, Reg. Papers*, vol. 64, no. 07, pp. 1781-1790, July 2017.
- [82] M. Kabir, C. E. Christoffersen, and N. Kriplani, "Transient Simulation based on state variables and waves," *Int. Journal RF Microwave Computer-Aided Engineering.*, vol. 21, pp. 314-324, May 2011.

- [83] M. Kabir and C. E. Christoffersen, "wave-based transient analysis using block Newton-Jacobi," *Proc. IEEE-CCECE*, pp. 000669-000673, 2011.
- [84] M. D. Al-Khaleel, "Optimized waveform relaxation methods for circuit simulations", Ph.D. dissertation, McGill Univ., Montreal QC, Canada, 2007.
- [85] V. B. Dmitriev-Zdorov and B. Klaassen, "An improved relaxation approach for mixed system analysis with several simulation tools," *Proc. EURO-DAC*, pp. 274-279, 1995.
- [86] V. B. Dmitriev-Zdorov, "Generalized coupling as a way to improve the convergence in relaxation-based solvers," in *Proc. EURO-DAC/EURO-VHDL Exhib.*, Geneva, Switzerland, Sep. 1996.
- [87] F. Nataf, F. Rogier, and E. de Sturler, "Optimal Interface Conditions for Domain Decomposition Methods", Tech. Report, CMAP (Ecole Polytechnique), Paris, France, 1994.
- [88] M. J. Gander, L. Halpern, and F. Nataf, C. Lai, P. Bjørstad, M. Cross, and O. Widlund, Eds., "Optimal convergence for overlapping and non-overlapping Schwarz waveform relaxation for time dependent problems," in *Proc. 11th Int. Conf. Domain Decomposition Methods*, Greenwich, U.K.
- [89] M. J. Gander and L. Halpern, "Méthodes de relaxation d'ondes pour l'équation de la chaleur en dimension 1," *C.R. Acad. Sci. Paris, Série I*, vol. 336, no. 6, pp. 519–524, 2003.
- [90] M. J. Gander, L. Halpern, and F. Nataf, "Optimal Schwarz waveform relaxation for the one dimensional wave equation," *SIAM J. Numer. Anal.*, vol. 41, no. 5, pp. 1643–1681, 2003.
- [91] M. J. Gander and L. Halpern, "Optimized Schwarz waveform relaxation methods for advection reaction diffusion problems," *SIAM J. Numer. Anal.*, vol. 45, no. 2, pp. 666–697, Feb. 2007.
- [92] W. LePage, *Complex Variables and the Laplace Transform for Engineers*, New York: Dover, 1980.
- [93] Volker Scheidemann, *Introduction to Complex Analysis in Several Variables*, Birkhäuser Verlag, Switzerland, 2005.
- [94] Clayton. R. Paul, *Analysis of Multiconductor Transmission Lines*, 2<sup>nd</sup> ed., Wiley Interscience, 2008.
- [95] J. Vlach and K. Singhal, *Computer Methods for Circuit Analysis and Design*, 2nd ed. Boston MA; Kluwer, 1993.
- [96] E. A. Guillemin, *Synthesis of Passive Networks*, New York, NY, USA: Wiley, 1957.
- [97] T. Menkad and A. Dounavis, "Resistive-based coupling waveform relaxation

- algorithm for analysis of interconnect circuits," *IEEE Trans. Circuits Syst. I, Reg. Papers*, vol. 64, no. 07, pp. 1877-1890, July 2017.
- [98] F.H. Branin, Jr., "Transient analysis of lossless transmission lines," *Proc. IEEE*, vol. 55, no. 11, pp. 2012-2013, Nov. 1967.
- [99] A. Odabasioglu, M. Celik and L. T. Pileggi, "PRIMA: passive reduced-order interconnect macromodeling algorithm," *IEEE Trans. Comput.-Aided Design Integr. Circuits Syst.*, vol. 17, no. 8, pp. 645-654, Aug. 1998.
- [100] P. Triverio, S. Grivet-Talocia, M. S. Nakhla, F. G. Canavero and R. Achar, "Stability, Causality, and Passivity in Electrical Interconnect Models," in *IEEE Trans. Adv. Packag.*, vol. 30, no. 4, pp. 795-808, Nov. 2007.
- [101] P. Henrici, *Applied and Computational Complex Analysis*, vol. 2. New York, NY, USA: John Wiley & Sons, 1986.
- [102] N. Nakhla, A. Dounavis, R. Achar and M. Nakhla, "DEPACT: Delay Extraction-Based Passive Compact Transmission-Line Macromodeling Algorithm," *IEEE Trans. Adv. Packag.*, vol. 23, no. 1, pp. 13-23, Feb. 2005.
- [103] N. Nakhla, M. Nakhla, and R. Achar, "Simplified delay Extraction-Based Passive Transmission Line Macromodeling Algorithm," *IEEE Trans. Adv. Packag.*, vol. 33, no. 2, pp. 498-509, May 2010.
- [104] A. Cangellaris, S. Pasha, J. Prince, and M. Celik, "A new discrete time-domain model for passive model order reduction and macromodeling of high-speed interconnections," *IEEE Trans. Comp., Packag., Manufact. Technol.*, pp. 356-364, Aug. 1999.
- [105] MATLAB and Statistic toolbox Release 2014a, The MathWorks Inc., Natick, Massachusetts, US.
- [106] "HSPICE U-2008.09-RA," Synopsis Inc.
- [107] A. Toselli and O. Widlund, *Domain decomposition methods-Algorithms and Theory*, New York, NY, USA: Springer Ser. Comput. Math., Springer, 2005, pp. 34.
- [108] R. A. Beauregard and J. B. Raleigh, *A first course in linear algebra; with optional introduction to groups, rings, and fields*, Houghton Mifflin Harcourt, Boston, MA, 1973.
- [109] K. Singhal and J. Vlach, *Computer Methods for Circuit Analysis and Design*, 2nd ed., Kluwer Academic Publisher, MA, USA, 2003.
- [110] HSPICE Signal Integrity User Guide, X-2005.09, Synopsys, Mountain View, CA, USA.

## Curriculum Vitae

**Name:** Tarik Menkad

**Post-secondary Education and Degrees:** Lakehead University  
Thunder Bay, Ontario, Canada  
2011-2013 MASc

Western University  
London, Ontario, Canada  
2013-2020 PhD

**Honors and Awards:** Province of Ontario Graduate Scholarship. 2012-2016.

**Related Work Experience** Electrical Engineer, Contract Lecturer  
ENIE, ENICAB, SONELGAZ, Lakehead University, Western University

### Publications:

#### In journals

T. Menkad and A. Dounavis, "Some results on the convergence of the dissipative coupling-based waveform relaxation algorithm for chains of circuits," In preparation.

T. Menkad and A. Dounavis, "Using strictly dissipative impedance coupling in the waveform relaxation method for the analysis of the analysis of interconnect circuits", Submitted to *IEEE Trans. Circuits Syst. I, Reg. Papers*, manuscript: *TCAS-I-01396-2020* on October 18, 2020. Accepted for publication on December 18, 2020.

T. Menkad and A. Dounavis, "Resistive coupling-based coupling waveform relaxation algorithm for analysis of interconnect circuits," *IEEE Trans. Circuits Syst. I, Reg. Papers*, vol. 64, no. 07, pp. 1877-1890, July 2017. DOI: [10.1109/TCSI.2017.2665973](https://doi.org/10.1109/TCSI.2017.2665973)

#### In conference proceedings

Tarik Menkad and Anestis Dounavis, "Longitudinal partitioning waveform relaxation algorithm for analysis of transmission line circuits", *Proc. International Domain-Decomposition Methods Symposium (DD25)*, July 2018.

T. Menkad, D. Alexandrov, and K. S. Butcher, "Modeling of metal-oxide-semiconductor capacitor on Indium Gallium Nitride-1: channel model," in *Proc. IEEE-CCECE*, April 2012. DOI: [10.1109/CCECE.2012.6334924](https://doi.org/10.1109/CCECE.2012.6334924)